INVESTIGATING THE MOLECULAR FUNCTION OF UBCH10

By

Ahmed Abdullah Al Awadh

A thesis submitted to

The University of Birmingham

For the degree of
DOCTOR OF PHILOSOPHY

Institute of Cancer and Genomic Sciences
College of Medical and Dental Sciences
The University of Birmingham

September 2020

Abstract

UbcH10 is an E2-conjugating enzyme specific for the Anaphase-Promoting Complex/Cyclosome (APC/C) and a proto-oncogene product that is overexpressed in many human cancers. The molecular basis of UbcH10 function is not, however, completely understood. To investigate the molecular function of UbcH10 in more detail and identify novel UbcH10-interacting proteins, our laboratory had previously performed UbcH10 interactomic studies. As such, it was hypothesised that novel UbcH10-associated proteins might be novel APC/C substrates or APC/C regulators. To this end, we investigated the function of the novel UbcH10-interacting protein and RhoA-specific RhoGEF, PDZ-RhoGEF in more detail. It was determined that PDZ-RhoGEF associates with UbcH10 both in vitro and in vivo and is targeted for proteasomal degradation in early mitosis. In this regard, it was determined that PDZ-RhoGEF associates with Cdc20, at least in part, through a highly conserved KEN box present in PDZ-RhoGEF and that ablation of the KEN box stabilises PDZ-RhoGEF protein levels. Moreover, it was determined that PDZ-RhoGEF is phosphorylated upon a number of S/TP sites in mitosis by Cdk1 and that pharmacological inhibition of Cdk1 in combination with proteasomal inhibitors limits the degradation of PDZ-RhoGEF in mitosis. These data suggest that PDZ-RhoGEF is targeted for APC/C-Cdc20-mediated degradation in a Cdk1- dependent manner.

Previous studies have suggested that UbcH10 might possess intrinsic E3 ubiquitin ligase activity. As such it was hypothesized that UbcH10 autoubiquitylation activity might affect UbcH10 function and that UbcH10 E3 ligase activity represented a potential therapeutic target. To this end, it was shown that UbcH10 possesses intrinsic

E3 ligase activity and is able to undergo extensive autopolyubiquitylation independent of the APC/C, on one or more lysine acceptor residues. Mutational analyses determined that K119 is the major lysine acceptor residue for polyubiquitin chain formation both in vitro and in vivo. In this regard, it was also determined that UbcH10 can assemble polyubiquitin chains with K6, K11 and K48 homotypic ubiquitin linkages. A high-throughput quantitative UbcH10 ubiquitylation assay for drug-screening was also developed and confirmed the requirement for lysine acceptor residues in UbcH10 autopolyubiquitylation activity. These data indicate that UbcH10 can potentially modify its own activity through self-polyubiquitylation and that UbcH10 E3 ligase activity could potentially be targeted pharmacologically in order to inhibit UbcH10 function.

Acknowledgements

First and Foremost, praise is to **ALLAH**, the Almighty, the greatest of all, on whom ultimately, we depend for guidance for giving me determination, and strength to do my work. I am deeply thankful to **Najran University** and **Saudi Arabian Cultural Bureau** for financially supporting my study.

I would like to express my deep and sincere gratitude to my supervisor, **Dr Andy Turnell** for giving me the opportunity to do research and providing invaluable guidance throughout this research. His patience, immense knowledge, motivation and trust have deeply inspired me. He has taught me the methodology to carry out the research and to present the research works as clearly as possible. It was a great privilege and honour to work and study under his supervision. I am extremely grateful for what he has offered me. I would like to thank all my lab mates from Turnell group for their friendship, advices and making the time in the lab great experience.

Prayers, caring, endless support and sacrifices from my family was worth more than I can express on paper. I would not reach this day without the support of my **Father,** my **Mother**, **my brother** and my **sisters.** Special thanks to my brother **Nasser** who was the source of all the encouragement and support. Any attempt at any level can't be satisfactorily completed without the support and understanding of **my wife**. I am grateful for everything you have done for me. I would also thank my friend **Abdullah AlAwam** for making the four years in Birmingham full of fun and being always there when I needed him. I would like also to thank my friend **Talal Madah** for his endless support.

Table of Contents

List of Figures

List of Tables

Abbreviations

53BP1	53 Binding Protein 1
λPPase	Lambda Phosphatase
β-Trcp	β transducin repeat-containing protein
AAD	Active adenylation domain
AMFR	Autocrine motility factor receptor
APC/C	Anaphase Promoting Complex/Cyclosome
AREL1	Apoptosis-resistant HECT-type E3 ubiquitin transferase 1
Arf	ADP-Ribosylation Factor
ATM	Ataxia Telangiectasia Mutated
ATP	Adenosine Triphosphate
BLAST	Basic Local Alignment Search Tool
BRCA1	Breast Cancer Type 1 Susceptibility Protein
BRCA1-BARD1	BRCA1-associated RING domain protein 1
BSA	Bovine Serum Albumin
Bub1	budding uninhibited by benzimidazoles 1)
Bub3	Budding uninhibited by benzimidazole-3
BubR1	BUB1-related protein 1
CBP/p300	CREB-Binding Protein/Histone Acetyltransferase p300
Cbl-b	Casitas B-lineage lymphoma proto-oncogene b
Cdc34	Cell division cycle 34
CDC6	Cell division control protein 6 homolog
Cdc20	Cell division-cycle protein 20
Cdh1	Cdc20 homologue 1
Cdk	Cyclin dependent kinase
cDNA	Complementary DNA
CHIP	Recombinant Human CHIP/Stub1
Cks	Cyclin-Dependent Kinase Regulatory Subunit
c-MAD2	Close MAD2
CRISPR	Clustered Regularly Interspaced Short Palindromic Repeat
Crn7	Coronin 7
CUE	coupling of ubiquitin conjugation to endoplasmic reticulum degradation
Cys	cysteine
DDR	DNA Damage Repair
DH	Dbi homology
DMBA	7,12-dimethylbenz(a)anthracene
DMEM	Dulbecco's Modified Eagle Medium
DMSO	Dimethyl Sulphoxide
DNA	Deoxyribonucleic acid
Dox	Doxycycline
DTX3L	Deltex E3 Ubiquitin Ligase 3L
DUBs	Deubiquitylating enzymes
E6AP	E6-Associated protein
E3 ligase TRAIP	E3 ligase TRAIP
Ect2	Epithelial cell-transforming sequence 2 oncogene
EGF	Epidermal growth factor
ELISA	Enzyme-linked immunosorbent assay
Emi1	Early mitotic inhibitor 1
FCS	Foetal Calf Serum
FRT	Flp Recombination Target
G1	Gap1
GAG	Group antigens polyprotein

GAP	GTPase Activating Proteins
GAT	Gga and TOM1
GDP	Guanosine Diphosphate
GEF	Guanine Nucleotide Exchange Factor
GFP	Green Fluorescent Protein
Gp78	Glycoprotein 78
GPCR	G-Protein Coupled Receptor
GST	Glutathione S-transferase
GTP	Guanosine Triphosphate
H2A	Histone 2A
H2B	Histone 2B
HACE1	HECT domain and ankyrin repeat-containing E3 ubiquitin-protein ligase 1
HECT	homologous to E6-associated protein C-terminus
HERC	HECT domain and RCC1-like domain-containing protein 1
HIF-2α	Hypoxia-inducible factor 2α
HOIL-1	Heme-oxidized IRP2 ubiquitin ligase 1
HOIP	HOIL-1 Interaction protein
HRP	Horseradish Peroxidase
HtrA2	High temperature requirement protein A2
HUWE1	HECT, UBA and WWE domain containing E3 ubiquitin protein ligase 1
IAD	Inactive adenylation domain
IAP	inhibitor of apoptosis
IgG	Immunoglobulin G
IKK	I kappa B kinase complex
IM	Interaction Motif
IP	Immunoprecipitation
IPTG	isopropyl-b-D-1-thiogalactopyranoside
ITCH	HECT-type E3 ubiquitin transferase Itchy homolog
K	Lysine
KLHL20	Kelch-like ECT2-interacting protein
LARG	Leukaemia Associated Rho Guanine Nucleotide Exchange Factor
LB	Luria Broth
LC-MS/MS	Liquid Chromatography Coupled Tandem Mass Spectrometry
LH	Lsc Homology
LPA	lysophosphatidic
LUBAC	Linear ubiquitin chain assembly complex
Mad2	Mitotic arrest deficient 2
MCC	Mitotic Checkpoint Complex
MEFs	mouse embryo fibroblasts
Met4	Methionine 4
MG132	Carbobenzoxy-Leu-Leu-leucinal
Mps1	Monopolar spindle 1
NCBI	National Centre for Biotechnology Information
NEBD	Nuclear Envelop Break Down
NEDD4	neural precursor cell expressed developmentally down-regulated protein 4
Nek2A	NimA-related protein kinase 2
NEMO	Nuclear factor-κB essential modifier
NETN	NaCl-EDTA-Tris-NP 40
NF-kB	Nuclear Factor Kappa Beta
NMR	Nuclear magnetic resonance spectroscopy
NZF	Npl4 zinc finger
o-MAD2	Open MAD2
OPD	o-phenylenediamine dihydrochloride
OPTN	Optineurin
OTUD7A	OTU Deubiquitinase 7A
OTUD7B	OTU Deubiquitinase 7B
PAZ	polyubiquitin associated ZINC finger
PBS	Phospho-Buffered Saline
PCR	Polymerase Chain Reaction
PDZ	PDS-96, DlgA, ZO-1

PDZ-RhoGEF	PDZ domain-containing Rho guanine nucleotide exchange facto
PH	Pleckstrin Homology
Plk1	Polo like kinase 1
pRB	Retinoblastoma
Pro-TAME	Prodrug Tosyl-L-arginine Methyl Ester
PTMs	Post Translation Modifications
pSer	Phosphor-Serine
pThr	Phosphor-Threonine
pTyr	Phosphor-Tyrosine
Rab	RAS- like proteins in brain
Ran	Ras-like Nuclea
RAS	Rat sarcoma
RASSF1A	Ras Association Domain Containing Family 1 Isoform A
RBRs	RING-between RING
RCC1	regulator of chromatin condensation 1
RGS	Regulators of G Proteins
RhoGDIs	Rho-specific guanine nucleotide dissociation inhibito
Rho	Ras Homologous
RhoGEF	RhoGEF
RING	Really Interesting New Gene
RNF144A	Ring Finger protein 144A
RNF144B	Ring Finger Protein 144B
RNF8	Ring Finger protein 8
RNP10	RNA binding protein 10
RTS	Rothmund-Thomson syndrome
SAC	Spindle assembly checkpoint
SAL A.	Salinosporsmide A
SCF	Skp, Cullin, F-box containing complex
SHARPIN	SHANK-associated RH domain-interacting protein
Sic1	stoichiometric inhibitor 1
siRNA	Small Interfering Ribonucleic Acid
Skp2	S-phase kinase associated kinase 2 (Skp2)
SMAC	Second mitochondria-derived activator of caspase
SQSTM1	Sequestosome-1
STING	Transmembrane protein
TANK	TRAF-interacting protein
TBE	Tris-Boric Acid-EDTA
TBST	Tris-Buffered Saline-Tween 20
TEMED	N, N, N', N;-tetramethylethylenediamine
TGN	trans-Golgi network
TNF-R1	TNF Receptor 1
TPR	Tetratricopeptide-repeat
TRAF6	Tumour necrosis factor receptor-associated factor 6
Tris	hydroxymethylaminomethane
TSG101	Tumour Susceptibility Gene 101
UBA	Ubiquitin Associated domain
UBA6	UbL modifier activating enzyme 6
UBA52	Ubiquitin A-52 Residue
UBA80	Ubiquitin A 80
UBAN	Ubiquitin binding in ABIN and NEMO
UB32G2	Ubiquitin-conjugating enzyme 2G2
UBB	Ubiquitin B
UBC	Ubiquitin C
UBD	Ubiquitin Binding Domain
UBE1	ubiquitin-activating enzyme 1
UBE2C	Ubiquitin-conjugating enzyme C
UBE1DC1	ubiquitin-activating enzyme E1 domain containing
UBE2N	Ubiquitin-conjugating enzyme 2N
UBE2S	Ubiquitin-conjugating enzyme 2S
UBE2T	Ubiquitin-conjugating enzyme 2T

Ub–VS	ubiquitin– vinylsulphone
UEV	Ubiquitin-conjugating enzyme variant
UFD	Ubiquitin Fold domain
UIM	Ubiquitin interacting motif
USP8	Ubiquitin Specific protease 8
UTB	Urea-Tris-b-Mercaptoethanol
UV	Ultra Violet
VCP	Valosin-containing protein
WHB	Winged-Helix B
Wnt	Wingless and Int-1
WT	Wild-Type
YB-1	Y-BOX binding protein 1
Zap-70	70 kDa zeta-chain associated protei
ZBR	Zinc-binding region

1 Introduction

1.1 The cell cycle

The cell cycle is a highly ordered and temporally-coordinated process, controlled by multiple regulatory mechanisms whose main purpose is to maintain genome integrity during cell growth and DNA replication, and during chromosomal segregation and cell division. The cell cycle is classically organized into four distinct stages, where Gap phase 0 - G0, also known as cellular quiescence, is a state where the cell is not committed to undergo a replicative cell cycle. Cells typically enter Gap phase 1 - G1 in response to mitogenic growth factors, whereupon the cell grows larger, organelles and other cellular contents are duplicated, and the proteins and molecular building blocks needed for DNA replication are synthesized. Synthetic phase - S is the cellular DNA replication stage where all 46 chromosomes are replicated. G2 phase is the proof-reading stage where DNA damage surveillance pathways ensure that any DNA errors of replication are recognized and repaired. Mitosis, or M-phase allows for faithful chromosomal segregation, cytokinesis and the formation of two identical daughter cells. Cell cycle checkpoints are an important regulatory layer that ensures the timely and ordered progression of cells through the cell cycle.

A number of essential checkpoints operate at different stages of the cell cycle:

- R- restriction point during G1 whereby the cell commits irreversibly to enter the cell cycle
- G1-S, to allow for the timely entry into S
- intra-S phase checkpoints that ensure the fidelity of DNA replication
- G2-M checkpoint that ensures that DNA damage is recognized and repaired
- The spindle assembly checkpoint (SAC) that ensures all sister chromatids are attached appropriately to the mitotic spindles prior to segregation.

Progression through cell cycle stages is controlled principally by fluctuations in the activities of a family of Cyclin-dependent kinases (Cdks), which bind to partner Cyclin proteins, whose synthesis and degradation are important for the Cdk activation and inactivation, respectively. In cells, there are four main types of Cdks and each type is activated by different cyclins - D, E, A and B in a cell cycle-dependent manner (Evans et al. 1983, Gautier et al. 1990, Elledge 1996). Cyclin D binds and activates Cdk4 and Cdk6 in response to mitogenic signalling and stimulates entry into G1. During quiescence and the early stages of G1, the Retinoblastoma protein (pRB) binds to the E2F1 transcription factor to inhibit its activity (Ewen et al. 1993). Activation of Cdk4/6 by Cyclin D promotes the Cdk4/6-dependent phosphorylation of pRB, which in turn primes E2F1-dependent transcription, passage of the cell through the restriction point, R, and commitment to the cell cycle.

E2F1 activation also allows for the synthesis of cyclin E that, in cooperation with Cdk2, is crucial for progression into S phase (Gautier et al. 1990, Koff et al. 1991, Baldin et al. 1993, Ewen et al. 1993). Indeed, further phosphorylation of pRB by Cyclin E-Cdk2 allows for pRB release from E2F1, the full activation of E2F1, the synthesis of proteins important for DNA replication and G1-S phase transition and the assembly of the MCM helicase in readiness for DNA replication (Coverley et al. 2002). Cyclin E-Cdk2 activity is regulated by the p27 Cdk inhibitor (Morisaki et al. 1997). p27 works to limit cyclin E-Cdk2 activation and ensures that S phase transition is inhibited until cells are ready for DNA replication. Activation of BCR-ABL and Src tyrosine kinases during G1 phosphorylate p27, which promotes its degradation by S phase Kinase-associated Protein 2 (Skp2) and the activation of Cyclin E-Cdk2 complexes (Chu et al. 2007, Grimmler et al. 2007). The Cyclin E- Cdk2 complex also regulates cell cycle

progression by modulating the activity of other cellular proteins such as E2F5. Cyclin E-Cdk2 phosphorylates E2F5 directly, which triggers the recruitment of CBP/p300 to the E2F5 complex to drive E2F5-dependent transcription and cell cycle progression (Morris et al. 2000).

Full activation of the E2F1 transcription factor stimulates the expression of the S phase cyclin, cyclin A, which stimulates DNA synthesis from origins of replication, which are specific sequences of DNA where the replication machinery associates to promote DNA replication. Indeed, a number of components of the DNA replication machinery are substrates for cyclin A-Cdk2. The single-stranded DNA binding complex component, RPA, which participates in DNA replication, is a substrate for Cyclin A-Cdk2, whilst the DNA elongation activity of DNA polymerase δ is also regulated by Cyclin A-Cdk2 (Pan et al. 1994, Voitenleitner et al. 1997). Cyclin A-cdk2 is also required to ensure that there is only one DNA replication cycle per cell cycle. As such, Cyclin A-cdk2- phosphorylates 'free' unbound CDC6 ensuring that CDC6 is targeted for degradation and that new replication complexes are not formed, whilst it also inhibits the activity of the MCM helicase through targeted phosphorylation of MCM4 (Coverley et al. 2000, Ishimi et al. 2000) . Cyclin A-Cdk2 complexes also serve to phosphorylate E2F1 and inhibit E2F1 transcriptional activity (Girard, et al. 1991, Hinds, et al. 1992, Xu, et al. 1994). Cyclin A is particularly interesting amongst the cyclin family for its ability to associate with and activate two different Cdks, Cdk2 and Cdk1 that function in S phase and mitosis, respectively. Cyclin A starts to accumulate in S phase following E2F1 activation and is destroyed at nuclear envelope breakdown during mitosis by the ubiquitin proteasome system. Cyclin A-Cdk2 activities are also important in G2-M phase transition, such that its localization to centrosomes promotes

Cyclin B1-Cdk1 activation and the timing of mitotic entry (Yam et al. 2002, De Boer et al. 2008). Cyclin A also enhances Cyclin B1 accumulation in the nucleus and nuclear envelope breakdown in early mitosis, whence it is inactivated (Gong et al. 2007).

Cyclin B1-Cdk1 activity is required for entry into, and progression through mitosis. Following chromosome segregation Cyclin B1-Cdk1 activity is inhibited to allow for mitotic exit (Brito and Rieder 2006). Cyclin B1-Cdk1 activity is inhibited during G2 phase by phosphorylation of Cdk1 by Wee1 (Russell and Nurse 1987). Upon G2-M checkpoint satisfaction, Polo- like Kinase 1 (Plk1) phosphorylates Wee1 and inhibits its activity (Watanabe et al. 2004). Cdk1 is subsequently dephosphorylated by the Cdc25 phosphatase which results in Cyclin B1-Cdk1 activation and entry into mitosis (Jin et al. 1998). Mitosis is divided into five morphologically distinct stages, which are prophase, prometaphase, metaphase, anaphase and telophase (**Fig. 1.1**). In prophase: centrosomes are replicated and move to opposite poles; microtubules begin to be synthesized; chromosomes condense; the Cohesin complex is removed from chromosome arms such that sister chromatids are resolved; Cohesin is maintained at centromeres such that sister chromatids are still physically connected. In prometaphase: nuclear envelope breakdown (NEBD) is initiated; the mitotic spindle begins to assemble and attaches to each sister chromatid at centromeres through protein complexes called kinetochores. In metaphase, sister chromatids align at the equator when all sister chromatids are associated with the mitotic spindle through their kinetochores. Upon satisfaction of the Spindle Assembly Checkpoint (SAC) Cohesin is removed from sister chromatids and chromosome segregation, is initiated at anaphase, such that sister chromatids move to different poles of the cell. In telophase the mitotic spindle disassembles, chromosomes decondense and the nuclear

membrane starts to reform. Mitosis is completed following cytokinesis and the formation of two, identical daughter cells by abscission- the physical separation of the daughter cells. Mitotic progression is ultimately regulated by the destruction of cyclins, namely cyclin A and cyclin B1 and other key cell cycle proteins in a temporally and spatially coordinated manner by the 1.2 MDa macromolecular E3 ubiquitin ligase, The Anaphase-Promoting Complex/Cyclosome (APC/C) that targets Cyclins and other key cell cycle proteins for ubiquitin-dependent degradation (Brito and Rieder 2006).

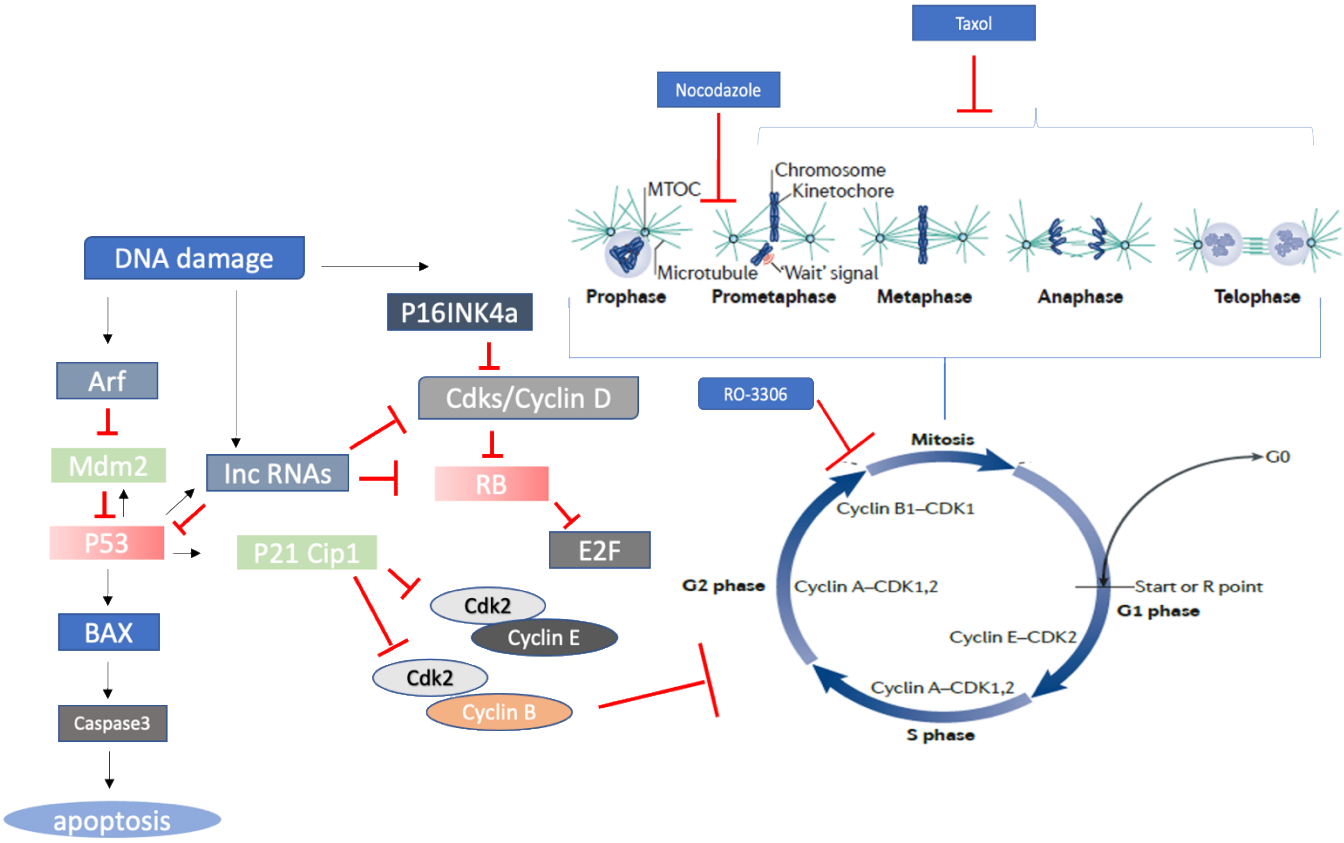

Figure 1.1: Schematic representation of the cell cycle. The cell cycle is controlled by different Cyclin-CDK partners. The cell cycle is divided into five important stages which are G0 phase, G1 phase, S phase, G2 phase and M phase. M phase or Mitosis is also divided into five different stages: prophase prometaphase, metaphase, anaphase and telophase – see text for details. Figure taken from Pines 2011. Retinoblastoma (Rb) and P53 control cell cycle progression in different ways. Rb stimulates cell cycle arrest in G1 and governs the S phase entry by modulating E2Fs activity. P53 mediate cell cycle by regulating different effectors causing G1, G2 arrest and promoting apoptosis.

1.2 The Ubiquitin-Proteasome System

Ubiquitylation (also known as ubiquitination) simply describes the enzymatic process of attaching the small, 76 amino acid protein, ubiquitin, to a target protein to modify the target protein's function (see section 1.3 for a more detailed description of ubiquitin) (Deshaies and Joazeiro 2009). This post-translational modification (PTM) is regulated by a multistep enzymatic cascade that is initiated by the ubiquitin-activating enzyme (known as E1) that, in an ATP-dependent manner, forms a covalent, high-energy thiol-ester bond with the carboxyl-terminal glycine of ubiquitin. The 'activated' E1-associated ubiquitin is then transferred to a ubiquitin-conjugating enzyme (known as E2), in a trans-thiolation reaction which similarly generates a high-energy thiol-ester bond between the E2 and the carboxyl-terminal glycine of ubiquitin. Finally, a substrate-specific ubiquitin ligase (E3) coordinates the transfer of ubiquitin from the E2-conjugating enzyme to the target substrate. Inspection of the human proteome indicates that there are 3 known human E1 enzymes, 37 known E2s and approximately 1000 E3s such that substrate specificity is controlled, predominantly by the E3 enzymes (**Fig. 1.2**; Deshaies and Joazeiro 2009).

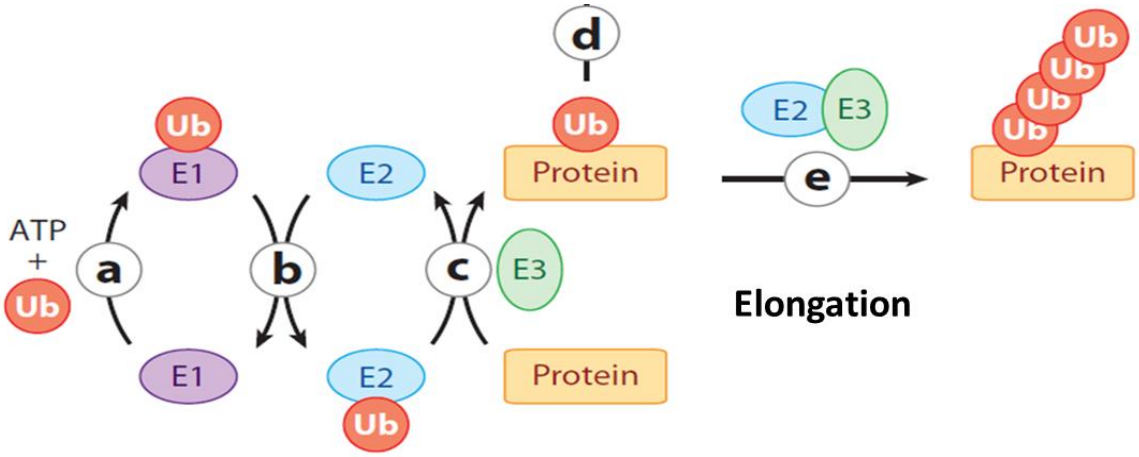

Figure 1.2: The Ubiquitin-Proteasome System. Schematic representation of ubiquitin attachment to a substrate in a multistep enzymatic pathway that requires activation of ubiquitin and its conjugation to the E1-activating enzyme (a), transfer of ubiquitin to an E2-conjugating enzyme (b) association of the E2 with an E3 ubiquitin ligase (c) and ultimately transfer of the ubiquitin to the substrate protein (d). Multiple ubiquitin transfers to the substrate result in polyubiquitylation (e). Adapted from Deshaies and Joazeiro 2009.

1.2.1 **E1-activating enzymes**

The first step of the ubiquitylation process is the activation of ubiquitin by an E1-activating enzyme. The first mammalian E1 enzyme was discovered in rabbit reticulocyte lysate and it was found to activate both ubiquitin and ubiquitin-like (UbL) proteins such as SUMO and Nedd8 (Hershko et al. 1980). In humans the known E1-activating enzymes are: ubiquitin-activating enzyme 1 (UBE1), ubiquitin-activating enzyme E1 domain containing 1 (UBE1DC1) and UbL modifier-activating enzyme 6 (UBA6) (Ciehanover et al. 1978, Handley et al. 1991, McGrath et al. 1991, Pelzer et al. 2007). In yeast, however, a single E1-activating enzyme can activate all ubiquitin and UbL proteins (McGrath et al. 1991). The activation of ubiquitin by E1 enzymes is an ATP-dependent reaction that involves two molecules of ATP and two molecules of ubiquitin. The E1 enzyme initially binds to ubiquitin and catalyses the adenylation of the C-terminal, G76 residue on one of the ubiquitin moieties by ATP and generates pyrophosphate as a by-product. This reaction promotes a conformational change at the active site of the E1 which means that the catalytic Cysteine (C) residue of the E1

comes into close contact with the ubiquitin adenylate allowing for nucleophilic attack of the ubiquitin adenylate by the E1 C residue. The reaction intermediate generated is unstable and a more stable thioester bond is ultimately formed between the E1 C residue and G76 of ubiquitin with the loss of AMP as a by-product (Holliday, et al. 2007). The second reaction then proceeds in the same manner with the generation of a G76 ubiquitin adenylate intermediate and E1 conformational changes that results in nucleophilic attack by the catalytic C residue of the E1 and the formation of a thioester linkage between the E1 and ubiquitin (Holliday et al. 2007).

E1-activating enzymes consist of three structural domains that are required for ubiquitin activation and ubiquitin transfer to E2-conjugating enzymes. Structural studies of Uba1 show that E1 function is highly dependent on the following structural domains. First, the adenylation domain facilitates the binding of ubiquitin and ATP and consists of two MoeB/Thif motifs containing an IAD (inactive adenylation domain) and an ADD (active adenylation domain). The active C half-domains, FCCH (First Catalytic C half-domain) and SCCH (Second Catalytic C half-domain) form the E1 active site, responsible for ubiquitin activation and binding. Finally, the Ubiquitin Fold domain (UFD) is important in the recruitment of the E2 and allowing for ubiquitin transfer to the E2 (Lake et al. 2001, Lois and Lima 2005, Szczepanowski et al. 2005, Lv et al. 2018; **Fig. 1.3**).

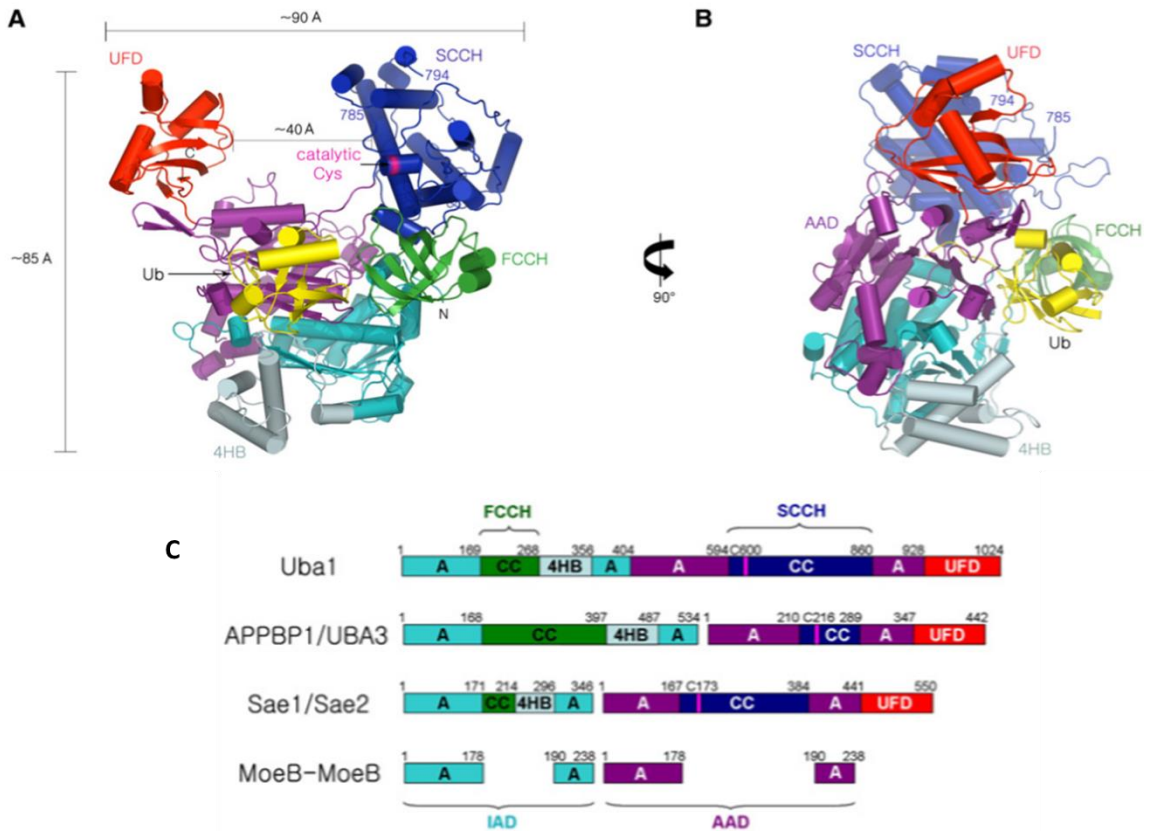

Figure 1.3: Structure of the E1-activating enzyme, Uba1. (A) The figure illustrates the structural domains of Uba1: IAD in Cyan, AAD in purple, FCCH in green, SCCH in blue, UFD in red, ubiquitin in yellow and catalytic Cys in pink (B) Alternative view of the Uba1 structure highlighting the association of Uba1 with ubiquitin. (C) Schematic illustration of the conserved domains present in Uba1, the NEDD8-E1 (Uba3), the Sumo-E1 (Sae1/Sae2) and bacterial E1 (MoeB-MoeB). Images taken from Lee and Schindelin 2008.

1.2.2 **E2 ubiquitin-conjugating enzymes**

The E2 family comprises 13 genes in *Saccharomyces cerevisiae* and at least 37 genes in humans; human E2s can be subdivided into 17 subfamilies based on phylogenetics (Michelle et al. 2009; Table 1.1). All E2-conjugating enzymes contain a main ubiquitin-conjugating domain (UBC) which possesses a catalytic C residue for binding to the E1. E2-conjugating enzymes are structurally divided into four different classes:

- Class I E2s contain only the conserved catalytic C residue
- Class II E2s possess an extended C-terminal region in addition to the catalytic domain
- Class III E2s contain an extended N-terminal region in addition to the catalytic domain
- Class IV E2s have both N- and C-terminal domains in addition to the catalytic domain.

These E2s-conjugating enzymes also contain additional functional domains within their structure that define the specificity of the E2.

Table 1-1 List of human E2-conjugating enzymes. Phylogenetic analysis of all protein belonging to E2-conjugating enzyme in seven species *Homo sapiens, Mus musculus, Drosophila melanogaster, Caenorhabditis elegans, Schizosaccharomyces pombe, Saccharomyces cerevisiae, and Arabidopsis thaliana* led to the identification of 37 E2 gene products in the human genome (Michelle, Vourc'h et al. 2009).

Gene	Protein	Amino acid length
UBE2A	HR6A	152
UBE2B	HR6B	152
UBE2C	UBCH10	179
UBE2D1	E2(17) KB1, SFT, UBC4/5, UBCH5, UbcH5a	147
UBE2D2	E2-17kDa2, UbcH5b	147
UBE2D3	E2-17kDa3, UbcH5c	147
UBE2D4	HBUCE1	147
UBE2E1	UBCH6	193
UBE2E2	UBCH8	201
UBE2E3	UBCH9	207
UBE2F	NCE2, MGC18120	185
UBE2G1	E2-17K	170
UBE2G2		165
UBE2H	UBCH2, E2-20k	183
UBE2I	SUMO1conjugating enzyme	158
UBE2J1	NCUBE1	318
UBE2J2	NCUBE2, UBC6p	292
UBE2K	HIP2, E2-25kDa, HYPG, LIG	200
UBE2L3	UBCH7, L-UBC	154
UBE2L6	RIG-B, UBCH8 (homonyme E2)	153
UBE2M	NEDD8 conjugating enzyme	183
UBE2N		152
UBE2NL	UBE2Nlike	153
UBE2O	E2-230K	1292
UBE2Q	UBE2Q1, NICE-5	422
UBE2Q2	UBCi	375
UBE2R1	CDC34, E2-32kDa	236
UBE2R2	FLJ20419, UBC3B	238
UBE2S	E2-24 kDa, E2-EPF	222
UBE2T	HSPC150	197
UBE2U		321
UBE2V1	CROC-1, UEV-1, Kua	170
UBE2V2	DDVIT1, EDAF-1, EDPF-1, MMS2, UEV-2	145
UBE2W		162
UBE2Z	HOYS7	246
BIRC6		4829
FTS	AKTIP	293

The first role of ubiquitin-specific E2-conjugating enzymes is to bind to ubiquitin-bound E1 enzymes, such that E2 ubiquitin-conjugating enzymes bind with high affinity to E1 enzymes associated with ubiquitin. In this regard, several structural studies have revealed that attachment of ubiquitin to E1 initiates conformational changes in the E1 that generates an E2 binding site that enhances the formation of E1-E2 complexes (Lois and Lima 2005, Huang et al. 2007, Lee and Schindelin 2008, Michelle et al. 2009). The second role for E2-conjugating enzymes is to catalyse the transfer of the activated ubiquitin from the catalytic C residue on E1 to the catalytic C residue on the E2. This transfer reaction proceeds once the E2 binds to the ubiquitin-bound E1 and the catalytic C of the E2 attacks the E1-bound ubiquitin in a nucleophilic manner that allows for the formation of a ubiquitin intermediate, which allows for conformational changes in the E1-E2 complex and the transfer of ubiquitin to the E2-conjugating enzyme and the formation of a thioester bond between the catalytic C residue on the E2 enzyme and G76 of ubiquitin (Holliday et al. 2007).

Once loaded with ubiquitin, E2s engage with specific E3 ubiquitin ligases to catalyse substrate ubiquitylation. Although structural studies have revealed that the interaction of E2-E3 is straightforward, the physiological determination of the E2-E3 interaction, particularly in humans, is more complicated. The E2 ubiquitin-binding domain within different E2s has a high degree of sequence homology and structure and is typically comprised of a conserved 3_{10}-helix (3_{10}), four α-helices, an anti-parallel β-pleated sheet of four strands and loop regions that link these defined structures (Olsen and Lima 2013). The catalytic C residue on the E2 enzyme is situated in a superficial groove linking α-helix 2 with α-helix 3. All E2-conjugating enzymes bind to E3 enzymes through α-helix 1 and L1 and L2 loops which all lie close to the surface of the E2. This

region possesses some sequence variation between E2s which allows for specificity of E3 binding. Moreover, a single E2 might interact with several E3 ligases, which recognise the E2s differently. For instance, UBE2N binds specifically to the E3 TRAF6 through R6 and K10 residues but interacts with the E3 ligase, CHIP through R7 and K10 (**Fig. 1.4** b and c; Zhang et al. 2005). Additionally, E2 binding to E3s is weak and of low affinity. This low affinity is beneficial however, as the E2 uses overlapping regions to bind both E1 and E3. Hence, E2 cannot bind both E1 and E3 at same time and therefore requires many rounds of E3 association and dissociation to assemble polyubiquitin chains on substrates (Eletr et al. 2005).

E2 enzymes have different capacities to allow for ubiquitin chain initiation and ubiquitin chain elongation on the target substrate. As such, E2s are classified into three groups: (i) E2- conjugating enzymes involved in ubiquitin chain initiation; (ii) E2-conjugating enzymes involved in ubiquitin chain elongation; (iii) E2-conjugating enzymes involved in both ubiquitin chain initiation and chain elongation. In this regard, some E2s only catalyse the monoubiquitylation on the target substrate. For instance, UBE2T initiates ubiquitin chain formation on its substrate FANCD2 but lacks the ability to elongate ubiquitin chains on the substrate (Alpi et al. 2008). In contrast, UBE2S is involved on the elongation of K11 ubiquitin chains but does not possess any initiation activity (Williamson et al. 2009). Finally, E2s such as the yeast E2, Cdc34 possesses both activities. As such, the E3 ligase, SCF associates with Cdc34 to initially promote monoubiquitylation and then the assembly of polyubiquitin chains with K48 linkages on the Cyclin-dependent kinase 1 inhibitor, Sic1 to promote Sic1 proteasomal-degradation (Petroski and Deshaies 2005, Gazdoiu et al. 2007). Those E2s that facilitate elongation often have more capacity to promote the processivity of ubiquitin

chain formation. For instance, human UBE2G2 and its yeast homologue, Ubc7 are able to assemble polyubiquitin chains on its active C residue both *in vivo* and *in vitro* before it is transferred to substrate. Mechanistic studies revealed that to allow for increased processivity UBEG2 forms a homodimer that associates with the gb78 E3 ligase (**Fig. 1.4**.a; Li et al. 2007). Other E2s are also known to form short ubiquitin chains on their catalytic C residue to facilitate elongation, whilst some E2s also possess inherent E3-ligase activity. Indeed, the yeast Cdc34 E2-conjugating enzyme can catalyse its own polyubiquitylation in the absence of a supporting E3 ubiquitin ligase. As such, it can assemble K48-linked polyubiquitin chains on four internal K residues to promote its own degradation; mutation of these K residues stabilises Cdc34 and reduces the ability of Cdc34 to catalyse auto-polyubiquitylation. These data suggested that some E2-conjugating enzymes do exhibit functional E3 ubiquitin ligase activity (Banerjee et al. 1993).

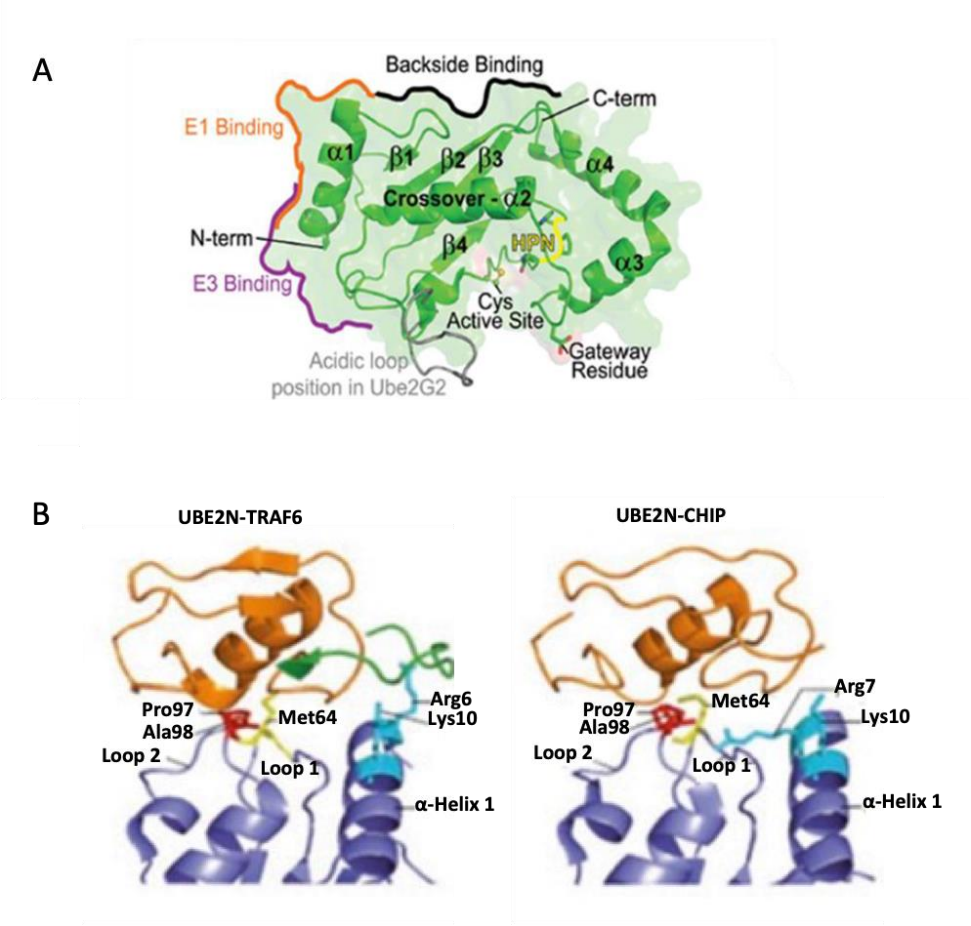

Figure 1.4: Structural features of E2-conjugating enzymes.(a) Overview of the E2 UBC domain structure indicating binding surfaces- E1-binding domain in orange, E3-binding surface in purple and acidic loop of the UBE2G2. (b) UBE2N structure indicating the role of specific residues in targeting two individual E3 ligases (shown in blue). Images taken from Ye and Rape 2009, Stewart, Ritterhoff et al. 2016.

1.2.3 **E3 ubiquitin ligases**

E3 ubiquitin ligases are responsible for catalysing the final step of the ubiquitylation process- the transfer of ubiquitin from the E2-conjugating enzyme to the Lys (K) residue of the target substrate. In humans, there are more than 600 E3 ubiquitin ligases which define substrate specificity (Berndsen and Wolberger, 2014). These E3-Ubiquitin ligases are categorized into three main classes which are: homologous to E6-AP carboxyl terminus (HECT); Really Interesting New Gene (RING); and RING-between RING (RBRs). Aside of the structural differences that exist between these

classes of E3 enzymes, a notable difference between them is the mechanism they adopt to promote ubiquitin transfer to the target protein (**Fig. 1.5**).

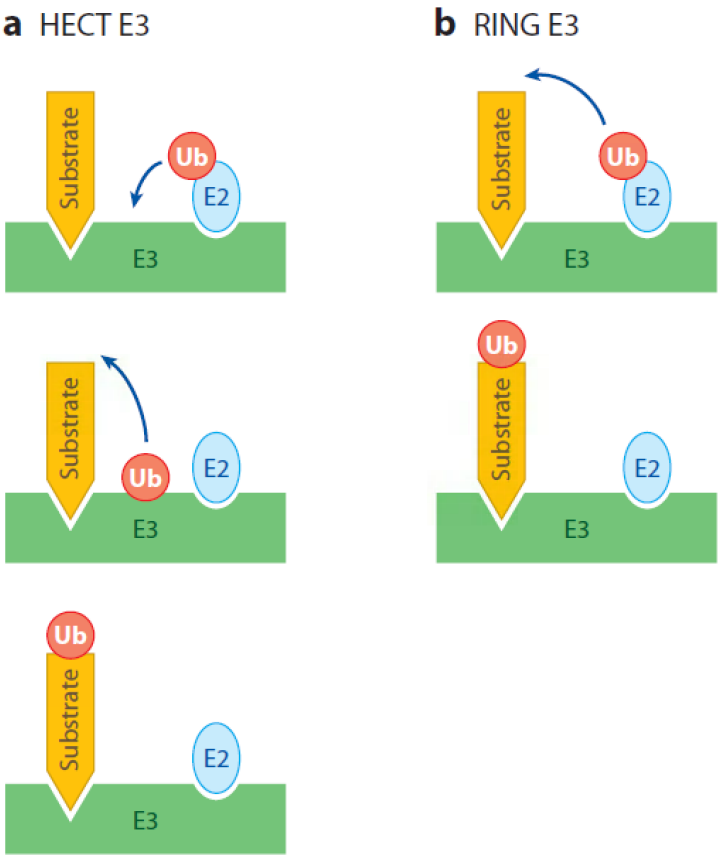

Figure 1.5: HECT and RING E3 ligases utilise different mechanisms. (A) HECT E3 ligases possess a conserved catalytic C residue that accepts ubiquitin from the E2 and forms an activated ubiquitin intermediate to allow for transfer of ubiquitin to the substrate. (B) RING E3 ligases catalyse the direct transfer of ubiquitin from the E2 to the substrate. Image taken from Deshaies and Joazeiro 2009.

1.2.3.1 HECT E3 ubiquitin ligases

HECT E3 ligases were the first identified class of E3 ubiquitin ligases (Li, Bengtson et al. 2008) The HECT E3 ligases can be distinguished from other E3 ligase types in that this class of enzyme has a catalytic C residue that forms an intermediate complex with ubiquitin prior to its transfer to substrates, which can allow HECT E3 ligases to override the preference of the E2 conjugating enzyme for generating specific ubiquitin linkages (Huibregtse et al. 1995). The first HECT E3 ligase identified was E6-Associated protein (E6AP) through its interactions with the human papillomavirus E6 oncoprotein

(Scheffner et al. 1990). Human papillomavirus E6 interacts with E6-AP and stimulates its ability to target p53, and other cellular proteins for proteasomal degradation (Scheffner et al. 1990). There are at least 28 HECT E3 ubiquitin ligases encoded for by the human genome, which consist of two structural lobes, the C-terminal lobe and the N-terminal lobe, linked together by a short flexible linker. The HECT domain is located in the C-terminal region of the E3 ligase which contains the active site C residue. HECT E3 ligases exhibit a variation in their N-terminal structural composition and accordingly are divided into NEDD4 (9 members incorporate N-terminal C2 motif and two-four WW domain), HERC (6 members, each contain regulator of chromatin condensation 1 (RCC1) and the heterogeneous subfamily (13 members, no homologous regions) (**Fig. 1.6**; Li et al. 2008, Lorenz 2018, Singh and Sivaraman 2020).

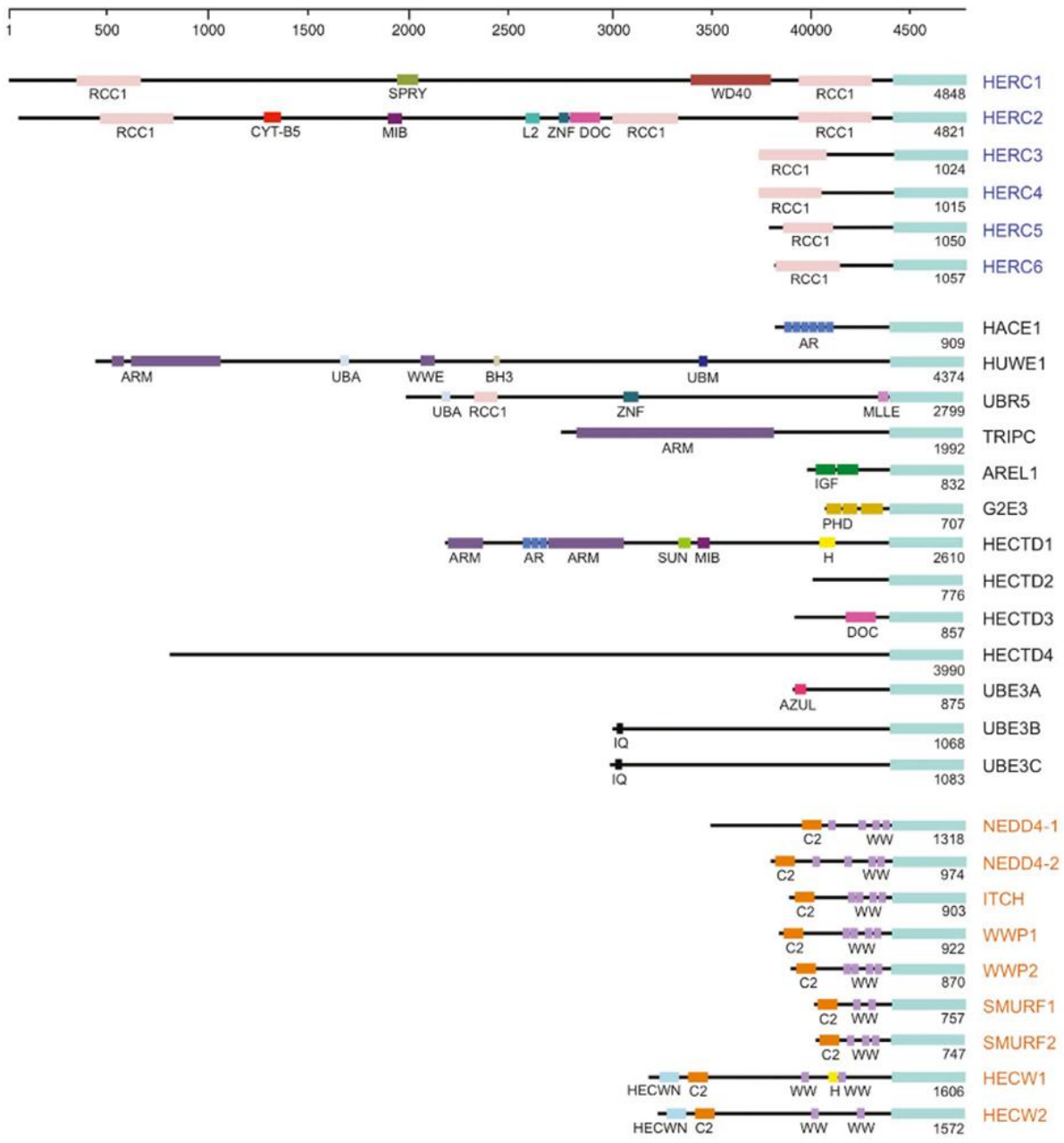

Figure 1.6: HECT E3 ligases subfamilies structural composition. Overview of the HECT E3 ligase domain showing structural domain features of the different subfamilies of the HECT E3 ligases. HERC subfamily member is shown in the top section, NEDD4 subfamily members in the bottom section, and heterogeneous members shown in the middle section. Image taken from Lorenz (2018).

1.2.3.2 RING-Between-RING E3 ubiquitin ligases

RING-Between-RING (RBR) E3 ubiquitin ligases were first identified based on their sequence similarity to two predicted RING domains linked through an in-between RING (IBR) domain (Moynihan et al. 1999, Shimura et al. 2000, Zhang et al. 2000, Wenzel et al. 2011). This family was initially thought to be a subclass of RING E3 ubiquitin ligases, however, the RBR E3 ligase was found to be fundamentally different from the canonical RING E3 ligases. Akin to RING E3 ubiquitin ligases, RBR E3 ligases recruit, and interact with, ubiquitin loaded-E2 conjugating enzymes via RING1. However, RING2 is found to contain an active C residue, which forms an activated ubiquitin intermediate, similar to HECT E3 ubiquitin ligases (Wenzel et al. 2011). As such, RBR E3 ligases adopt a RING/HECT hybrid mechanism to allow for ubiquitin transfer to the substrate. The first RBR members identified were Parkin and HHAR1, and the hybrid mechanism has also been confirmed for HOIP, HOIL-1L, TRIAD1, and RNF144A (**Fig. 1.7**; Smit et al. 2012, Stieglitz et al. 2012, Kelsall et al. 2013, Ho et al. 2014).

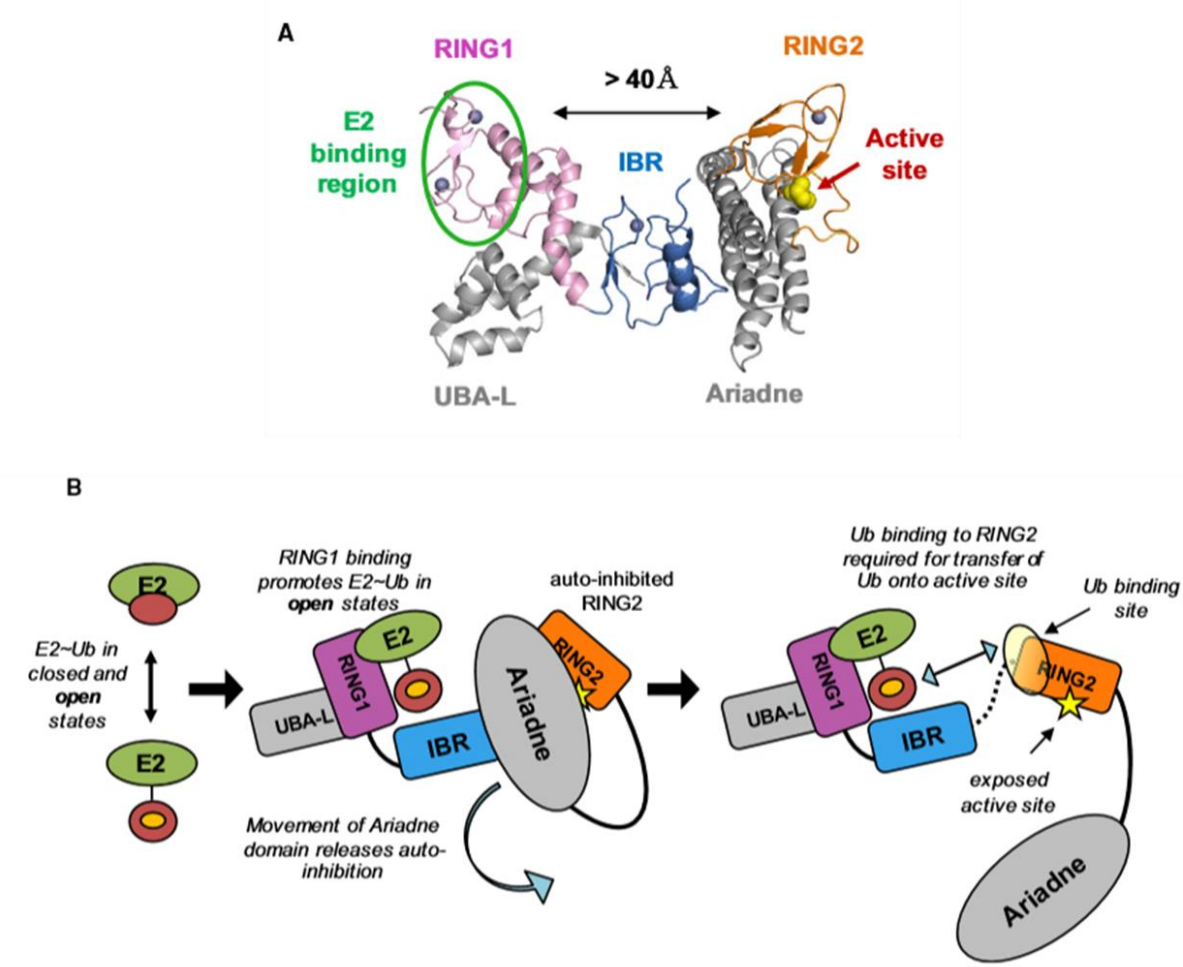

Figure 1.7: RBR E3 ligase structural domains and mechanism of ubiquitin transfer. (A) cartoon representation of RBR E3 ligases structural domains, RING1 in pink, RING2 in orange, E2 binding site in green oval, IBR connect the RING1 and RING2 and the Ariadne domain in grey that possesses the active site C residue in yellow. (B) a schematic representation of the mechanism of ubiquitin transfer by RBR E3 ligases using HHARI as an example. Images taken from Dove, Stieglitz et al. 2016.

1.2.3.3 RING E3 ubiquitin ligases

The domain that was finally characterized as a RING E3 ligase was initially identified as a C-rich sequence common amongst a number of proteins, including Ring1- hence the name adopted for its description; it was originally postulated that this domain might bind zinc and possess biological activity (Freemont et al. 1991). Structural studies revealed that conserved C and H residues (with C3HC4 architecture) within these domains chelated two zinc atoms to allow for the formation of a Zn-finger, which was shown to be functional and possess transactivation capacity (Barlow et al. 1994,

Borden et al. 1995). To date more than 600 RING-containing proteins have been identified. The first explicit demonstration that RING-domain containing proteins might possess E3 ubiquitin ligase activity was established in yeast for the known RING-containing protein, radiation sensitivity protein 18 (Rad18), which formed a heterodimer with Rad6 (its cognate E2-conjugating enzyme) to ubiquitylate histone H2B *in vitro* (Bailly et al. 1997). There exists a second class of RING ligases- the U-box family of RING E3 ligases, which adopt a similar structure to Zn-finger RING ligases, but they do not coordinate Zinc ions (**Fig.1.8**; Koegl et al. 1999, Hatakeyama et al. 2001).

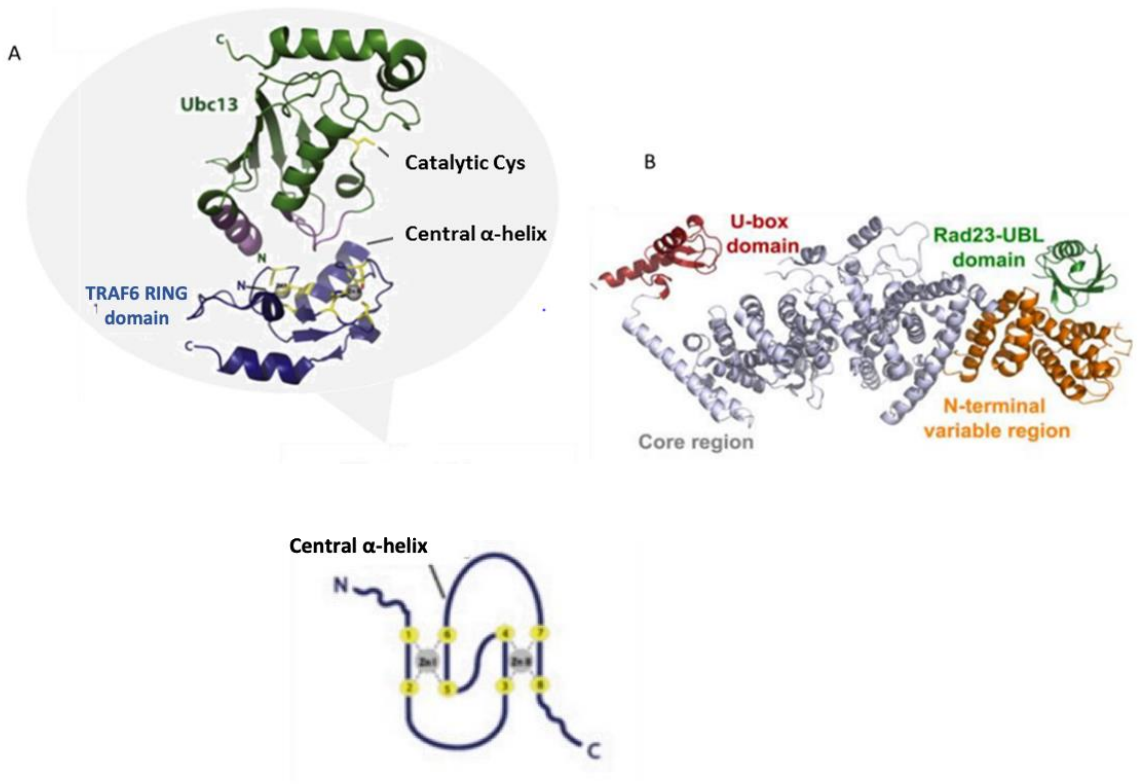

Figure 1.8: Structural domains of RING E3 and U-box RING E3 ligases. (A) Schematic representation of a RING E3 ligase (TRAF6 as an example) structural domains: RING domain in blue, the interacting region in purple, linked to E2 in green, and the catalytic C in yellow. It also shows the coordination of Zn2 + forming the RING structure; (B) Ribbon representation of the structure of the U box E3 ligase (UFD2) bound to (Rad23-UBL) in green. The core region is shown in grey, the N-terminal region in orange and the U-box domain in red. Images taken from Hänzelmann, Stingele et al. 2010 and Metzger, Pruneda et al. 2014.

RING E3 ligases are non-conjugating enzymes, which means they function by bringing both substrate and the ubiquitin-bound E2-conjugating enzyme into close proximity with its catalytic core. It has been suggested that the RING domain facilitates structural changes in the ubiquitin-bound E2, such that it positions ubiquitin in a 'closed' conformation which facilitates its transfer to the substrate through an oxyanion intermediate that is coordinated transiently at the active site of the E2 by an N residue. As such, the E3 ligase facilitates the hydrolysis of both thioester and oxyester ubiquitin species to allow for transfer of ubiquitin and the formation of an amide bond between ubiquitin and the K acceptor in the substrate (Holliday et al. 2007). RING E3 ligases typically adopt homodimer, or heterodimer configurations, or are components of multi-subunit platforms (Lorick et al. 1999). However, the RING domain alone is able to catalyse the transfer of ubiquitin from the E2 conjugating enzyme to the substrate (Lorick, et al. 1999). The human genome encodes two multi-subunit RING E3 ligases which are the SCF (Skp1/cullin/F-box protein) and the Anaphase-Promoting Complex/Cyclosome (APC/C; Sivakumar and Gorbsky 2015, Nakayama et al. 2000).

1.3 Ubiquitin

Ubiquitin is a small polypeptide protein, 76 amino acids in length and a molecular weight of 8.5 kDa. It was initially identified in rabbit reticulocyte extracts and investigated for its role in ATP-dependent protein conjugation (Hershko et al. 1984). Ubiquitin exists in all eukaryotes and some prokaryotes and is involved in a wide variety of cellular processes (Wolf et al. 1993; Hochstrasser 1996). In humans, ubiquitin is encoded by four genes which are UBC, UBB, UBA52 and UBA80, which are first transcribed as either ribosomal protein fusions (UBA80 and UBA52) or as linear ubiquitin chains (UBC and UBB; Wiborg et al. 1985, Ozkaynak et al. 1987).

Ubiquitin has been found to exist, as both monomers and polymers, either unbound and ‘free’, or covalently bound to cellular proteins, in which ubiquitin forms covalent isopeptide linkages with its target (Chau et al. 1989, Hochstrasser 1996).

The diverse functions attributed to ubiquitin reside in its ability to regulate the function of other proteins by tagging them with single or multiple ubiquitin proteins on specific residues, in a specific conformation (Haas et al. 1982, Pines 1994, Hochstrasser 1996). The best known role for ubiquitin is its ability to promote, through conjugation with cellular proteins, their proteasomal-mediated degradation. Such examples include cyclins, the p53 transcription factor and tumour suppressor, and myc and fos proto-oncogene products that also serve as transcription factors and coordinate to regulate cell growth and cell death pathways (Scheffner et al. 1990, Ciechanover et al. 1991, Glotzer et al. 1991). However, proteasomal degradation is not the only biological outcome of ubiquitin conjugation indicating that specific polyubiquitin topologies dictate protein fate. For example, ubiquitin conjugation to nuclear histones (H2A and H2B) modulates transcription (Mayer, Arnold et al. 1991), whilst ubiquitin conjugation to substrate proteins can also regulate DNA repair, mitochondrial integrity and autophagy (Ordureau et al. 2014), cell surface protein trafficking, post-Golgi protein trafficking and lysosomal function among others (Yuan et al. 2014).

Ubiquitin binding proteins (UBPs) normally contain an independent domain consisting of 20-150 amino acids by which these proteins interact with mono-or poly ubiquitin chains. These structural domains known as Ubiquitin-binding domains (UBDs) are usually found in deubiquitylating enzymes (DUBs) that cleaves the ubiquitin chain from ubiquitylated proteins, in E3 enzymes and/or in ubiquitin acceptor proteins (Hicke et

al. 2005). UBDs were first identified in the proteasomal subunit protein, S5A/RPN10. A short sequence of basic amino acids in S5A was found to be required for ubiquitin binding, which was subsequently called a ubiquitin interacting motif (UIM; Young et al. 1998). As such, sequence homology searches for UIMs, identified functional UIMs in several different proteins. In addition, another ubiquitin-binding motif, the ubiquitin-associated domain (UBA) was also identified by bioinformatic analysis in a number of proteins later shown to be involved in ubiquitylation/deubiquitylation processes (Hofmann 1996). Following the discovery of UIMs and UBAs, many other ubiquitin binding motifs were identified, such as CUE (coupling of ubiquitin conjugation to endoplasmic reticulum degradation), GAT (Gga and TOM1) and PAZ (polyubiquitin associated ZINC finger), NZF (Npl4 zinc finger) motif, and finally the UEV (Ubiquitin-conjugating enzyme variant). Interestingly, UBDs are found in many proteins with distinct functions yet, all are required for the interaction with both mono- or poly ubiquitin chains (**Fig. 1.9**; Hook et al. 2002, Meyer et al. 2002, Pornillos et al. 2002, Donaldson et al. 2003, Shiba et al. 2004).

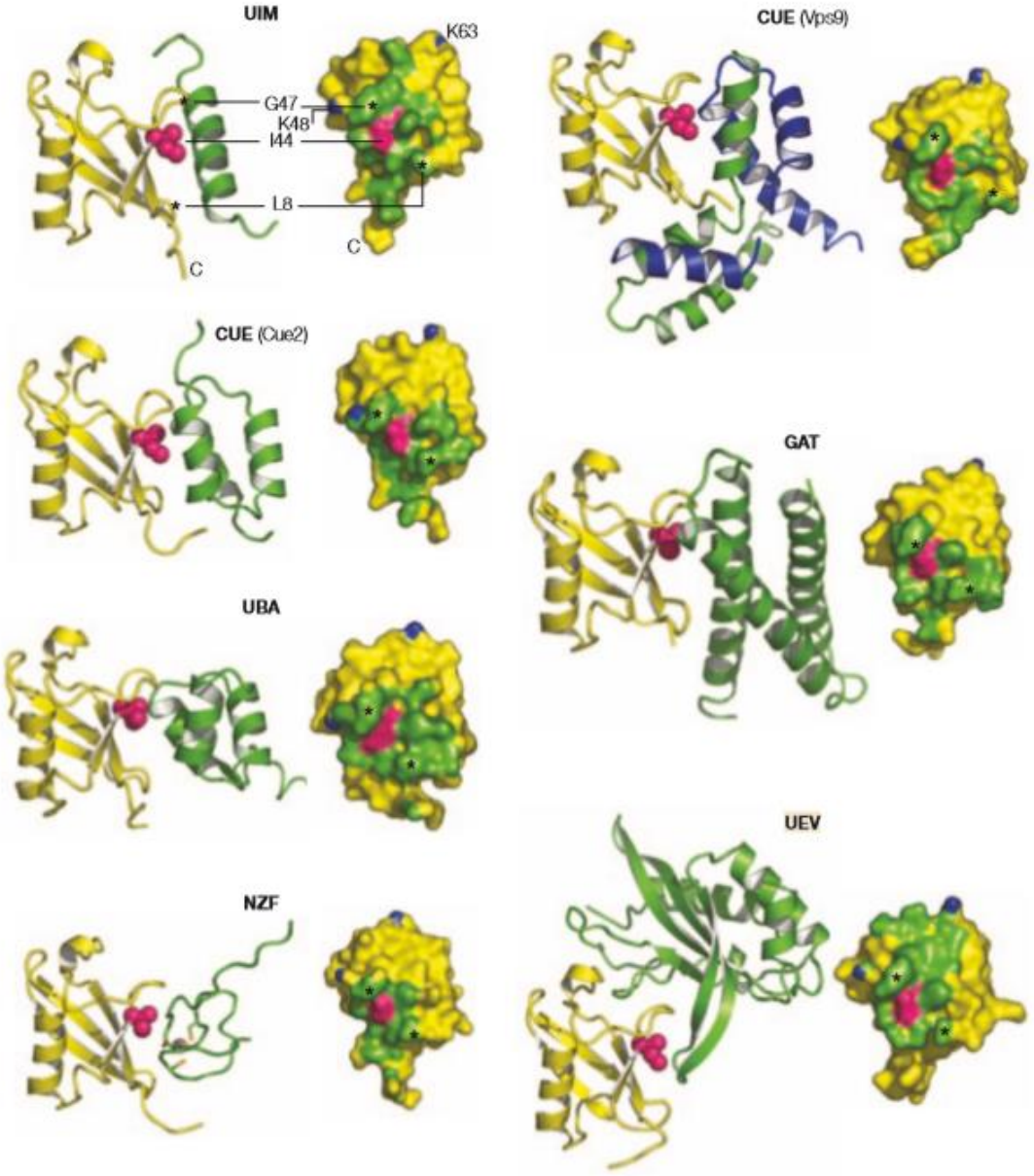

Figure 1.9: Ribbon structures of UBDs and ubiquitin in association. X-Ray crystallography or NMR spectroscopy for different UBDs showing their structure and localization of each complex. Ubiquitin is shown in yellow, UBD in green (green and blue for CUE). Ubiquitin residue, Ile144 important for non-covalent association is shown in red. Image taken from Hicke, Schubert et al. 2005**.**

Ubiquitin possesses a number of structural characteristics allowing for its diversity in protein recognition. It is a highly stable protein that possesses a compact β-grasp fold with a flexible C-terminal tail (see **Fig. 1.9**). The β1/β2 loop that encompasses Leu8 of ubiquitin provides the needed flexibility for protein recognition (Vijay-Kumar et al. 1987) The hydrophobic surface of ubiquitin consisting of Ile44, Leu8, Val70 and His68

is required for its role in protein degradation as it is recognised by proteasomes and most UBDs (Dikic et al. 2009) (**Fig. 1.10** a). The Ile36 patch that also encompasses Leu71 and Leu73 is important in regulating ubiquitin conjugation to substrates as it is recognised by HECT E3s (Kamadurai et al. 2009) DUBs (Hu, Li et al. 2002) and UBDs (Reyes-Turcu et al. 2006). Moreover, the Phe4 patch containing Gln2, Phe4, and Thr12 has been shown to be important for protein trafficking and yeast cell division (Sloper-Mould et al. 2001) and also binds to Ubiquitin-specific protease (USP) domains of UBDs (Rahighi et al. 2009). An important molecular feature that facilitates polyubiquitin chain assembly on substrates is the TEK box, which is a region on the surface of ubiquitin that serves to nucleate substrates, E3 ligase to ubiquitin and allow the formation of K11-linked chains on substrates (Jin et al. 2008). Together, these features help UBD-containing proteins to recognise the ubiquitin chain to achieve signal specificity.

Proteins can be ubiquitylated on one or more lysine residues with a single ubiquitin protein (i.e. mono- or multi- monoubiquitin). However, probably the most important factor that determines ubiquitin functional diversity is its inherent ability to form discrete polyubiquitin chains of different lengths with distinct ubiquitin linkages that form different conformations and overall topologies. As such, ubiquitin possesses seven distinct lysine residues within its primary sequence, which all can form different ubiquitin linkages. Ubiquitin proteins can be ligated to one another via its internal K6, K11, K27, K29, K33, K48 and K63 residues or through its N-terminal M residue (M1) (Komander and Rape, 2012). Polyubiquitin chains can be homotypic, i.e. polyubiquitin chains possessing one type of ubiquitin linkage, or can be heterotypic and contain mixed chain-linkages within the same ubiquitin polymer that often generates branching

of polyubiquitin chains. Another level of complexity is that a single ubiquitin protein can be ubiquitylated on two or more residues at once, which provides a multitude of possibilities in which to assemble different ubiquitin linkages that ultimately determines the function of the ubiquitin-conjugated protein (**Fig.1.10**; Meyer and Rape, 2014).

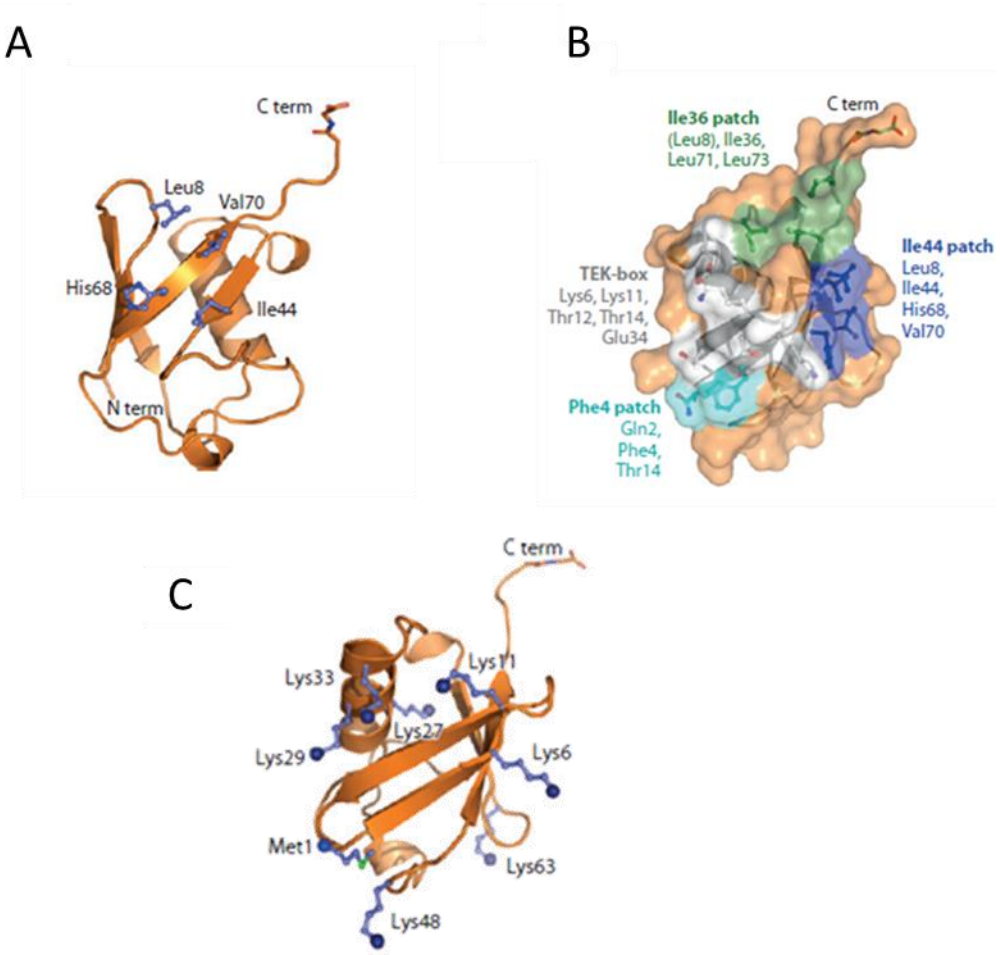

Figure 1.10: Ubiquitin structural features. (A) ubiquitin structure indicting N and C terminal residues as well as the Ile44 patch. (B) The ubiquitin surface patches are shown: Ile36 (green), Ile44 (blue) and TEK box (white). (C) Structure of ubiquitin indicating the seven lysines residues and N-terminal methionine upon which ubiquitin linkages are formed. Image taken from Komander and Rape, 2012.

1.3.1 **Ubiquitin linkages**

Ubiquitin linkages, i.e. the covalent attachment of one ubiquitin protein to another were first discovered in mechanistic studies determining the role of ubiquitin in proteasomal degradation (reviewed by Pickart 2004). Early studies concluded that polyubiquitin chains possessing K48 ubiquitin linkages on protein substrates targeted them for

proteasomal degradation, such that polyubiquitin chains with K48 linkages were a proteasome delivery signal (Finley et al. 1994). More recently, polyubiquitin chains with K63 linkages were found to have non-proteolytic roles in DNA repair (Liu et al. 2018). Such studies provided evidence to indicate that structurally distinct linkages lead to different functional signals. To date studies using X-ray crystallography, nuclear magnetic resonance (NMR) spectroscopy and small angle X-ray scattering (SAXS), have identified and structurally-characterized five distinct ubiquitin linkages with distinct structures. These linkages were classified as having either compact or open conformations. K6, K11 and K48 linkages where found to form intramolecular interfaces, such that they were more compact in nature, whereas K63 and Met1 linkages formed a more open and extended conformation (**Fig. 1.11**; Hospenthal et al, 2013; Datta et al. 2009; Komander et al. 2012).

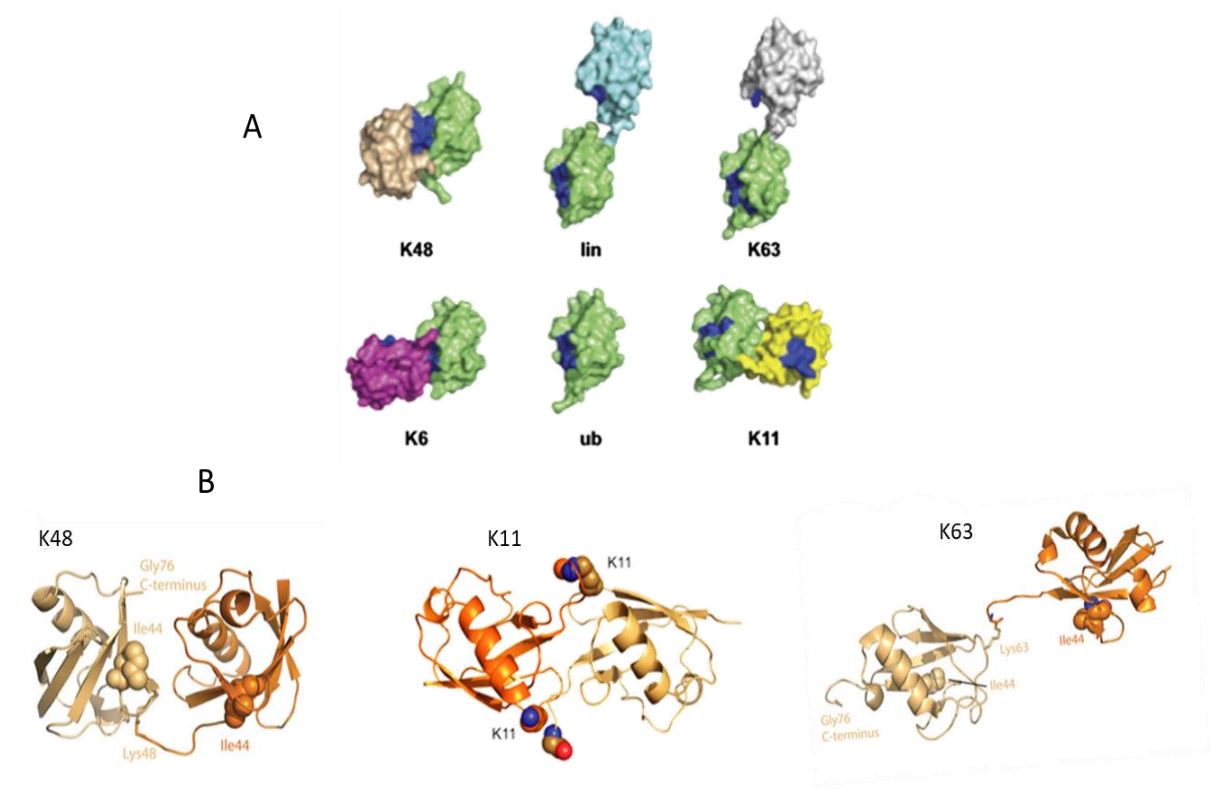

Figure 1.11: Structure of diubiquitin linkages. (A) Surface representation of mono and di-ubiquitin showing the structure of K48, Met1, K63, K6 and K11 diubiquitin species. (B) Ribbon structure representation of the K48, K63 and K11 di-ubiquitin structures showing the first ubiquitin in light orange, the distal ubiquitin in dark orange and the Ile144 surface as spheres. Taken from Matsumoto et al. 2010, Hurley and Stenmark 2011, Clague, Barsukov et al. 2013.

1.3.2 **Classic linkages**

1.3.2.1 K48 linkages

K48 is the most abundant ubiquitin linkage found in cells (Elsasser, et al. 2004). It is well established that K48 linkages are the major signal for proteasomal degradation as mass spectrometry identifies the rapid accumulation of K48 linkages following proteasomal inhibition (Xu et al. 2009; Chau, et al. 1989). The proteolytic role of K48 ubiquitin linkages has been extensively studied particularly in relation to the Anaphase-Promoting Complex/Cyclosome (Rodrigo-Brenni et al. 2010; see section 1.4 for more detail). Polyubiquitin chains with K48 linkages are targeted for proteasomal degradation as the 19S regulatory complex, possesses two subunits,

Rpn10 and Rpn13 that bind selectively to polyubiquitin chains with K48 linkages. Mutation of specific residues in these receptors decreases the affinity of the proteasome for polyubiquitin chains with K48 linkages by upto four-fold.

Interestingly, other studies have also identified a novel non-proteolytic role for K48 linkages. An example is the role of K48 in the regulation of transcription factor, Met4 in *Saccharomyces cerevisiae*. Met4 activity is highly sensitive to the level of methionine in cells, such that the repletion of methionine promotes Met4 polyubiqutylation with K48 ubiquitin linkages and the inhibition of Met4 transcriptional activity (Kaiser, et al. 2000); Met4 possesses a UBD that limits the chain length below the threshold required for proteasome recognition such that it is not targeted for protein degradation (Flick, et al. 2006). Another non-proteolytic role for K48 ubiquitin linkages is the activation of the ubiquitin-dependent p97 segregase (also known as valosin-containing protein, VCP), a member of the ATPase family. p97 serves to interact with substrates with polyubiquitin K48 linkages and extract them from larger protein complexes. For example, p97 promotes the release of the yeast membrane-bound transcription factor, Spt23, which ultimately allows for deubiquitylation and stabilisation of the substrates (Rape et al. 2001). Other studies have also shown that the p97-Ufd1-Np14 complex serves to recognise K48 linkages on Aurora B kinase and extract Aurora B from chromatin during mitosis to allow for chromosome decondensation (Ramadan et al. 2007).

1.3.2.2 K63 linkages

K63 is the second most abundant polyubiquitin linkage in cells and it has been found to function in multiple cellular processes. K63 was first described as an important

modification in yeast plasma membrane transporters, particularly uracil permease (Chen and Sun, 2009). Since then, K63 linkages have been found in different plasma membrane proteins from yeast to mammals, such as the TNF Receptor 1 (TNF-R1; Fritsch et al. 2014), LDL receptors (Zhang et al. 2013), Prolactin receptor (Varghese, et al. 2008) and Interferon receptor, IFNAR1 (Kumar et al. 2004) for sorting into the endosomal multivesicular body pathway (Lauwers et al. 2009). K63 linkages are also known to play non-proteolytic roles in the DDR. For instance, E3 ubiquitin ligase RNF8 and RNF168 assemble K63 ubiquitin linkages on core histones and the recruitment of various repair factors to chromatin (Liu et al. 2018). K63 linkages are also important for its role in protein synthesis, and it is required for proper translational functions, such that ablation of K63 linkage formation promotes hypersensitivity of cells to translational inhibitors through their effect on the rate of protein synthesis (Spence et al. 2000). K63 ubiquitin linkages are also important in many other non-proteolytic processes such as regulating mitochondrial integrity (Sugiura et al. 2013), cell motility (Didier et al. 2003), and the cell's inflammatory response (Sun and Chen 2004).

K63 ubiquitin linkages are also important in the regulation of autophagy, a cellular process that eliminates damaged organelles which are too large to be handled by cellular proteases such as the proteasome. p62/sequestosome-1 is a member of Ubi/UBA family that possess both a ubiquitin-binding domain (UBA) and ubiquitin-like fold (Ubi). These family members recognise ubiquitylated proteins through their UBA domain. It has been shown that p62 serves as an autophagy receptor for cargo decorated with polyubiquitin chains possessing K63 linkages that have been assembled by E3 ligases such as Parkin. Once recognised by p62, polyubiquitylated substrates are cleared by phagosomes (Torrecilla et al. 2017)

1.3.3 **Atypical linkages**

The revolution in the generation and commercialisation of ubiquitin discovery tools has helped increase our understanding of the function of the less studied, atypical ubiquitin linkages. Atypical ubiquitin linkages include K6, K11, K27, K29, K27, K33 and the N-terminal, M1. Amongst these K11 and Met1 are perhaps the mostly widely studied.

1.3.3.1 K11 linkages

The best known role for K11 ubiquitin linkages is proteasomal degradation and, it is a linkage used particularly by the APC/C E3 ligase to promote substrate degradation (see sections 1.4. and 1.5 for more details). As mentioned previously the APC/C utilises two different E2 conjugating enzymes, UbcH10/Ube2C and Ube2S to assemble K11 ubiquitin linkages on mitotic substrates (Jin et al. 2008). UbcH10-APC/C complexes initiate ubiquitin chain formation on targeted proteins whilst Ube2S-APC/C complexes elongate the polyubiquitin chain. UbcH10 preferentially forms K11 linkages although it can also assemble K48 and K63 linkages (Jin et al. 2008), whilst Ube2S assembles branched, K11 polyubiquitin chains on substrates (Meyer and Rape 2014). Indeed, homotypic K11 linkages are poor substrates for the proteasome, yet branched ubiquitin chains are recognised more efficiently by the 5SA proteasome receptor (Meyer and Rape 2014).

Homotypic K11 linkages have also been suggested to play important roles in the cellular response to hypoxia. However, the exact mechanism is still not fully understood. K11 linkage-specific DUBs Cezanne (OUTD7B) and Cezanne 2 (OTUD7A) are known to regulate hypoxia factors HIF-1α and HIF-2α, such that knockdown of Cezanne results in the non-proteasomal mediated degradation of HIF-

1α, suggesting a requirement for autophagy (Bremm et al. 2010). Cezanne also regulates the expression of HIF-2α by the transcription factor E2F1. (Moniz, Bandarra et al. 2015) and also regulates NF-kB signalling (Hu et al. 2013), T-cell activation (Hu et al. 2016) EGF receptor function (Pareja, et al. 2012) though the precise role of K11 homotypic K linkages in these processes is not known.

1.3.3.2 Met1 (M1) linkages

M1 ubiquitin linkages generate linear polyubiquitin chains that are important in inflammatory and immune responses through the activation of the transcription factor, NF-kB. The linear ubiquitin chain assembly complex (LUBAC) is a multi-subunit E3 ligase consisting of HOIP, HOIL-1L and SHARPIN that participates in inflammatory and immune responses through the HOIP-dependent assembly of M1 ubiquitin chains on target proteins (Gerlach et al. 2011; Park, et al. 2016). As such, the Met1 specific domain UBAN (Ubiquitin binding in ABIN and NEMO) in an element of the kB kinase IKK complex, NEMO is a substrate for Met1 linkages and serves to activate IKK to modulate NF-kB transcriptional activity (**Fig. 1.12**; Rahighi et al. 2009).

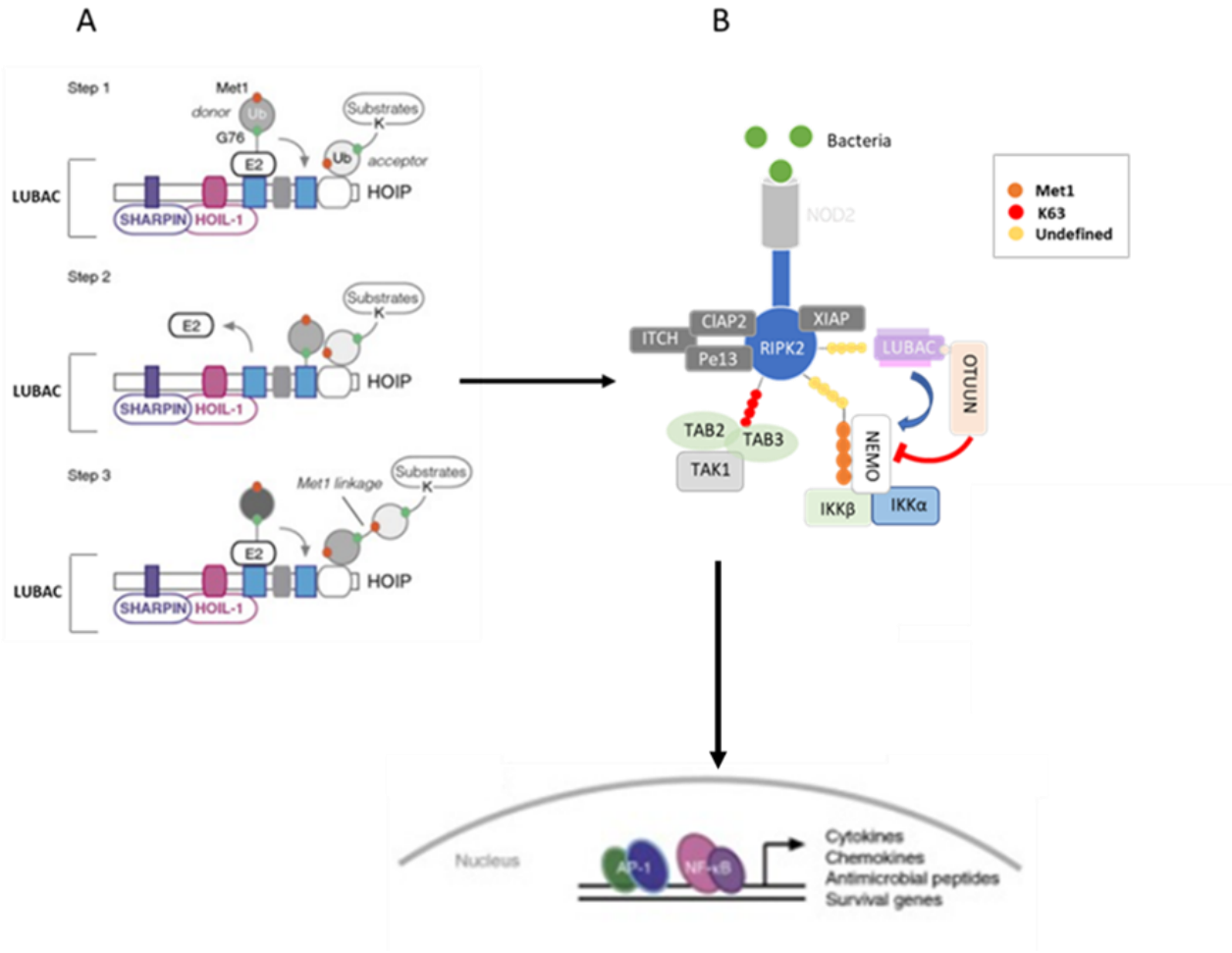

Figure 1.12: Model of Met1 ubiquitylation in immune signalling. (A) Schematic representation of the LUBAC subunits and the formation of Met1 linkages by HOIP, HOIL-1 and SHARPIN. (B) Schematic model for the role of Met1. RIPK2 serves as important adaptor for the association of signalling complex that are targeted for ubiquitylation. The assembly of Met1 polyubiquitin chains is important to activate the NF-kB pathway. Images taken from Fiil and Gyrd-Hansen 2014.

1.3.3.3 K6 linkages

The exact physiological role of K6 ubiquitin linkages is not well understood. Generally, K6 linkages are described as a non-degradative signal, as the overall abundance of these linkages does not correlate positively with proteasomal inhibition (Kim et al. 2011, Wagner et al. 2011). Recent proteomic investigation has linked K6 linkages with two different cellular functions. Firstly, the abundance of K6 and K33 linkages have been shown to be upregulated following UV radiation (Elia et al. 2015). Consistent with a potential role in the DNA damage repair cascade, the heterodimeric E3 ligase,

BRCA1-BARD1, an important regulator in the DDR is known to assemble K6 linkages on substrates (Morris and Solomon 2004). A recent study generated K6- (and K33-) affimers that could recognise specifically these ubiquitin linkages *in vitro* and *in vivo,* greatly improving their ability to study the biology of these linkage types. Using these affimers they were able to demonstrate that RNF144A/B were able to assemble K6-linked chains, in addition to K11- and K48- linked chains *in vitro*, and moreover, they determined that the HECT E3 ligase, HUWE1 was the major E3 for E6-chains and that Mitofusin-2 was a major *in vivo* substrate for HUWE1-targeted K6 ubiquitylation (Michel et al. 2017).

Other studies implicate K6 linkages in mitochondrial homeostasis. In response to mitochondrial depolarization mitochondrial outer membrane proteins are polyubiquitylated by the E3 ligase, Parkin, which assembles predominantly K6 and K11 linkages, and a smaller amount of K48 and K63, on mitochondrial outer membrane proteins. Interestingly, overexpression of K6 and K63 mutants results in delayed mitophagy suggesting a significant role for these linkages in the mitophagy pathway. Moreover, the DUB, USP30 that maintains mitochondrial integrity displays a particular preference for K6 linkages. USP8 similarly disassembles K6 ubiquitin linkages on mitochondrial substrates deposited by Parkin (Bingol et al. 2014, Ordureau et al. 2014 Cunningham, et al. 2015, Liang et al. 2015, Ordureau et al. 2015).

1.3.3.4 K29 linkages

K29 ubiquitin linkages are suggested to modulate the Wnt signalling pathway whose activity is essential in embryogenesis and its dysregulation is important in tumourigenesis, Alzheimer's and cardiovascular disease (Clevers and Nusse 2012). It

is well established that Wnt ligands are a major regulator of β-catenin stability, and that ubiquitylation modulates Wnt signaling at multiple levels. Under basal conditions when Wnt signaling is switched off, the β-Trcp E3 ubiquitin ligase assembles K48 and K63 –linked polyubiquitin chains on phosphorylated β-catenin and targets its degradation. Upon Wnt ligand activation β-catenin is stabilized, whereupon it translocates to the nucleus and promotes the transcription of Wnt target genes (Clevers and Nusse 2012). It has been shown that the HECT E3 ligase, Smurf1 assembles polyubiquitin chains with K29 linkages on axin which serves to disrupt its interaction with the Wnt coreceptors LRP5 and LRP6, to ultimately repress Wnt/β-catenin signalling in a non-proteolytic manner (Fei et al. 2013). Intriguingly, Trabid, a DUB of the OUT family, which is an important regulator of Wnt transcriptional activity displays an increased specificity for K29 and K33 ubiquitin linkages further establishing K29 ubiquitin linkages in the regulation of the Wnt/β-catenin cascade (Kristariyanto et al. 2015).

1.3.3.5 K27 linkages

Recent data suggests that K27 ubiquitin linkages modulate both the DDR and innate immunity. Studying the functional significance of different ubiquitin linkages using selected reaction-monitoring mass spectrometry in DDR has indicated that K27 is a major ubiquitin linkage on chromatin following the activation of the DDR (Gatti, et al. 2015). As such, the RING E3 ligase, RNF168 promotes K27 linkages on histones H2A and H2AX and these K27 linkages serve as scaffolds for the recruitment of important DDR mediators such as 53PB1, Rap80 and RNF169 at sites of DNA damage (Gatti et al. 2015). K27 linkages also modulate the host immune response following microbial DNA invasion, which triggers the activation of both the Interferon regulatory factor 3

(IRF3) and NF-kB signaling pathways and the release of IFN type 1 and pro-inflammatory cytokines. Upon the release of pro-inflammatory cytokines, the E3 ligase complex, AMFR/INSIG1 decorates STING with K27-linked polyubiquitin chains, which serves as a scaffold to recruit the TANK-binding kinase and facilitate its translocation from the ER to a perinuclear compartment (Wang, Liu et al. 2014). Another E3 ligase, HACE1 was found to assemble K27 linkages on Optineurin (OPTN) which in turn facilitates OPTN interaction with p62/SQSTM1 to create a complex that promotes autophagy (**Fig. 1.13**; Liu et al. 2014). Additionally, HACE1 targets the Y-BOX binding protein (YB-1) for K27 ubiquitin linked polyubiquitylation. The ubiquitylation of YB-1 is required for the interaction with TSG101 (Tumour Susceptibility Gene 101), in order to promote its secretion from the cell (Palicharla and Maddika 2015).

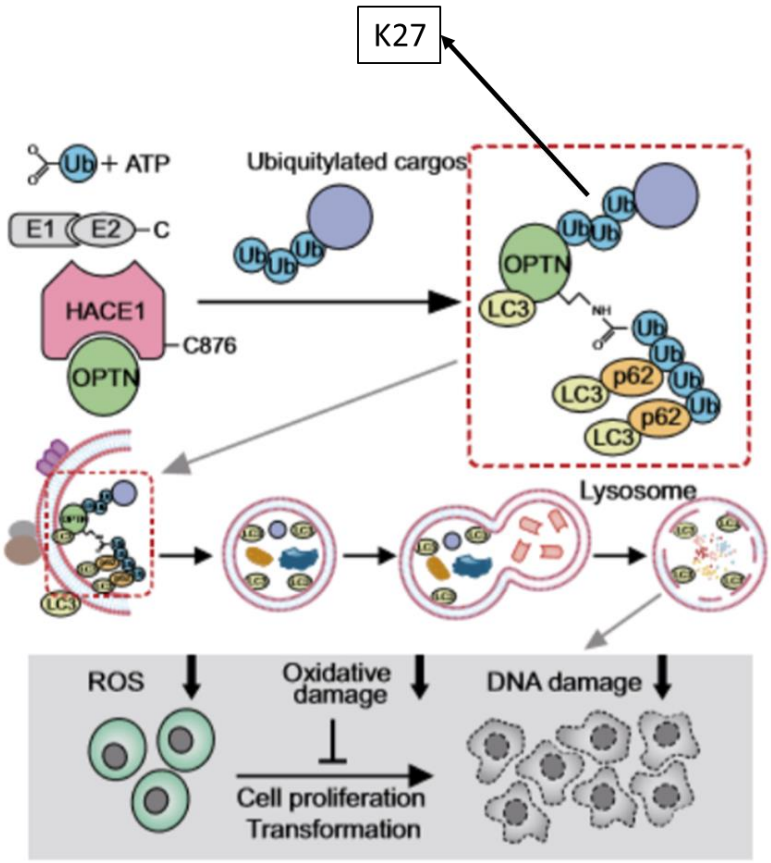

Figure 1.13: K27 assembly facilitates autophagy. Schematic representation of K27 assembly by HACE1 on OPTN which promotes interaction with p26 and accelerates autophagy. Image taken from Liu, Chen et al. 2014.

1.3.3.6 K33 linkages

K33 linkages have been linked to different cellular processes such as the negative regulation of T-cell receptor signalling such that depletion of Cbl-b and Itch E3-ligases, known to decorate substrates with K33-linkages, augments TCR activation. As such, Cbl-b and Itch decorate TCR-zeta with polyubiquitin chains possessing K33-linkages, which ultimately promote TCR-zeta phosphorylation and its association with the protein kinase, Zap-70 (Huang et al. 2010). Recently, the HECT ligase, ARLEE was also shown to assemble K33 ubiquitin linkages on antagonists of inhibitor of apoptosis (IAP) proteins to target them for ubiquitin-mediated proteolysis. Indeed, *in vitro* assays demonstrated that AREL1 assembled polyubiquitin chains with K33 linkages principally on three substrates: SMAC, HtrA2 and ARTS (Michel, et al. 2015). Polyubiquitin chains with K33 linkages are also suggested to have a role in post-Golgi membrane protein trafficking where the BTB domain-containing adapter protein, KLHL20 associates with a cullin-3 E3 ligase complex to tag Coronin 7 (Crn7) with non-degradable K33 ubiquitin linkages, which serve to promote the recruitment of Crn7 to the trans-Golgi network (TGN), for anterograde trafficking (Yuan, et al. 2014).

1.4 The Anaphase-Promoting Complex/Cyclosome (APC/C)

The APC/C was first discovered in *Clam* and *Xenopous oocyte* extracts. In *Clams*, an E3 ligase, termed the Cyclosome, was identified that could target mitotic cyclins A and B for ubiquitin-mediated proteolysis. In *Xenopous oocyte* extracts, an E3 ligase was also found to target cyclin B1 for proteasomal degradation and called the Anaphase-Promoting Complex (Sudakin et al. 1995; King et al. 1995), hence the name, Anaphase-Promoting Complex/Cyclosome or APC/C. Since then, the APC/C has been of major interest for its major role in regulating the cell cycle particularly during mitosis. The function of the APC/C has been strongly linked to metaphase-anaphase

checkpoint control (i.e. Spindle-assembly checkpoint) satisfaction, G1 progression and DNA replication regulation (Holloway et al. 1993).

The APC/C is a cullin-RING E3 ubiquitin ligase that operates as a master regulator of many cellular processes through the spatio-temporal degradation of many cellular proteins. The APC/C assembles, predominantly, K11-linked ubiquitin linkages on its substrates and targets them for proteasomal degradation. The APC/C has been linked to the targeted degradation of more than 100 substrates, most of which are degraded during mitosis and G1 phases, allowing for the fidelity of chromosomal segregation, an orderly mitotic exit and progression through the successive G1 phase. The APC/C's role is not confined to cell cycle progression, however, and has been implicated in other cellular process such as the DDR, metabolism, and post-mitotic functions such as the formation of dendrites in neurons and synaptic function and consequently, learning and memory processes (van Zon et al. 2010, Mocciaro and Rape 2012, Sivakumar and Gorbsky 2015, Brown et al. 2016).

1.4.1 **APC/C structure**

The APC/C is a 1.22 MDa multi-protein complex formed of 14 different protein subunits. The APC/C is divided structurally and functionally into three identifiable domains which are the platform, the TPR lobe and the catalytic core that function as the scaffolding module, the substrate recognition module and the catalytic module, respectively (**Fig. 1.14**; Gieffers et al. 2001, Passmore et al. 2005, Chang et al. 2015). The APC/C adopts a triangular shape with a central cavity, with the back and top of the APC/C being formed by the TPR lobe, whilst the catalytic core of the APC/C occupies a peripheral position within the structure. The catalytic core and TPR lobe

are held together by the platform domain which acts as a scaffolding bridge bringing the TPR lobe and catalytic core together and maintaining the overall structure. The central cavity of the APC/C is where the E2-conjugating enzymes, UbcH10 or Ube2S, APC/C substrates and coactivators are positioned to allow for substrate ubiquitylation (Zhang et al. 2010A, Zhang et al. 2010B, Chang et al. 2014).

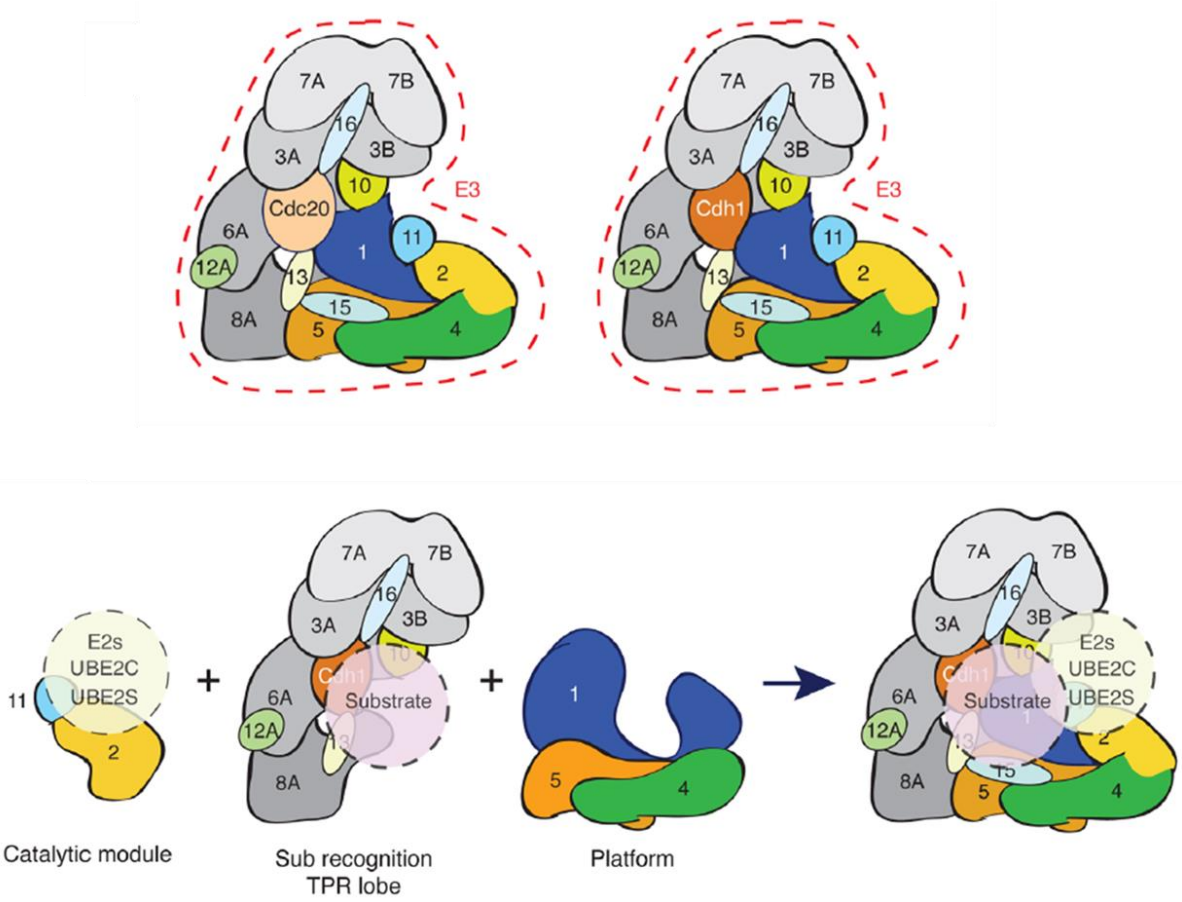

Figure 1.14: Cartoon depiction of APC/C structure. The figure shows relative APC/C structure as described in the text and the relative positions of each subunit and: the catalytic module, the TPR lobe and the platform, which together form the APC/C. Image taken from Yamano 2019.

1.4.2 **The Catalytic core**

The catalytic core is located at the periphery of the APC/C on the right-hand side of the platform and lies close to the opening of the central cavity of APC/C. It comprises of APC2- the cullin subunit, APC11- the RING ligase, and APC10. The catalytic module subunits are key functional subunits highlighted by their high degree of

conservation amongst species. The APC2 and APC11 subunits define the cullin-RING ligase activity of the APC/C - the N-terminal region of APC11 is associated with the central α/β-domain of APC2. These two subunits are also known to possess two highly conformational-flexible domains which are the RING domain of APC11 and the WHB domain of APC2. The conformational flexibility of these domains is important in the catalytic function of APC/C. The WHB domain of APC2 cooperates with the RING domain of APC11 to associate with ubiquitin-bound UbcH10, which upon binding promotes a conformational change in APC2 to position ubiquitin-bound UbcH10 close to the substrate to facilitate ubiquitin transfer. This conformational change in APC2 upon UbcH10 binding is reminiscent of the structural changes that occur in classical Cullin-containing CRLs when their WHB domain is NEDDylated for activation, indicating why APC2 does not possess the homologous K acceptor residue and is not a substrate for NEDDylation. The catalytic core also lies in close proximity to the TPR component, APC10 which participates with APC/C coactivators to form substrate recognition domains. As such, substrates bind to the WD40 domain of Cdc20 or Cdh1 and APC10 in the central cavity of APC/C and their K acceptor residue lies in close proximity to ubiquitin-bound UbcH10 tethered to APC2 to allow for substrate ubiquitylation (Zachariae et al. 1998, Burton and Solomon 2001, Kraft et al. 2005, Brown et al. 2015, Alfieri et al. 2017).

1.4.3 **The TPR lobe**

The TPR (Tetratricopeptide-repeat) lobe is the predominant structural feature of the APC/C. The TPR lobe is composed of seven large scaffolding proteins which are APC3, APC6, APC7, APC8, APC12, APC13 and APC16. The four, structurally-related, TPR-containing proteins are APC3, APC6, APC7 and APC8 which all form

homodimers in the APC/C and undergo significant PTMs, mediate numerous protein-protein interactions and interact functionally with the catalytic core. APC3, APC6 and APC8 were initially identified as being important to APC/C function in yeast whereby the mutation of any of these subunits resulted in a terminal G2/M arrest. Structural studies of the TPR domain-containing subunits show that the N-terminal region of these subunits is important for homodimer interactions whilst the C-terminal TPR domains allow for protein-protein interactions and interaction with other subunits, and more importantly the substrates and coactivators. As such, the TPR lobe serves as a regulatory centre in which cell cycle-dependent PTMs of the TPR proteins modulates the whole APC/C structure, and hence, APC/C catalytic activity (Hirano et al. 1990, Sikorski et al. 1990, Vodermaier et al. 2003, Wang et al. 2009, Zhang et al. 2010B, Zhang, et al. 2013). The stability of the four TPR subunits is important for the whole function of APC/C, thus TPR-accessory subunits such as APC12, APC13 and APC16 which lack the TPR protein-protein interaction motif function to stabilise the TPR lobe (Passmore et al. 2003, Schwickart et al. 2004, Kops et al. 2015, Kataria and Yamano 2019). Indeed, it has been proposed that APC13 mediates the stability of APC3 and APC6 within the APC/C holoenzyme, whilst APC12 associates with, and stabilises, APC6 (Wang et al. 2009, Torres et al. 2010). Additionally, APC16 associates with APC3 and plays an important role in the recruitment of APC7 to the APC/C complex (Yamaguchi et al. 2016).

1.4.4 **The platform**

The platform of the APC/C forms the base of the whole structure and consists of APC1, APC4, APC5 and APC15. In addition to the structural role of the platform domain in keeping the catalytic core and TPR lobe linked, the platform subunits also serve as a

regulatory centre for the APC/C and is subjected to cell cycle specific PTMs that modulate APC/C activity. Moreover, structural features such as the WD40 β-propeller domain of APC1 play an important role in the conformational changes that occur within the APC/Cs structure upon association with its coactivators. Indeed, APC1 is the largest APC/C subunit, and possesses a distinct motif that is also shared by the Rpn1 and Rpn2 subunits of the proteasome with exact order and number. This 40 amino acid motif is called the PC-repeat (proteasome-cyclosome repeat) and was found to be important in forming the interface of APC/C subunits. Rothmund-Thomson syndrome (RTS) Type-1, which is characterized by a number of clinical features such as poikiloderma, sparse hair and nail abnormalities, as well as bilateral juvenile cataracts is caused by either homozygous mutations in APC1 or mono-allelic mutation of APC1 and another distinct accompanying mutation (Ajeawung et al, 2019).

APC4 is comprised of a WD40 domain that is split by a helical bundle domain and serves to maintain structural interactions with APC5 (Cronin et al., 2015). APC4 is subject to PTMs but how this modulates overall APC/C structure is not known, although APC4 SUMOylation at amino acids 772 and 798 is known to recruit Kinesin-like protein KIF18B to the APC/C for ubiquitylation (Eifler et al. 2018). APC5 occupies a central region within the platform domain and forms interactions with many other APC/C subunits, including APC1, APC4, APC15 and APC8. Work from our laboratory and others indicate that APC5 is a substrate for PTM though the functional significance of this is not known (Maria Tilotta, PhD thesis, The University of Birmingham, 2019). APC15 also provides structural integrity for APC5 and performs an important function in negatively regulating the SAC to facilitate Cdc20 autoubiquitylation (Mansfeld et al. 2011, He et al. 2012, Cronin et al. 2015, Zhang et al. 2016, Kataria and Yamano 2019).

1.4.5 **Regulation of APC/C activity**

1.4.5.1 APC/C coactivators

The intrinsic E3 ligase activity of the APC/C is stimulated via its temporally-coordinated association with one of two, closely-related coactivators, Cell division-cycle protein 20 (Cdc20) or Cdc20 homologue 1 (Cdh1). These two coactivators enhance the enzymatic activity of APC/C by facilitating the recognition of substrates and increasing the affinity of the APC/C for its E2-conjugating enzyme, UbcH10. Both Cdc20 and Cdh1 recognise the APC/C via their C-terminal IR tails and N-terminal C-boxes which interact with APC3 and APC8, respectively. Upon binding to the APC/C, Cdc20 and Cdh1 facilitate the recruitment of APC/C substrates through their C-terminal WD40 β-propeller domains which interact with degron sequences within APC/C substrates and together with APC10 form a recognition target motif, termed the 'degron receptor' (**Fig. 1.15**; Peters 1998, Schwab et al. 2001, Kraft et al. 2005, Matyskiela and Morgan 2009).

Cdc20 associates with, and activates, the APC/C from NEBD to anaphase-onset, whilst Cdh1 associates with, and activates, the APC/C from anaphase-onset until the APC/C is inactivated at the end of G1. Indeed, despite the high similarities between Cdc20 and Cdh1 both proteins show differential selectivity and specificity for APC/C substrates. As such, APC/C-Cdh1 complexes possess higher affinities for APC/C substrates and can promote the degradation of all mitotic substrates, yet regulatory mechanisms exist to ensure that the APC/C-Cdh1 is selective and promotes the timely degradation of substrates, which is important for an ordered mitotic exit (Pines 2011, Davey and Morgan 2016).

Upon mitotic entry the APC/C subunit, APC3 is phosphorylated on multiple residues by Cdk1, which subsequently facilitates APC1 phosphorylation by Cdk1. APC1 phosphorylation causes a conformational change within APC1 such that an autoinhibitory helix that, in the inactivated state, occupies the activator-binding site on APC8 is displaced. This conformational change ultimately favours the binding of Cdc20 to the APC/C allowing for APC/C activation. Conversely, phosphorylation of the activator Cdh1 at this time by Cdk1 inhibits its association with the APC/C (reviewed by Sivakumar and Gorbsky 2015). APC/C-Cdc20 complexes promote metaphase-to-anaphase transition by targeting Securin and Cyclin B1 for ubiquitin-mediated proteolysis. Securin normally functions to inhibit Separase activity towards the Scc1 Cohesin subunit, which serves to hold sister chromatid together following DNA replication. Once all chromosomes are aligned on the metaphase plate, APC/C-Cdc20 targets Securin for degradation which allows for Separase activation, Cohesin cleavage and anaphase onset, characterized by the commencement of chromosome segregation (Clute and Pines 1999, Zur and Brandeis 2001, Hagting et al. 2002, Foe et al. 2011, Gavet and Pines 2010, Alfieri et al. 2017). The APC/C-Cdc20 mediated degradation of Cyclin B1 at anaphase-onset ensures that unphosphorylated Cdh1 can associate with the APC/C and promote the degradation of a new cohort of substrates, such as Cdc20, which, ultimately allows for mitotic exit and progression into and through G1.

The APC/C-Cdh1 complex ensures proper mitotic exit by targeting mitotic kinases such as Polo-like kinase 1 (Plk1), Aurora A and Aurora B for degradation, whilst its ability to target Cdc20 and UbcH10 for degradation prevents uncoordinated re-entry into mitosis. APC/C-Cdh1 also targets Geminin for degradation during G1, allowing for

the formation of new pre-replication complexes and ensuring that re-replication does not occur and that DNA replication only occurs once per cell cycle. In addition, the APC/C-Cdh1 complex also targets S-phase kinase associated kinase 2 (Skp2) for degradation during G1, which allows for the accumulation of proteins required for S phase entry (**Fig. 1.15**; McGarry and Kirschner 1998, , Alfieri, et al. 2017, Kataria and Yamano 2019, Diffley 2004, Wirth, et al. 2004).

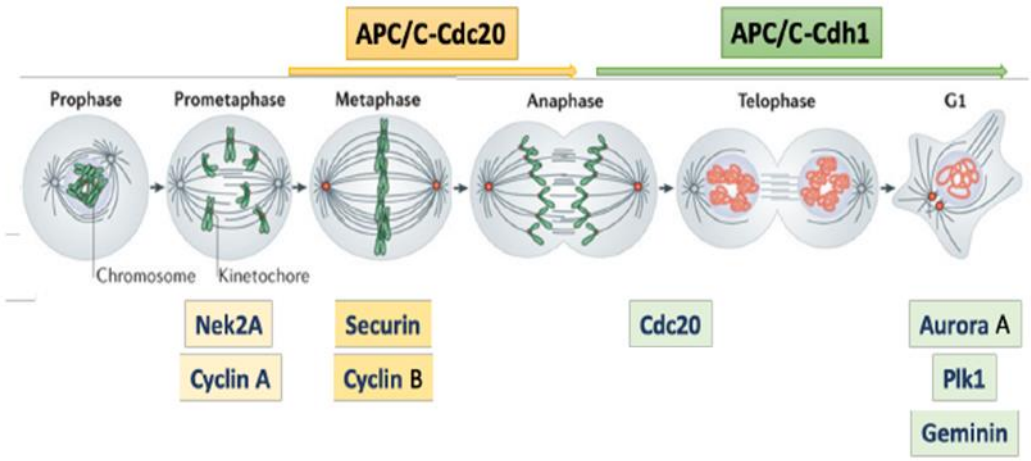

Figure 1.15: Sequential activation of the APC/C by Cdc20 and Cdh1. APC/C binds to its coactivators in a cell cycle-dependent manner and facilitates the timely degradation of APC/C substrates. Image taken from Sivakumar and Gorbsky (2015).

1.4.5.2 APC/C substrate recognition

As the APC/C governs the degradation of many different substrates it is crucial that these substrates are recognised with high specificity. In contrast to many ubiquitin ligases, the APC/C employs a unique method to recognise unmodified substrates at distinct times in the cell cycle. The APC/C recruits substrates predominantly through their interaction with the C-terminal WD40 domain of, one of its coactivators, Cdc20 or Cdh1, alone or in combination with APC10. The WD40 domain possesses surface-exposed binding pockets that recognise short amino acids motifs in substrates termed degrons (Schwab et al. 1997, Visintin et al. 1997, Fang et al. 1998). APC/C classical

degrons are the: D-box typified by the consensus sequence, RXXLXXI/VXN; KEN box characterized by the sequence, KENXXXN/D; and the ABBA motif which conforms to the consensus sequence, FX[ILV][FHY]X[DE]. The D-box is the most common APC/C degron and is incorporated in the sequences of many APC/C substrates including cyclin A, cyclin B1, Geminin, Securin and Nek2A. In addition to the degrons described above, other less utilised APC/C degrons have been identified. These include the: A-box (AQRXLXPSN) in Aurora A; CRY-box (CRYXPS) in Cdc20; GXEN-box in Xkid; and O-box (LXXXN) which have been found in *Drosophila melanogaster* APC/C substrates, Orc1 and Asp (Littlepage and Ruderman 2002, Castro et al. 2003, Araki et al. 2005, Reis et al. 2006, Di Fiore et al. 2015).

In order to ensure the correct timing and order of mitotic events, APC/C recognition of substrates is affected by different regulatory mechanisms, some of which are related to the PTM of substrates and regulatory proteins that are related to the affinity of different substrates for the APC/C. Although the APC/C has a remarkable ability to recognise unmodified substrates, substrate PTMs can, in some instances, modulate the timing of APC/C substrate recognition and degradation. Indeed, phosphorylation of Aurora A and Nek2A promotes their degradation. Computational analysis shows that the phosphorylation of the S residue close to the KEN box of both substrates (S-P-K-E-N) promotes ubiquitin chain assembly on these substrates, such that phosphorylation at this residue enhances their ubiquitin-dependent degradation (Min et al. 2015). In contrast, PTMs can also function in an inhibitory manner to prevent APC/C accessibility to degron motifs. Thus, the acetylation of BubR1 at K250 close to the KEN box renders it a poor APC/C substrate, whilst the deacetylated form of BubR1 can be readily targeted for degradation. This BubR1 acetylation/deacetylation switch

provides a crucial regulatory mechanism in switching of the SAC, as BubR1 is integral to SAC signalling and the timely regulation of the metaphase-to-anaphase transition (Choi et al. 2009).

The binding affinity of substrates for the APC/C also plays an important role in their timely association with the APC/C. As such, an increased number of degron motifs within same substrate increase the binding affinity of the substrate for Cdc20 and/or Cdh1. In agreement with this proposed mechanism, structural studies with the Cdh1 inhibitor and pseudosubstrate, Acm1 bound to Cdh1 in *S. cerevisiae* determined that the Acm1 D-box, KEN box and ABBA motifs are recruited simultaneously to the WD40 domain pockets in Cdh1 (Bu et al. 1995). This mechanism of multiple degrons is also employed by SAC-insensitive substrates Cyclin A and Nek2A and yeast Clb5, such that they utilise multiple motifs to increase their binding affinity for the APC/C (Di Fiore Net al. 2015, Lu, et al. 2015). Consistent with these observations inactivation of the Clb5 motif by mutation results in the delayed degradation of Clb5 (Lu, et al. 2014), whilst the addition of an ABBA motif to cyclin B1 enhances the rate of its ubiquitin-mediated degradation (Di Fiore, et al. 2015). The underlying mechanism of how the number of degrons affects the rate of degradation is not understood fully, yet it might be that substrates with multiple degrons out-compete substrates with fewer degrons for accessibility to the APC/C.

1.4.5.3 APC/C regulators

In the context of the temporal degradation of substrates by the APC/C and the overall role of Cdc20 and Cdh1 in this process, there are other APC/C regulators that modulate the timing of substrate degradation. Indeed, cells are subjected to molecular

checkpoints to ensure the correct timing and ordering of the cell cycle events. As such, APC/C activity following binding to its coactivators is inhibited to allow for the accumulation of essential proteins. The Spindle Assembly Checkpoint (SAC) works to inhibit APC/C-Cdc20 activity until all chromosomes are aligned in a bi-oriented manner on the metaphase plate (Hoyt et al. 1991, Li and Murray 1991, Lara-Gonzalez et al. 2012). Additionally, APC/C-Cdh1 activity is restrained at the end of G1 phase to allow for cellular progression into S phase. In this regard, the Early mitotic inhibitor 1 (Emi1) associates with APC/C-Cdh1 and inhibits its activity to allow for the accumulation of cyclins and Geminin (Reimann et al. 2001A, Reimann et al. 2001B, Hsu et al. 2002). In addition, there are other proteins regulators such as Rae1-Nub98, 53BP1 and RASSF1A, CBP and p300 which interact with APC/C at different phases of cell cycle to modulate its activity (Dreijerink, Braga et al. 2001, Jeganathan, Malureanu et al. 2005, Turnell, Stewart et al. 2005, Kucharski, Minshall et al. 2017).

1.4.5.3.1 Emi1

Emi1 is an F-box protein that inhibits APC/C activity at different stages of the cell cycle. This protein has three functional domains. The N-terminal domain is responsible for the localisation of Emi1, the F-box domain facilitates its association with Skp1 but has no role in APC/C activity regulation, whilst its C-terminal domain, which is important for APC/C inhibition contains a D-box, a Zinc-binding region (ZBR) and a C-terminal tail. This C-terminal tail of Emi1 functions as pseudo-substrate inhibitor of APC/C activity at the end of G1 and during G2. In the late stages of G1, the E2F transcription factor induces the expression of Emi1, which binds to the Cdh1 WD40 domain via its ZBR domain to inhibit APC/C-Cdh1 activity (Dong et al. 1997, Miller S et al. 2006, Frye et al. 2013). During G2, Emi1 inhibits APC/C activity and overcomes APC/C binding

to the WD40 domain of Cdc20, thus inhibiting their association. Upon entry into mitosis Emi1 activity is inhibited by Plk1, which promotes its degradation in an SCF-dependent manner.

1.4.5.3.2 The Spindle-Assembly Checkpoint

The Spindle-Assembly Checkpoint (SAC) is basically a genome-safeguarding mechanism that targets APC/-Cdc20 activity to ensure timely APC/C-Cdc20 activation and the fidelity of chromosome segregation at the metaphase-to-anaphase transition. The SAC serves to ensure that sister chromatids are associated, through their kinetochores to the mitotic spindle, in a bi-oriented manner. The Mitotic Checkpoint Complex (MCC) functions as a surveillance complex to monitor chromosome attachment to kinetochores. The MCC is a trimeric complex that detects unattached kinetochores and propagates an inhibitory signal to prevent mitotic progression through activation of the SAC and inhibition of APC/C-Cdc20. The MCC is comprised of a group of highly conserved proteins: Mitotic arrest deficient 2 (Mad2), Budding uninhibited by benzimidazole-3 (Bub3), and BubR1 (Sudakin 2001, Yu 2002, Díaz-Martínez and Yu 2007). The Monopolar spindle 1 (Mps1) kinase is the main effector of the MCC inhibitory signal. At unattached kinetochores, Mps1 is recruited and phosphorylates some of the SAC proteins, including MAD1, which facilitates its binding to MAD2. MAD1 association with MAD2 acts as a molecular switch that converts the open MAD2 conformation (o-MAD2) to a closed conformation (c-MAD2) which binds to Cdc20 (Davenport, Harris et al. 2006, Musacchio 2015 et al. 2019). Robust inhibition of APC/C-Cdc20 also requires the BubR1 and BuBb3 association with c-MAD2-Cdc20 complexes, which together form the MCC. In this regard, BubR1 serves as pseudo-substrate that outcompetes Cdc20 for APC/C binding though its two KEN boxes (King

et al. 2007) that ultimately limits substrate recognition and binding of UbcH10 to the APC/C. However, some studies also suggest that BUBR1 and BUB3 can also act alone to inhibit APC/C-Cdc20 (Tang et al. 2001, Davenport et al. 2006, Nilsson et al. 2008, Di Fiore et al. 2015).

The inhibitory role performed by the MCC facilitates the accumulation of APC/C substrates, cyclin B1 and Securin which consequently prevent premature metaphase-to-anaphase transition (**Fig. 1.16**; Li and Murray 1991, Rieder et al. 1994, Zou et al. 1999). The ability of Cdc20 to associate differentially with the APC/C during SAC activation and upon SAC satisfaction ensures APC/C substrate selectivity. In the absence of the SAC, Cdc20 associates with both APC3 and APC8 to activate the APC/C, but in the presence of the SAC, Cdc20 associates only with APC8 in order to activate the APC/C. This differential binding capacity of Cdc20 allows for the degradation of SAC-insensitive substrates during an active SAC and prevents the degradation of SAC-sensitive substrates when the SAC is active. The SAC also promotes the ubiquitylation of Cdc20 which serves as an autoinhibitory feedback mechanism to allow for disassembly of the SAC when the SAC has been satisfied and all chromosomes are aligned on the metaphase plate. APC15 performs a crucial role in this process whereby it accelerates Cdc20 ubiquitylation and MCC disassembly (Wolthuis et al. 2008, Geley et al. 2001, Mansfeld et al. 2011,Izawa and Pines 2011).

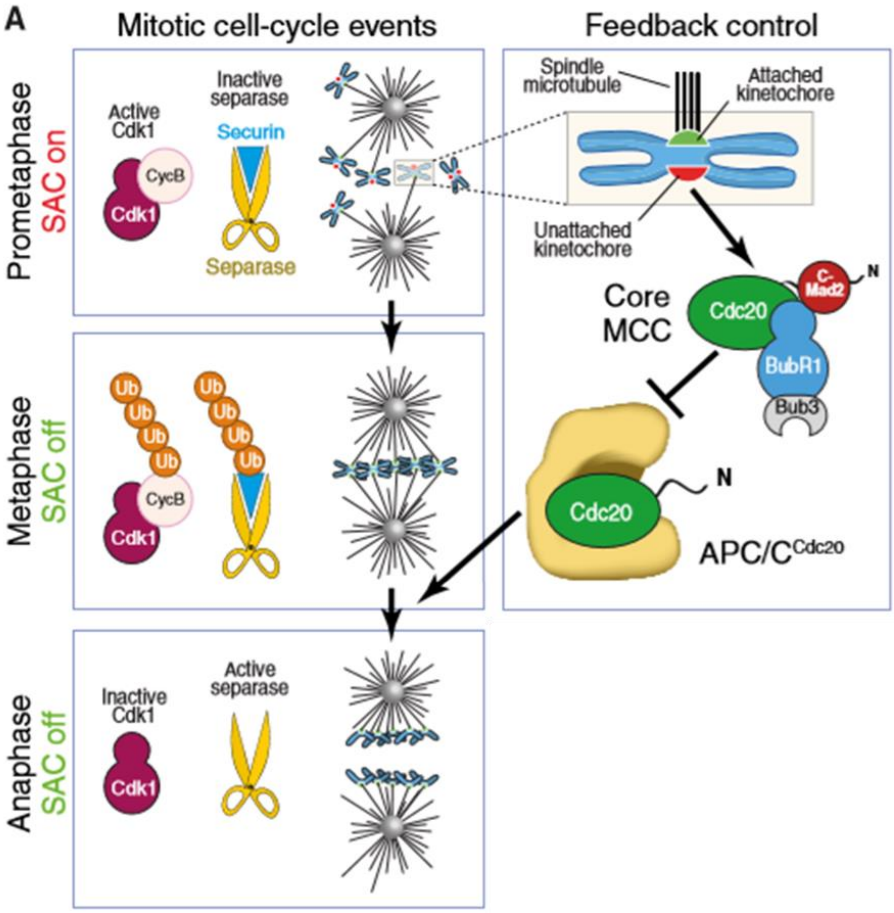

Figure 1.16: Regulation of the Spindle Assembly Checkpoint in mitosis. (A) Cdk1 promotes kinetochore attachment to the mitotic spindle, whilst SAC activity in prometaphase ensures that chromosomes attach to the Spidle correctly. Unattached kinetochores, shown in Red, emit the SAC inhibitory signal and facilitate MCC assembly and prevent the binding of Cdc20 to the APC/C. Image taken from Musacchio 2015.

1.4.5.3.3 SAC-insensitive substrates

As alluded to above, SAC-insensitive substrates such as Nek2A, Cyclin A and 53BP1 are degraded independently of SAC activation (Hoyt et al. 1991, Thornton and Toczyski 2003, Geley et al. 2001, Kucharski et al. 2017). Cyclin A is a highly stable protein during both S and G2 phase, yet becomes extermely short-lived during early mitosis. The degradation of cyclin A begins after cyclin B1 has entered the nucleus and is coincident with NEBD. Cyclin A degradation occurs prior to cyclin B1 degradation, but is required for metaphase-to-anaphase transition as overexpression of cyclin A arrests cells in metaphase. (Geley et al. 2001). The ability of APC/C-Cdc20

to target cyclin A for degradation independent of the SAC is dependent on two factors. Firstly, cyclin A possesses an extended D-box within its N-terminal region that facilitates its recognition by Cdc20. Second, cyclin A binds to Cks (a Cdk cofactor) during mitotic entry which is crucial in cyclin A outcompeting SAC proteins for binding to Cdc20. As such, Cks binding triggers a structural conformational alteration in cyclin A which exposes its N-terminal D box and further increases its affinity for Cdc20. cyclin A is therefore a more efficient substrate for the APC/C-Cdc20 than cyclin B1 and Securin as it requires less Cdc20 activity, while cyclin B1 and Securin degradation require full Cdc20 activity (Klotzbücher et al. 1996 Geley et al. 2001).

APPOLON (also termed BRUCE or BIRC6) is an E3 ligase, important in the regulation of apoptosis, that has been suggested to have a role in the degradation of cyclin A during SAC activation. In this regard, APPOLON is thought to interact with 'free' cyclin A that is not bound to Cdks. As such knockout of APPOLON causes the accumulation of the total amount of cyclin A during mitotic entry but does not affect the amount of cyclin A associated with Cdks. Interestingly, it has been shown that the UBC domain of APPOLON is not involved in this process, but interacts with APC3 and APC11 to facilitate recruitment of free cyclin A to the APC/C (Kikuchi et al. 2014). The APC/C substrate, Nek2A is a serine/thrionine kinase involved in chromatin condensation, centrosome disjunction and the formation of bipolar mitotic spindles (Hames et al. 2001). Akin to cyclin A, Nek2A levels peak during S and G2 phases, whilst its levels decrease dramatically upon APC/C activation in mitosis. APC/C-Cdc20 targets Nek2A for degradation in early mitosis independently of the SAC via a cyclin A-like D-box. Nek2A also possesses an MR motif similar to the C-terminal IR motif of Cdc20 and Cdh1 by which Nek2A binds directly to the APC/C. in addition, Nek2A interacts with

the leucine zipper motif of APC8 which enhances its degradation in a SAC-insensitive manner (Hames et al. 2001, Sedgwick et al. 2013).

1.4.6 **The mechanism of APC/C ubiquitylation**

The Cullin-containing, APC2, and the E3 RING ligase, APC11 constitute the minimal module required for ubiquitylation of protein substrates (Tang et al., 2001). APC11 is a zinc-dependent enzyme that associates directly with the APC/Cs two E2-conjugating enzymes. Ubiquitin chain initiation on APC/C substrates is initiated by the E2, UbcH10 (Ube2C), whilst Ube2S is the E2 responsible for the polyubiquitylation elongation process. APC/C association with UbcH10, but not Ube2S, is triggered by a conformational change in the APC/C structure from a ‘down’ to an ‘up’ position in a process regulated by coactivator binding. In the ‘down’ position, APC5 interacts with APC11 and prevents UbcH10 association, whilst upon coactivator binding to the APC/C, APC5 is displaced and the core-domain of UbcH10 associates with the C-terminal region of APC11 at the catalytic core of APC/C, with aproximately 10-fold higher afiinity. As the core domain of UbcH10 binds to APC11 the ‘backside’ of UbcH10 interacts specifically with the APC2 WHB domain and further causes structural rearrangements facilitating substrate binding. This interaction keeps ubiquitin-bound UbcH10 close to the APC/C substrates for rapid monoubiquitylation of target substrates. UbcH10 interaction with ubiquitin and substrates is mediated through the TEK box, which is a small cluster of amino acids that are evolutionarily conserved in ubiquitin and many APC/C substrates (see section 1.3; Jin et al. 2008). It is proposed that the TEK-box is recognised by UbcH10, which consequently nucleates the APC/C, substrate and coactivator to facilitate both the initiation, and subsequent elongation, of polyubiquitin chains on substrates by the APC/C. In this

regard, the TEK box in ubiquitin favours the formation of K11-linked polyubiquitin chains on substrates while the TEK box in substrates faciliates the positioning of the ubiquitin acceptor K residue close to ubiquitin-loaded UbcH10 and APC11 to ensure the APC/C-directed ubiquitylation of the substrate (Jin et al., 2008). Ube2S binding to the APC/C is different from UbcH10, APC2 interacts with the Ube2S C-terminal LRRL motif. Ube2S recruitment to the APC/C requires a docking site on APC11s surface, called the exosite. Binding of Ube2S to APC11 allows Ube2S access to the APC/C catalytic core and its coactivators to facilitate highly processive polyubiquitin chain formation on substrates (**Fig. 1.17**; Williamson et al. 2009, Chang et al. 2014, Meyer and Rape 2014).

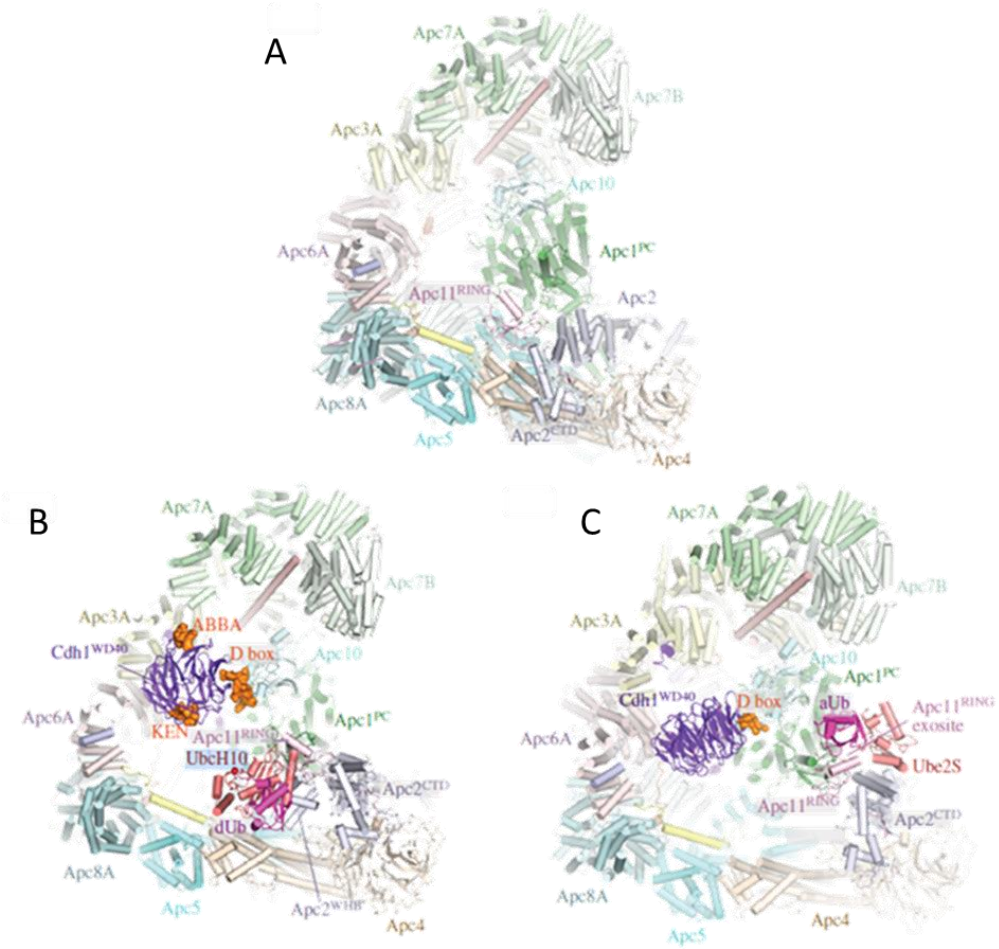

Figure 1.17: APC/C association with UbcH10 and Ube2S. (A) In the coactivator unbound state, APC11 binds to APC5 and blocks the UbcH10 binding site. (B) the 'up' position of the APC/C following interaction with coactivators (Cdh1 model) and the binding of UbcH10 to the APC/Cs catalytic core. (C) APC/C binding to Ube2S through it C-terminal LRRL motif at the APC11 exosite surface. Image taken from (Alfieri, Zhang et al. 2017).

Several mutation classes of APC11 have defined further the UbcH10-Ube2S-APC/C interaction sites at the amino acid level. One class of mutations including I25, R27, W63 and R77 APC11 affect the canonical E2-Ub site and show a high impact on UbcH10 ubiquitylation ability but not Ube2S. Interestingly, another class of RING mutations including K81, F82 and M57 limits APC-Ube2S dependent ubiquitylation with no effect on UbcH10, and impairs Cdc20 mediated polyubiquitylation of cyclin B, suggesting a fundamental role of the RING subunit in the elongation process with Ube2S. Most importantly, NMR and X-ray crystallography show the existence of these

amino acids on different surfaces of APC11 forming the canonical surface for UbcH10 and Ube2S binding association (**Fig. 1.18**; Brown et al. 2014).

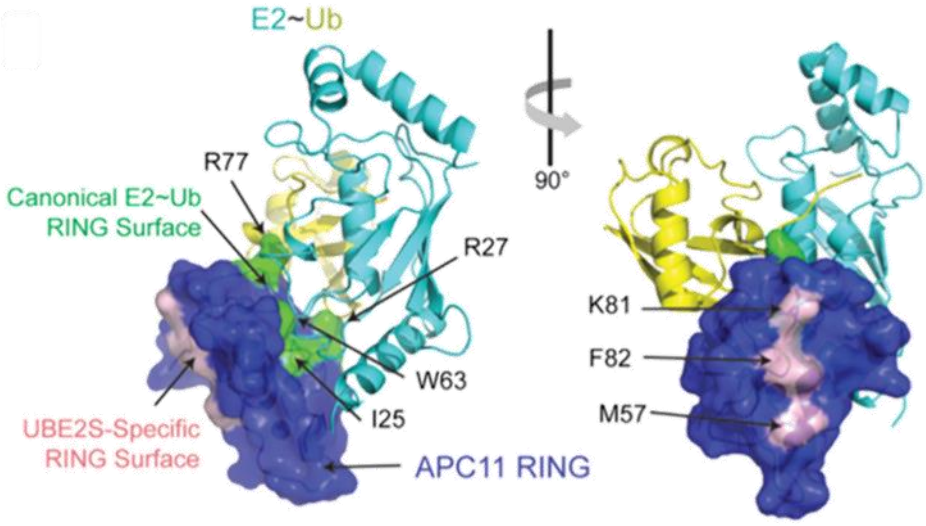

Figure 1.18: UbcH10 and Ube2S interaction sites on APC11. Representation of the APC11 surfaces required for UbcH10 and Ube2S association with the APC/C. The canonical UbcH10 binding-site requires amino acids I25, R27, W63 and R77, whilst Ube2S uses a non-canonical binding site that possesses amino acids K81, F82 and M57. Taken from (Brown, Watson et al. 2014).

1.5 UbcH10

1.5.1 UbcH10 structure

UbcH10 is an APC/C-specific E2-conjugating enzyme that is important in the initiation of ubiquitin chain formation on APC/C substrates. UbcH10 is a class III E2 consisting of the catalytic UBC domain which contains the active site Cysteine (C114) and an N-terminal extension, comprising the first 28 amino acids. UbcH10 is 179 amino acids (19.65 kDa) in size. Its crystal structure has been determined; UbcH10 adopts a triangular prism conformation comprising four-stranded antiparallel β-sheets, four α-helices and a 3_{10}-helix, which is located close to the active site C114 residue (**Fig. 1.19**; Aristarkhov et al. 1996, Townsley et al. 1997, Lin et al. 2002).

1.5.1.1 UbcH10 UBC domain

The catalytic domain of UbcH10 comprises approximately 150 amino acids and contains the catalytic C114 residue which is important in associating with ubiquitin and mediating ubiquitin chain initiation on APC/C substrates (Rape, Reddy et al. 2006). The UBC domain of UbcH10 also contains essential amino acids Q36, L39, L59 and F60, which contribute towards the thioesterification activity of UbcH10 and also form the E1 binding site (Olsen and Lima 2013). The UBC domain also comprises the L1 and L2 loops required for binding to the APC/C (as described in section 1.2.2; Summers et al. 2008, Nagy et al. 2012). The catalytic C114 is positioned next to the NH2 terminal region of the 3_{10} helix, comprising residues, 115-119 (LDILK), which are believed to enhance the transfer of ubiquitin from the E1 to UbcH10. As such, it is believed that the positively-charged K119 ε-amino group, reduces the pKa of C114 making it more reactive towards E1-bound ubiquitin (**Fig. 1.19**; Lin et al. 2002). The α-helix extending from residue L125 also includes the D-box, R^{129}TILLSIQS^{137} that coordinates the cell cycle-dependent degradation of UbcH10 (**Fig. 1.19**; see section 1.5.2 for further description). As outlined in section 1.4.6 UbcH10 interacts directly with APC11 in promoting the transfer of ubiquitin from UbcH10 to APC/C substrates. UbcH10 interacts with APC11 through residues, Y^{91} and A^{124}, whilst structural studies indicate that residues on the opposite face to Y^{91} and A^{124} are likely to interact with other APC/C subunits, simultaneously (Lin et al. 2002).

1.5.1.2 The N- terminal extension

The N-terminal extension of UbcH10 is not essential for the ubiquitylation activity of UbcH10 but does define interaction sites with the APC/C and is important in regulating APC/C specificity and the ordering of APC/C substrate ubiquitylation. The N-terminal

region of UbcH10 comprises the first 28 amino acids, and deletion of this region results in increased ubiquitylation on multiple K residues of APC/C substrates in a D-box-independent manner. Deletion of this region also decreases the sensitivity of the APC/C to APC/C intrinsic pseudosubstrate inhibitors, Emi1 and BubR1 *in vitro*, and allows for cells to bypass the SAC *in vivo*. As such, the N-terminal extension of UbcH10 is important in defining the specificity of the APC/C but also important in regulating APC/C substrate selectivity (Summers et al. 2008).

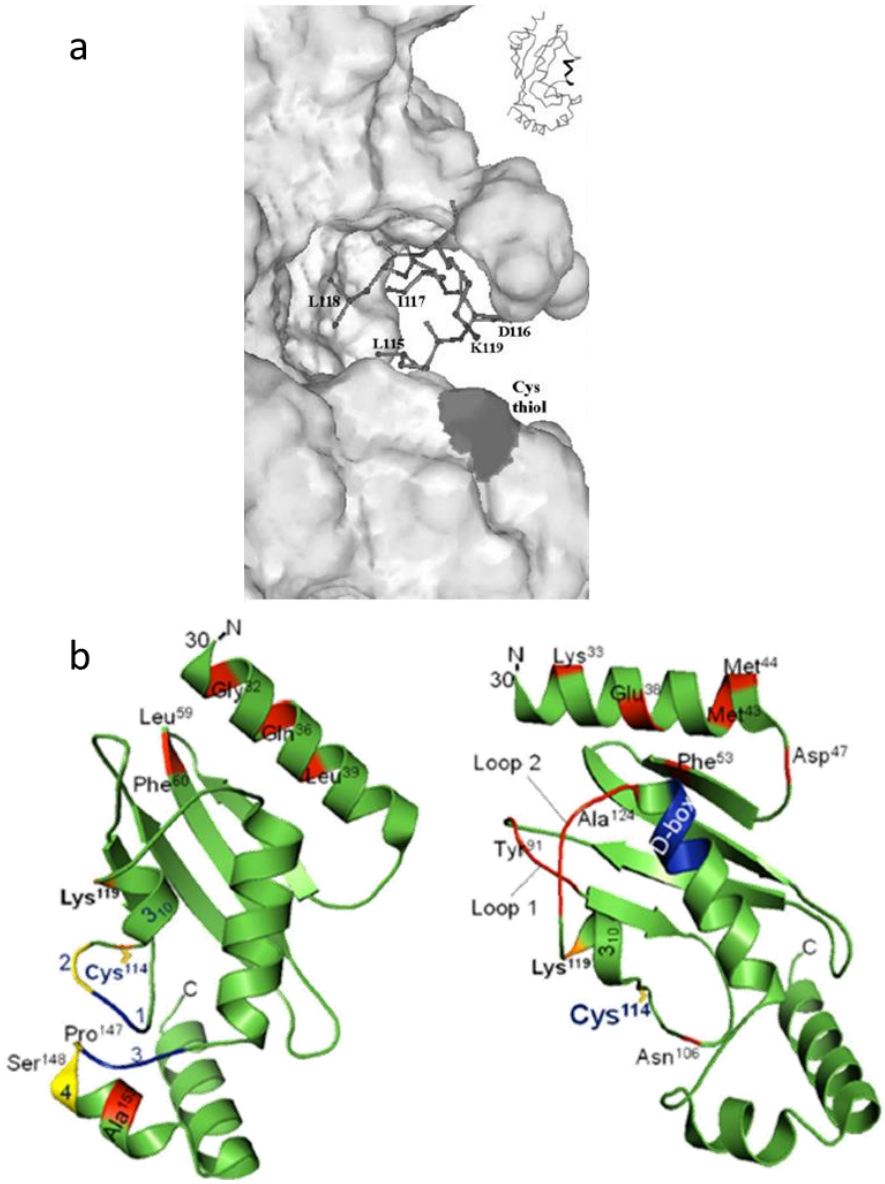

Figure 1.19: UbcH10 structure. (A) structural representation of the 310 helix positioned close to the C114 of UbcH10 showing the residues surrrounding the catalytic C114 residue. (B) Secondary structure of UBC in green, showing C114, the UbcH10 D-box, Loops 1 and 2 that interact with E1, and amino acids important in binding to the APC/C (e.g. Y91 and A124). Taken from Lin, Hwang et al. 2002 and Xie, Powell et al. 2014.

1.5.2 **UbcH10 regulation**

UbcH10 stability is regulated in a cell cycle-dependent manner. The levels of UbcH10 are low in late G1, gradually increase in G2 and peak in mitosis. An increase in UbcH10 levels in mitosis is regulated both by the UPS and at the transcriptional level (Nath et al. 2011). It is well established that the APC/C associates with transcriptional

coactivators, CBP/p300 in order to regulate their acetyltransferase activities (Turnell, Stewart et al. 2005). It has been determined that APC/C-Cdc20 and CBP/p300 associate with the UbcH10 promoter in order to induce the expression of UbcH10 (Nath et al. 2011). It has been proposed that Cdc20 overexpression promotes tumourigenesis by inducing the overexpression of UbcH10 and promoting aneuploidy through mitotic slippage (Nath et al. 2011). UbcH10 is known to be targeted for ubiquitylation by APC/C-Cdh1, but not APC/C-Cdc20, in late G1 (Rape and Kirschner 2004). Like other APC/C-Cdh1 substrates, UbcH10 ubiquitylation is distributive, meaning that ubiquitylation occurs through repeated rounds of substrate association/dissociation with the APC/C, whilst APC/C-Cdc20 substrates undergo processive ubiquitylation, only binding once to the APC/C and, as such, are degraded faster. UbcH10 degradation also inactivates APC/C-Cdh1 activity allowing for the accumulation of cyclin A that is required for DNA replication during S phase. Although UbcH10 can be ubiquitylated by the APC/C it also been established that UbcH10 can undergo auto-monubiquitylation in the absence of the APC/C, though the significance of these observations is not known (Rape and Kirschner, 2004).

The N-terminal extension of UbcH10 is suggested to have a role in the modulation of UbcH10 degradation. Indeed, deletion of UbcH10's N-terminal extension inhibits APC/C-Cdh1 activity towards UbcH10 but enhances the APC/C-Cdc20-mediated degradation of UbcH10 (Rape, Reddy et al. 2006, Williamson et al. 2011). In this regard, the N-terminal extension of UbcH10 possesses an initiation motif (IM) comprising charged residues R6, R17 and K18. Interestingly, the IM is a motif consisting of a cluster of charged (K and R) amino acids, which are normally located close to a D-box and are found in many APC/C substrates like cyclin B1, Geminin and

Securin. IMs determine both the efficiency of substrate degradation and the rate of substrate degradation. It has been proposed that UbcH10 associates with substrates directly through their IM to help nucleate APC/C, coactivators and substrates, and that the number of charged residues within the IM motif dictates its binding affinity for UbcH10 and the APC/C (Williamson et al. 2011). Although it is not yet clear how UbcH10's IM is recognised by the APC/C it is interesting to note that the IM of UbcH10 is not as positively charged as other APC/C-Cdh1 substrates, potentially indicating why UbcH10 is the last APC/C substrate to be degraded at the end of G1 phase. It has also been determined that when ubiquitylated UbcH10 dissociates from the APC/C it undergoes rapid deubiquitylation by an unknown deubiquitylase which also modulates UbcH10 degradation (Rape et al, 2006).

1.5.3 **UbcH10 and cancer**

The UbcH10 proto-oncogene product is found to be overexpressed in many human cancers including bladder, brain, breast, colon, gastric, lung, oesophageal, ovarian, thyroid and uterine, amongst others. Overexpression of UbcH10 typically correlates positively with poor prognostic outcome such that UbcH10 levels often serve as a biomarker with both diagnostic and prognostic potential. Furthermore, UbcH10 is a potential therapeutic target as the siRNA knockdown of UbcH10 in ovarian and pancreatic carcinoma cell lines limits cell proliferation (Welsh et al. 2001, Pallante et al. 2005, Lin et al. 2006, Berlingieri et al. 2007, Jiang et al. 2008, Fujita et al. 2009). Indeed, CRISPR/CAS9-mediated knockout of UbcH10 results in delayed kinetics of progression through mitosis (NEBD to anaphase onset) and mitotic exit, relative to control cells, which was exacerbated by inhibition of APC/C-Cdc20 complexes with the APC/C inhibitor, proTAME (Wild et al. 2016). Despite UbcH10, like other E2

conjugating enzymes, being touted as cancer therapuetic targets, no specific E2 active site inhibitors have been identified to date, though an allosteric inhibitor of hCDC34, in the CRL-Skp2-dependent uiquitylation of $p27^{KIP1}$, has been identified (Ceccarelli, Tang et al. 2011). The lack of characterised E2 inhibitors indicate that, despite well characterized catalytic domain structures, there are no natural compounds, or synthesized drugs, tested to date that associate with the active site of E2s to modulate their catalytic activity.

The molecular function of UbcH10 as a proto-oncogene product has been investigated in a transgenic mouse model. Consistent with the oncogenic nature of UbcH10, transgenic mice overexpressing *UbcH10* are prone to develop a broad spectrum of spontaneous tumours, including lipomas, liver and skin tumours, lung adenomas and lymphomas, as well as carcinogen-induced (7,12-dimethylbenz(a)anthracene, DMBA) lung tumours (Van Ree et al. 2010). Indeed, normal mouse embryo fibroblasts (MEFs) taken from *UbcH10* transgenic animals display considerable aneuploidy and aberrant mitosis, characterized by supernumerary centrioles and anaphases with lagging chromosomes and chromatin bridges (Van Ree et al. 2010). Consistent with these observations the overexpression of UbcH10 in transgenic mice promotes the precocious degradation of cyclin B1 in mitosis by the APC/C. As such, the ability of UbcH10 to act as an oncogene product is thought to be dependent solely upon its ability to stimulate APC/C E3 ligase activity towards its substrates.

1.6 Aims and objectives

As detailed throughout the introduction, UbcH10 is an integral component of the APC/C, which is required for normal cell cycle progression through mitosis. Indeed, its overexpression results in the hyperactivation of the APC/C, chromosome missegregation, aneuploidy and cancer, whilst ablation of UbcH10 expression results in prolonged mitotic progression and a reduction in cellular proliferation (Van Ree et al. 2010). Despite the key role performed by UbcH10 in the cell and its potential role as a biomarker and cancer therapeutic target it is perhaps surprising that UbcH10 is, relative to other proto-oncogene products, less well studied. In order to begin to redress this balance our laboratory developed αUbcH10 antibodies to perform immunoprecipitation coupled to tandem mass spectrometry to identify and characterize the UbcH10 interactome (Jessica Foster PhD thesis, University of Birmingham, 2018). That study successfully identified a number of UbcH10-interacting proteins, of which, the RGS-containing RhoGEF, PDZ-RhoGEF (RhoGEF11) was the most abundant (by number of peptides identified and % sequence coverage) interacting protein identified. These preliminary studies suggested that PDZ-RhoGEF was potentially, a novel APC/C substrate that was targeted for degradation in early mitosis (Jessica Foster PhD thesis, University of Birmingham, 2018).

- A major aim of the current study therefore was to expand on these preliminary findings and determine the molecular relationship between UbcH10, the APC/C and PDZ-RhoGEF degradation. In this regard, specific aims were to: generate αPDZ-RhoGEF antibodies to facilitate molecular studies of PDZ-RhoGEF function; address the role for the APC/C in PDZ-RhoGEF degradation in mitosis and establish the molecular basis of PDZ-RhoGEF targeting to UbcH10 and the APC/C. It was envisaged that such

studies would provide new insight into the role of PDZ-RhoGEF in the cell cycle and provide further insight into the molecular basis of UbcH10 and APC/C function.

- The second major aim of this thesis was to explore the intrinsic UbcH10 E3 ligase activity and UbcH10 autoubiquitylation in more detail. In this regard, it has long been known that UbcH10 can undergo auto-monoubiquitylation in the absence of the APC/C (Rape et al. 2006). However, the molecular role of UbcH10 autoubiquitylation has yet to be explored. As such, the initial aims of this part of the project were to characterise those K acceptor residues in UbcH10 that were substrates for autoubiquitylation, to characterise the ubiquitin linkages utilised in polyubiquitin chains assembled on UbcH10, and investigate UbcH10 autoubiquitylation *in vivo*. These studies were aimed to provide futher molecular insight into the role of UbcH10 autoubiquitylation and UbcH10 function.

2 Materials and Methods

2.1 Tissue culture

2.1.1 Cell culture

Descriptions of all the cell lines used during the course of my study are presented in Table 2.1. HeLa, RPE1 and U2OS cells were grown in HEPES-buffered Dulbecco's Modified Eagle Medium (DMEM; Sigma-Aldrich) supplemented with 8% v/v FCS (Sigma-Aldrich) and 2mM L-glutamine (complete medium; Sigma-Aldrich). The U2OS FlpIn TREX cell lines generated for this project were also grown in complete medium supplemented with 200μg/ml of the selection antibiotic, Hygromycin B (Gibco). Retrovirus cell lines generated during this project were similarly grown in complete medium with 500 μg/ml of the selection antibiotic, G418/Geneticin (Gibco). All cells were incubated in a Nuaire humidified incubator at 37°C and 5% v/v CO_2. For cell passage, cells were washed in warmed Phosphate-Buffered Saline (PBS; Oxoid) and then detached from the surface of the culture dish or flask using trypsin (TrypLE express; Gibco). Depending on the cell line, cells were incubated with trypsin for up to 5 min at 37 ºC in a humidified incubator. Once detached from the dish/flask, cells were re-suspended in complete medium and centrifuged at 1600 rpm at room temperature (RT). The cell pellet was then re-suspended in fresh complete medium and cell density calculated using a haemocytometer. Cells were then split into new dishes/flasks at the required density. For long term storage cells were re-suspended in complete medium + 10% v/v DMSO and incubated in sterile cryotubes in a Mr Frosty containing Propan-2-ol at -80°C overnight, after which cryotubes were transferred to cryoboxes in liquid nitrogen. To retrieve cells from liquid nitrogen, cells were thawed rapidly at 37°C, washed twice in complete medium and then incubated in fresh complete medium until

needed. All the tissue culture procedures were performed in a Scanlaf Mars Safety Class hood 2 sterile-cabinet.

Table 2-1 List of cell models used during this study.

Cell line	Description	source
HeLa	Human, adenocarcinoma, integrated HPV-18 genome, cervical epithelial cells	ATCC CCL-2
RPE-1	Human, hTERT-immortalized retinal pigment epithelial cells, wild-type p53	ATCC CRL-4000
U2OS	Human, osteosarcoma, epithelial cells, wild-type p53	ATCC HTB96
U2OS FlpIn T-REX	U2OS cell line with an engineered, integrated FRT recombination site and expression of a TET repressor	Dr.Garry Sedgwick, UoCopenhagen
U2OS FlpIn T-REX W.T. UbcH10-HA	U2OS cell line that expresses W.T. UbcH10-HA under the control of a tetracycline-responsive (TET-ON) promoter	This study
U2OS FlpIn T-REX K119R UbcH10-HA	U2OS cell line that expresses K119R UbcH10-HA under the control of a tetracycline-responsive (TET-ON) promoter	This study
U2OS FlpIn T-REX K121R UbcH10-HA	U2OS cell line that expresses K121R UbcH10-HA under the control of a tetracycline-responsive (TET-ON) promoter	This study
U2OS FlpInT-REX ΔPDZ UbcH10-HA	U2OS cell line that expresses ΔPDZ UbcH10-HA under the control of a tetracycline-responsive (TET-ON) promoter	This study
RPE-1 WT Myc-PDZRhoGEF	RPE-1 cell line that expresses WT PDZ-RhoGEF under the control of an immediate early CMV promoter for continual expression	This study
RPE-1 ΔKEN Myc-PDZ-RhpGEF	RPE-1 cell line that expresses ΔKEN PDZ-RhoGEF under the control of an immediate early CMV promoter for continual expression	This study
RPE-1 S27A Myc-PDZ-RhpGEF	RPE-1 cell line that expresses S27A PDZ-RhoGEF under the control of an immediate early CMV promoter for continual expression	This study
RPE-1 S1518A Myc-PDZ-RhpGEF	RPE-1 cell line that expresses S1518A PDZ-RhoGEF under the control of an immediate early CMV promoter for continual expression	This study

2.1.2 Generation of cell lines

2.1.2.1 Generation of U2OS FlpIn T-REX cell lines

For the generation of clonal U2OS FlpIn T-REX cell lines, FlpIn T-REX-U2OS cells were seeded at 90% confluence on 10cm dishes. 1.5μg of the appropriate pcDNA5-FRT vector containing the gene of interest was mixed with 13.5μg of the pOG44 vector (expressing the Flp recombinase to allow the integration of the gene of interest at the FRT recombinant site in U2OS FlpIn T-REX cells) in a 1:9 ratio and diluted in 200μl reduced-serum medium, Opti-MEM (Life Technologies). 15μl of the transfection reagent Lipofectamine 2000 (Life Technologies) was prepared separately in 200μl Opti-MEM. Plasmid DNA-Opti-MEM and transfection reagent-Opti-MEM mixtures were incubated for 5 min at RT and then combined and left at RT for an additional 45 min to allow plasmid DNA-transfection reagent complexes to form. After this time cells were washed with Opti-MEM and then incubated in 5 ml of Opti-MEM medium. Plasmid DNA/Lipofectamine mixtures were then added drop-wise to the cells and incubated for 6 h in a humidified incubator at 37°C and 5% v/v CO_2, after which cells were washed with complete medium and then incubated in the same medium. 24 h post-transfection, cells were split by trypsinization onto 4 x 10 cm dishes. After an additional 48h incubation, cells were incubated in HEPES-buffered DMEM (+8% v/v FCS and 2mM L-glutamine) supplemented with 200μg/ml hygromycin B to allow for selection of cells that had integrated the gene-of-interest, successfully at the FRT site in the U2OS-FlpIn T-REX cells. Colonies were observed approximately 2 weeks post-transfection and individual colonies were isolated with a 1 ml pipette using the microscope under sterile conditions in the tissue culture hood. Colonies were plated and expanded on 24-well, and then 6-well, plates in complete medium containing 200μg/ml hygromycin B. Individual cell lines were then tested for their ability to express

the gene-of-interest +/- 0.1µg/ml of Doxycycline for 24 h, after which time cells were harvested and subject to Western blot (WB; section 2.3.5) for the gene product of interest. Stocks of cell lines of interest were frozen in liquid Nitrogen in complete medium + 10% v/v DMSO for long-term storage.

2.1.2.2 Generation of retrovirus and retrovirus transduction of cell lines

To generate cell lines that expressed a gene-of-interest constitutively, the pQCXIN retroviral vector system (Clontech) was used. As such our gene-of-interest was first cloned into pQCXIN and then transfected along with a plasmid expressing viral envelope in to the retroviral packaging cell line, GP2-293 cells (which are HEK293 cells that constitutively express viral factors, gag (Group antigens polyprotein) and pol (reverse transcriptase gene)) to generate retrovirus particles for cell transduction and generation of cell lines that express the gene-of-interest. One day before transfection, GP2-293 cells were plated on 75cm^2 flasks such that they would be 80% confluent the following day. For transfection, 10 µg of pQCXIN-WT / ΔKEN / S27A / S1518A PDZ-RhoGEF construct and 10 µg of pCMV-VSV-G plasmid were diluted in 200 µl of Opti-MEM. Similarly, 20 µl of Lipofectamine 2000 was added to 200 µl of Opti-MEM in a separate Eppendorf. As described earlier, plasmid DNA-OptiMEM and transfection reagent-OptiMEM mixtures were incubated for 5 min at RT and then combined and left at RT for an additional 45 min to allow for plasmid DNA-transfection reagent complexes to form. GP2-293 cells were then washed twice with Opti-MEM and then incubated in 5ml of complete medium. After this time the DNA-Lipofectamine mixture was added to the cells and incubated for 6 h at 37°C, after which cells were incubated in complete medium.

72 h post-transfection, retrovirus particles were collected from the GP2-293 cell medium and filtered using a 0.45μM filter (Sartorious). GP2-293 cells typically produce high titre virus and RPE-1 cells transduce very well, such that the virus did not need concentration by ultra-centrifugation or add cationic reagents (e.g. Polybrene) to aid cell transduction with the retrovirus. As retroviruses infect mitotically-active cells, RPE-1 cells were seeded at very low density (10%) on 75 cm^2 flasks prior to infection and then transduced overnight with one quarter of the retrovirus supernatant isolated from 10 ml of GP2-293 cells. Cells were then incubated in complete medium for an additional 48h, prior to being seeded at 500 cells/10cm dish and incubated in complete medium with 500 μg/ml G418 for selection. Individual clones were then picked and expanded as described in section 2.1.2.1 and tested for gene product expression by WB. Stocks of cell lines of interest were frozen in liquid Nitrogen in complete medium + 10% v/v DMSO for long-term storage.

2.1.3 **Transient transfection**

Transient transfections for gene product expression were performed on RPE-1 cells, typically at 30-40% confluence. As such, the appropriate amount of plasmid DNA diluted in 200 μl Opti-MEM and the appropriate amount of Lipofectamine 2000, also diluted in 200 μl Opti-MEM were incubated separately for 5 min, and then together for 45 min, at RT (see Figure legends for details). At this time cells were washed twice with Opti-MEM and incubated in 5 ml of Opti-MEM in a humidified atmosphere at 37°C and 5% v/v CO_2. The DNA plasmid-Lipofectamine mixture was then added drop-wise to cells. After 6 h incubation in a humidified atmosphere at 37°C and 5% v/v CO_2, Opti-MEM was replaced with complete medium and cells were further incubated in a humidified atmosphere at 37°C and 5% v/v CO_2 until needed.

2.1.4 **siRNA transfection**

RNA interference is generally used to knockdown the endogenous expression of a specific gene; small-interfering (si)RNA was used in the current study to knockdown PDZ-RhoGEF expression. As described above, transfection was performed using cells at 30-40% confluence. As such, 30nM silencing control siRNA (siCTRL) or 30nM siRNA-directed towards PDZ-RhoGEF (see Table 2.2) were diluted in 200 μl Opti-MEM, whilst 5 μl of Lipofectamine RNAiMAX (Life Technologies) was also diluted in 200 μl Opti-MEM. In the meantime cells were washed twice with Opti-MEM and incubated in 5 ml of Opti-MEM in a humidified atmosphere at 37°C and 5% v/v CO_2. After 5 min incubation mixtures were combined and incubated together for 45 min, at RT (see Figure legends for details). The siRNA-transfection mix was then added drop-wise to cells and incubated in a humidified atmosphere at 6h at 37°C, 5% v/v CO_2. The transfection mixture was then discarded from the cells and replaced with complete medium, after which time cells were incubated in a humidified atmosphere at 37°C and 5% v/v CO_2 until needed.

Table 2-2 siRNAs used in this study.

siRNA	Sequence	manufacturer
siRNA PDZ-RhoGEF	CGUUUAGAGGGCUACCAGAtt	Ambion
siCTRL	CGUACGCGGAAUACUUCGAtt	Ambion

2.2 Synchronization experiments and drug treatments

2.2.1 **Synchronization of cells in mitosis**

For mitotic synchronisation, cells were seeded into 25cm^2 or 75cm^2 sterile culture flasks (Corning). Cells were then incubated with complete medium + 10μM spindle

fibre assembly inhibitor, nocodazole (Sigma-Aldrich) or 10µM spindle fibre stabiliser, Taxol (Sigma-Aldrich) for 16 h. Mitotic cells were then harvested by mechanical shake-off, and pelleted by centrifugation at 1600 rpm. Cells were then either washed twice with ice-cold PBS by successive rounds of resuspension and centrifugation, prior to harvesting in the appropriate lysis buffer (see sections 2.3.1) or subjected to 'nocodazole-release' for re-entry into the cell cycle. For nocodazole-release experiments cells harvested by mechanical shake-off were washed twice in complete medium that was warmed to 37°C to release cells back into the cell cycle and incubated in complete medium in a humidified incubator at 37°C and 5% v/v CO_2. Cells were then harvested after washing with ice-cold PBS, as detailed above, at appropriate time points for subsequent analyses (see section 2.3.1). In cell synchronisation experiments using U20S FlpIN T-REX cell lines, cells were treated with 0.1µg/ml Doxycycline for 18hr to induce the expression of the gene of interest prior to treatment with the appropriate drug. In some experiments the 26S proteasome inhibitor, MG132 was added to the cells (at 10µM) 30 min following nocodazole or Taxol withdrawal to stabilize proteins normally targeted for degradation as cells progress through mitosis.

2.2.2 **Synchronization of cells in G2/M phase**

To synchronise cells at the G2/M border, cells were treated with 9µM of Cdk1 inhibitor, RO-3306 (Sigma-Aldrich) in complete medium for 16 h before harvesting in the appropriate lysis buffer. As described above, for cell synchronisation experiments using U20S FlpIn T-REX cell lines, cells were treated with 0.1µg/ml Doxycycline for 18 h to induce the expression of the gene of interest prior to treatment with RO-3306.

2.2.3 **Inhibition of mitotic kinases**

For mitotic kinase inhibition, cells were initially treated with 10μM nocodazole for 16 h. Mitotic cells were then collected by mechanical shake-off and seeded onto fresh 10cm dishes in the presence of nocodazole. To inhibit Cdk1, RO-3306 was added to a final concentration of 9μM; To inhibit Aurora B, Hesperadin was added to a final concentration of 10μM (Cayman Chemical); To inhibit Plk1, BI-6727 was added to a final concentration of 250nM (Cayman Chemical). The mitotic kinase inhibitors were added either separately, or together with 10μM MG132, to inhibit the 26S proteasome, and harvested at the appropriate times post-treatment.

2.2.4 **26S Proteasome inhibition**

Cells were grown on 10cm dishes or in 75cm^2 flasks to the appropriate density and either left untreated, or treated with the drugs described above. To inhibit the 26S proteasome cells were treated with either 5μM or 10μM MG132 for the time indicated (see figure legends for specific details).

2.2.5 **Induction of cellular genotoxic stress**

Genotoxic stress and DNA damage was induced by treatment of cells with hydroxyurea (HU), UV light or X-rays. For treatment with UV, all the medium covering the cells on a 6cm or 10cm dish was removed and stored in a sterile universal. The lid of the dish was removed and cells were then subjected to 25 J/m^2 UV (at 254nm) using the UV light source, (UVP Blak-Ray). The old medium was then replaced and cells were incubated at 37°C and 5% v/v CO_2 and then harvested at the appropriate time post-irradiation. For HU treatment, cells were incubated with 1mM HU for the appropriate time prior to harvesting. Typically cells grown in 75cm^2 flasks were

subjected 5 Gy of X-ray irradiation, which were delivered using an X-Ray irradiator from CellRad.

2.3 Protein biochemistry

2.3.1 Cell lysate preparation for Western blots

For cell harvesting, medium was removed from the cells, which were then washed twice with ice-cold PBS. After the removal of residual PBS, cells were lysed in the appropriate amount of UTB lysis buffer (9M Urea, 50mM Tris-HCl (Tris(hydroxymethyl)aminomethane) pH 7.5, 0.15M β-mercaptoethanol) and incubated at RT for 5-10 min. Cell lysates were then collected using a cell scraper and transferred to a clean, non-sterile Eppendorf. Lysates were then sonicated by sonication using a Microson Ultrasonic Cell Distrupter at 3-4 KHz with a continuous pulse for 15 s. Cell lysates were then subject to centrifugation for 20 min at 13000rpm and 4°C to remove insoluble material, prior to storage at -80°C until required.

2.3.2 Cell lysate preparation for Immunoprecipitation

For immunoprecipitation (IP), cells were washed twice with ice-cold PBS and then lysed in either NETN containing 250mM NaCl (20 mM Tris (pH 7.5), 250 mM NaCl, 25 mM NaF, 25 mM β-glycerophosphate, 1 mM EDTA (pH 8.0), 1% (v/v) Nonidet P-40), or HiLo buffer (50mM Tris (pH 7.5), 0.825M NaCl, 1%(v/v) Nonidet-P40). Cells were then incubated for 5-10 min at 4°C prior to being transferred to a non-sterile Eppendorf with a cell scraper and pipette. Cells harvested in NETN were disrubted with 2 x 15 strokes (separated by a 5 min interval) using a dounce homogenizer with a tight pestle (Wheaton) and then centrifuged at 13000rpm, 4°C for 20 min to pellet the cellular debris. The supernatant was then collected using a small gauge needle to avoid disturbing the lipid layer on the surface of the supernatant. Cells harvested in

HiLo buffer were then clarified, on ice, by sonication using a Microson Ultrasonic Cell Distrupter at 3-4 KHz with a continuous pulse for 15 s.

For IP, samples were typically incubated overnight at 4°C with either an IgG control or with a specific antibody targeting the protein of interest (see figure legends for details). The following morning 20µl of packed protein G agarose beads were added to the samples and incubated for an additional 3 h at 4°C. The samples were then centrifuged to pellet the beads and the supernatant was removed. The beads were then washed 3 times in the same buffer used to harvest them. Following the final wash any residual supernatant was removed using a small gauge needle. 30µl of sample buffer (1 volume 10% v/v SDS: 2 volumes 9 M Urea, 50 mM Tris (pH 7.4), 150 mM β-mercaptoethanol) was added to the immunoprecipitated proteins on the Protein G beads, which were then subject to heating at 95°C for 5 min and SDS-PAGE and WB analysis (sections 2.3.4 and 2.3.5)

2.3.3 **Protein determination by Bradford assay**

We used the Bradford assay to measure the protein concentration in the cell lysates isolated in UTB, NETN or HiLo lysis buffers. Bovine serum albumin 1mg/ml (BSA; Melford Chemicals) diluted in 1ml of Bradford reagent (Bio-Rad) was used to create a standard curve of BSA at 0µg, 5µg, 10µg, 20µg and 30µg. The absorbance for the standards was read at 595nm on a Cecil CE9200 spectrophotometer. Typically, between 2 and 5µl of the cell lysate was also diluted in 1ml of Bradford reagent and the absorbance also taken at 595nm. The protein lysate absorbance was compared with standard curve readings to calculate the protein concentration of the cell lysate.

2.3.4 **SDS-PAGE**

Sample buffer (as described in section 2.3.2) was typically added in equal volume to 50 µg of the protein sample. After mixing, all samples were boiled at 95°C to facilitate protein denaturation. Samples were then separated by SDS-PAGE (sodium dodecyl sulphate–polyacrylamide gel electrophoresis) using a 10% w/v acrylamide gel (37.5/1 acrylamide/bisacrylamide, 0.1 M Tris, 0.1M Bicine, 0.1% w/v SDS, 0.3% v/v TEMED [N, N, N', N;-tetramethylethylenediamine], 0.06% w/v ammonium persulphate) in the presence of running buffer (0.1 M Tris, 0.1 M Bicine, 0.1% w/v SDS). For SDS-PAGE we used a Hoefer vertical gel electrophoresis system and typically ran gels at constant mA until the proteins were suitably resolved.

2.3.5 **Western blot (WB) analysis**

For WB analysis, the gel was transferred to nitrocellulose membranes (PALL) in transfer buffer (25 M Tris, 192 mM glycine, 20% v/v methanol) at 280 mA for 6 h. The membrane was then blocked in either 5% w/v milk powder, or 5% w/v BSA, in TBST (Tris-buffered saline-Tween; 0.02 M Tris [pH 7.6], 0.2 M NaCl, 0.1% (v/v) Tween 80) for 1 h at RT. The membrane was then incubated with the primary antibody at an appropriate dilution in either 5% w/v milk powder, or 5% w/v BSA, in TBST at 4°C overnight (Table 2.3). After washing with TBST for 15 min, the membrane was next incubated with the appropriate secondary antibody in either 5% w/v milk powder, or 5% w/v BSA, in TBST for 3 h at RT. Following washing of the membranes with TBST for 3 x 15 min, Immobilon ECL (Thermo Scientific) was applied to the membrane and protein bands were visualised by exposure of blue X-ray film (SLS) for different lengths of time and developed using an X-ograph developer.

Table 2-3 Primary and secondary antibodies used during this study.

Antibody name	Diluted in	Catalogue /Clone #	Dilution	Species	Manufacturer
APC3	Milk	610455	1:2000	Mouse	BD Transduction Lab
PDZ-RhoGEF	Milk	847/848	1:2000	Rabbit	Home-made: Eurogentec
Bub1	Milk	ab-54893	1:1000	Mouse	Abcam
Cdc20	Milk	Sc-245/H175	1:2000	Mouse	Santa-Cruz Biotechnology
Cyclin A	Milk	Sc-53227/AT10.2	1:500	Mouse	Santa-Cruz Biotechnology
Cyclin B1	Milk	Sc-245/GNS1	1:1000	Mouse	CRUK
Geminin	BSA	Sc-13015/FL-209	1:1000	Rabbit	Santa-Cruz Biotechnology
GST	Milk	Ab-1	1:500	Rabbit	Oncogene Science
Nek2A	Milk	610594	1:2000	Mouse	BD Transduction Lab
Myc	Milk	9E10	1:20	Mouse	David Lane
pH3 Ser10	Milk	sc-17783	1:3000	Rabbit	Cell Signalling
Plk1	Milk	9701	1:2000	Mouse	Santa-Cruz Biotechnology
Aurora B	Milk	ab-2254	1:2000	Rabbit	Abcam
UbcH10	Milk	49	1:500	Rabbit	Home-made: Eurogentec
P53	Milk	DO-1	1:20	Mouse	David Lane
Normal Mouse IgG	Milk	12-371	1:1000	Mouse	Sigma-Aldrich
Normal Rbbit IgG	Milk	12-370	1:1000	Rabbit	Millipore
K6-Afimmer	Milk	AVK6	1:1000	Human	Avacta
Ubiquitin FK2	Milk	BMLPW13350025	1:2000	Mouse	Enzo Life Sciences
α-Anti-mouse Ig HRP	Milk	P0447	1:2000	Goat	Dako
α-Anti-rabbit Ig HRP	Milk	P0399	1:3000	Swine	Dako
β-actin	Milk	A2228	1:40000	Mouse	Sigma-Aldrich

2.3.6 λ-phosphatase assay

λ-Phosphatase assays (dephosphorylation and gel-shift assay) were conducted using the lambda phosphatase kit (New England BioLabs). Cell lysates were prepared for IP from both asynchronous and mitotic cells in NETN lysis buffer and subjected to IP

using the appropriate antibodies (section 2.3.2- see figure legends for details). After IP, Protein G beads containing precipitated proteins were washed three times in NETN buffer and once in 25mM Tris pH 7.4. IPs were then incubated in 30μl of phosphatase buffer (containing 3μl 10X NEBuffer (PMP), 3μl of 10mM $MnCl_2$ and 23μl nuclease-free water) +/- 1000 units λ-phosphatase and incubated for 1 h at 30°C. Sample buffer was then added to the sample which after heating at 95°C was separated by SDS-PAGE (section 2.3.4) and analysed by WB (section 2.3.5).

2.3.7 **Expression and Purification of GST fusion proteins**

cDNAs of genes-of-interest were cloned into pGEX 4T-1 (GE Healthcare) which contains an N-terminal Glutathione–S-Transferase (GST) tag and validated for sequence integrity by Sanger sequencing (section 2.5.5). Validated constructs were used to transform BL21 Codon plus (RIPL) competent cells (Agilent) and plated onto 1.5% w/v agar (DIFCO)- Luria Broth (LB- 1% w/v NaCl, 1% w/v Tryptone (DIFCO), 0.5% w/v yeast extract (DIFCO))- plates supplemented with 100μg/ml ampicillin for selection and incubated at 37°C overnight. Individual colonies were then picked using a plastic inoculating loop and grown in 20 ml LB/ampicillin again overnight at 37°C in an orbital shaker at 200 rpm. The following morning the culture was transferred to 500 ml LB, supplemented with 100ug/ml ampicillin and incubated at 37°C for 3 h in an orbital shaker at 200 rpm. The culture was then incubated at 30°C, 200rpm for 30 min, after which GST protein expression was induced by the addition of 0.5mM IPTG (Isopropyl-β-D-thio-galactoside; Sigma) and incubated in an orbital shaker for a further 3 h at 30°C and 200rpm.

After induction the bacteria were pelleted by centrifugation for 10 min at 5000 rpm and the supernatant removed. The pellet was resuspended in 28ml of GST lysis buffer (1x PBS, 1% (v/v) Triton X-100, 1mM EDTA). Complete bacterial lysis was achieved by 5 rounds of 1 min sonication cycles on ice (power setting 5), separated by 1 min sonication-free intervals using a Misonix Microson Ultrasonic Cell Disrupter. Bacterial lysates were then clarified by two rounds of centrifugation at 16000rpm for 15 min at 4°C. The supernatant was collected and 1ml of glutathione agarose beads (Sigma) prepared in GST lysis buffer was incubated with the bacterial lysate overnight by rotation at 4°C. The beads were then centrifuged at 3000rpm for 2 min and washed three times with GST lysis buffer and three times with GST wash buffer (1x PBS, 1, 1mM EDTA PH 8.0). The glutathione-Sepharose beads containing the GST fusion protein of interest were incubated with 2 ml of glutathione elution buffer (25mM reduced glutathione, 50mM Tris, pH 8.0) and incubated by rotation at 4°C for 2 h, followed by a second elution with 1 ml glutathione elution buffer under the same conditions. The GST proteins were then dialysed using cellulose dialysis tubing with 12,000-14,000 molecular weight cut-off (Fisher Scientific) against 1 x 5L (overnight) and 2 x 2L (4 h each) dialysis buffer containing 25mM Tris pH 8.0, 150mM NaCl, 1mM Dithiothreitol (DTT; Sigma) and 10% v/v glycerol (SLS). After the third round of dialysis the protein was isolated and its concentration determined by Bradford assay and stored at -80°C until required. Purity was assessed by SDS-PAGE (section 2.3.4) and coomassie blue staining. As such, gels were first stained with a solution of 0.1% w/v coomassie Brilliant Blue R-250 (Fisher Scientific) in 20% v/v methanol, and 10% v/v glacial acetic acid for 1 h, and then destained with a solution of 10% v/v glacial acetic acid and 20% v/v methanol until proteins were visible.

2.3.8 *In vitro* ubiquitylation assays

30 μl of a ubiquitylation assay mix (5 mM $MgCl_2$, 5 mM ATP, 10 mM creatine phosphate (Sigma-Aldrich), 100U/ml creatine phosphate kinase (Sigma-Aldrich), 500μM ubiquitin (Table 2.4) 100nM of E1 [his-tagged recombinant hUB1 (Boston biochem)]) in 50mM Tris, pH 7.4 was added to the substrate under investigation (see figure legends for details). Reactions were incubated in a water-bath at 37°C for 1 h. Samples were then separated by SDS PAGE (section 2.3.4) and analysed by WB (section 2.3.5). K6 affimer blots were visualised by autoradiography on a Fusion Fx (Vilber Lourmat) autoradiographer.

Table 2-4 list of ubiquitin forms using during this study

Ubiquitin	manufacturer	Final concentration
WT	Boston Biochem	500μM
K6O	Boston Biochem	500μM
K11O	Boston Biochem	500μM
K48O	Boston Biochem	500μM
K6R	Boston Biochem	500μM
K11R	Boston Biochem	500μM
K48R	Boston Biochem	500μM

2.3.9 Development of ELISA for *in vitro* ubiquitylation assays

Polysorb 96 wells plates were coated overnight at 4°C with 200ng/well of Glutathione Casein (Merck) prepared in 50mM carbonate buffer, pH 9.6. Thereafter, purified GST and GST-UbcH10 were then prepared at 0.2 μg/μl in blocking buffer and incubated for 2 h at RT and the wells were then washed twice with 50mM Tris PH 7.4. The *in vitro* ubiquitylation assays were then conducted in final volume of 200μl (Section 2.38) and

incubated at 37°C. The wells were then washed three times with 50mM Tris pH 7.4 and were then blocked for 1 h at RT with 100 μl of blocking buffer 0.2% (w/v) casein in PBS 0.5% (v/v) Tween 20). Primary antibody was then diluted in blocking buffer and 100 μl was added to each well. The wells were then washed, and secondary antibody added for 1 h. Finally, the wells were washed 6 times with 50mM Tris PH 7.4 and the ubiquitylation activity were detected using o-phenylenediamine dihydrochloride/ Horse Radish Peroxidase. The plate then was subjected to SpectraMax ABS plus plate reader, Softmax pro 7 /ELISA endpoint with absorbance read at 492nm.

2.3.10 **Statistical analysis**

To quantify the ubiquitylation activity of WT GST- UbcH10 vs GST and GST-UbcH10 mutants, the absorbance read-outs of ELISA assays were analysed using two tailed t-test where statistical significance was measured. Error bars represent standard deviation about the mean.

2.3.11 **Proteasomal degradation assays**

100 ng of purified 26S proteasome (Ubiquigent) in which DUB activity has been inactivated was added to GST-UbcH10 alone, or GST-UbcH10 loaded with different polyubiquitin chains in degradation buffer (50mM Tris, pH 7.4, 5mM ATP and 5mM $MgCl_2$). The reactions were incubated at 37°C for different times after which samples were heated at 95°C in sample buffer for 5 min, separated by SDS PAGE (section 2.3.4) and analysed by WB with an anti-GST antibody (section 2.3.5).

2.4 Mass spectrometry

2.4.1 In gel trypsinisation

Asynchronous and mitotic cells lysates were prepared in NETN as discussed in section 2.3.2. Protein lysates were then incubated with either normal rabbit IgG control or anti-PDZ-RhoGEF antibodies for IP and collected on protein G agarose beads (section 2.3.2). Novex LDS sample buffer (Life Technologies) containing 50mM DTT was added to the samples, which were then heated at 95°C and loaded onto a pre-cast NuPAGE 4-12% BIS-TRIS acrylamide gel (ThermoFisher Scientific) and run with 1x MES running buffer (50mM 2-(N-morpholino)ethanesulfonic acid (MES), 50mM Tris, 0.1% w/v SDS, 1mM EDTA (pH 7.3)) at constant mA. The gel then was stained overnight in Colloidal Coomassie (0.08% (v/v) Coomassie Brilliant Blue G250, 1.6% v/v orthophosphoric Acid, 8% w/v ammonium sulphate, 20% v/v methanol) and then destained in distilled water.

The gel was then cut into individual slices using a sterile scalpel and put into sterile, low protein-binding microcentrifuge tubes (Sorenson Bioscience Inc). Samples were then washed 3 times, for 45 min in total, in 50% v/v acetonitrile (Millipore) and 50mM ammonium bicarbonate on a rocker for 1 h. Proteins were then reduced by incubating the gel slice in 10% v/v acetonitrile, 50 mM ammonium bicarbonate and 50mM DTT at 56°C for 1 h. Following reduction, cysteine residues were carboxymethylated with 100 mM iodoacetamide (Sigma Aldrich) in 10% v/v acetonitrile and 50 mM ammonium bicarbonate for 30 min in the dark. Samples were then washed 3 times, for 45 min in total, in 10% v/v acetonitrile and 40 mM ammonium bicarbonate. 200μl of 100% v/v acetonitrile was then added to dehydrate the sample and left on a rocker, for approximately 30 min until the gel slice became white. The samples were then rehydrated, then immersed, in a solution containing 10% v/v acetontrile, 20mM

ammonium bicarbonate and sequence-grade modified trypsin (Promega) and incubated overnight at 37°C. Supernatants containing trypsinized peptides were then collected by centrifugation and transferred to a fresh low protein-binding tube and temporarily stored in the fridge. The gel bands were then immersed in 3% v/v formic acid (Sigma Aldrich) and left on a rocker for 1 h to wash residual peptides free from the gel slice. The supernatants were then combined and the samples were dried using a vacuum centrifuge (Eppendorf Concentrator 5301). Samples were then stored at -20°C until analysis. Unless otherwise stated all reagents were prepared in high performance liquid chromatography (HPLC) grade water (Fisher Scientific, Chromanorm).

2.4.2 **Mass spectrometry analysis**

Samples were thawed at RT and then resuspended in 20µl 1% v/v acetonitrile, 1% v/v formic acid. Peptides were then analysed by tandem mass spectrometry using a Q Exactive™ HF hybrid Quadrupole-Orbitrab™ mass spectrometer as part of the University of Birmingham Mass Spectrometry Facility in Biosciences. PDZ-RhoGEF phosphorylated peptides identified from asynchronous and nocodazole-treated cells were compared to generate a list of mitosis-specific phosphorylation sites for PDZ-RhoGEF.

2.5 Molecular Biology

2.5.1 **PCR cloning**

DNA was amplified by PCR from an appropriate DNA template in a 50 µl reaction containing 10-50ng plasmid DNA, 500nM oligonucleotide primers (Forward and Reverse), 200µM dNTPs, 10µl 5x Q5 buffer and 1U Q5 high-fidelity DNA polymerase

(New England BioLab). Oligonucleotides primers (Table 2.5) were designed to include specific endonuclease restriction sites to facilitate sticky-end cloning of the amplified DNA into the desired vector. PCR reactions were conducted using a 2720 Thermal cycler PCR machine (Applied Biosystems) using this generic protocol unless otherwise stated: 98°C for 30 sec, 25-35 cycles of 95°C for 10 sec, 50-72°C for 30 sec, 30 sec/kb at 72°C, 72°C for 7 min. PCR products were separated by agarose gel electrophoresis (section 2.5.2) and visualised with SYBR safe DNA dye (Life Technologies). The DNA bands of interest were cut with a scalpel and purified (also described in section 2.5.2).

Following DNA purification, the DNA to be cloned and the host vector were both digested with the appropriate restriction enzymes (New England BioLab). Typically, digestion reactions included 500ng-2µg DNA/vector, 5µl 10X Cut smart buffer (New England BioLab) and 25 units of each of the restriction enzymes and were allowed to proceed for 3 h at 37°C in a water bath. The digested DNA and vector were again subjected to agarose gel electrophoresis, gel extraction and DNA purification. Digested DNA was then cloned into the digested vector by ligation. The ligation reaction was carried out by adding appropriate amounts of insert DNA and vector (molar ratios varied from 1:1 to 5:1), 3µl of 10X T4 buffer, 1 unit of T4 DNA ligase, to 30µl with Nuclease-free water (Ambion). The ligation reaction was performed overnight in 14-16°C after which they were incubated for 10 min at 65°C to inactivate the T4 DNA ligase. The ligation mixture was then used to transformed bacteria to isolate clonal, ligated plasmids (section 2.5.3).

Table 2-5 Primers used for the PCR cloning during the study.

Primers	Sequence (5'→3')	Manufacturer
5' EcoR1 PDZ RhoGEF	5'-ATCGAATTCATGAGTGTAAGGTTACCCCAGAGTATA	Sigma-Aldrich
3' Xhol PDZ-RhoGEF FRG1	5'-AATCTCGAGTTAACTGTCTAGCCCAGGGTCTGACAGTAC	Sigma-Aldrich
3' Xhol PDZ-RhoGEF FRG2	5'-AATCTCGAGTTAACTCTCCAGCAGGTCCTCAGGAAAGCTTCC	Sigma-Aldrich
5' EcoR1 PDZ-RhoGEF FRG3	5'-ATTGAATTCATGGACAGTTCACGCTCAGAGATTCGCCTGGG	Sigma-Aldrich
3' Xhol PDZ-RhoGEF FRG3	5'-ATACTCGAGTTAGCTGGGTGTGGGGCCCTGCTGGGCTGGCTC	Sigma-Aldrich
5' EcoR1 PDZ-RhoGEF FRG4	5'-TTTGAATTCATGAGGGTAGAACTGGATGACTCAGACGTGTTC	Sigma-Aldrich
3' Xhol PDZ-RhoGEF FRG4	5'-AATCTCGAGTTATGGTCCTGGTGACGCGGCTGC	Sigma-Aldrich

2.5.2 **Gel purification of PCR products**

A 0.8% w/v agarose gel was made up by dissolving agarose (Life Technologies) in 1xTBE (100mM Tris, 100mM boric acid and 2mM EDTA, pH 8.3) and cast with 1μl/gel SYBR safe-dye (Life Technologies) using Flowgen electrophoresis equipment. 6x loading buffer (30% (v/v) glycerol, 0.25% (w/w) Bromophenol blue, 0.25% (w/w) xylene cyanol FF) was added to the PCR products which were then separated by agarose-gel electrophoresis at 60V until the sample had migrated a sufficient distance to ensure good resolution. The gel was then visualized on a Blue-light transilluminator (Invitrogen safe imager). The relevant DNA bands were excised (with reference to the 1kb+ DNA ladder (Life Technologies)) using a scalpel and the DNA extracted using QIAquick Gel Extraction Kit (Qiagen). As such, the gel band was weighed and 3x volume of QG buffer was added; the gel band was then incubated at 55 °C until the gel had fully dissolved. 1x volume Isopropanol was then added to the solution to facilitate binding to a QIAquick column; samples were loaded on the QIAquick column by centrifugation at 13000 rpm for 1 min. The column was then washed successively

with 500μl QG buffer and then 750μl PE buffer containing 70% v/v ethanol (QIAgen). The column was then dried by centrifugation at 13000 rpm for 1 min and then transferred to a clean tube whereupon 50 μl of nuclease-free H_2O was added. The column was left to hydrate for a further 5 min after which the DNA was eluted by centrifugation at 13000 rpm for 2 min.

2.5.3 **Bacterial Transformation**

A number of different strains of chemically-competent bacteria were used for transformation (see Table 2.6). Usually 100ng of purified DNA, 5μl of the ligation reaction, or 5μl mini-prep DNA was used to transform 20μl of the most appropriate bacterial strain, which was dependent upon the chosen application (Table 2.6). Typically transformation mixtures were incubated on ice for 30 min, followed by 1 min heat-shock at 42°C, and then incubated on ice for a further 5 min. 300μl of SOC medium was then added to the transformation mixture and incubated at 37°C, 200rpm for 1 h. The transformation mix was then cultured on LB agar-plates (1.5% (w/v) bacto-agar (DIFCO) in LB containing the appropriate antibiotic and incubated at 37°C overnight. The next day, individual colonies were selected and incubated with 5ml of LB plus the appropriate antibiotic and allowed to grow in an orbital shaker at 37°C, 200rpm overnight.

Table 2-6 Competent bacterial strains used during this study.

Bacteria	Source
Subcloning efficient DH5α	Invitrogen
Library efficient DH5α	Invitrogen
MAX Efficiency Stbl2	Invitrogen
BL21 CodonPlus (DE3)-RIPL	Agilent
XL1-Blue supercompetent	Agilent
XL10-Gold ultracompetent	Agilent
NEB stable high efficiency	NEB

2.5.4 **Mini-prep of plasmid DNA**

5ml bacterial cultures grown to saturation were pelleted by centrifugation at 5000rpm for 5 min. The supernatant was then removed and DNA purified using a GenElute plasmid mini-prep kit (Sigma-Aldrich). First, the bacteria were re-suspended in 200μl of resuspension buffer (+RNase) and then lysed by the addition of 200μl lysis buffer, inversion and incubation for 5 min. Second, 300μl of neutralization buffer was added to the lysed cells, which were mixed and incubated for an additional 3 min. The sample was then centrifuged at 13000 rpm for 10 min. During this time the DNA purification column was wetted with 500μl of column preparation buffer by centrifugation at 13000 rpm for 1 min. Next, the sample was loaded onto the column by centrifugation at 13000 rpm for 1 min and the flow-through discarded. The column was then washed with 500μl of wash buffer (containing 70% v/v ethanol) by centrifugation at 13000 rpm for 1 min. The column was then dried by centrifugation and transferred to a fresh, collection tube, to which 100μl of nuclease-free water was added. After 5 min hydration the plasmid DNA was eluted by centrifugation at 13000 rpm for 3 min. The concentration of the DNA was measured using a NanoDrop ND-1000 spectrophotometer (ThermoFisher

Scientific) and the accompanying ND-1000 spectrophotometer v3.2 software (ThermoFisher Scientific).

2.5.5 **Sanger DNA sequencing**

Sequencing reactions were carried out by PCR. Typically, a 20µl reaction mixture was set up containing 10ng/µl sequencing primer (Table 2.7), 4µl 5x sequencing buffer, 1µl Big Dye Terminator (Applied Biosystems), 5µl of mini-prep or 100ng purified DNA. Sequencing protocols for PCR were: 25 cycles of 96°C for 10s, 55°C for 5s, and 60°C for 4 min. After PCR, the DNA was purified in preparation for sequencing. First, 62.5µl absolute ethanol, 3µl 3 M Sodium Acetate, and 14.5µl nuclease-free water was added to the PCR products and incubated at RT for 30 min to precipitate the DNA. The samples were then centrifuged at 13000rpm for 20 min to pellet the DNA, after which pellets were washed twice with 100µl 70% v/v ethanol by centrifugation at 13000rpm for 15 min. Purified DNA was then dried for 1 min at 90°C, re-suspended in 11µl HiDi and subsequently heated at 100°C for 5 min. The samples were then loaded into 96 wells plates and sequenced using a 3500xl Genetic Analyser (Applied Biosystems); sequences were then extracted and analysed by BLAST (NCBI, NIH).

Table 2-7: Sequencing primers used during this study

Primers	Sequence (5'→3')	Manufacturer
RhoGEF Myc	5'-GCCAGCCTTCGGATGCCTCTGAGAGA-3'	Sigma-Aldrich
RhoGEF 1 (351)	5'-CACCCTCCTGGGCTCTTCACCTTC-3'	Sigma-Aldrich
RhoGEF 2 (731)	5'-TGTCAGCACCCTGGGCTAGACA-3'	Sigma-Aldrich
RhoGEF 3 (1111)	5'-AAAAATGCGCCTCTGAGAGTGAAG-3'	Sigma-Aldrich
RhoGEF 4 (1461)	5'-TCGAGAGGCACGACCTTCCAACAC-3'	Sigma-Aldrich
RhoGEF 5 (1731)	5'-GTATGATGCCCCAGAACCTGGGAC-3'	Sigma-Aldrich
RhoGEF 6 (2111)	5'-TGTCTGACCTGGAGCCAGAGCCAG-3'	Sigma-Aldrich
RhoGEF 7 (2491)	5'-CAGTTCTGTTCCTATCAGTCAATA-3'	Sigma-Aldrich
RhoGEF 8 (2875)	5'-CTGGATCTTACAACCAGAAAAATG-3'	Sigma-Aldrich
RhoGEF 9 (3251)	5'-ACCCCGGAGCTGGGGGAATGCCCG-3'	Sigma-Aldrich
RhoGEF 10 (3631)	5'-CTGATCCTGTGGAGCCTGCTGCCA-3'	Sigma-Aldrich
RhoGEF 11 (4015)	5'-GAGAGTGGCCAGTCAGAGCCTGGG-3'	Sigma-Aldrich
RhoGEF 12	5'-ACTCTCAAGCTCAACAGGCTCAAG-3'	Sigma-Aldrich
R3 RhoGEF R3 (571-565)	5'-TTTCTTCCTGCCTCAGCATATTCC-3'	Sigma-Aldrich
pGEX forward	5'-GGGCTGGCAAGCCACGTTTGGTG-3'	Sigma-Aldrich
pGEX reverse	5-'CCGGGAGCTGCATGTGTCAGAGG-3'	Sigma-Aldrich

2.5.6 **Maxi-prep of plasmid DNA**

Following the validation of DNA clones by sequencing, clones were used to transform the most appropriate bacterial strain (section 2.5.3) and were grown overnight at 37°C on LB-agar plates supplemented with the relevant antibiotic. The following day, individual colonies were picked using a plastic inoculating loop and grown in 5ml of LB + antibiotic in an orbital shaker at 37°C for 6 h. The culture was then transferred to a flask containing 250 ml of LB + antibiotic and incubated overnight at 37°C in an orbital shaker. DNA extraction and purification were performed using the PureLink HiPure Plasmid MaxiPrep kit (Invitrogen). As such, the bacterial culture was pelleted by

centrifugation at 5000rpm for 10 min and the supernatant discarded. The pellet was resuspended in 12 ml of resuspension buffer (+ RNase) and transferred into a fresh 50ml sterile tube, after which 12 ml of lysis buffer was added to the sample, mixed by inversion and then incubated for 5 min at RT. During this time the DNA-binding column was equilibriated with 25ml of EQU solution by gravity-flow through. After lysis the bacterial lysate was neutralised by addition of 12 ml neutralisation buffer. Neutralized samples were then added to the column for DNA-binding by gravity-flow through. After the sample had passed through the column it was washed with 15ml of EQU buffer and 25ml of wash buffer (containing 70% v/v ethanol). Plasmid DNA was then eluted from the column with 15 ml of elution buffer. The eluted DNA was then precipitated with 10.5 ml of isopropanol and pelleted by centrifugation at 15000rpm for 30 min at 4°C, after which time the DNA pellet was washed twice with 70% v/v ethanol. The pellet was then left to air-dry and then re-suspended in 150-400µl nuclease-free water, dependent on the pellet size. Plasmid DNA concentration measured with a NanoDrop ND-1000 spectrophotometer as detailed earlier (section 2.5.4).

2.5.7 **Site-Directed Mutagenesis**

2.5.7.1 Quick-change site-directed mutagenesis

pGEX-2T-1-UbcH10 was used as a template for site-directed mutagenesis (SDM) using the QuickChange SDM kit (Agilent). PCR for SDM was performed in 50 µl reaction volumes. Each reaction contained 5 µl 10x reaction buffer, 25 ng pGEX-2T-1-UbcH10 DNA template, 500 nM of the appropriate forward and reverse primers (primers listed in Table 2.8), 2 mM dNTPs, 2.5 U/µl PfuUltra DNA polymerase (Agilent) and made up to 50µl with nuclease-free water. The PCR protocol for SDM was as follows: 95°C for 1 min, 18 cycles of 95°C for 50 sec, 60°C for 50 sec, 1min/kb at 68°C,

68°C for 6 min. Following PCR, the PCR product was digested with the Dpn1 restriction enzyme (10U/µl), in order to digest parental DNA, and incubated in water-bath at 37°C for 1 h. DNA was then used to transform XL1 blue supercompetent bacteria as described in section 2.5.3. Multiple transformants were then selected for DNA mini-prep and DNA sequencing to isolate clones which has successfully incorporated the mutation in the context of the entire UbcH10 open-reading frame (sections 2.5.4. and 2.5.5).

Table 2-8 List of primers used in this study for QuickChange site-directed mutagenesis.

Primers	Sequence (5'→3')	Manufacturer
UbcH10 K119R For	5'-CTGGACATCCTGAGGGAAAAGTGGTCTGCC-3'	Sigma-Aldrich
UbcH10 K119R Rev	5'-GGCAGACCACTTTTCCCTCAGGATGTCCAG-3'	Sigma-Aldrich
UbcH10 K121R For	5'-ATCCTGAAGGAAAGGTGGTCTGCCCTG-3'	Sigma-Aldrich
UbcH10 K121R Rev	5'-CAGGGCAGACCACCTTTCCTTCAGGAT-3'	Sigma-Aldrich
UbcH10 K164R For	5'-ACAGCTTTTAAGAGGTACCTGCAAGAAACC-3'	Sigma-Aldrich
UbcH10 K164R Rev	5'-GGTTTCTTGCAGGTACCTCTTAAAAGCTGT-3'	Sigma-Aldrich
K119-121R UbcH10 For	5'-ATCCTGAGGGAAAGGTGGTCTGCCCTG-3'	Sigma-Aldrich
K119-121R UbcH10 For	5'-CAGGGCAGACCACCTTTCCCTCAGGAT-3'	Sigma-Aldrich

2.5.7.2 Q5 site-directed mutagenesis

The Q5 site-directed mutagenesis kit (NEB) was used to generate specific mutations in the PDZ-RhoGEF open-reading frame. PCR reactions were performed in a total volume of 25µl and contained 25ng plasmid DNA template, 12.5µl Q5 hot start high-fidelity 2x master mix (NEB), 500 nM forward primer, 500 nM reverse primer (Table 2.9) and 9µl nuclease-free water. The PCR conditions used for Q5 SDM were: 98°C for 30 s; 25 cycles of 98°C for 10 s, 68°C for 20 s, 72°C for 6.5 min; 72°C for 7 min. Following PCR, 11µl PCR product was mixed with 5 µl 2x KLD reaction buffer (NEB),

1 µl KLD enzyme mix (NEB) and 3 µl nuclease-free water and incubated at RT for 5 min. DNA was then used to transform bacteria as described in section 2.5.3. Multiple transformants were then selected for DNA mini-prep and DNA sequencing to isolate clones which has successfully incorporated the mutation in the context of the entire PDZ-RhoGEF open-reading frame (sections 2.5.4. and 2.5.5).

Table 2-9 List of primers used in this study for Q5 site-directed mutagenesis.

Primers	Sequence (5'→3')	Manufacturer
RhoGEF S27 For	5'GCACCAGAGCGCAAGGCCCCTTCCCACCATCGC-3'	Sigma-Aldrich
RhoGEF S27 Rev	5'GCGATGGTGGGAAGGGGCCTTGCGCTTCGCGTCTGGTGC-3'	Sigma-Aldrich
RhoGEF S1414 For	5'AGACGCCCCAGCCGCGCTCCTCCAAGCCTGGCC-3'	Sigma-Aldrich
RhoGEF S1414 Rev	5'GGCCAGGCTTGGAGGAGCGCGGGCTGGGGCGTCT-3'	Sigma-Aldrich
RhoGEF S1518 For	5'GCAGACGCAGCCGCGGCACCAGGACCAGGACCATAA-3'	Sigma-Aldrich
RhoGEF S1518 Rev	5'TTATGGTCCTCCTGGTGCCGGCTGCGTCTGC-3'	Sigma-Aldrich
RhoGEF S27ii For	5'GCACCAGAGCGCAAGGCCCCTTCCCACCATCGC-3'	Sigma-Aldrich
RhoGEF S27ii Rev	5'GCGATGGTGGGAAGGGGCCTTGCGCTTCGCGTCTGGTGC-3'	Sigma-Aldrich
RhoGEF ΔKEN For	5' GGCCCTGATGCCCCGGGAG-3'	Sigma-Aldrich
RhoGEF ΔKEN Rev	5' GCCGCCTTCCATTCGCTGGTAGAAGATCAGG-3'	Sigma-Aldrich

3 INVESTIGATING THE RELATIONSHIP BETWEEN THE APC/C AND PDZ-RHOGEF

3.1 Introduction

3.1.1 Rho GTPase and RhoGEF

Small GTPases are G-proteins that respond to different cellular stimuli and serve as molecular switches to trigger different signalling pathways in order to regulate a wide variety of cellular processes. GTPases possess high affinity binding for GDP and GTP and their functional activity resides in their capacity to cycle between the GTP-bound active form and the GDP-bound inactive form (Gilman 1987 et al. 2002, Margarit et al. 2003). The interconvertible GTP/GDP states of these GTPases is mediated by GTPase-Activating Proteins (GAPs) and intrinsic GTPase activities, and Guanine nucleotide Exchange Factors (GEFs). An upstream stimulus (e.g. tyrosine kinase receptor activation) triggers the activation of a GEF that stimulates the dissociation of GDP from the inactive GTPase form and promotes the formation of the GTP active form. GEF activation and GTP-binding to the GTPase causes conformational changes in the protein which facilitates association with downstream factors and the transduction and amplification of the cellular signal (Bourne et al. 1990, Takai et al. 2001). GAPs subsequently bind to GTPases and enhance their inrinsic GTPase activity to promote the formation of the GDP inactive form and inhibition of the signalling capacity of the GTPase (Hall et al. 2002).

The Rat sarcoma (RAS) is a superfamily of small GTPases that consist of more than 150 members and have similar structure and biochemical features. Despite the structural similarities, these proteins exhibit versatile and multiple roles, being key

regulators of many fundamental physiological processes. Dysregulation of RAS proteins have been suggested to contribute to the pathogenesis of human diseases including cancer and other developmental syndromes. The RAS family is structurally and functionally divided into five subfamilies which are Ras, Rho, Ran, Arf and Rab; RAS protein members commonly contain conserved G Box GTP/GDP binding motifs, G1, G2, G3, G4 and G5 (Goitre et al. 2014).

The Ras family of proto-oncogene proteins consist of more than 36 members and has been widely studied due to their role in human oncogenesis. Ras proteins act as molecular switches that respond to external factors to activate downstream effectors important in the regulation of cell proliferation and differentiation, gene expression and cell survival (Johnson and Chen 2012). The Rab family of proteins is the largest of the RAS superfamily containing 61 members. Rab proteins serve as crucial regulators of intracellular transport and play key roles in endocytosis, secretory pathways and cellular protein trafficking. The RAS-like nuclear (Ran) family are the most abundant RAS GTPase in cells and are important for nuclear-cytoplasmic transport of proteins and mRNA (Moore 1998), whilst the ADP-ribosylation factor (Arf) family of RAS GTPases is important for the control of vesicular transport (Zerial and McBride 2001, Weis 2003, Memon 2004, Repasky, Chenette et al. 2004). Finally, the Ras homologous (Rho) proteins are crucial regulators of the actin cytoskelton and control actin dynamics in order to regulate cell cycle progression and gene expression. The Rho family consists of 20 members with RhoA, Rac1 and Cdc42 being the most well studied, which serve to regulate cell shape, cell movement and cell polarity (Iden and Collard 2008). For such functional diversity, RhoA, Rac1 and Cdc42 employ different GEFs and GAPs to modulate their biological activities. Additionally, RhoGTPases are

subject to another regulatory layer- Rho-specific guanine nucleotide dissociation inhibitors (RhoGDIs) which bind the C-terminal region of RhoGTPases to inhibit nucleotide exchange and prevent GTPase association with membranes (**Fig 3.1;** Grizot et al. 2001, Etienne-Manneville and Hall 2002, Schmidt and Hall 2002, Moon and Zheng 2003).

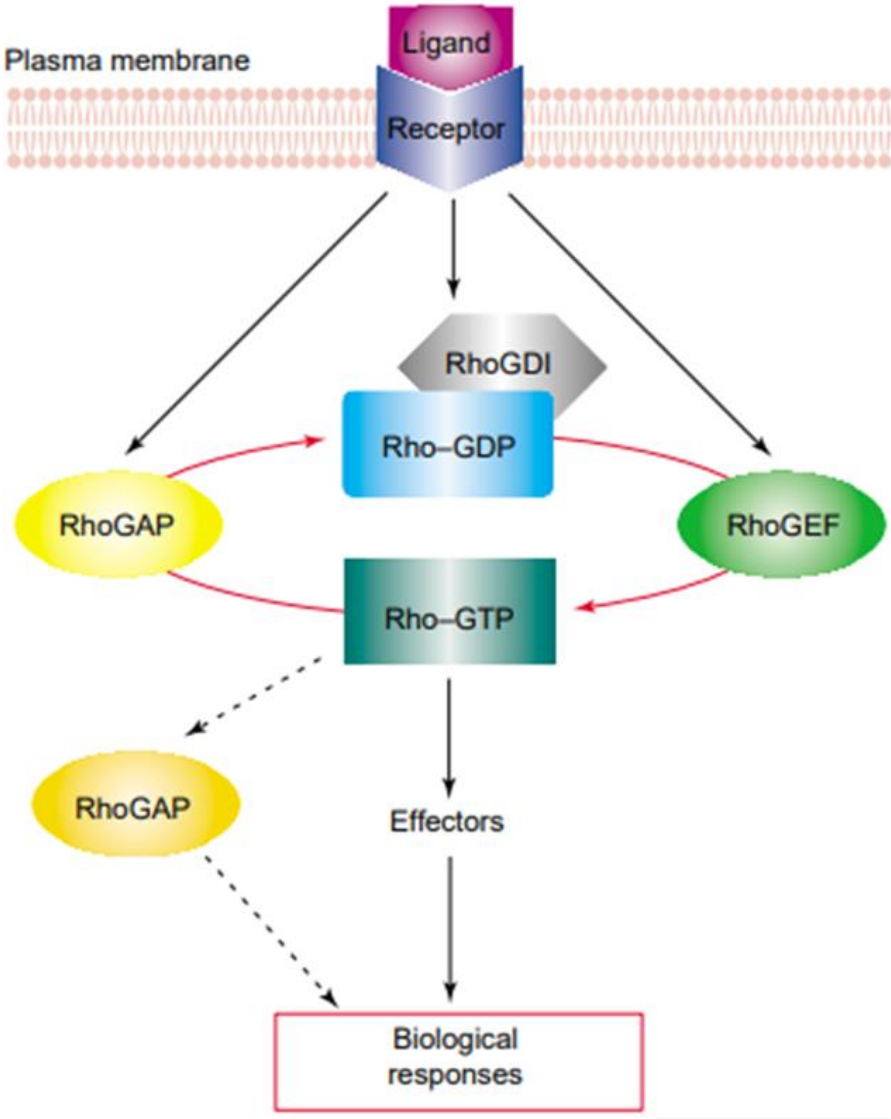

Figure 3.1: Rho GTPases activation-inactivation model. Schematic representation of the switch between the GTP-active form and the GDP-inactive form which is regulated by guanine exchange factors (GEFs), GTPase-activating proteins (GAPs) and guanine nucleotide dissociation inhibitors (GDIs). Taken from (Moon and Zheng 2003).

All RhoGEF proteins share the same structural features with Dbl homology (DH) and Pleckstrin Homology (PH) domains being the elements required for GEF catalytic activity and membrane interaction, respectively. A subfamily of RhoGEFs also possess a Regulator of G protein signalling (RGS) domain that is important in enhancing the GTPase activity of Gα subunit of G-protein coupled receptors to modulate their activity. In humans, there are three RGS-containing RhoGEFs which are PDZ-RhoGEF (also known as RhoGEF11 or ARHGEF11), Leukaemia-associated RhoGEF (LARG) and p115 RhoGEF (Banerjee and Wedegaertner 2004). The p115-RhoGEF is the most studied member of the RGS-containing RhoGEFs and has been identified for its major role in linking heterodimeric G protein α subunit signalling to Rho activation (Hart et al. 1998).

3.1.2 **PDZ-RhoGEF structure**

PDZ-RhoGEF is a protein of 1522 amino acids in length which contains highly conserved structural and functional domains (**Fig 3.2**). In addition to DH and PH domains, PDZ-RhoGEF possesses an N-terminal PDZ domain that is also found within LARG, but not p115 RhoGEF (**Fig. 3.2**). The PDZ domain is named after the first three proteins in which it was identified: **P**DS95, **D**lgA and **Z**O-1 and it serves as an important protein-protein interaction module. The PDZ domain typically binds to a PDZ interaction motif found, in most instances, at the C- terminus of the interacting protein. Type I domains recognize the sequence, X-S/T-X-Φ-COOH, Type II domains recognize the sequence X-Φ-X-Φ-COOH and Type III domains recognize C-termini with the sequence, X-X-C-COOH (where X is any amino acid and Φ is a hydrophobic residue); PDZ-RhoGEF is a Type I PDZ-containing protein (Fukuhara, Murga et al. 1999, Banerjee and Wedegaertner 2004; Woods and Bryant 1991, Cho et al. 1992,

Itoh et al. 1993). The PDZ domain of PDZ-RhoGEF has been shown to regulate actin cytoskeleton re-arrangements. As such, Plexin B transmembrane receptors interact with the PDZ domain of PDZ-RhoGEF in order to activate Rho and induce sphingosine 1-phosphate-dependent stress fibre formation and cell contraction/rounding (Driessens et al. 2002; Oinuma et al. 2003). PDZ-RhoGEF and the related RhoGEF, LARG have also found to regulate ligand-induced axonal growth through their PDZ domains, such that they mediate the NGF and semaphorin 4D –dependent activation of Rho A, respectively (Swiercz et al. 2002; Swiercz et al. 2009).

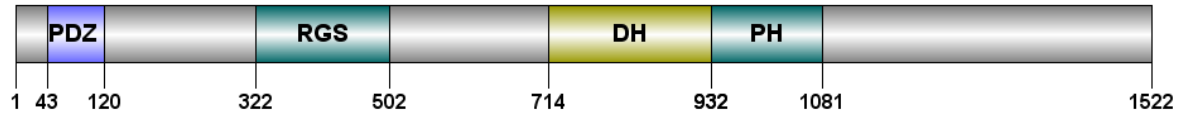

Figure 3.2: PDZ-RhoGEF structure. Schematic representation of PDZ-RhoGEF. The DH domain is responsible for GEF catalytic activity, PH domain controls PDZ-RhoGEF interaction with GPCR subunits and the plasma membrane, whilst the PDZ domain important for protein-protein interactions.

Previous unpublished, mass spectrometric interactomic studies from our laboratory using the E2-conjugating enzyme, UbcH10 as bait identified a large number of UbcH10-interacting proteins in both RPE-1 and HeLa cells. Of these, PDZ-RhoGEF had the best sequence coverage in both cell lines (Jessica Foster, PhD thesis, University of Birmingham, 2018). This study also indicated that the levels of PDZ-RhoGEF were low in early mitosis, however the molecular relationship between PDZ-RhoGEF, UbcH10 and the APC/C was not studied in any detail. Given that UbcH10 functions in mitosis in conjunction with the APC/C these data suggested that PDZ-RhoGEF might modulate mitotic entry and/or progression and be a target for APC/C targeted E3 ubiquitin ligase activity. As such, the principle aims of the study presented herein were to:

1. Generate a new anti PDZ-RhoGEF antibody for use in IP and WB studies.
2. Investigate further the levels of the PDZ-RhoGEF protein in mitosis and determine the role of PDZ-RhoGEF PTMs in mitosis.
3. Determine the relationship between UbcH10, the APC/C and APC/C coactivators and PDZ-RhoGEF at the molecular level.
4. Determine the effects of PDZ-RhoGEF silencing on mitotic entry and progression.

Results of these studies are presented below.

3.2 Results

3.2.1 Generation of GST-tagged PDZ-RhoGEF fragments

In order to create a new a-PDZ-RhoGEF antibody and study the biochemical interactions between PDZ-RhoGEF and UbcH10, GST-tagged PDZ-RhoGEF fragments that covered the entire PDZ-RhoGEF open reading frame were initially generated (**Fig. 3.3 A**). To ensure that the fragments were generated with intact secondary structure the PDZ-RhoGEF sequence was interrogated using JPred (a secondary structure prediction programme, www.compbio.dundee.ac.uk/jpred) to ensure that the fragments were generated with intact secondary structure (data not shown). Appropriate DNA fragments were generated by PCR using full-length PDZ-RhoGEF cDNA as a template and cloned into the bacterial expression vector PGEX-4T-1 in order to generate recombinant GST-PDZ-RhoGEF fusion proteins (see section 2.3.7). After validation of DNA sequences (see section 2.5.5) pGEX-4T-1 constructs containing PDZ-RhoGEF fragments were used to transform the protease-deficient bacterial strain BL21. Protein expression and GST purification was then performed as described (see section 2.3.7) after which GST-PDZ-RhoGEF fragments were seperated by SDS-PAGE and analysed by Coomassie blue staining (**Fig. 3.3 B**). Coomassie staining revealed that in most instances the most abundant protein band corresponded to the expected size of the GST-PDZ-RhoGEF fusion protein, except fragment 3, in which a truncated species was the most abundant (**Fig. 3.3 B**). Taken together, these data indicated that GST-fusion proteins corresponding to the entire open reading frame of PDZ-RhoGEF were successfully cloned and expressed.

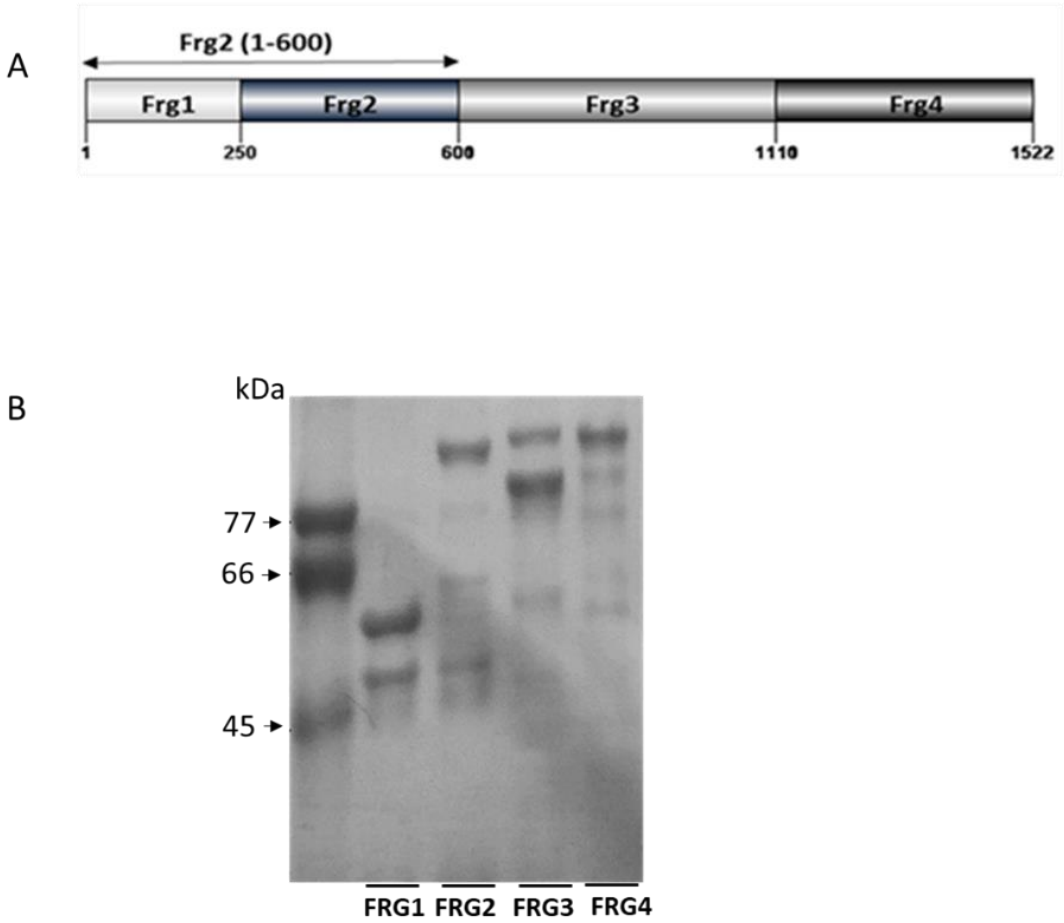

Figure 3.3: Expression of GST-PDZ-RhoGEF protein fragments. (A) Schematic representation of PDZ-RhoGEF fragment coverage. (B) PDZ-RhoGEF fragments were expressed in BL21, purified using glutathione agarose and quantified by Bradford assay. 20 µg of GST-PDZ-RhoGEF fragments 1, 2, 3 and 4 were separated on SDS-PAGE and stained with Coomassie blue.

3.2.2 Generation and validation of a new rabbit anti-PDZ-RhoGEF polyclonal antibody

Previous work in our laboratory found that the only commercially available polyclonal anti-PDZ-RhoGEF antibody at the time, although clean, was expensive and had low avidity for its antigen in both WB and IP. Therefore, Eurogentec was employed to generate a new polyclonal antibody using GST-PDZ-RhoGEF fragment 2 as an antigen (**Fig. 3.3 B**) using their 87-day immunisation programme. The final-bleed serum was first cleaned by incubation with GST-loaded agarose beads to remove anti-GST antibodies and then incubated with protein G Sepharose to purify PDZ-RhoGEF IgG which was then dialysed extensively against PBS. WB analysis with this antibody

recognised one major protein band from a number of different human cell lines at molecular weight of approximately 180kDa (**Fig. 3.4 A**). To validate that the protein band identified was PDZ-RhoGEF, RPE-1 cells were transfected with non-silencing control siRNA or PDZ-RhoGEF siRNA and subjected cell lysates, taken at 48 h and 72 h post-transfection, to WB analysis with the new anti PDZ-RhoGEF antibody. Significantly, when PDZ-RhoGEF expression was reduced by knockdown, the ability of the antibody to recognise the reactive protein band was similarly reduced, indicating that the new antibody was specific for PDZ-RhoGEF (**Fig. 3.4 B**).

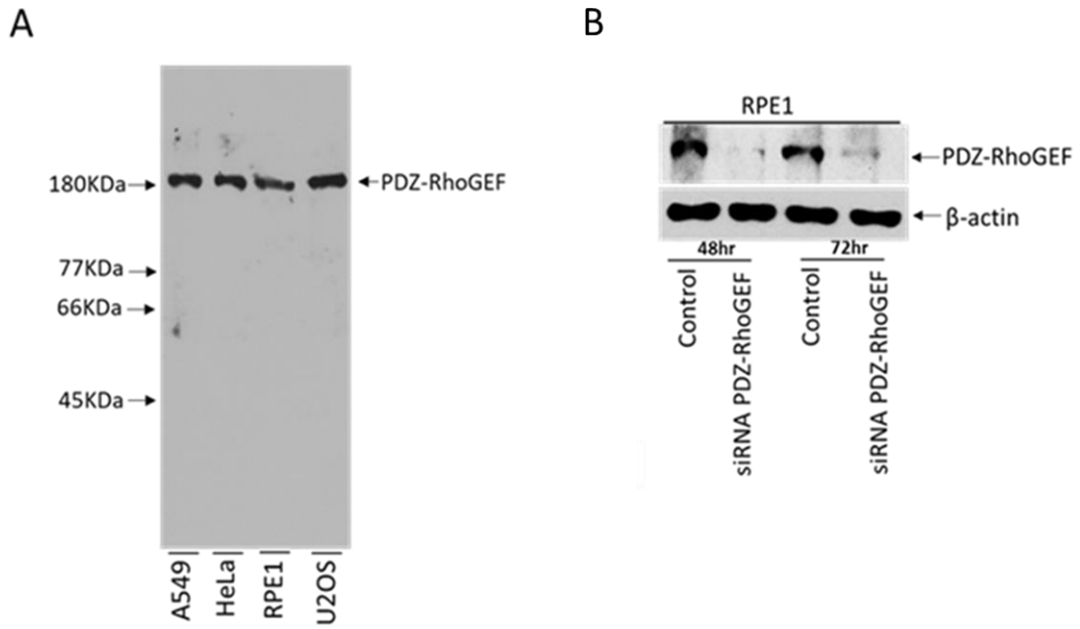

Figure 3.4: Validation of the new rabbit polyclonal anti-PDZ-RhoGEF antibody. (A) GST-PDZ-RhoGEF fragment 2 was used to make a new polyclonal antibody, which after purification was used to analyse PDZ-RhoGEF protein levels from different human cell lines. (B) siRNA validation of the anti-PDZ-RhoGEF antibody. RPE1 cells were transfected with either non-silencing control siRNA, or siRNA specific for PDZ-RhoGEF; cells were harvested at 48- and 72-hours post transfection and analysed by WB. Results taken from one experiment, representative of two other identical experiments.

3.2.3 Validation of PDZ-RhoGEF antibody for immunoprecipitation and PDZ-RhoGEF as a UbcH10-interacting protein

To validate the new anti PDZ-RhoGEF antibody for IP, series of IPs with both IgG control and the anti-PDZ-RhoGEF antibody were performed. Using RPE-1 and U2OS

cells, and analysed the IPs by WB. The immunoblot revealed that the PDZ-RhoGEF antibody worked well for IPs but that it was not able to co-precipitate UbcH10 (**Fig. 3.5 A**). Potential explanations for the inability of the anti-PDZ-RhoGEF antibody to co-precipitate UbcH10 will be considered in the discussion. Consistent with earlier studies (Jessica Foster, PhD thesis, University of Birmingham, 2018) reciprocal IP with an anti-UbcH10 antibody revealed that PDZ-RhoGEF co-immunoprecipetated with UbcH10 indicating that these two proteins interact *in vivo* (**Fig 3.5 B**).

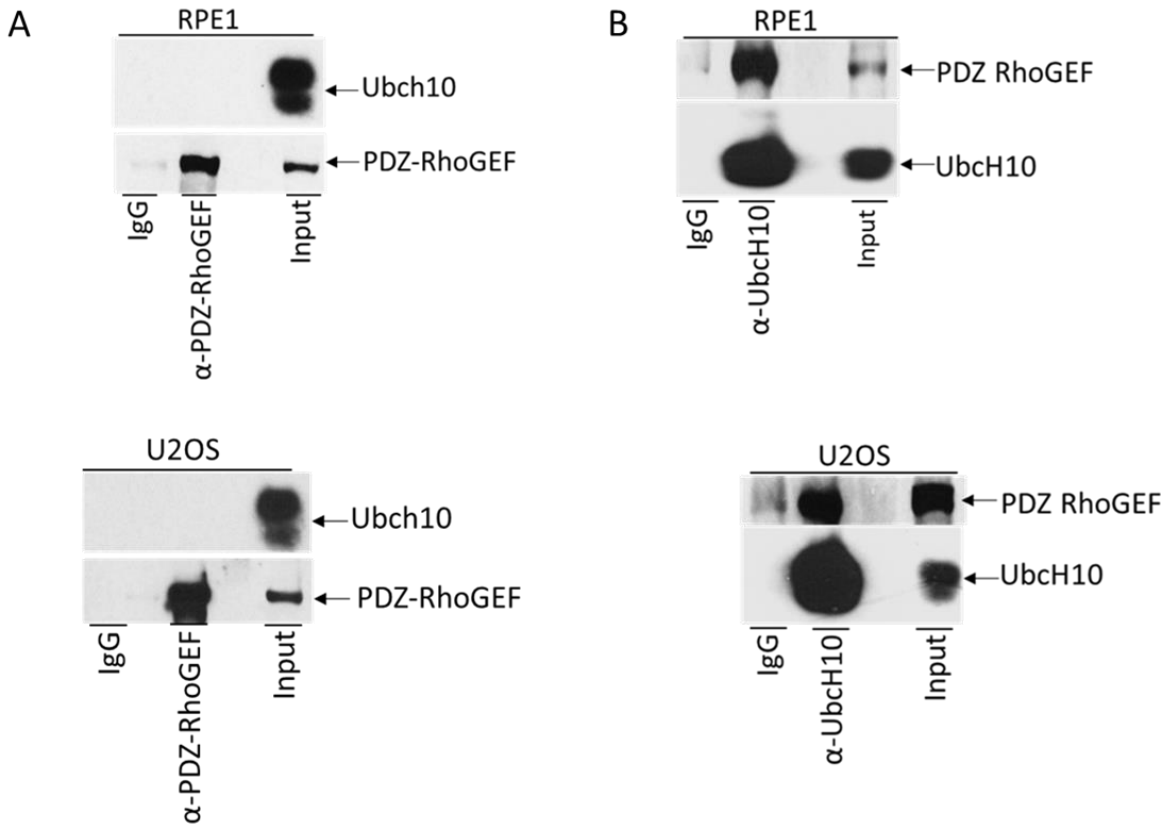

Figure 3.5: PDZ-RhoGEF is a UbcH10-interacting protein. RPE-1 and U2OS cells were used to test the ability of the newly-generated anti-PDZ-RhoGEF antibody to work in IP (A) and the ability of UbcH10 to interact with PDZ-RhoGEF *in vivo*. (B) Cells were harvested in NETN lysis buffer and subjected to IP with rabbit IgG, anti-PDZ-RhoGEF antibody, or anti-UbcH10 antibody and protein G Sepharose isolation. Immunoprecipitated proteins and 50 µg of the total protein lysate were separated by SDS-PAGE and analysed by WB. Results taken from one experiment, representative of two other identical experiments.

3.2.4 **PDZ-RhoGEF is post-translationally modified in early mitosis**

Previous studies from our laboratory have indicated that the protein levels of PDZ-RhoGEF are low in nocodazole-arrested mitotic cells, suggesting that it might be a target for APC/C-directed ubiquitylation and proteasome-mediated degradation during early mitosis. To establish whether the new anti-PDZ-RhoGEF antibody similarly showed a reduction in PDZ-RhoGEF protein levels in mitosis, PDZ-RhoGEF levels during mitotic progression were then investigated by WB. RPE-1 and U2OS cells were therefore treated with nocodazole (a spindle polymerization inhibitor) to arrest the cells in prophase. Cells were then released from the mitotic block following nocodazole withdrawal and the addition of complete medium; cells were subsequently harvested at different time-points post-release and analysed by WB. Analyses revealed that both U2OS and RPE-1 cells had been successfully synchronised in mitosis as indicated by the hyperphosphorylation of APC3 and progressed through mitosis following nocodazole-withdrawal as APC3 became increasingly dephosphorylated (panel i, **Fig. 3.6**). In agreement with these observations, SAC-dependent substrates cyclin B1 and Geminin both accumulated in mitotic cells and, consistent with increased APC/C activity were reduced in levels following nocodazole-release (panels iv and v, **Fig. 3.6**). In contrast, the SAC-independent APC/C substrate, Nek2a, was degraded in early mitosis as indicated by reduced protein levels in mitotic cells compared to asynchronous cells (panel iii, **Fig. 3.6**). Likewise, PDZ-RhoGEF protein levels were very low in mitotically-arrested cells, in agreement with previous findings (Jessica Foster, PhD thesis, University of Birmingham, 2018). However, these analyses also revealed that PDZ-RhoGEF is likely to be subject to PTMs as indicted by the faint PDZ-RhoGEF protein band detected with reduced mobility in mitotically-arrested U2OS and RPE-1 cells, which had not been seen previously (panel ii, **Fig. 3.6**). Taken

together, these analyses confirm that PDZ-RhoGEF protein levels are low in early mitosis and, moreover suggest that PDZ-RhoGEF is subject to PTM in mitosis.

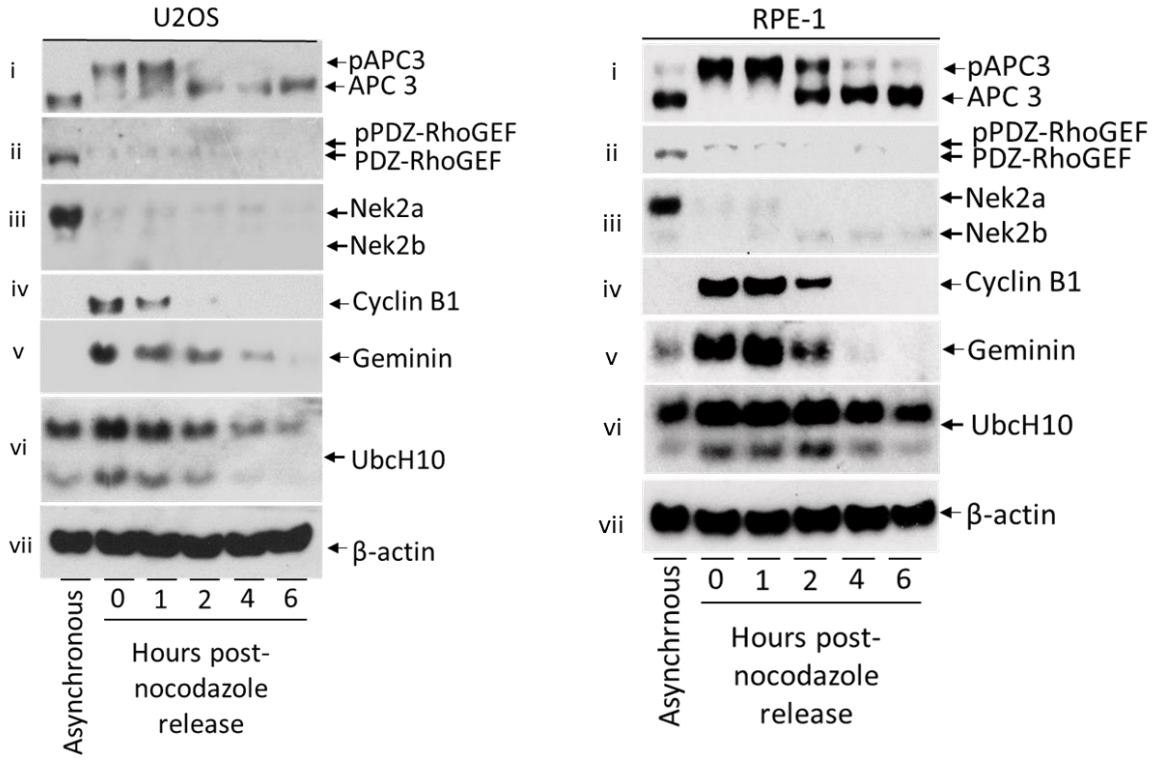

Figure 3.6: PDZ-RhoGEF is post-translationally modified in mitosis. RPE-1 and U2OS cells were arrested in mitosis with nocodazole. The cells were then released from the nocodazole block and harvested at different time-points. Lysates were then sonicated, and protein concentration was determined by Bradford assay. 50µg of total protein were separated by SDS-PAGE and the level of cellular proteins were analysed by WB. The blot shows that PDZ-RhoGEF is degraded akin to Nek2a in early mitosis and is, potentially, post-translationally modified in mitosis. Results taken from one experiment, representative of several identical experiments.

3.2.5 **PDZ-RhoGEF protein levels are reduced following mitotic entry**

Work presented above indicated that PDZ-RhoGEF protein levels were low in prophase, in the presence of nocodazole (**Fig. 3.6**). To extend these findings further and investigate the timing of PDZ-RhoGEF protein loss, the anti-PDZ-RhoGEF antibody was used to determine the effects of synchronising cells at the G2/M boundary with the cdk1 inhibitor, RO-3306 and the effects of SAC activation with the nocodazole, as before, but also the effects of treating cells with the spindle-depolymerization inhibitor, Taxol. RPE-1 cells were therefore synchronised at different

stages of cell cycle with these drugs. Treated cells were then harvested and subjected to WB analysis to investigate the level of PDZ-RhoGEF in these different stages of cell cycle (**Fig. 3.7**).

WB analyses suggested that the cells had been arrested successfully at different stages of the cell cycle as indicated by the hyperphosphorylation status of APC3 in mitotically-arrested cells, and the hypophosphorylation status of APC3 in asynchronous and RO-3306-treated cells (panel i, **Fig 3.7**). In agreement with these data the SAC-dependent APC/C substrates, cyclin B1 and Plk1 accumulated in mitotically-arrested cells when compared to asynchronous and RO-3306 treated cells (panels iii and iv, **Fig 3.7**). This experiment also confirmed that PDZ-RhoGEF protein levels were reduced substantially in both nocodazole- and Taxol- treated cells, whereas PDZ-RhoGEF protein levels were elevated in both asynchronous cells and cells treated with the cdk1 inhibitor, RO-3306 (panel ii, **Fig. 3.7**). Moreover, it was evident that PDZ-RhoGEF was not phosphorylated in cells treated with the cdk1 inhibitor (cf lanes 1 and 2, panel ii, **Fig. 3.7**). Interestingly, the PDZ-RhoGEF expression pattern matched the expression pattern of the well-known early APC/C substrate, Nek2a which is degraded independently of SAC (panel v, **Fig. 3.7**). Together, these data suggest that PDZ-RhoGEF might be an APC/C substrate that is degraded early in mitosis in a SAC-Insensitive manner and that PDZ-RhoGEF is post-translationally modified, specifically in mitosis. Studies with the spindle-depolymerisation inhibitor, Taxol also revealed that PDZ-RhoGEF protein levels in mitosis are not reduced due to the loss of the mitotic spindle.

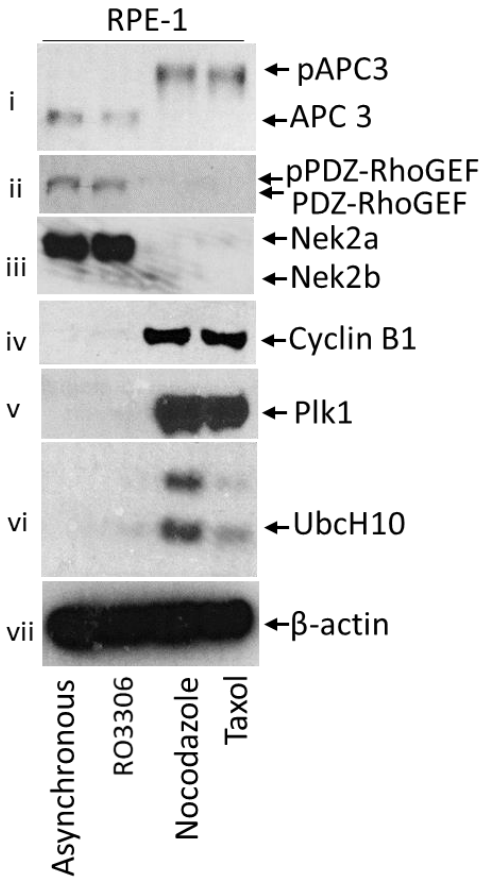

Figure 3.7: PDZ-RhoGEF is expressed at low levels in early mitosis akin to SAC-Independent APC/C substrates. RPE-1 cells were treated with different drugs to arrest the cells at different stages of cell cycle. Cells were harvested in UTB lysis buffer, sonicated, and protein concentration was determined by Bradford assay. 50µg of total protein were separated by SDS-PAGE and the level of cellular proteins were analysed by WB. Results taken from one experiment, representative of several identical experiments.

3.2.6 PDZ-RhoGEF is stabilized following 26S proteasome inhibition

As the experiments performed thus far indicate that PDZ-RhoGEF protein levels mirror those of Nek2a, a known APC/C substrate in early mitosis, the next aim was to investigate whether PDZ-RhoGEF was subjected to 26S proteasome-targeted degradation in mitosis. To investigate this possibility RPE-1 cells were arrested in mitosis by nocodazole treatment, and subsequently treated with 26S proteasomal inhibitors, MG132 or Salinosporamide A (SAL A), in an attempt to stabilize PDZ-RhoGEF levels. Following treatment with these inhibitors PDZ-RhoGEF levels were analyzed by WB (**Fig 3.8**). Consistent with cells being arrested in mitosis APC3 was

hyperphosphorylated in mitosis in the absence, or presence of the proteasome inhibitors (panel i, **Fig 3.8**). In agreement with these observations SAC-sensitive substrates cyclin B1 and Plk1 were stable throughout the time course of the experiment and not affected by the addition of the proteasome inhibitors, whilst the SAC insensitive substrates, cyclin A and Nek2a were stabilised upon the addition of either MG132 or SALA (panels iii-vi, respectively, **Fig 3.8**). Akin to cyclin A and Nek2a, the levels of PDZ-RhoGEF were stabilized upon the addition of the proteasome inhibitors, MG132 or SAL A, although SAL A required 4h to restore PDZ-RhoGEF protein levels fully in mitosis (panel ii, **Fig 3.8**). Taken together, these data suggest that PDZ-RhoGEF is subject to 26S proteasomal degradation during early mitosis. Moreover, upon proteasomal inhibition PDZ-RhoGEF is maintained in its PTM form (panel ii, **Fig 3.8**).

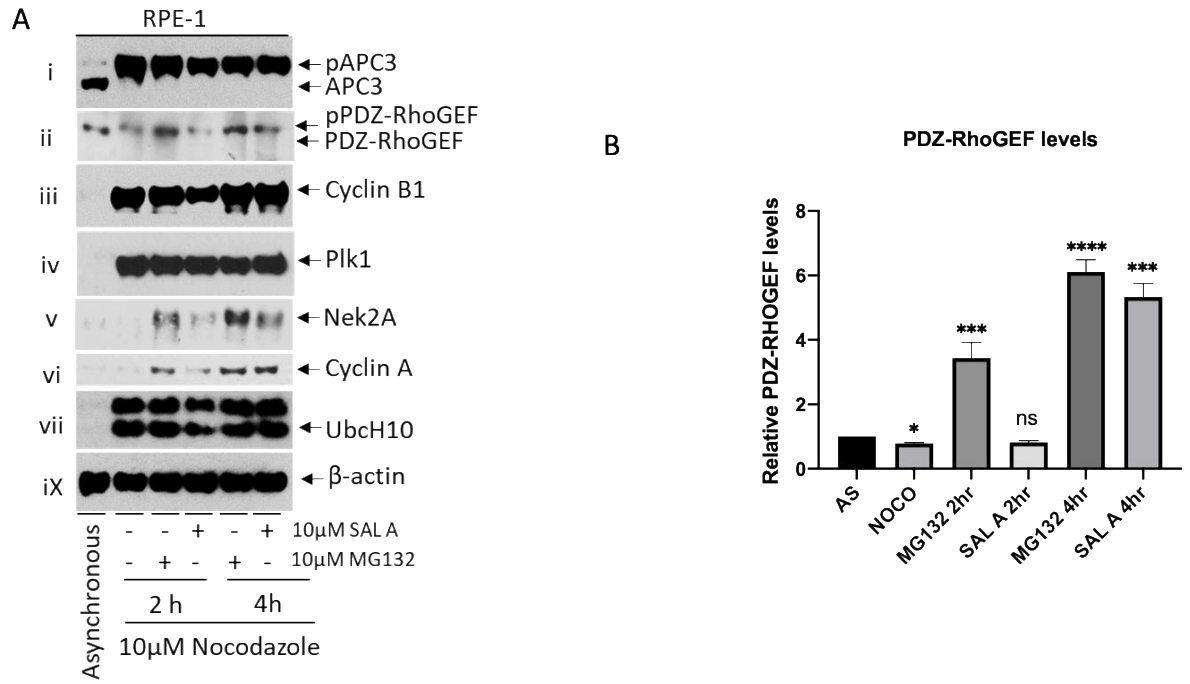

Figure 3.8: Proteasomal inhibition stabilizes PDZ-RhoGEF protein levels in mitotically-arrested cells. Mitotically-arrested cells isolated by mechanical shake-off were treated with proteasomal inhibitors MG132 and SAL A for 2 and 4 h, respectively. Cells were subsequently harvested in UTB lysis buffer and processed for analysis. 50μg of total protein samples were separated by SDS-PAGE and the levels of key cellular proteins were investigated by WB. Results taken from one experiment, representative of two other identical experiments. B) Using ImageJ, the band densities of PDZ-RhoGEF were measured and normalised to the β-actin loading control. Protein levels of the normalised band densities were calculated and are presented as a bar-graph showing the mean reading +/- Standard Deviation where (*) $P \leq 0.05$, (**) $P \leq 0.01$, (***) $P \leq 0.001$ and (****) $P \leq 0.0001$ (N=3).

3.2.7 **UbcH10 overexpression promotes PDZ-RhoGEF degradation in mitosis**

UbcH10 is a specific E2-conjugating enzyme for the APC/C whose overexpression causes the inappropriate activation of the APC/C in mitosis, resulting in the premature degradation of APC/C substrates (Van Ree et al. 2010). A Tetracycline/doxycycline-inducible UbcH10-HA Flp-In U2OS cell line that had been generated previously in Tarnell's laboratory to investigate UbcH10 function (Jessica Foster, PhD thesis, University of Birmingham). To investigate whether UbcH10-HA overexpression affected the protein levels of PDZ-RhoGEF, WT UbcH10-HA Flp-In U2OS cells (+/- Doxycycline) were arrested in mitosis with nocodazole and determined the rate of PDZ-RhoGEF and APC/C substrate degradation +/- UbcH10-HA following nocodazole

withdrawal. WB analyses revealed that the rate of degradation of SAC-sensitive substrates cyclin B1 and Plk1 were moderately faster following the over-expression of UbcH10-HA, which was most noticeable at 2 h post-nocodazole withdrawal (cf lanes 4 and 10, panels iv and v, **Fig. 3.9**). Examination of PDZ-RhoGEF levels following nocodazole release suggested that UbcH10-HA overexpression did enhance PDZ-RhoGEF protein loss, relative to cells where UbcH10-HA expression was not induced (cf lanes 2-6 with lane 8-12, panel ii, **Fig. 3.9**). These data suggest that the overexpression of UbcH10 does enhance the degradation of known APC/C substrates such as cyclin B1 and Plk1, but also suggests that PDZ-RhoGEF is also a potential APC/C substrate as protein levels were lower following nocodazole withdrawal in UbcH10-HA overexpressing cells, relative to cells where UbcH10 is not over-expressed.

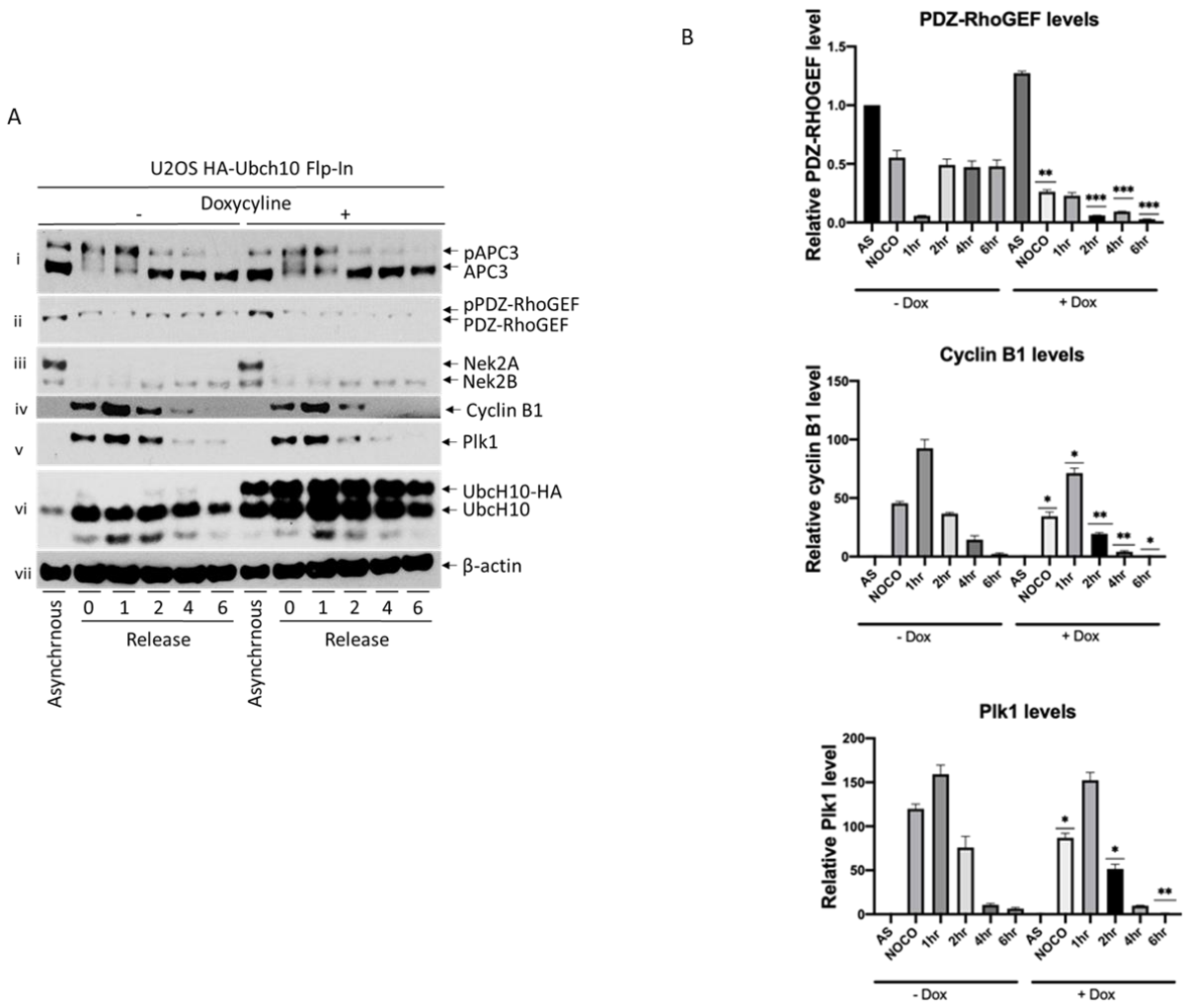

Figure 3.9: UbcH10 overexpression promotes the degradation of PDZ-RhoGEF. Mitotically-arrested doxycycline-inducible UbcH10-HA Flp-In U2OS cells (+/- Dox) were released back into mitosis following nocodazole withdrawal and harvested at different time points post-release. Lysates were processed for analysis by SDS-PAGE and WB. 50µg protein samples were separated by SDS-PAGE and the level of key cellular proteins were analysed by WB for the indicated proteins. The blot shows that PDZ-RhoGEF degradation is enhanced following UbcH10 overexpression. Results taken from one experiment, representative of two other identical experiments. B) Using ImageJ, the band densities of PDZ-RhoGEF, Cyclin B1 and PLK1 in both (+/-) Dox U2OS HA UcH10 cells were measured and normalised to the β-actin loading control. Protein levels of the normalised band densities were calculated and are presented as a bar-graph showing the mean reading +/- Standard Deviation where (*) $P \leq 0.05$, (**) $P \leq 0.01$, (***) $P \leq 0.001$ and (****) $P \leq 0.0001$ indicated significant differences between – Dox and, corresponding + Dox sample (N=3).

3.2.8 **PDZ-RhoGEF knockdown affects APC/C activity**

As PDZ-RhoGEF is targeted for proteasomal degradation early in mitosis it is likely that inappropriate expression of PDZ-RhoGEF during mitosis might affect the normal timing of mitotic progression. Indeed, it has been suggested previously that the APC/C

substrate, 53BP1 is also an APC/C inhibitor, such that 53BP1 knockdown enhances APC/C activity and promotes the premature degradation of other APC/C substrates (Kucharski et al. 2017). Moreover, as previously discussed UbcH10 overexpression enhances APC/C activity, whilst the N-terminal region of UbcH10 negatively regulates APC/C activity (Summers, et al. 2008). Therefore, PDZ-RhoGEF knockdown might also affect APC/C activity. To investigate this possibility PDZ-RhoGEF expression was reduced in interphase RPE-1 cells by transfecting cells with siRNA directed against PDZ-RhoGEF or a non-silencing siRNA control. The cells were then harvested at 48 h and 72 h and analysed by WB to determine whether PDZ-RhoGEF knockdown affected APC/C substrate degradation. WB analyses revealed that PDZ-RhoGEF knockdown was successful as indicated by the loss of PDZ-RhoGEF immunoreactive signal in cells treated with PDZ-RhoGEF siRNA, relative to control cells (panel ii, **Fig. 3.10**). Interestingly, PDZ-RhoGEF knockdown also affected APC/C activity against other substrates, such that PDZ-RhoGEF knockdown reduced the levels of both SAC-insensitive substrates, Nek2a and cyclin A (panels ii and iii, **Fig. 3.10**) as well as SAC-sensitive substrates, Geminin, Plk1, cyclin B1 and UbcH10 (panels iv-vii, respectively, **Fig. 3.10**). These data suggest that PDZ-RhoGEF knockdown enhances APC/C activity towards its substrates. The molecular explanation for this will be considered in the discussion.

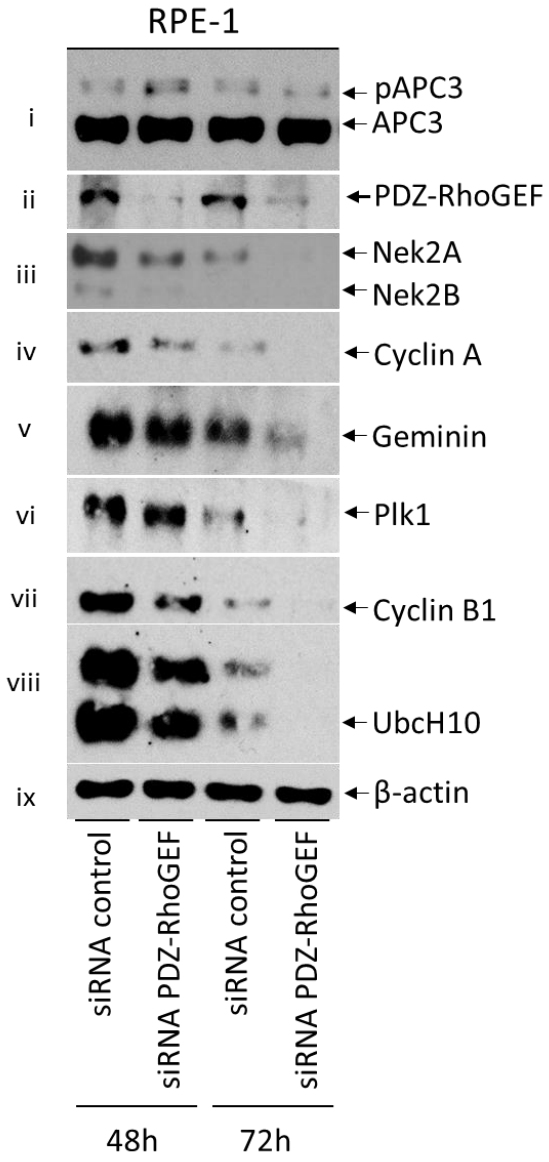

Figure 3.10: PDZ-RhoGEF knockdown reduces the protein levels of APC/C substrates. RPE-1 cells were transfected with both siRNA control oligonucleotides and siRNA oligonucleotides targeted against PDZ-RhoGEF and harvested at 48 h and 72 h post-treatment. Lysates were processed for analysis by SDS-PAGE and WB. 50µg protein samples were separated on SDS-PAGE and the level of key APC/C substrates were analysed by WB for the indicated proteins. Results taken from one experiment, representative of two other identical experiments.

3.2.9 **PDZ-RhoGEF is phosphorylated in mitosis**

Data presented earlier suggested that PDZ-RhoGEF is subject to PTM in mitotically-arrested cells (see **Fig. 3.6**). Given these findings it was important to determine, in the first instance whether PDZ-RhoGEF was subject to PTM in mitosis. As phosphorylation is the most common PTM in mitosis, is known to affect APC/C activity

and the recruitment of some substrates to the APC/C, as well as resulting in the reduced mobility of some proteins on SDS-PAGE, to investigate whether PDZ-RhoGEF was phosphorylated in mitosis. PDZ-RhoGEF was isolated from mitotic cells by IP and subject IP's to treatment with λ-protein phosphatase, a broad-range phosphatase that dephosphorylates non-specifically all phosphorylation sites (i.e. S, T and Y) in a target protein (Mackiewicz et al. 2020). To do this, RPE-1 cells were treated +/- nocodazole and subsequently subjected to IP with both rabbit IgG and rabbit anti-PDZ-RhoGEF antibodies. IPs were then treated with λ-protein phosphatase and subjected to WB analyses to establish whether PDZ-RhoGEF is phosphorylated in mitosis (**Fig 3.11**). WB results indicated that PDZ-RhoGEF protein levels were reduced in mitotic cells compared to asynchronous cells as well as being post-translationally modified (cf lane 4 and 6, **Fig. 3.11**). Significantly, treatment of anti-PDZ-RhoGEF IPs from mitotic cells with λ-protein phosphatase reduced the apparent molecular weight of PDZ-RhoGEF to that of PDZ-RhoGEF in asynchronous cells (cf lanes 4-6, **Fig. 3.11**). Taken together, these data indicate that PDZ-RhoGEF is phosphorylated in mitosis.

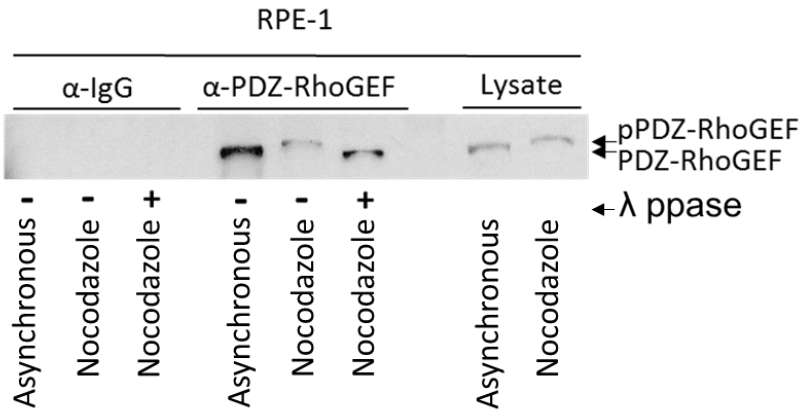

Figure 3.11: PDZ-RhoGEF is phosphorylated in mitosis. RPE-1 cells (+/- nocodazole) cells were subject to IP with α- PDZ-RhoGEF antibodies or with mouse α-IgG overnight at 4°C followed by 3 h incubation with protein G Sepharose at 4°C. IPs were then treated with λ-protein phosphatase (λ PPase) at 30°C for 1 h. IPs and 50μg protein lysate were then separated by SDS-PAGE and analysed by WB for PDZ-RhoGEF. Results taken from one experiment, representative of two other identical experiments.

3.2.10 Mass spectrometric determination of mitotic PDZ-RhoGEF phosphorylation sites

As have been shown that PDZ-RhoGEF is phosphorylated in mitosis, the next aim was to identify mitosis-specific phosphorylation sites in PDZ-RhoGEF. In order to do this, IP coupled to mass spectrometric analysis was performed. Therefore treated RPE-1 cells +/- nocodazole and isolated PDZ-RhoGEF by IP with the anti-PDZ-RhoGEF antibody and then subjected IPs to SDS-PAGE. Gel slices corresponding to the molecular weight of PDZ-RhoGEF were then processed for in gel tryptic digestion and mass spectrometric analysis (see section 2.4.1). Peptides were analysed using a Q ExactiveTM HF hybrid Quadrupole-Orbitrab TM Mass spectrometer (Mass spectrometry facility, The School of Biosciences, The University of Birmingham). Identified PDZ-RhoGEF phosphopeptides from asynchronous and nocodazole cells were compared to generate a list of mitosis-specific phosphorylation sites for PDZ-RhoGEF in mitosis (Tables 3.1 and 3.2). The mass spectrometry data revealed that PDZ-RhoGEF was heavily phosphorylated in both interphase and mitosis. The data also revealed that PDZ-RhoGEF was phosphorylated upon 7 distinct sites, exclusively during mitosis, 3 of which were consensus Cdk1 sites; Rho kinase, PKC, Casein Kinase and ATM kinase consensus phosphorylation sites were also identified as being mitosis-specific (**Fig 3.12**).

Table 3-1 PDZ-RhoGEF phosphorylation sites in asynchronous and mitotic cells. RPE-1 cells (+/- nocodazole) were subjected to IP with an anti-PDZ-RhoGEF antibody and then separated by SDS-PAGE and processed for analysis by mass spectrometry. Peptides were identified using SEQUEST.

Asynchronous		Mitosis	
Sequence	**Residue**	**Sequence**	**Residue**
NSVLSDPGLDSPRTSPVIMAR	S255	SSSQSTFHIPLSPVEVKPGNVR	S556
SLENPTPPFTPK	T272	FPSLSESLMNR	S232
HQVLLEDPEQEGSAEE	S1115	TRNSGIWESPELDR	S1295
SSSQSTFHIPLSPVEVKPGNVR	S556	SLGGESSGGTTPVGSFHTEAAR	S1452
SRSDVDMDAAAEATR	S632	KSPSHHRQPSDASETTGLVQR	S27
WTDGSLSPPAKEPLASDSR	S1489	SPPSLALR	S1414
LSTGSFPEDLLESDSSR	S603	SLENPTPPFTPK	T272
TRNSGIWESPELDR	S1295	LHQSASSSTSSLSTR	S594, S597
LHQSASSSTSSLSTR	S594, S597	SRSDVDMDAAAEATR	S632
SLGGESSGGTTPVGSFHTEAAR	S1452	LSTGSFPEDLLESDSSR	S603
NSVLSDPGLDSPRTSPVIMAR	S255	NSHELGPCPEDGSDAPLEDSTADAAASPGP	S1518
		TAVGSSDSKQTFSPVLK	S1030
		WTDGSLSPPAKEPLASDSR	S1489
		LSLDSQEGDSGLDSGTER	S215
		NSVLSDPGLDSPR	S255
		HQVLLEDPEQEGSAEEEELGVLP	S1115

Table 3-2: PDZ-RhoGEF sites phosphorylated exclusively in mitosis. Table illustrates those phosphopeptides identified in both asynchronous and mitotic cells, showing the 7 PDZ-RhoGEF phosphorylation sites identified as specifically occurring in mitosis. Xcorr = cross correlation value with other peptides (score > 2, high confidence, though smaller peptides might have Xcorr values lower than 2); Percolator q-Value =the minimum false discovery rate (score of < 0.01, high confidence).

Mitosis-specific phosphorylation sites	**XCorr**	**Percolator q-Value**	**Residue**	**kinase**
NSHELGPCPEDGSDAPLEDSTADAAASPGP	2.73	0	S1518	CDK1
TAVGSSDSKQTFSPVLK	2.86	0	S1030	ROK
LSLDSQEGDSGLDSGTER	2.58	0	S215	ATM/ATR
SPPSLALR	1.89	0	S1414	CDK1
FPSLSESLMNR	2.8	0	S232	PKC
KSPSHHRQPSDASETTGLVQR	1.67	0	S27	CDK1
EPAQQGPTPSRVELDDSDVFHGEPEPEELPGGTGSQQR	2.96	0	S1117	CK

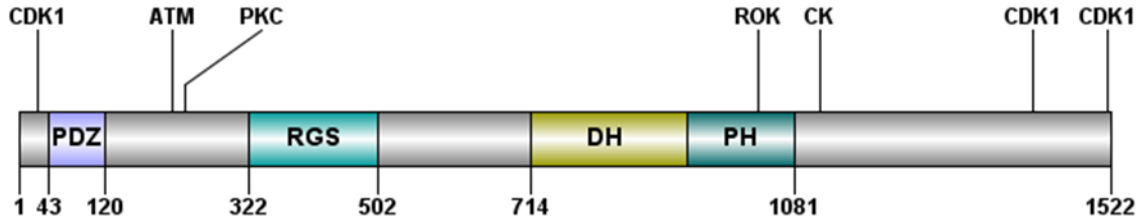

Figure 3.12: Phosphorylation sites on PDZ-RhoGEF identified by mass spectrometry. Schematic illustration of the mitotic-specific phosphorylation sites in the context of the whole PDZ-RhoGEF primary sequence detailing kinases responsible for phosphorylation.

3.2.11 **Cdk1 is required for PDZ-RhoGEF phosphorylation in mitosis**

As mentioned in section 1.4.5, the APC/C is regulated in mitosis by a multi-layered regulatory system that constitutes APC/C coactivators, the SAC and PTMs. Cdk1, Plk1 and Aurora B are the principal mitotic kinases that contribute towards the timely regulation of mitotic events. For example, Cyclin B1-Cdk1 phosphorylates APC/C subunits that allows for Cdc20 recruitment to the APC/C. The degradation of cyclin B1 by APC/C-Cdc20 and APC/C-Cdh1 results in the inhibition of Cdk1 activity and mitotic exit. Plk1 is also a key regulator of mitotic progression and plays central roles in mitotic entry, spindle assembly and cytokinesis, whilst Aurora B is required for chromosome segregation and cytokinesis (D'Avino and Capalbo 2016). Like cyclin B1, Plk1 and Aurora B are targeted for degradation by APC/C-Cdh1; there is also considerable cross-talk between each of these kinases. Given this findings that Cdk1 consensus phosphorylation sites in PDZ-RhoGEF are targeted for phosphorylation during mitosis, and the cross-talk between Cdk1, Plk1 and Aurora B, it was important to confirm that Cdk1 was responsible for PDZ-RhoGEF phosphorylation during this time and to also establish whether other mitotic kinases such as Plk1 and Aurora B contributed to PDZ-RhoGEF phosphorylation during mitosis. Moreover, as PDZ-RhoGEF is degraded in mitosis, it is possible that Cdk1 and other kinases might promote PDZ-RhoGEF

degradation through phosphorylation such that it was interesting to establish whether these mitotic kinases contributed towards PDZ-RhoGEF degradation.

To check the effect of Cdk1 inhibition on the phosphorylation status of PDZ-RhoGEF in mitosis RPE-1 cells were first arrested in mitosis with nocodazole and isolated mitotic cells by mechanical shake-off. Cells were then treated with RO-3306 to inhibit Cdk1 activity. However, as it is well known that the inhibition of Cdk1 by RO-3306 in mitotically-arrested cells causes mitotic slippage and mitotic exit it was necessary to add the proteasome inhibitor, MG132, to RO-3306-treated cells in order to prevent cyclin B1 degradation and mitotic exit. Inhibition of mitotic exit was necessary to avoid potential changes in cell cycle status that might impact upon PDZ-RhoGEF phosphorylation status.

WB analyses revealed that treatment of RPE-1 cells with RO-0336 alone in nocodazole-treated cells promoted mitotic exit as evidenced by the loss in cyclin B1 and Geminin protein levels (panels iv and v, **Fig. 3.13).** However, MG132 was able to prevent cyclin B1 and Geminin degradation, consistent with the cells still being in mitosis (cf lanes 3 and 4, and lanes 7 and 8, panels iv and v, **Fig. 3.13**). In this scenario the Cdk1-dependent phosphorylation of APC3 was also inhibited (cf lanes 2 and 4, and lanes 5 and 8, panel i, **Fig. 3.13**). Interestingly Cdk1 inhibition, in the context of MG132 treatment, led to a loss in PDZ-RhoGEF phosphorylation status and an increase in PDZ-RhoGEF levels (cf lane 2 with lane 4, and lane 5 with lane 7, panel ii, **Fig. 3.13**). Interestingly, treatment of RPE-1 cells with MG132 also rescued the protein levels of the SAC-insensitive APC/C substrate, Nek2a (cf lanes 3 and 4, and 7 and 8, panel iii, **Fig 3.13**). Taken together, these data suggest that PDZ-RhoGEF11 is a

target for Cdk1-directed phosphorylation in mitosis, and that phosphorylation might contribute towards the targeting of PDZ-RhoGEF for proteasomal degradation.

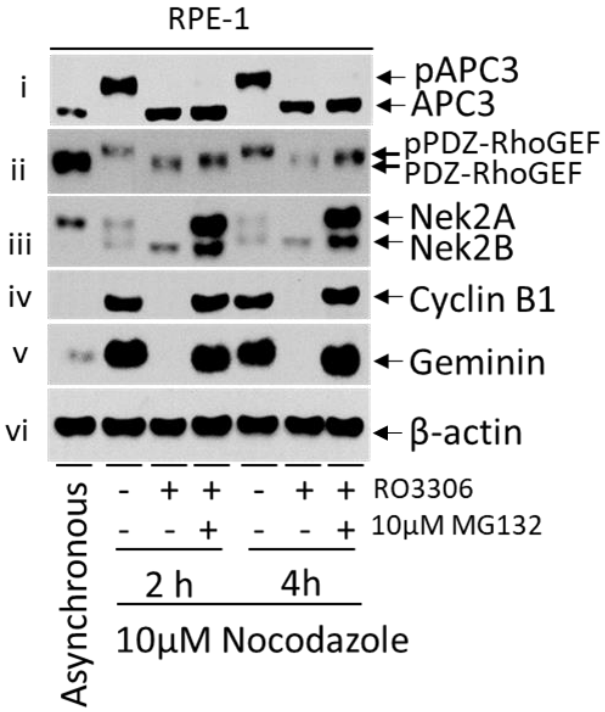

Figure 3.13: PDZ-RhoGEF is phosphorylated by Cdk1 in mitosis. RPE-1 cells were arrested in mitosis with nocodazole. Cdk1 inhibitor RO-3306 was then added to the cells to inhibit Cdk1 activity either in the absence, or presence of MG132, which inhibited mitotic exit. Cells were then harvested after 2 h and 4 h treatment; 50μg protein samples were separated by SDS-PAGE and the levels of key cell cycle proteins were analysed by WB. Results taken from one experiment, representative of two other identical experiments.

3.2.12 **Aurora B kinase is required for PDZ-RhoGEF phosphorylation in mitosis**

Although Cdk1 is the kinase most likely responsible for PDZ-RhoGEF targeted phosphorylation given the mass spectrometric data and the data presented in **Fig. 3.13**, given that Aurora B kinase is known to phosphorylate cyclin B1 and target it to the spindle midzone during anaphase (Afonso et al. 2019) it was considered that inhibition of Aurora B might also inhibit cyclin B1-Cdk1 activity and limit PDZ-RhoGEF phosphorylation in mitosis. In this context it is important to stress that inspection of the PDZ-RhoGEF sequence indicates that it does not possess any consensus Aurora B phosphorylation motifs inhibition on the phosphorylation status of PDZ-RhoGEF. To investigate this possibility, similar protocol to the one detailed for Cdk1 was used

(section 3.2.11). RPE-1 cells were first arrested in mitosis using nocodazole then isolated by mechanical shake-off and treated with the Aurora B inhibitor, Hesperidin +/- the proteasomal inhibitor MG132, to avoid mitotic slippage. Cells were then harvested at 2 and 4 hours post-treatment and analysed by WB for PDZ-RhoGEF and other key cell cycle proteins (**Fig 3.14**).

Results indicated that MG132 treatment prevented Hesperadin-induced mitotic slippage and mitotic exit as evidenced by the levels of cyclin B1 and Aurora B in these samples (cf lanes 3 and 4 and lanes 5 and 6, panels iv and vi, **Figure 3.14**). Interestingly, inhibition of Aurora B prevented the known cyclin B1-Cdk1 dependent phosphorylation of APC3 (panel i, **Fig. 3.14**) and similarly inhibited PDZ-RhoGEF phosphorylation (panel ii, **Fig. 3.14**). Moreover, prolonged treatment with MG132 stabilised PDZ-RhoGEF protein levels (panel ii, **Fig. 3.14**). Treatment of RPE-1 cells with MG132 also rescued the protein levels of the SAC-insensitive APC/C substrate, Nek2a (panel iii, **Fig 3.14**). Consistent with histone H3 S10 being an Aurora B target during mitosis, histone H3 S10 phosphorylation (pH-Ser10) was inhibited in the presence of Hesperadin (panel vii, **Fig 3.14**). Taken together, these data are highly supportive of the notion that Aurora B regulates the cyclin B1-Cdk1-targeted phosphorylation of PDZ-RhoGEF during mitosis.

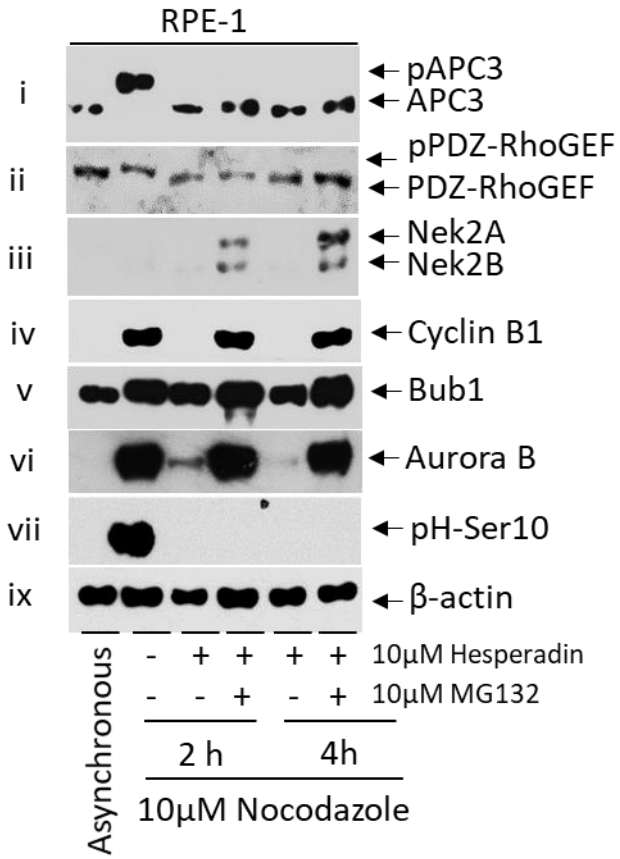

Figure 3.14: Aurora B kinase inhibition prevents PDZ-RhoGEF phosphorylation in mitosis. RPE-1 cell were arrested in mitosis by treating the cells with nocodazole. The cells were then isolated by mechanical shake-off and treated with the Aurora B kinase inhibitor, Hesperadin (+/-) MG132. The cells were then harvested at 2 and 4 h post-treatment. 50μg protein samples were separated by SDS-PAGE and the levels of key cell cycle proteins were analysed by WB. Results taken from one experiment, representative of two other identical experiments.

3.2.13 Plk1 is required for PDZ-RhoGEF phosphorylation in mitosis

As for Aurora B, there are no consensus Plk1 phosphorylation sites in PDZ-RhoGEF, though like Aurora B, Plk1 is known to modulate cyclin B1-Cdk1 activity; Plk1-directed phosphorylation of cyclin B1 targets it to the nucleus (Yuan et al. 2002). To investigate whether Plk1 participates in the phosphorylation of PDZ-RhoGEF the same protocol to the one detailed for Cdk1 and Aurora B was used (sections 3.2.11 and 3.2.12). RPE-1 cells were thus arrested in mitosis with nocodazole, isolated by mechanical shake-off and treated with the Plk1 inhibitor, BI-6727 +/- the proteasomal inhibitor MG132, to avoid mitotic slippage. Cells were then harvested at 2 and 4 hours post-

treatment and analysed by WB for PDZ-RhoGEF and other key cell cycle proteins (**Fig 3.15**). Results indicated that Plk1 inhibition does not cause mitotic slippage as evidenced by the stable levels of cyclin B1, Plk1 and phospho-histone H3 (pH-Ser10) in cells treated with Plk1 inhibitor alone (panels iv, v and vi, **Fig. 3.15**). PlK1 inhibition reduced modestly the cyclin B1-Cdk1-dependent phosphorylation of PDZ-RhoGEF and reduced PDZ-RhoGEF phosphorylation, particularly at 2 h post-treatment (panel ii, **Fig. 3.15**). Taken together, these results suggest that Plk1 might influence the phosphorylation of PDZ-RhoGEF in mitosis.

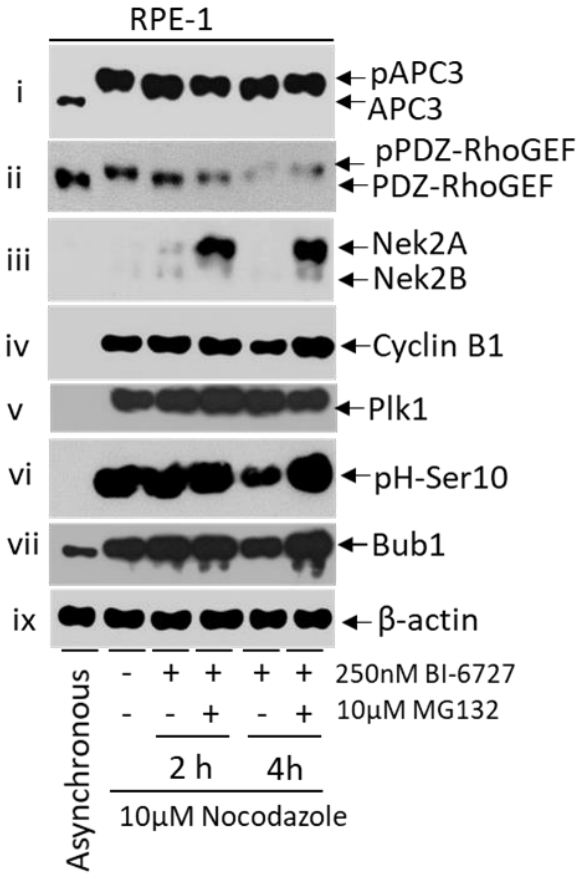

Figure 3.15: Plk1 inhibition prevents PDZ-RhoGEF phosphorylation in mitosis. RPE-1 cell were arrested in mitosis by treating the cells with nocodazole. The cells were then isolated by mechanical shake-off and treated with the Plk1 inhibitor, BI-6727 (+/-) MG132. The cells were then harvested at 2 and 4 h post-treatment. 50μg protein samples were separated by SDS-PAGE and the levels of key cell cycle proteins were analysed by WB. Results taken from one experiment, representative of two other identical experiments.

3.2.14 PDZ-RhoGEF is not phosphorylated or targeted for proteasomal degradation in response to DNA damage

The APC/C is known to play an important role in the cellular response to DNA damage. The APC/C-Cdh1 complex is reactivated in G2 phase in order to target Plk1 for proteasomal degradation to prevent mitotic progression (Bassermann et al. 2008, Stracker et al. 2009). Interestingly, the mass spectrometric analysis of PDZ-RhoGEF phosphorylation sites indicated that S215 was phosphorylated specifically in mitosis; S215 is part of an SQE ATM/ATR consensus site. Although limited studies do indicate that ATM and ATR participate in mitosis (Palazzo et al. 2014, Kabeche et al. 2018) given their well-established roles in DNA damage, the next aim was to investigate the phosphorylation status, as well as protein levels of PDZ-RhoGEF following genotoxic insult. To do this, RPE-1 cells were subjected to UV and hydroxyurea treatment in order to activate ATR kinase, and treated with X-rays to activate the ATM kinase. Cells were then harvested at different time-points post treatment and subjected to WB analyses for PDZ-RhoGEF and p53 (**Fig. 3.16**). DNA damage was successfully induced following all treatments as indicated by the stabilization in p53 protein levels (panel ii, **Fig. 3.16 A, B** and **C**). However, DNA damage treatment did not appear to promote PDZ-RhoGEF phosphorylation or degradation (panel i, **Fig 3.16. A, B** and **C**), although there was a suggestion that PDZ-RhoGEF might undergo PTM after 1 h UV treatment (panel i, **Fig. 3.16 A**). These data suggest that PDZ-RhoGEF is not phosphorylated or targeted for degradation in response to DNA damage.

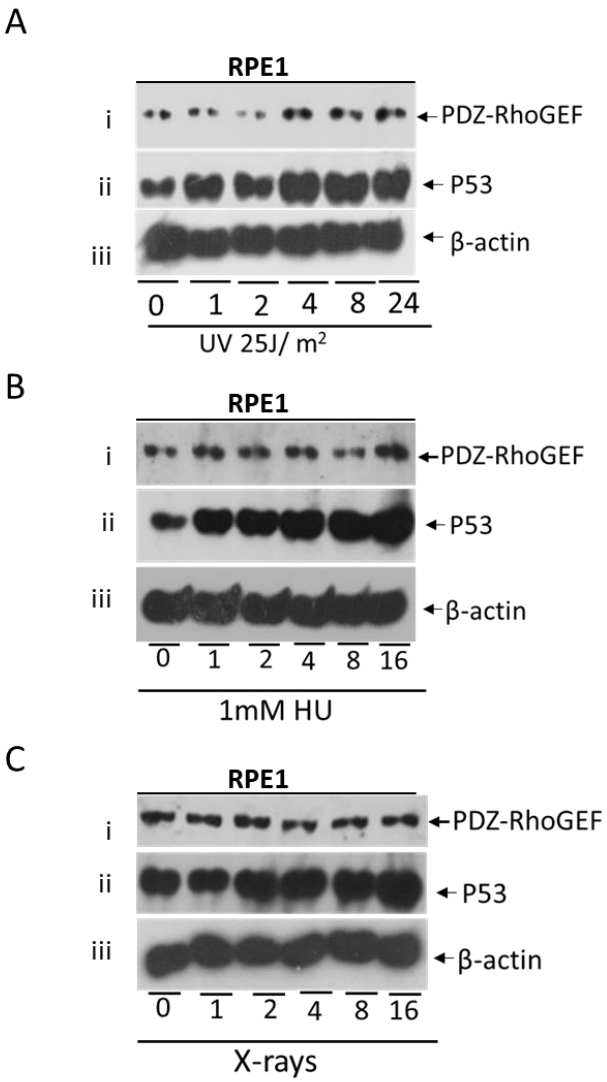

Figure 3.16: DNA damage induction does not promote PDZ-RhoGEF phosphorylation or degradation. RPE-1 cells were subjected to UV, hydroxyurea (HU) and X-rays to evaluate the effect of DNA damage on PDZ-RhoGEF phosphorylation. Cells were then harvested at different time-points. 50µg protein samples were then separated by SDS-PAGE and the phosphorylation status and p53 protein levels were analysed by WB. Results taken from one experiment, representative of two other identical experiments.

3.2.15 Generation of Cdk1 phosphorylation-site mutants in PDZ-RhoGEF to investigate the role of Cdk1 in its degradation

The mass spectrometry results, and mitotic kinase inhibitor studies suggest that cyclin B1-Cdk1 is the kinase that is most likely responsible for the phosphorylation of PDZ-RhoGEF in mitosis (**Figs. 3.12** and **3.13**). In light of these results, firstly, multiple PDZ-RhoGEF sequence alignments was performed from *Homo sapiens, Pan Troglodytes,*

Mus musculus, Rattus Norvegicus and Danio rerio to evaluate the conservation of the Cdk1 sites in different species. The results suggested that Cdk1 sites, SP^{27} and SP^{1518} were well conserved amongst different species, whilst S1414 was only conserved amongst primates (**Fig. 3.17**).

Figure 3.17: Conservation of Cdk1 sites within the PDZ-RhoGEF sequence from different species. Clustal Omega multiple alignment of potential Cdk1 sites obtained by mass spectrometry, S27, S1414 and S 1518 from *Homo sapiens, Pan Troglodytes, Mus musculus, Rattus Norvegicus and Danio rerio.*

Given these levels of conservation, the Cdk1-dependent phosphorylation of PDZ-RhoGEF might be important in targeting PDZ-RhoGEF for proteasomal degradation. To investigate this possibility further all the PDZ-RhoGEF Cdk1 sites were mutated in the context of full-length PDZ-RhoGEF. To do this a WT Myc-tagged PDZ-RhoGEF construct was first generated and cloned it into the retrovirus vector, pQCXIN (**Fig. 3.18 A** and **B**). Next, using the Q5-Sited directed mutagenesis kit we attempted to mutate residues, S27, S1414 and S1518 to alanine, in isolation and combination, to test the effect of abolishing S acceptor residues on the phosphorylation status of PDZ-RhoGEF in mitosis. Subsequently isolated S27A and S1518A clones were validated

using Sanger sequencing (**Fig. 3.18 C and D**). Unfortunately, however, despite numerous attempts with different oligonucleotide combinations we were not able to generate the S1414A mutant so were not able to progress in the allocated time to make the triple mutant. In order to generate clonal cell lines that expressed S27A and S1518A, retrovirus particles were generated first by transfecting pQCXIN-Myc-PDZ-RhoGEF (WT, S27A and S1518A mutants) along with VSV-G (viral envelope) into GP2-293 cells, then transduced RPE-1 cells with the retroviruses obtained and selected clonal cell lines with G418 (see materials and methods, section 2.1.1.2). Taking this approach, cell lines were isolated with comparable expression, for further analysis as determined by WB (**Fig 3.18 E**).

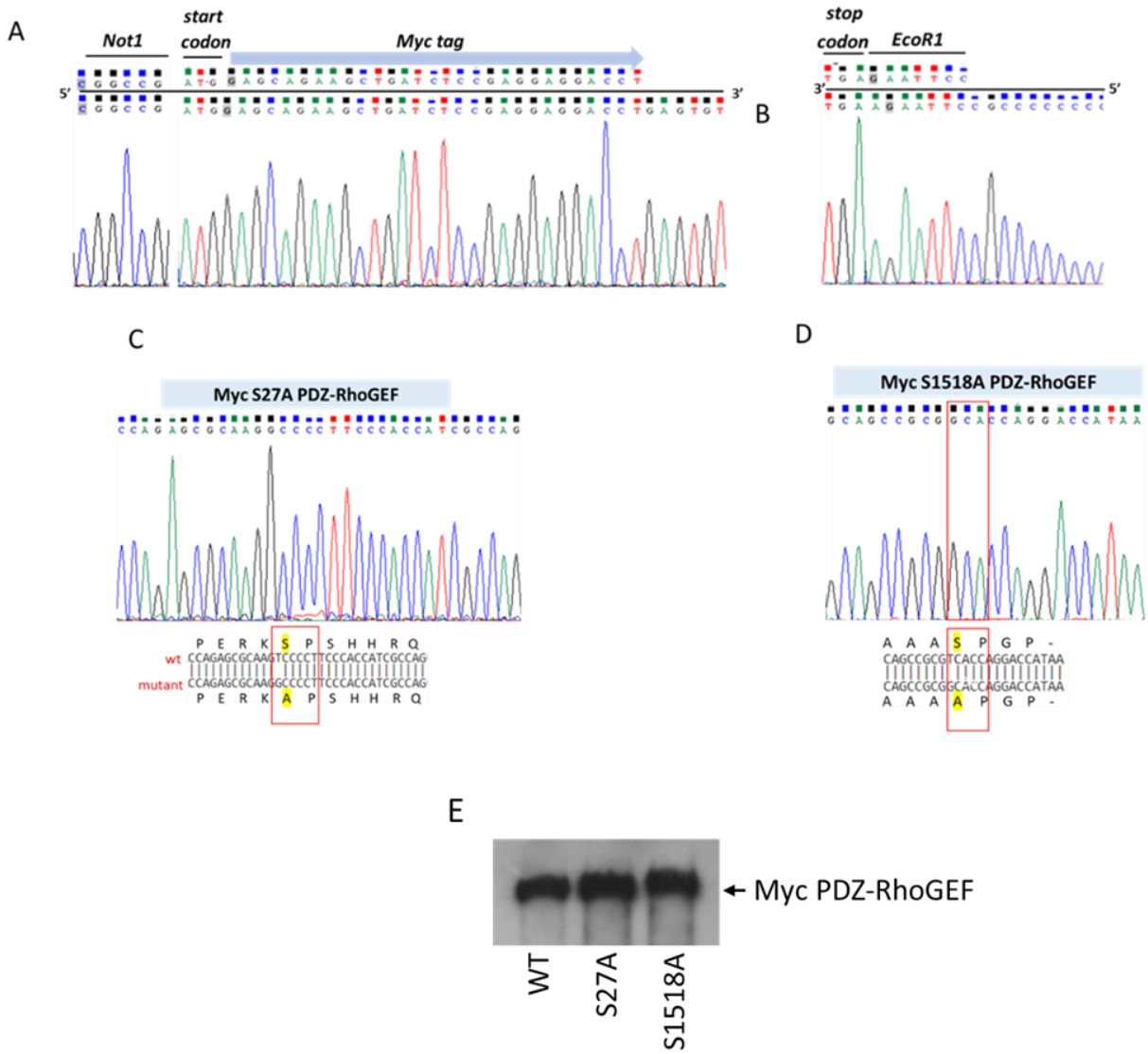

Figure 3.18: Generation of PDZ-RhoGEF phosphorylation mutants. Using Q5 site directed mutagenesis, we mutated Cdk1 sites S27 and S1518 to alanine. (A) Cloning of WT Myc-tagged PDZ-RhoGEF into the pQCXIN vector, illustrating the 5' NotI cloning site and the incorporation of the Myc-tag. (B) Cloning of WT Myc-tagged PDZ-RhoGEF into the pQCXIN vector, illustrating the 3' end of the PDZ-RhoGEF sequence with the stop codon and the EcoRI cloning site. (C) chromatogram illustrating the incorporation of the S27A mutation. (D chromatogram illustrating the incorporation of the S1518A mutation. The images presented were made using Chromas following Sanger sequencing. (E) Asynchronous RPE-1 cells showing isolated, clonal WT, S27A and S1518A Myc-tagged RhoGEF mutants.

3.2.16 Investigating the effect of S27A and S1518A mutation on PDZ-RhoGEF phosphorylation status and degradation pattern in mitosis

Although we were not able to mutate all Cdk1 phosphorylation sites in the Myc-tagged PDZ-RhoGEF construct we decided to investigate whether ablation of either S27 or S1518 Cdk1 sites affected PDZ-RhoGEF phosphorylation, or degradation in early

mitosis. To address these questions Myc-tagged WT, S27A and S1518A PDZ-RhoGEF cell lines were treated with nocodazole to arrest them in mitosis, isolated by mechanical shake-off and released back into the cell cycle following nocodazole withdrawal. WT, S27A and S1518A PDZ-RhoGEF protein levels were then analysed at specific times during mitotic progression by WB (**Fig. 3.19**). The results indicated that WT, S27A and S1518A Myc-tagged PDZ-RhoGEF species were phosphorylated in mitotically-arrested RPE-1 cells, although it appeared that the phosphorylation status of S27A and S1518 mutants was only transient when compared to WT, as S27A and S1518A mutants appeared to undergo dephosphorylation during the time-course of the experiment, whereas the WT species remained phosphorylated throughout (panel ii**, Fig. 3.19, A-C**). Furthermore, it appeared that the protein levels of S27A and S1518A returned almost to the levels of these mutants in interphase cells, whilst the WT species remained low throughout the experiment suggesting that mutation of these sites did affect the degradation of PDZ-RhoGEF (panel ii, **Fig 3.19, A-C**). These data suggest that Cyclin B1-Cdk1 affects the temporal nature of PDZ-RhoGEF phosphorylation in mitosis and also the degradation of PDZ-RhoGEF during mitosis.

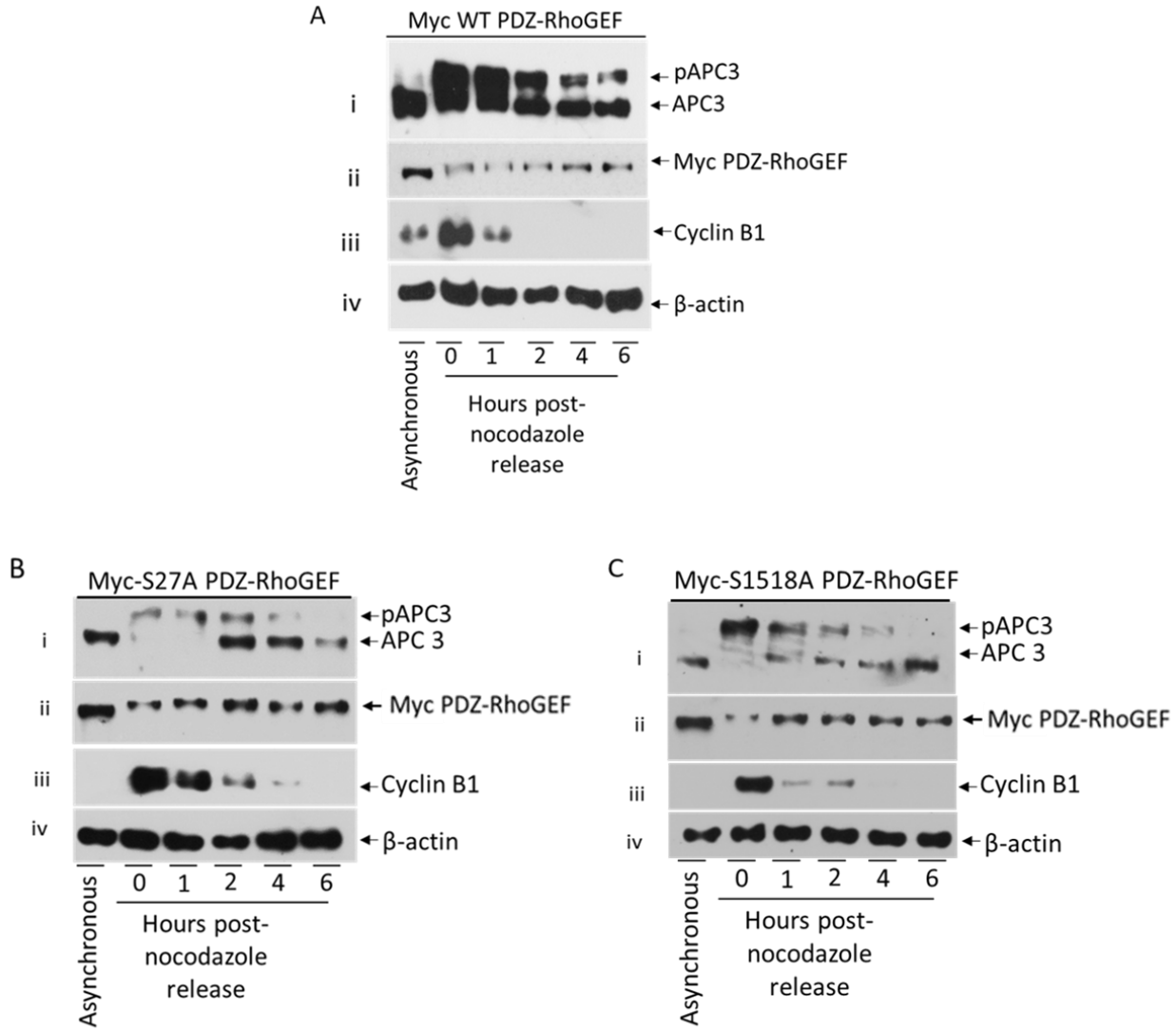

Figure 3.19: Investigating the role of S27 and S1518 in the phosphorylation and degradation of PDZ-RhoGEF in mitosis. WT, S27A and S1518A Myc-tagged PDZ-RhoGEF cells were arrested in mitosis with nocodazole. The cells were then released from the nocodazole block and harvested at different time-points post release. 50µg protein samples were separated by SDS-PAGE and the levels of Myc-PDZ-RhoGEF and key cell cycle proteins were analysed by WB. Results taken from one experiment, representative of two other identical experiments.

3.2.17 PDZ-RhoGEF possesses multiple APC/C degrons within its primary sequence

The APC/C coordinates the timely degradation of its substrates in mitosis by recognising degradation motifs (degrons) within the primary sequence of the substrate. APC/C degrons include the: D-box typified by the consensus sequence, RXXLXXI/VXN; KEN box characterized by the sequence, KENXXXN/D; and the ABBA

motif which conforms to the consensus sequence, FX [ILV][FHY]X[DE] (see section 1.4.5.2). Previous work in analysed the human PDZ-RhoGEF amino acid sequence for all possible APC/C classical degrons and determined that PDZ-RhoGEF possessed 12 potential D-boxes and one very well conserved KEN box (Jessica Foster, PhD thesis, University of Birmingham; **Fig. 3.20 A**). Given the conservation of the KEN box, the location of the ^{766}KEN^{768} box was investigated in the crystal structure of PDZ-RhoGEF DH/PH domains in complex with GTP gamma-S activated RhoA at resolution 2.70 Å (PDB 3KZ1; Chen et al. 2010). Using Chimera software, the KEN box of PDZ-RhoGEF was shown, in the context of this partial fragment at least, is surface-exposed and located at the end of an α-helix suggesting that Cdc20 would be able to access this region for association with the PDZ-RhoGEF KEN box (**Fig 3.20 B**). Therefore, the hypothesis was that the PDZ-RhoGEF KEN box is a major degron by which AP/C-Cdc20 complex targets RhoGEF for degradation in mitosis. As such, the next aim was to investigate the relationship between Cdc20 and PDZ-RhoGEF further.

A

```
PDZ-RhoGEF degrons
  65    RIVLVQSVRPGGAAMKAGVKEGDRIIKVNG
 183    RNMLRQEEKELQDILPLYGDTSQRPSEGRL
 211    RLSLDSQEGDSGLDSGTERFPSLSESLMNR
 398    RGVLCEAQEAAMPEIQEQIHDYRTKRTLGL
 766    KENLMPREELARLFPNLPELIEIHNSWCEA
 772    REELARLFPNLPELIEIHNSWCEAMKKLRE
 822    REELQQVAAQFCSYQSIALELIKTKQRKES
 852    RFQLFMQEAESHPQCRRLQLRDLIISEMQR
 868    RLQLRDLIISEMQRLTKYPLLLESIIKHTE
 914    REILKYVNEAVKQTENRHRLEGYQKRLDAT
 930    RHRLEGYQKRLDATALERASNPLAAEFKSL
1111    RVELDDSDVFHGEPEPEELPGGTGSQQRVQ
1447    RELLKSLGGESSGGTTPVGSFHTEAARWTD
```

B

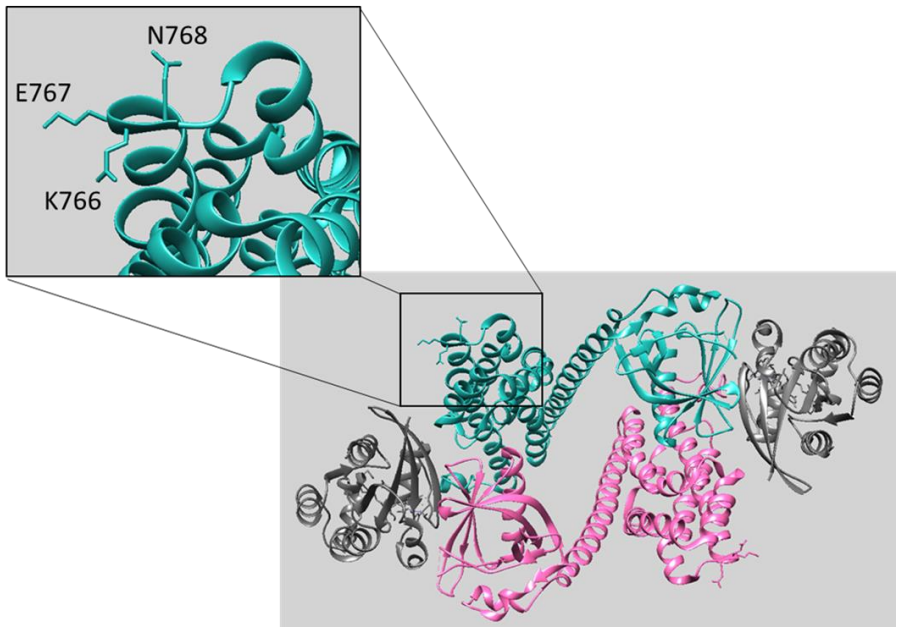

Figure 3.20: Analysis of PDZ-RhoGEF APC/C degrons. (A) PDZ-RhoGEF amino acid FASTA sequence showing the potential APC/C degrons of PDZ-RhoGEF. These sites have been identified previously in a multiple alignment analysis (Jessica Foster, PhD thesis, University of Birmingham 2018). (B) Ribbon structure representation of PDZ-RhoGEF in complex with activated RhoA showing the surface-exposed KEN box.

3.2.18 **Cdc20 interacts with PDZ-RhoGEF *in vitro***

Research presented to date indicates that PDZ-RhoGEF is a UbcH10-interacting protein that is targeted for degradation in a SAC-insensitive manner in early mitosis. As PDZ-RhoGEF possesses an accessible, well-conserved KEN box motif (^{766}KEN^{768}) within its primary sequence, the ability of Cdc20 to interact with PDZ-RhoGEF was

investigated by performing WT GST-PDZ-RhoGEF pulldowns using RPE-1 and HeLa mitotic cell extracts as source of Cdc20 and monitoring interaction with Cdc20 by WB. In this context GST PDZ-RhoGEF fragments were used that covered the entire open reading frame of the PDZ-RhoGEF sequence. WB results showed that GST-PDZ-RhoGEF fragments 2, 3 and 4 all had the ability to co-precipitate Cdc20 from mitotic cell lysates; GST and GST-PDZ-RhoGEF fragment 1 did not co-precipitate Cdc20 from either HeLa, or RPE-1 cells (**Fig. 3.21).** It appeared that GST-PDZ-RhoGEF fragment 3 (amino acids 601-1110) has the greatest propensity to interact with Cdc20 in RPE-1 cells, which interestingly contained the ^{766}KEN^{768} box motif and a conserved D box (^{930}RHRL^{933}) that is situated proximal to major ubiquitin acceptor lysine K938 (listed on phosphosite plus). Taken together, these data indicate that PDZ-RhoGEF and Cdc20 can associate *in vitro*, potentially through multiple sites that might involve the PDZ-RhoGEF KEN box and D-box.

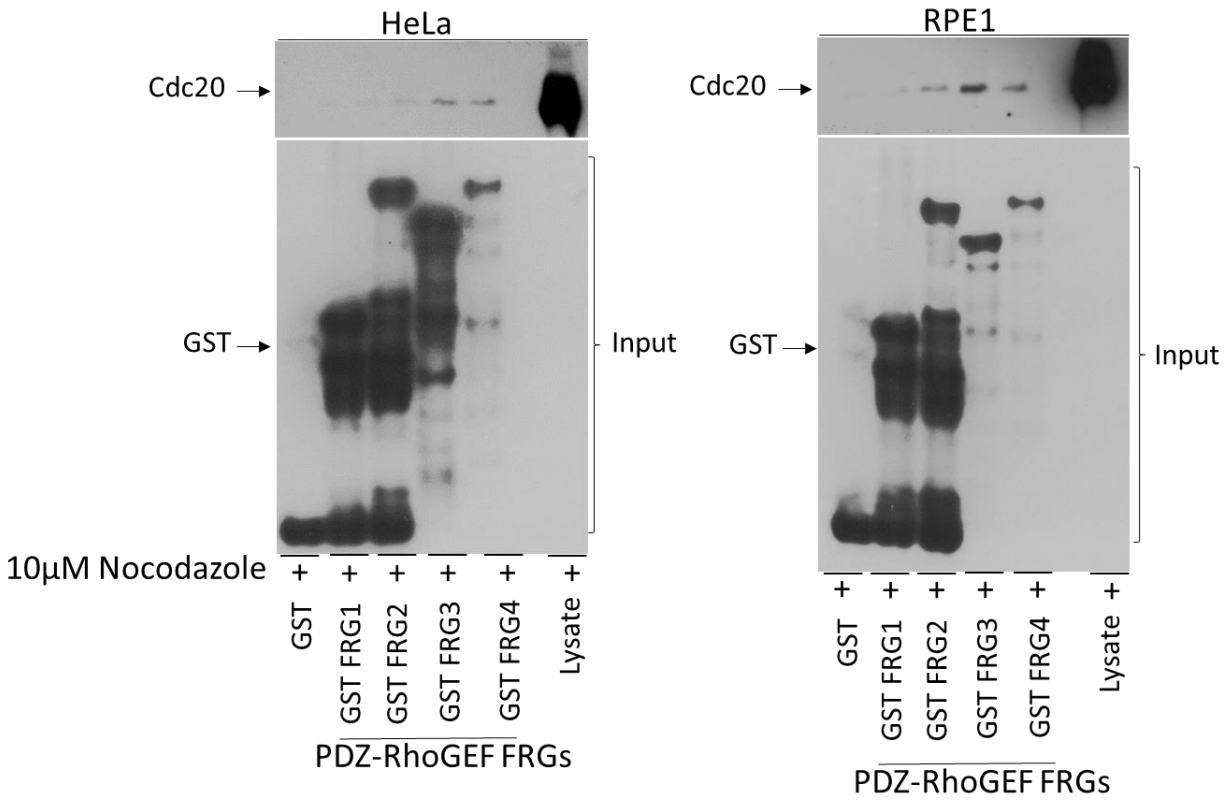

Figure 3.21: Cdc20 interacts with PDZ-RhoGEF *in vitro.* Mitotically-arrested RPE1 and HeLa cells were isolated by mechanical shake-off and harvested in NETN lysis buffer. 5µg of each GST-PDZ-RhoGEF fragment and GST alone was then added to the cell lysate containing 1 mg of protein and were mixed by rotation at 4°C overnight. Samples were then subjected to glutathione agarose pulldown by rotation for 3h at 4°C. Precipitated proteins were then separated by SDS-PAGE and analysed by WB for Cdc20 and GST, to show loading of GST fusion proteins. Results taken from one experiment, representative of one other identical experiment.

3.2.19 **PDZ-RhoGEF interacts with UbcH10 *in vitro***

As have been shown previously that PDZ-RhoGEF interacts with UbcH10 *in vivo* (**Fig. 3.5)** and have also been shown that GST-PDZ-RhoGEF fragments are able to interact with Cdc20 *in vitro*, the ability of UbcH10 to interact similarly *in vitro* with PDZ-RhoGEF was investigated. To do this, WT UbcH10-HA expression was induced in Flp-In TREX U2OS cells and mixed cell lysates with GST-PDZ-RhoGEF fragments that covered the entire open reading frame of the PDZ-RhoGEF sequence. WB results showed that GST-PDZ-RhoGEF fragments 2, 3 and 4 all had the ability to co-precipitate UbcH10-HA from U2OS cell lysates (**Fig. 3.22**); GST and GST-PDZ-RhoGEF fragment 1 did

not co-precipitate UbcH10 from U2OS cells induced to express UbcH10-HA (**Fig. 3.22**). Taken together, these data indicate that UbcH10 associates with PDZ-RhoGEF via multiple sites of interaction.

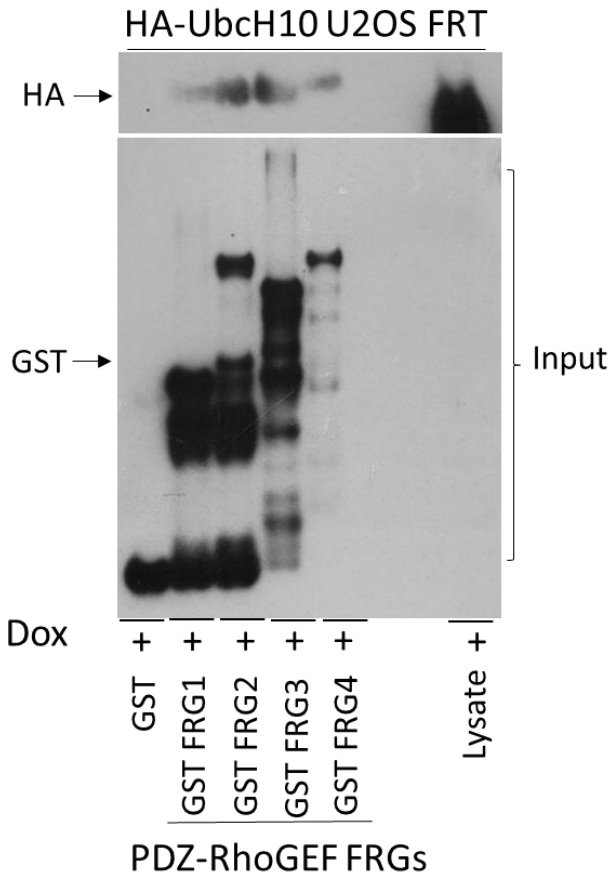

Figure 3.22: UbcH10 interacts with PDZ-RhoGEF *in vitro*. Asynchronous FlpIn TREX WT UbcH10-HA cells induced to express WT UbcH10-HA were harvested in NETN lysis buffer. 5µg of each GST-PDZ-RhoGEF fragment and GST alone was then added to the cell lysate containing 1 mg of protein and were mixed by rotation at 4°C overnight. Samples were then subjected to glutathione agarose pulldown by rotation for 3h at 4°C. Precipitated proteins were then separated by SDS-PAGE and analysed by WB for UbcH10 and GST, to show loading of GST fusion proteins. Results taken from one experiment, representative of one other identical experiment.

3.2.20 **Generation of Myc-tagged ΔKEN PDZ-RhoGEF RPE-1 cells**

To further investigate the role of PDZ-RhoGEF in mitosis and to study further the molecular basis of the relationship between APC/C-Cdc20 and PDZ-RhoGEF, a clonal cell line that expressed a PDZ-RhoGEF mutant lacking the ^{766}KEN^{768} box which is likely targeted by Cdc20 was made. Thus, a Q5 Site-Directed mutagenesis kit was used and

the pQCXIN Myc-tagged WT PDZ-RhoGEF construct to generate a ΔKEN PDZ-RhoGEF expression plasmid where the ^{766}KEN^{768} motif was mutated to AAA, in order to knockout KEN box functionality (**Fig 3.23 A**). The resulting pQCXIN-Myc-tagged ΔKEN PDZ-RhoGEF construct was then transfected along with a plasmid expressing viral envelope (VSV-G) in the retroviral packaging cell line, GP2-293 cells. Four days post transfection isolated retroviral particles were used to transduce RPE-1 cells for the isolation of clonal cell lines using G418 selection (see materials and methods, section 2.1.1.2). Using this technique, cell lines that constitutively expressed Myc-tagged ΔKEN PDZ-RhoGEF at similar levels to Myc-tagged WT PDZ-RhoGEF was successfully generated (**Fig 3.23 B**).

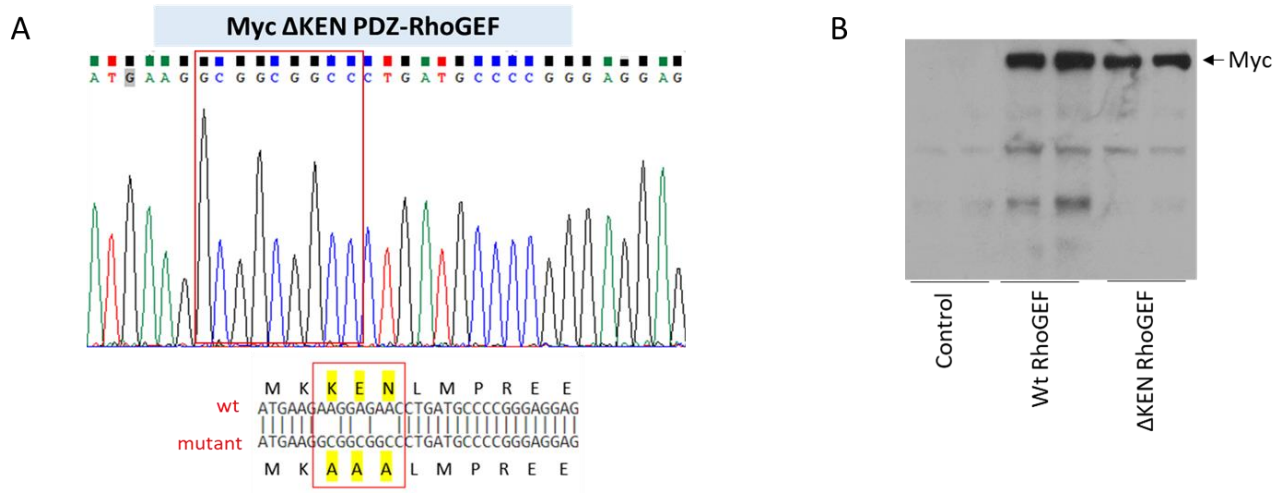

Figure 3.23: Generation of Myc-tagged ΔKEN PDZ-RhoGEF cell lines. **(**A) Chromatogram illustrating the incorporation of the AAA mutation and ablation of the KEN box in Myc-PDZ-RhoGEF. (B) Expression of WT and ΔKEN, Myc-tagged RhoGEF in clonal RPE-1 cells. WT and ΔKEN Myc-tagged PDZ-RhoGEF cells were harvested and processed for SDS-PAGE. 50µg of total protein lysate was separated on SDS-PAGE and the protein levels analysed by WB. Controls are RPE-1 cells alone.

3.2.21 Cdc20 associates with PDZ-RhoGEF KEN box *in vivo*

Once generated, the WT and ΔKEN Myc-tagged PDZ-RhoGEF RPE-1 cell lines were used to investigate whether WT and ΔKEN Myc-tagged species interacted with Cdc20 *in vivo*. As Cdc20 is predominantly functional in mitosis both asynchronous and

mitotically-arrested WT and ΔKEN Myc-tagged PDZ-RhoGEF RPE-1 cell lines were harvested and subjected lysates to IP with anti-Cdc20 antibodies, then WB for Myc-tagged PDZ-RhoGEF species and Cdc20. WB analyses revealed that Cdc20 associates with PDZ-RhoGEF in mitosis, predominantly through its KEN box motif as the Cdc20 interaction with PDZ-RhoGEF in WT Myc-PDZ-RhoGEF cells was almost ablated when the KEN box was inactivated by mutation (cf lanes 6 and 8, **Fig. 3.24**). These data suggest that Cdc20 interacts with PDZ-RhoGEF in mitosis which is mediated in the most part by a functional KEN box in PDZ-RhoGEF (^{766}KEN^{768}). It also suggests that PDZ-RhoGEF is targeted for proteasomal degradation.in early mitosis by APC/C-Cdc20.

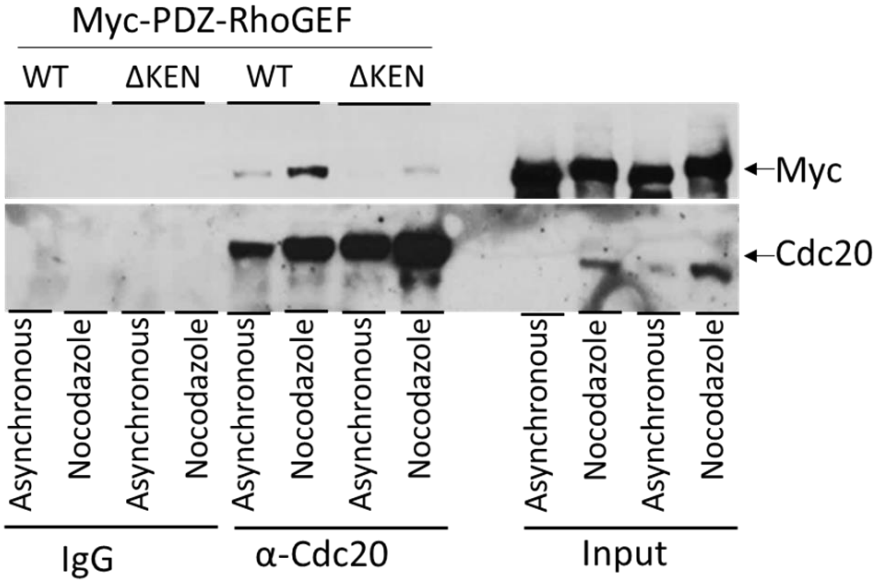

Figure 3.24: The PDZ-RhoGEF KEN box interacts with Cdc20 in mitosis. Myc-tagged WT and ΔKEN PDZ-RhoGEF RPE-1 cell lines were arrested in mitosis by nocodazole. Asynchronous and mitotically-arrested Myc-tagged WT and ΔKEN PDZ-RhoGEF RPE-1 cell lines were then harvested in NETN lysis buffer and subjected to IP with mouse IgG or an anti-Cdc20 antibody by end-to-end mixing at 4°C overnight. Immunocomplexes were then isolated on protein G Sepharose beads by incubation for 3 hours at 4°C and then separated along with 50 µg of the total protein lysate by SDS-PAGE and analysed by WB for Myc (PDZ-RhoGEF) and Cdc20. Results taken from one experiment, representative of one other identical experiment.

3.2.22 Mutation of PDZ-RhoGEF KEN box stabilises PDZ-RhoGEF at different stages of cell cycle

Following the generation of Myc-tagged WT PDZ-RHOGEF and ΔKEN PDZ-RhoGEF RPE-1 cell lines, the next aim was to investigate whether the protein levels of these PDZ-RhoGEF species were affected at different stages of cell cycle by the loss of the KEN box. Therefore, WT and ΔKEN PDZ-RhoGEF RPE-1 cell lines were treated with RO-3306, which synchronises cells at the G2/M boundary, with nocodazole which causes cell synchronisation in prophase by inhibiting spindle polymerization, and Taxol which prevents spindle depolymerisation and arrests cells at different stages of mitosis. Treated cells were then harvested and subjected to WB analysis to investigate the level of PDZ-RhoGEF in these stages of cell cycle (**Fig 3.25**). Consistent with the known effects of these cell cycle inhibitors, nocodazole and Taxol promoted the phosphorylation of APC3 and the stabilisation of cyclin B1 (panels i and iii, **Fig 3.25**). Interestingly, the protein levels of Myc-tagged ΔKEN PDZ-RhoGEF were higher at all stages of the cell cycle than WT PDZ-RHOGEF (panel ii, **Fig 3.25**). It was interesting to note that the ΔKEN PDZ-RhoGEF species was still a target for Cdk1-dependent phosphorylation in mitosis, and that a good proportion of this species was still targeted for degradation (panel ii, **Fig 3.25**). Taken together, these results indicate that KEN box of PDZ-RhoGEF does modulate the stability of PDZ-RhoGEF throughout the cell cycle but that other regions of the protein, presumably D-boxes, contribute towards its stability.

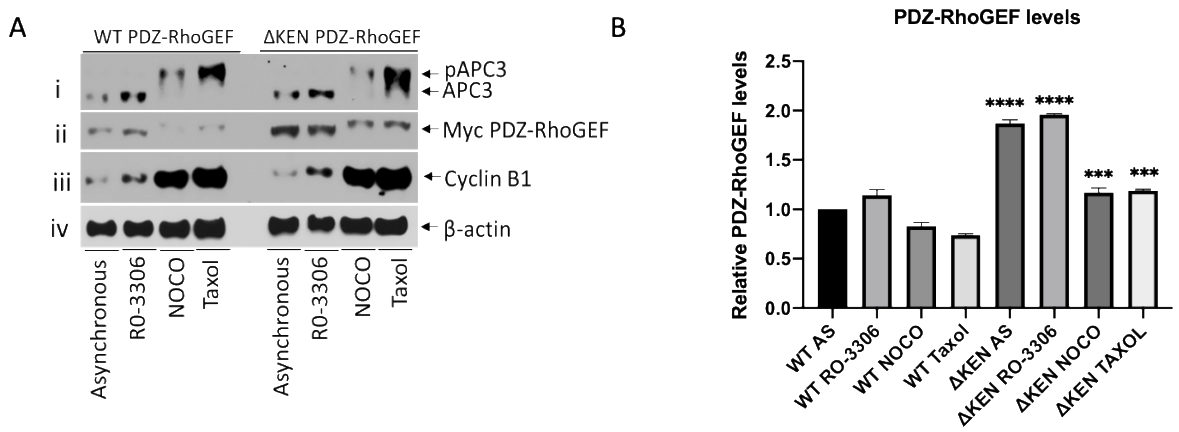

Figure 3.25: Mutation of the PDZ-RhoGEF KEN box facilitates the stabilisation of PDZ-RhoGEF. Myc-tagged WT PDZ-RhoGEF and ΔKEN PDZ-RhoGEF RPE-1 cells were treated with RO-3306 to arrest cells at the G2/M boundary, and nocodazole and Taxol to arrest cells in mitosis. The cells were subsequently harvested and 50µg of total protein lysates were separated by SDS-PAGE. (A) The protein levels of WT and ΔKEN PDZ-RhoGEF species and other cell cycle proteins were analysed by WB. Results taken from one experiment, representative of one other identical experiment. (B) Using ImageJ, the band densities of PDZ-RhoGEF at different cell stages in both WT PDZ-RhoGEF and ΔKEN PDZ-RhoGEF cells were measured and normalised to the β-actin loading control. Protein levels of the normalised band densities were calculated and are presented as a bar-graph showing the mean reading +/- Standard Deviation where (*) $P \leq 0.05$, (**) $P \leq 0.01$, (***) $P \leq 0.001$ and (****) $P \leq 0.0001$ indicated significant differences between corresponding WT and ΔKEN samples (N=3).

3.2.23 UbcH10 interacts PDZ-RhoGEF *in vivo* independently of PDZ-RhoGEFs KEN box

The WT and ΔKEN Myc-tagged PDZ-RhoGEF RPE-1 cell lines were also used to investigate whether WT and ΔKEN Myc-tagged species also interacted with UbcH10 *in vivo*. As previously been determined that UbcH10 can associate with PDZ-RhoGEF in interphase (**Fig. 3.5**) asynchronously growing WT and ΔKEN Myc-tagged PDZ-RhoGEF RPE-1 cell lines were harvested and subjected lysates to IP with anti-UbcH10 antibodies, then WB for Myc-tagged PDZ-RhoGEF species and UbcH10. WB results suggested that WT and ΔKEN Myc-tagged PDZ-RhoGEF species bound with

equal avidity to UbcH10, indicating that the PDZ-RhoGEF KEN box did not contribute to PDZ-RhoGEF association with UbcH10 (**Fig. 3.26**).

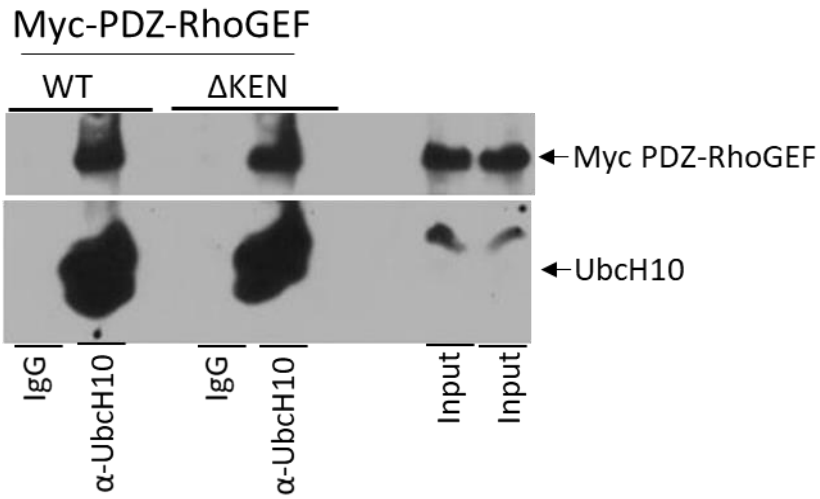

Figure 3.26 PDZ-RhoGEF interaction with UbcH10 is not dependent upon its KEN box. Asynchronous Myc-tagged WT and ΔKEN PDZ-RhoGEF RPE-1 cell lines were harvested in NETN lysis buffer and subjected to IP with rabbit IgG or an anti-UbcH10 antibody by end-to-end mixing at 4°C overnight. Immunocomplexes were then isolated on protein G Sepharose beads by incubation for 3 hours at 4°C and then separated along with 50 µg of the total protein lysate by SDS-PAGE and analysed by WB for Myc (PDZ-RhoGEF) and UbcH10. Results taken from one experiment, representative of one other identical experiment.

3.3 Discussion

Previous work in our laboratory identified PDZ-RhoGEF as a novel UbcH10-interacting protein; PDZ-RhoGEF protein levels were low in early mitosis suggesting that it was an APC/C substrate that was targeted for degradation in a SAC-independent manner (Jessica Foster, PhD thesis, University of Birmingham, 2018). The commercial anti-PDZ-RhoGEF antibody our laboratory used for those studies, although highly specific, had low avidity for PDZ-RhoGEF and was deemed unsuitable for either IP or Western blot. Therefore, a new homemade anti-PDZ-RhoGEF antibody was generated using a GST-PDZ-RhoGEF fragment possessing the first 600 amino acids. The antibody worked well in IP and WB and was validated by siRNA (**Figs. 3.4 and 3.5**); this antibody was used in all subsequent experiments. The study presented herein was to extend to confirm our laboratory's initial findings previous findings with the newly generated anti-PDZ-RhoGEF antibody and extend these findings to characterise further the biological relationship between PDZ-RhoGEF and UbcH10 and APC/C-Cdc20.

3.3.1 PDZ-RhoGEF is likely targeted for APC/C-Cdc20 dependent proteasomal degradation in early mitosis

The APC/C is a RING-Cullin E3 ubiquitin ligase that functions to control cell progression through mitosis and G1 by targeting key cell cycle proteins for proteasomal degradation (see section 1.4). Data presented in this thesis indicates that PDZ-RhoGEF is degraded in early mitosis, like cyclin A and Nek2a, in a 26S-proteasome-dependent manner, as treatment of mitotic cells with proteasomal inhibitors increases the protein levels of PDZ-RhoGEF, cyclin A and Nek2a, suggestive of a common mechanism of inactivation (**Fig. 3.8**). Early mitotic substrates, Nek2a and cyclin A are targeted for degradation by APC/C-Cdc20 through the

recognition of D-box and protein-protein interaction motifs that are found in these substrates (Hoyt, Totis et al. 1991; Thornton and Toczyski 2003; Geley et al. 2001). Bioinformatic analysis of the primary sequence of PDZ-RhoGEF indicates that it possesses many potential APC/C degrons, namely 12 putative D-boxes, typically targeted by Cdc20, and one KEN box, which is typically targeted by Cdh1 (**Fig. 3.20**). Interestingly however, previous collaborative work in Turnell's laboratory determined that, 53BP1 a KEN-box containing APC/C substrate, is primarily targeted by APC/C-Cdc20 in a KEN box-dependent manner for degradation (Kucharski et al 2017). In the same context, work presented herein indicated that PDZ-RhoGEF interacted with Cdc20, both *in vitro* and *in vivo,* and that PDZ-RhoGEF interaction with Cdc20 in mitosis was dependent on a functional KEN box as mutation of the KEN box to AAA reduced the extent of the interaction considerably (**Figs. 3.21 and 3.24**). Moreover, ablation of the functional KEN box in PDZ-RhoGEF stabilized PDZ-RhoGEF in both interphase and mitosis, indicative of a requirement for this APC/C degron in PDZ-RhoGEF stability (**Fig. 3.25**). These observations are the first to suggest that PDZ-RhoGEF is targeted for degradation by APC/C-Cdc20 in early mitosis.

IP studies performed here suggested that IP with UbcH10 antibodies was able to co-IP PDZ-RhoGEF but that IP with PDZ-RhoGEF antibodies was not able to co-IP UbcH10 (**Fig. 3.5**). The reasons for this discepancy are not immediately apparent though could suggest that epitopes on PDZ-RhoGEF targeted by the anti-PDZ-RhoGEF antibodies sterically prevent the association of PDZ-RhoGEF with UbcH10. Consistent with this notion, *in vitro* pulldowns indicated that UbcH10 had the ability to associate with GST-PDZ-RhoGEF fragment 2, comprising amino acids 1-600, that was used to generate the PDZ-RhoGEF antibody (**Figs 3.3, 3.4** and **3.22**). The siRNA-

mediated knockdown of PDZ-RhoGEF was shown to cause the loss of both SAC-sensitive and SAC-insensitive APC/C substrates (**Fig 3.10**). Interestingly, previous studies have suggested that knockdown or knockout of the early mitotic APC/C-Cdc20 substrate, 53BP1, similarly promoted the loss of APC/C substrates suggesting that 53BP1 was an APC/C inhibitor (Kucharski et al. 2017). Indeed, it was shown tha loss of 53BP1 led to the activation of the APC/C, and that *in vitro* at least 53BP1 could inhibit APC/C activity towards cyclin B1. Given these results it will be of considerable interest to see if loss of PDZ-RhoGEF, also leads to activation of the APC/C and whether PDZ-RhoGEF protein can inhibit APC/C activity towards other substrates.

The SAC-insensitive, APC/C, substrates cyclin A and Nek2A are important for mitotic entry and bipolar spindle formation, respectively (Hoyt et al. 1991; Thornton and Toczyski 2003; Geley et al. 2001), yet their degradation by the APC/C is required for mitotic progression. To date, there has been no published evidence that PDZ-RhoGEF is required for mitotic entry or events that occur early in mitosis. As discussed in the introduction to this chapter PDZ-RhoGEF is an important regulator of RhoA activity and has previously been shown to be targeted for ubiquitin-mediated degradation by CUL3-KHLH20, such that the degradation of PDZ-RhoGEF by CUL3-KHLH20 inhibits RhoA activity in order to modulate neurite growth (Lin et al. 2011). Interestingly however, Rho A activity is found to peak during the early stage of mitosis whereupon RhoA activity is significantly reduced upon anaphase initiation and is activated once more during cytokinesis. It has been determined that RhoA functions to modulate the arrangment of the cortical actin cytoskeleton during mitotic entry that promotes mitotic cell rounding (Maddox and Burridge 2003). The study further suggested that a RhoGEF is responsible in part for the activation of RhoA in mitosis and particularly in

cell rounding (see **Fig 3.27** for a pictorial description). The study also determined that the serine/threonine-dependent phosphorylation of p190RhoGAP resulted in its inhibition and the potentiation of RhoA activity (Maddox and Burridge 2003). In this regard, Rho kinase was found to promote the phosphorylation-dependent inhibiton of p190RhoGAP. Given these findings we can postulate that PDZ-RhoGEF might participate in the RhoA-dependent cell rounding in early mitosis. Consistent with our hypothesis, investigation of PDZ-RhoGEF specific phosphorylation sites in interphase and mitotic cells identified two potential Rho kinase phosphorylation sites (R/KXS/T or R/KXXS/T), KQTF^{1030} and RNSG^{1295} which could suggest that PDZ-RhoGEF might be targeted by Rho kinase to modulate its activity towards RhoA activation to promote mitotic cell rounding and that APC/C-Cdc20 inhibits RhoA activity by promoting PDZ-RhoGEF degradation. In this regard, it would be interesting to determine the affect of ablating the Rho kinase phosphorylation sites on PDZ-RhoGEF on mitotic cell rounding.

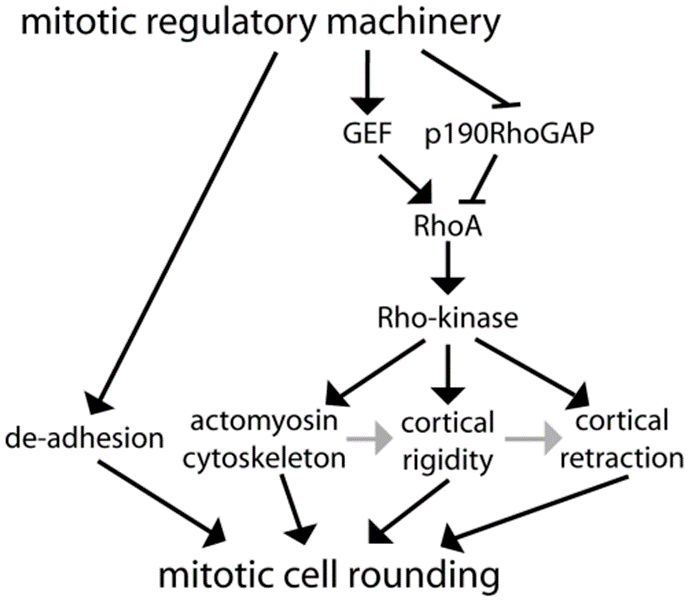

Figure 3.27: Role of RhoA in cell rounding during early mitosis. RhoA is regulated in mitosis by different RhoGEFs and RhoGAPs to regulate actin cytoskeleton rearrangements, cortical rigidity and cortical retraction (Maddox and Burridge 2003).

Other studies have, however, suggested regulatory roles for different RhoGEFs in mitosis. LARG, which is an RGS-containing RhoGEF is found to be the RhoGEF responsible for activating RhoA during cytokinesis, such that knockdown of LARG inhibits cytokinesis and promotes apoptosis in mitotis, in a process that is highly dependent on Aurora B kinase (Martz et al. 2013). Ect2 RhoGEF is also known to play an important role in cytokinesis and abscission; Ect2 relocalises to the spindle fibre in a process highly dependent on MgcRacGAP, whereupon Ect2 is subjected to sequential phosphorylation, first by Cdk1, and then by Plk1 after cyclin B1 is degraded; Ect2 is then targeted for degradation by APC/C-Cdh1 complexes during mitotic exit (Niiya, Tatsumoto et al. 2006, Nishimura and Yonemura 2006). More relevant to this studies, Ect2 is also involved in cell rounding in mitosis as it relocalises from from nucleus to cytpolasm in order to activate RhoA, which subsequently induces cell rigidity and rounding (Matthews et al. 2012). Given these findings it would be extremely interesting to perform confocal microscopy studies to establish the cellular localisation

of PDZ-RhoGEF as cells enter mitosis, in relation to Ect2, and moreover establish whether these RhoGEFs cooperate to regulate RhoA activity in early mitosis. Moreover, the ability of Ect2 to be differentially activated in mitosis has been suggested to be dependent upon its ability to be targeted for phosphorylation at multiple sites, particularly by Cdk1 (Hara et al. 2006, Niiya et al. 2006, Su et al. 2011). Indeed, Ect2 is phosphorylated at T^{341} at the G2/M boundry by Cdk1 and dephosphrylated at this site prior to cytokinesis (Hara, Abe et al. 2006). It will be interesting to determine whether ablation of any of the Cdk1 sites identified in PDZ-RhoGEF specifically modulate its ability to activate Rho.

3.3.2 **Investigating the role of PDZ-RhoGEF degrons and phosphorylation in mitosis**

The APC/C coactivators, Cdc20 and Cdh1, exhibit significant ability to recognise APC/C substrates at distinct mitotic stages, in order to promote their timely degradation (see Introduction, section 1.4.5.1). Indeed, the binding affinity of substrates for the APC/C is found to be a critical factor in ensuring the orderley association of substrates with the APC/C. In this regard, an increased number of degrons within the substrate correlates positively with Cdc20 and/or Cdh1 binding affinity (Bu et al. 1995). As such, previous work in Turnell's laboratory has identified 12 putative D-boxes and one conserved KEN box in PDZ-RhoGEF (Jessica Foster, PhD thesis, University of Birmingham, 2018). Indeed, as discussed in section 3.3.1 the KEN box of PDZ-RhoGEF is targeted by Cdc20 and does participate in PDZ-RhoGEF stability. However, the role of D Boxes in PDZ-RhoGEF stability is not known and further study is needed to analyse their contribution in the targeting of PDZ-RhoGEF for APC/C-Cdc20 dependent degradation. In this context it would be

interesting to investigate the PDZ-RhoGEF D box (^{930}RHRL^{933}), amongst others, which is highly conserved between species, and is positioned proximal to the major ubiquitin acceptor lysine, K938 (Hornbeck, Zhang et al. 2015). In this context we could inactivate D-boxes by mutation and investigate using co-IP (e.g. **Fig 3.24**) or GST-PDZ-RhoGEF pulldowns (e.g. **Fig. 3.21**) their contribution in targeting PDZ-RhoGEF to Cdc20.

It is well known that PTM of APC/C substrates, particularly phosphorylation, plays a key role in mediating the timely association of substrates with APC/C. For instance, the timely degradation of Securin is control by phosphorylation. As such, Cdk1 phosphorylates Securin at a S residue close to a D-box degron which inhibits Securin degradation by the APC/C-Cdc20, whilst Cdc14-mediated dephosphorylation of Securin promotes Securin degradation (Holt, Krutchinsky et al. 2008). Additionally, the targeting of Cdc6, an essential pre-replication complex component, for degradation by APC/C in mitosis is modulated by phosphorylation. Indeed, the cyclin E-Cdk2-dependent phosphorylation of Cdc6 at a residue close to its D-box inhibits its degradation and allows for its accumulation and the formation of pre-replication complex (Mailand and Diffley 2005). Perhaps more relevantly for a consideration of how PDZ-RhoGEF is targeted for degradation, phosphorylation can also influence positively APC/C substrate degradation. Both Nek2A and Aurora A are phosphorylated at a S residue proximal to their KEN box (SKEN) that promotes the degradation of both substrates by APC/C-Cdc20 complexes although the kinase(s) responsible for degradation were not identified (Min, Mayor et al. 2013). PDZ-RhoGEF does not, however, possess a S residue preceding its KEN box. Interestingly, both forms of the tumour suppressor gene product, MCPH1 (long and short forms) have recently been

shown to be phosphorylated by Cdk1 in mitosis and targeted for degradation later in mitosis by APC/C-Cdh1 (Meyer et al. 2019).

It was also showed that PDZ-RhoGEF is subjected to Cdk1-dependent phosphorylation in early mitosis and that Cdk1 inhibition limits PDZ-RhoGEF phosphorylation in mitosis, such that in the presence of MG132, PDZ-RhoGEF protein levels increased (**Figs 3.11** and **3.13**). We attempted to investigate the direct effects of PDZ-RhoGEF phosphorylation on its stability by attempting to ablate all Cdk1 S phospho-acceptor sites by mutation, though unfortunately, we were not able to make this PDZ-RhoGEF mutant (section 3.2.16). Interestingly we were able to make S27A and S1518A single mutants, which are the most highly conserved Cdk1 phosphorylation sites in PDZ-RhoGEF (**Fig 3.17**). Interestingly, ablation of these phosphorylation sites appeared to limit PDZ-RhoGEF degradation at the later stages of mitosis (**Fig 3.19**), although we need to substantiate these findings in future work by generating the triple-mutant that cannot undergo Cdk1-directed phosphorylation and investigating whether this mutant is targeted for degradation or not. Moreover, it would be interesting to see if the triple phospho-mutant was able to interact with Cdc20 *in vivo* in a KEN box (or D-box)-dependent, or independent manner to determine whether they function as genuine phosphodegrons (**Fig. 3.28**). In this regard, it would be interesting, at the structural level, and in the context of the whole protein to establish where S acceptor sites lie in relation to the KEN box, or D-boxes, as analysis of the primary sequence does not suggest they lie in close proximity. Moreover, it will be important to establish whether PDZ-RhoGEF is a direct substrate for the APC/C *in vitro* and whether the addition of Cdk1 can enhance the APC/C-Cdc20-dependent polyubiquitylation of PDZ-RhoGEF.

In summary data presented in this chapter suggests that PDZ-RhoGEF is targeted for APC/C-Cdc20 degradation in early mitosis, in a manner that is likely to be dependent upon Cdk1-dependent phosphorylation.

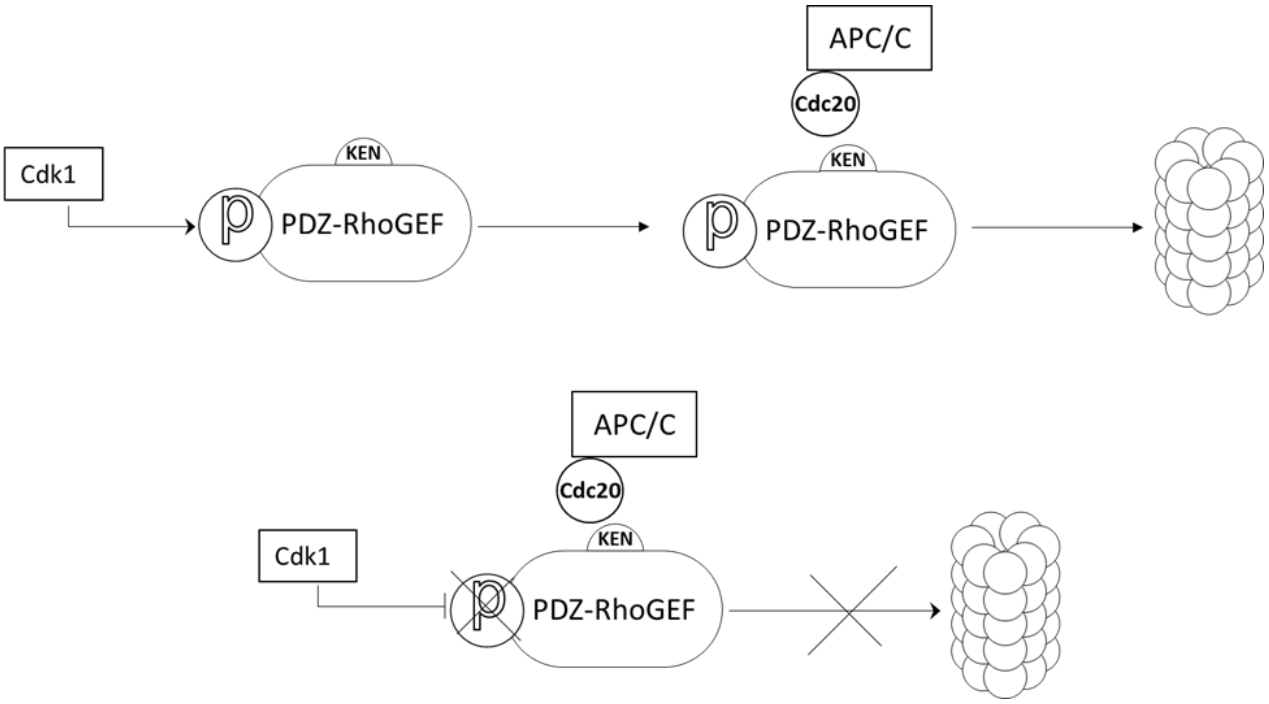

Figure 3.28: Schematic presentation indicating potential role of Cdk1 in the degradation of PDZ-RhoGEF. Mass spectrometric results presented in this chapter indicate that PDZ-RhoGEF is phosphorylated at 3 distinct sites during early mitosis (Fig 3.10), whilst Cdk1 inhibitors (in the presence of the proteasome inhibitor, MG132) were shown to inhibit PDZ-RhoGEF phosphorylation which led to the elevation of PDZ-RhoGEF protein levels.

4 INVESTIGATING THE INTRINSIC E3 UBIQUITIN LIGASE ACTIVITY OF UBCH10

4.1 Introduction

UbcH10 is a specific E2-conjugating enzyme for the APC/C that also serves to modulate APC/C E3 ligase activity through its N-terminal extension (Summers, Pan et al. 2008). UbcH10 is responsible primarily for the initiation process of ubiquitin chain formation on APC/C substrates. UbcH10 derives its initiation activity via its ability, when conjugated to ubiquitin to recognise threonine, glutamic acid and lysine residues in APC/C substrates, the TEK box, which is positioned in close proximity to APC/C recognition D box and KEN box motifs (Jin et al. 2008, Meyer and Rape 2014). As such, UbcH10 aids the nucleation of substrates to the APC/C for the initiation of APC/C substrate ubiquitylation (Jin et al. 2008, Meyer and Rape 2014). The TEK box is also present in ubiquitin and is formed of K6, L8, T9, E34, and I36 residues on its surface, which serves to promote the elongation of K11 chains on APC/C substrates in a UbcH10-dependent manner (Jin, et al. 2008).

In addition to its role as an E2-conjugating enzyme, UbcH10 possesses intrinsic E3 ubiquitin ligase activity and is known to undergo effective self-directed monoubiquitylation though the consequences of such autoubiquitylation are not known (David, Ziv et al. 2010). UbcH10 is known however, to be a substrate for polyubiquyitylation by the APC/C-Cdh1 complex in G1, which targets it for proteasomal-mediated degradation (Rape et al. 2006; Jin et al. 2008; Ye and Rape 2009). In general, E3 ligases catalyse polyubiquitin chain formation on target substrates, yet a number of E2s are known to possess intrinsic E3 ligase activity and undergo mono and, in some instances, short chain ubiquitylation (David et al. 2010).

Studies have investigated the molecular basis of UbcH10 ubiquitylation; it has been shown that APC/C-mediated UbcH10 ubiquitylation is distributive in nature, such that UbcH10 enhances the processivity of other APC/C substrates (Rape and Kirschner 2004). Indeed, the addition of competitive substrates, such as Securin that undergo processive degradation by the APC/C, to *in vitro* degradation assays, resulted in the inhibition of UbcH10's ability to be ubiquitylated by the APC/C (Rape, Reddy et al. 2006).

The molecular details, and requirement for UbcH10 autoubiquitylation have yet to be discerned fully. Given the known intrinsic E3 ligase activity of UbcH10 we wished to study this in more molecular detail. As such we hypothesised that UbcH10 might, like other E2-conjugating enzymes, possess the ability to undergo auto-polyubiquitylation. The principle aims of the study presented herein were to:

1. Investigate UbcH10 self-directed ubiquitylation activity *in vitro* and *in vivo*
2. Study the type of ubiquitin linkages assembled on UbcH10
3. Determine the the Lysine residues upon UbcH10 targeted for autoubiquitylation
4. Establish a high-throughput UbcH10 autoubiquitylation assay to screen drug libraries for UbcH10 inhibitors

4.2 Results

4.2.1 UbcH10 exhibits intrinsic E3 ligase activity and can self-assemble polyubiquitin chains

The ability of UbcH10 to undergo monoubiquitylation has been suggested to play an important role in the APC/C-dependent regulation of mitotic substrates, whilst the APC/C-Cdh1 K11-mediated polyubiquitylation of UbcH10 promotes UbcH10 degradation by the 26S proteasome. To validate the autoubiquitylation activity of UbcH10, an *in vitro* ubiquitylation assay was optimised that utilised WT GST-UbcH10, and UbcH10 catalytic cysteine mutants. The reactions were performed in the presence of a His_6-tagged E1 activating enzyme, Mg-ATP and WT ubiquitin and incubated for one hour at 37 °C after which time samples were separated by SDS-PAGE. We then transferred proteins to a nitrocellulose membrane and employed WB analyses to investigate the extent of UbcH10 ubiquitylation. For the detection of polyubiquitin chains on UbcH10 the membrane was first stained with Ponceau S red stain.

As such, the reconstitution of the UPS in this regard is aimed at mimicking the ubiquitylation pathway in order to investigate UbcH10 E3 ligase intrinsic activity. Moreover, as UbcH10 species used were typically GST-tagged, GST alone was used as a negative control. Initial results showed that UbcH10 underwent extensive auto-polyubiquitylation in the presence of E1 enzyme (**Fig. 4.1**). This is indicated by the discrete higher molecular weight protein bands that correspond to ubiquitin moieties attached to UbcH10 and that migrate slower than unmodified UbcH10 (cf lane 4 with lane 3, **Fig. 4.1**). In the absence of E1, WT UbcH10 is not modified by ubiquitin (cf lane 4 with lane 3, **Fig. 4.1**). To investigate the role of UbcH10's catalytic cysteine (Cys114) in this reaction two UbcH10 catalytic cysteine mutants were utilised. Previous studies have indicated that the mutation of Cys114 to Alanine abrogates both

the ubiquitylation and conjugation activity of UbcH10, whereas Mutation of Cys114 to Serine forms monoubiquitin conjugates alone (Townsley, Aristarkhov et al. 1997). Data presented here indicates that the C114A UbcH10 mutant is unable to undergo autoubiquitylation (cf lane 6 with lane 5, **Fig. 4.1**), whilst the C114S UbcH10 mutant only undergoes auto-monoubiquitylation (cf lane 8 with lane 8**, Fig. 4.1**). These results indicate that UbcH10 possesses intrinsic E3 ubiquitin ligase activity that catalyses auto-polyubiquitylation that is dependent upon its catalytic cysteine residue. Moreover, as these studies were conducted in the presence of reducing agents these data also indicate that polyubiquitin chain formation is on one or more K acceptor residues and not at the catalytic C residue.

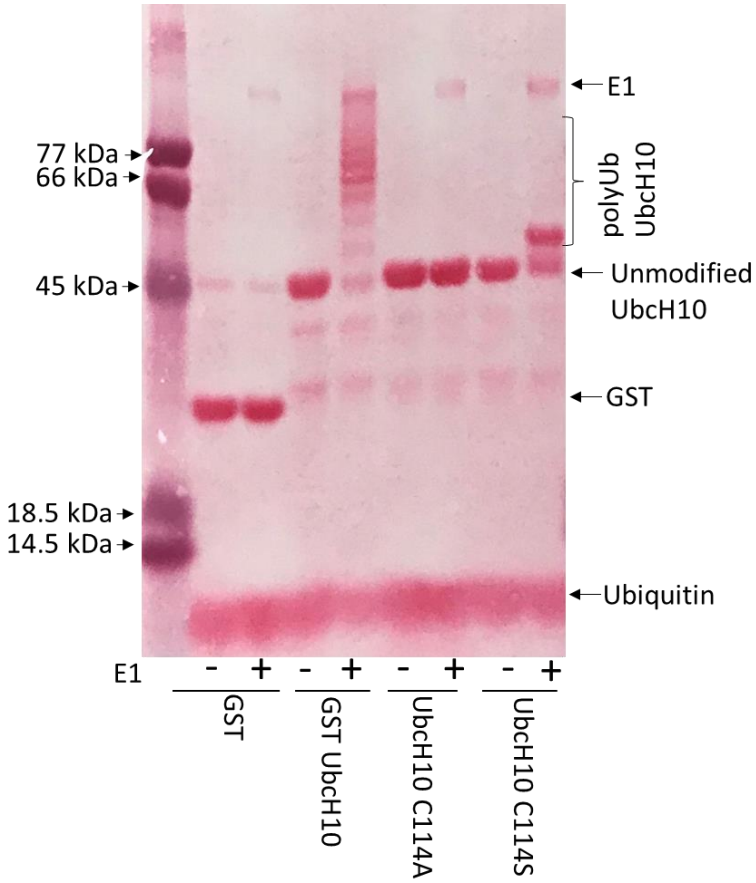

Figure 4.1: UbcH10 undergoes auto-polyubiquitylation which is dependent upon its catalytic cysteine residue. GST, GST-UbcH10, GST-C114A UbcH10 and GST-C114S UbcH10 were incubated with E1, MgATP and WT ubiquitin for one hour at 37 °C and resolved by SDS-PAGE and transferred to nitrocellulose (2.3.4). Proteins were stained with Ponceau S to visualise polyubiquitin chains. This Figure is representative of several similar experiments.

4.2.2 UbcH10 self-assembles polyubiquitin chains with different ubiquitin linkages

UbcH10 is a crucial component of the APC/C destruction machinery of mitotic substrates. As mentioned earlier (Chapter 1, section 1.4.6), the APC/C associates with two E2 conjugating enzymes to assemble branched polyubiquitin chains containing both K11 and K48 linkages on substrates in order to promote the proteasomal degradation of APC/C substrates. In collaboration with Prof. Robert Layfield (The University of Nottingham) ubiquitin linkages assembled on UbcH10 were analysed by mass spectrometry. In this experiment, polyubiquitylated UbcH10 formed from an *in*

vitro ubiquitylation assay and captured on glutathione agarose beads were trypsinised and UbcH10-derived peptides subjected to tandem array mass spectrometry on an LTQ-Orbitrap-Velos mass spectrometer. Peptide identification was conducted in data-dependent mode. Raw data files pertaining to individual LC-MS/MS acquisitions were compared with the Uniprot human database. Ubiquitin linkages were identified by inspection of ms/ms analyses for di-gly modified peptides (+114) using Scaffold proteome software and Mascot and X! tandem search engines for the validation of assigned spectra (unpublished observations, Prof. Robert Layfield, The University of Nottingham).

Results shown in **Figure 4.2** indicate that UbcH10 was able to form several different ubiquitin linkages. Consistent with the known role of K11 ubiquitin linkages in the degradation of APC/C substrates it is perhaps not surprising that K11 linkages were the most predominant ubiquitin linkage found on UbcH10 (**Fig. 4.2**). Likewise, given the role of K48 ubiquitin linkages in APC/C targeted ubiquitylation of substrates that this linkage is also found to a large extent (**Fig. 4.2**). Perhaps surprisingly, however UbcH10 was also able to form non-degradative linkages to high levels. As such, K6 ubiquitin linkages were the most abundant non-degradative linkage formed on UbcH10, followed by K63 and K29 being the less abundant linkages formed on UbcH10 (**Fig. 4.2**). Interestingly, the extent of K6 linkages on UbcH10 were comparable to K48 suggesting a potential role for K6 linkages in UbcH10 function. Taken together, these data confirm the role of UbcH10 in forming K11 and K48 linkages for proteasomal degradation of APC/C substrates but also establish that UbcH10 can form K6 as well as K63 and K29 linkages, suggesting that UbcH10 might participate in non-proteolytic pathways regulated by these linkages.

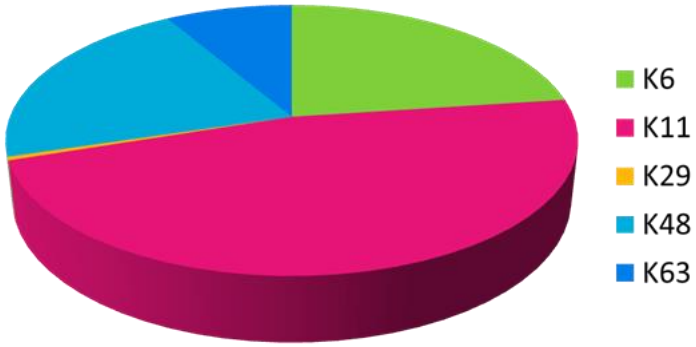

Figure 4.2: Characterisation of ubiquitin linkages on polyubiquitylated UbcH10. On-bead, immunoprecipitated, samples were first reduced using 50 mM dithiothreitol, then alkylated using 100 mM chloroacetamide and finally digested with sequencing-grade trypsin at 0.02 mg/ml. Following trypsinization, samples were submitted to MS/MS on an LTQ-Orbitrap-Velos spectrometer with nano-flow LC screening for daughter ions pertaining to di-gly modified peptides.

4.2.3 **Confirmation that UbcH10 self-assembles K6 ubiquitin linkages *in vitro***

The role of K6 ubiquitin linkages in biology is poorly understood. Thus, following the observation that UbcH10 possesses the ability to self-decorate with polyubiquitin chains that contain a high proportion of K6 linkages (**Fig. 4.2**), the next aim was to confirm that UbcH10 can indeed self-assemble polyubiquitin chains with K6 linkages. To do this, series of *in vitro* ubiquitylation assays were conducted with GST, GST-UbcH10 and GST-UbcH10 catalytic cysteine mutants, C114A and C114S as described (Chapter 2, section 4.2.1). After separation on SDS-PAGE samples were transferred to nitrocellulose and subjected to WB analysis. In order to identify whether UbcH10 formed polyubiquitin chains with K6 linkages we used an affimer that has previously been shown to detect K6 di-ubiquitin specifically and that is commercially available (Michel, Swatek et al. 2017). Affimers are non-antibody proteins that are engineered to recognise particular protein epitopes with high specificity and avidity in a similar manner to monoclonal antibodies. As such the K6 affimer has high specificity and affinity for K6 di-ubiquitin linkages and can be used to detect K6 di-ubiquitin linkages

in polyubiquitlated proteins. In this study GFP-tagged K6 affimer was used for better visualisation.

Consistent with the mass spectrometry data presented above, WB analysis with the GFP-tagged K6 affimer determined that UbcH10 could self-assemble K6-linked ubiquitin chains (see GFP-stain of discrete high molecular weight ubiquitin moieties on UbcH10 in lane 4, **Fig. 4.3**). Moreover, these data indicated that the catalytic cysteine residue, Cys114, was required for UbcH10 to self-assemble K6-linked polyubiquitin chains (as indicated by the lack of a GFP signal in lane 6, **Fig. 4.3**), whilst the K6 affimer used to detect the K6 linkages was not able to recognise UbcH10-conjugated to monoubiquitin in the presence of the catalytic mutant Cys114S (as indicated by the lack of a GFP signal in lane 8, **Fig. 4.3**). These data confirm the ability of UbcH10 to undergo auto-polyubiquitylation *in vitro* and assemble atypical K6-linked ubiquitin chains in this process.

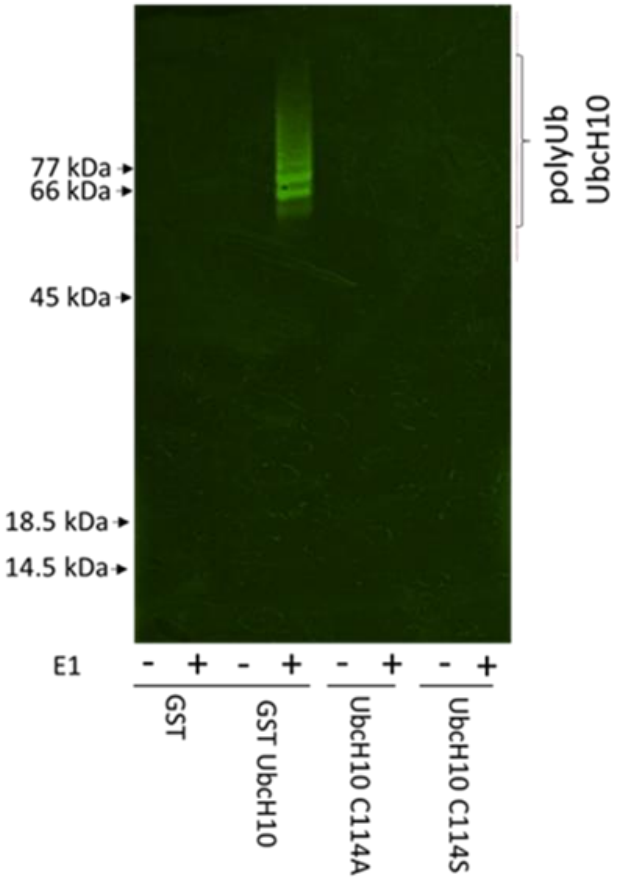

Figure 4.3: UbcH10 self-assembles polyubiquitin chains possessing K6 ubiquitin linkages. GST, GST-UbcH10, GST-C114A UbcH10 and GST-C114S UbcH10 were incubated with E1, MgATP and WT ubiquitin for one hour at 37 °C. The reactions then subjected to SDS-PAGE and subject to WB with the GFP-tagged K6 affimer. These data are representative of three identical experiments.

4.2.4 **The GST moiety does not contribute to UbcH10 E3 ligase activity**

The Glutathione S- transferases (GSTs) are a family of enzymes that catalyse the conjugation of glutathione to substrates. It is often used as a tag in biology to aid the purification of proteins synthesized in bacterial or other cellular systems (Sheehan et al. 2001). As such, this tag was utilised to obtain purified GST-UbcH10 for use in *in vitro* assays. However slim, to discount the possibility that GST intrinsic enzymic transferase activity enhanced UbcH10 E3 ubiquitin ligase activity, *in vitro* ubiquitylation assays were carried out using His_6-tagged UbcH10 in addition to GST-UbcH10, in the presence of His_6-tagged E1, MgATP and WT ubiquitin to eliminate the possibility that GST contributed towards UbcH10 autoubiquitylation. Ubiquitylation reactions were

separated by SDS-PAGE, transferred to nitrocellulose membrane and initially stained with Ponceau S red stain to visualise UbcH10 and polyubiquitylated UbcH10 (panel i, **Fig. 4.4**). The membrane was then subjected to WB analysis with the GFP-tagged K6 **affimer** to detect K6 di-ubiquitin linkages on both GST-UbcH10 and His-UbcH10 (panel ii, **Fig. 4.4**).

Ponceau S staining revealed that both GST-tagged UbcH10 and His_6-tagged UbcH10 were able to self-decorate with polyubiquitin chains in the presence of an E1 activating enzyme (cf lanes 1 and 2, and lanes 3 and 4, panel i, **Fig. 4.4**.) indicating that the GST moiety did not contribute towards the formation of polyubiquitin chains on UbcH10. Further WB analyses with the GFP-linked K6 di-ubiquitin affimer revealed that both GST-tagged UbcH10 and His_6-tagged UbcH10 were able to form K6-linked polyubiquitin chains (panel ii, **Fig 4.4**). Taken together these data indicate that E3 ligase activity is an inherent property of UbcH10.

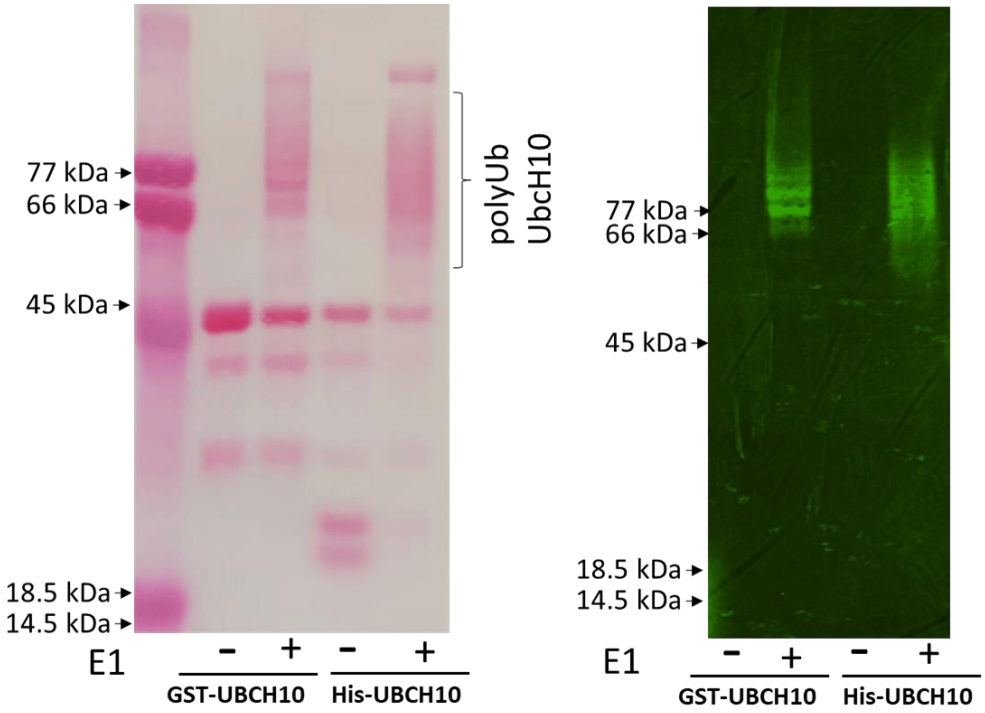

Figure 4.4: UbcH10 undergoes auto-polyubiquitylation containing K6-linked ubiquitin chains. GST-UbcH10 and HIS6-UbcH10 were incubated with E1, MgATP and WT ubiquitin for one hour at 37 °C, resolved by SDS-PAGE and transferred to nitrocellulose. Proteins were stained with Ponceau S (panel i) and K6-specific diubiquitin linkages were detected with a K6-specific affimer (labelled with GFP; panel ii). * creatine kinase runs at the same molecular weight as unmodified GST-UbcH10. These data are representative of three identical experiments.

4.2.5 **UbcH10 catalyses auto-polyubiquitylation using different ubiquitin linkages**

The mass spectrometric analysis of specific ubiquitin linkages on UbcH10 that had been subject to auto-polybiquitylatiuon *in vitro,* revealed that the most abundant ubiquitin linkages on polyubiquitylated UbcH10 were K11, K48 and K6 (**Fig. 4.2**). Given these findings, it was important to analyse UbcH10 autoubiquitylation in the context of different ubiquitin mutants to determine whether UbcH10 could self-decorate with polyubiquitin chains with homotypic K ubiquitin linkages and/or self-decorate with polyubiquitin chains with heterotypic K ubiquitin linkages.

To investigate these possibilities, the ability of UbcH10 to generate polyubiquitylated UbcH10 species with homotypic K ubiquitin linkages was initially investigated. As such, a number of *in vitro* autoubiquitylation assays were performed with UbcH10 using a panel of ubiquitin mutants that possessed only one K residue in its primary sequence. As before, *in vitro* ubiquitylation assays with GST-UbcH10 were performed in the presence of His_6-E1, Mg-ATP and WT ubiquitin or, in some case with K6 only (K6O), K11 only (K11O) or K48 only (K48O) ubiquitin. Assays were allowed to proceed at 37°C for one hour, after which time the reactions were separated by SDS-PAGE and transferred to a nitrocellulose membrane. The membrane was first stained with Ponceau S red stain to visualise proteins and then subjected to WB with the GFP-tagged affimer to identify K6-diubiquitin-containing UbcH10 species (**Fig. 4.5**).

Ponceau S staining indicated that UbcH10 could assemble homotypic polyubiquitin chains with either K6O, K11O or K48O ubiquitin (panel i, **Fig. 4.5**). Close inspection of the stained membrane revealed that autoubiquitylation with K6O, K11O and K48O ubiquitin was as efficient as autoubiquitylation with WT ubiquitin (cf unmodified GST-UbcH10 levels in lanes 2, 4, 6 and 8, **Fig. 4.5**). Moreover, WB analyses revealed that the K6 affimer recognised K6-polyubiquitin chains on UbcH10 more efficiently when K6O was the ubiquitin source when compared to UbcH10 polyubiquitylated in the presence of WT ubiquitin (cf lanes 2 and 4, panel ii, **Fig. 4.5**). This is presumably indicative of the heterotypic nature of ubiquitin linkages when WT ubiquitin is used and the lower proportion of K6-linkages relative to when K6O is used as the ubiquitin source. Interestingly, further analysis of the GFP blot revealed that there was some minor cross reactivity with K11 ubiquitin linkages on polyubiquitylated UbcH10, as evident by the detection of a weak GFP smear when K11O was used as the sole

ubiquitin source; there was no obvious cross-reactivity with K48 linkages however (cf lanes 4, 6 and 8, panel ii, **Fig. 4.5**). Taken together, these data indicate that UbcH10 can assemble K6, K11 and K4 homotypic ubiquitin linkages during autoubiquitylation.

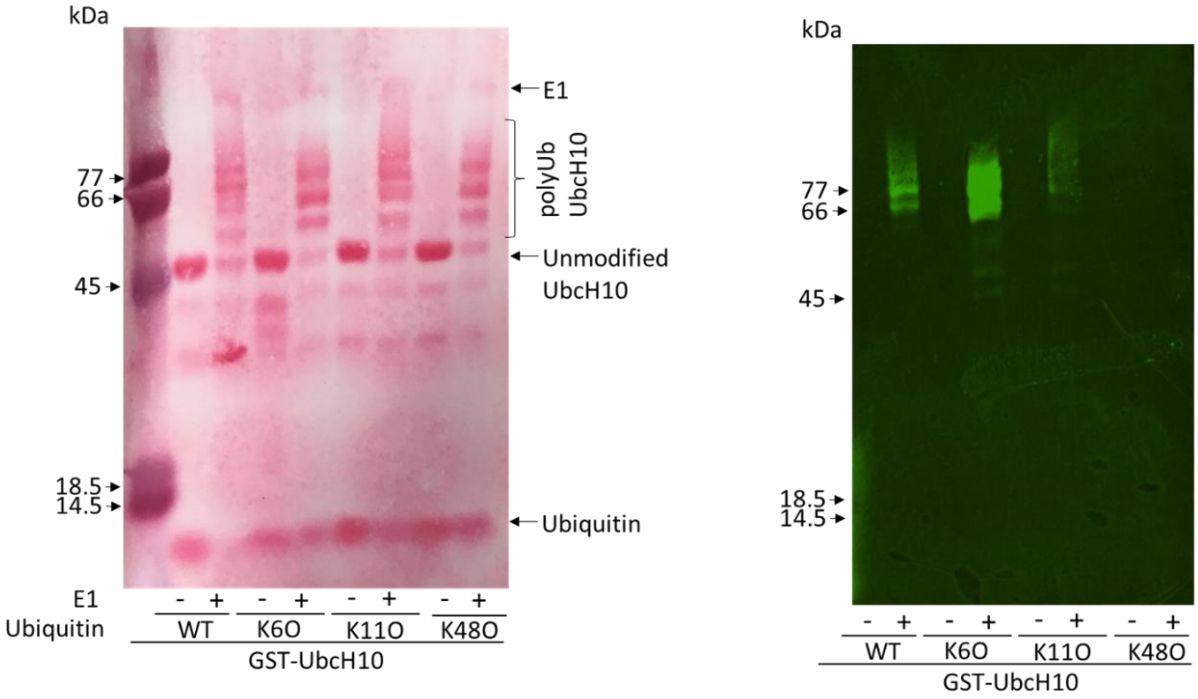

Figure 4.5: UbcH10 can self-assemble K6, K11 and K48 ubiquitin linkages on auto-polyubiquitylated UbcH10. GST-UbcH10 was incubated with E1, Mg-ATP and either WT, K6O, K11O or K48O ubiquitin for one hour at 37 °C. Samples were resolved by SDS-PAGE and transferred to nitrocellulose. Proteins were stained with Ponceau S, whilst K6-specific diubiquitin linkages were detected with a K6-specific affimer (labelled with GFP). These data are representative of three identical experiments.

4.2.6 Ablation of K6, K11 or K48 ubiquitin linkages does not affect UbcH10 auto-polyubiquitylation

To investigate further the requirement for ubiquitin linkages in UbcH10 auto-polyubiquitylation, ubiquitylation assays were performed with UbcH10 and ubiquitin mutants in which K6, K11 and K48 are mutated to arginine, to inhibit their ability to act as ubiquitin donors (**Fig. 4.6**). As such, these ubiquitin mutants negate the formation of K6, K11 and K48 ubiquitin linkages, respectively, which might impact UbcH10 auto-polyubiquitylation. To investigate this possibility GST-UbcH10, His_6-E1 and Mg-ATP

were incubated with the appropriate ubiquitin mutant for one hour 37°C. Samples were then separated by SDS-PAGE and transferred to nitrocellulose membrane prior to staining with Ponceau S red stain WB for K6 diubiquitin with the GFP-tagged K6 affimer.

The data presented in **Figure 4.6** indicates clearly that ablation of K6, K11, or K48 linkages does not impact, dramatically on the ability of UbcH10 to generate polyubiquitin chains, relative to WT ubiquitin (cf lanes 2, 4, 6 and 8, panels i and ii, **Fig. 4.6**). Consistent with the data using single K ubiquitin linkages (**Fig. 4.5**) these data suggest that UbcH10 can self-assemble polyubiquitin chains through multiple K ubiquitin linkages and, in the absence of a *bona fide* E3 ubiquitin ligase at least, does not show an intrinsic preference for different ubiquitin linkages. Inspection of the Ponceau S stained gel showed that the K48R polyubiquitin pattern of polyubiquitylated UbcH10 is different to polyubiquitylated UbcH10 that has undergone polyubiquitylation with WT ubiquitin, K6R or K11R ubiquitin (cf lane 8 with lanes 2, 4 and 6, panel i, **Fig. 4.6**). This presumably reflects the conformation of the K48R ubiquitin moiety, relative to WT, K6R and K11R ubiquitin. It was also evident from the GFP-stained gel that more K6 diubiquitin linkages were formed when K48 linkages were ablated through mutation, though not when K11 linkages were ablated (cf lanes 6 and 8 with lanes 2 and 4, panel ii, **Fig. 4.6**). As indicated previously, it appeared there was some low level, non-specific GFP staining when K6R was used as the ubiquitin donor (see lane 4, panel ii, **Fig. 4.6**), which presumably reflects K11 diubiquitin linkages identified in **Fig. 4.5**.

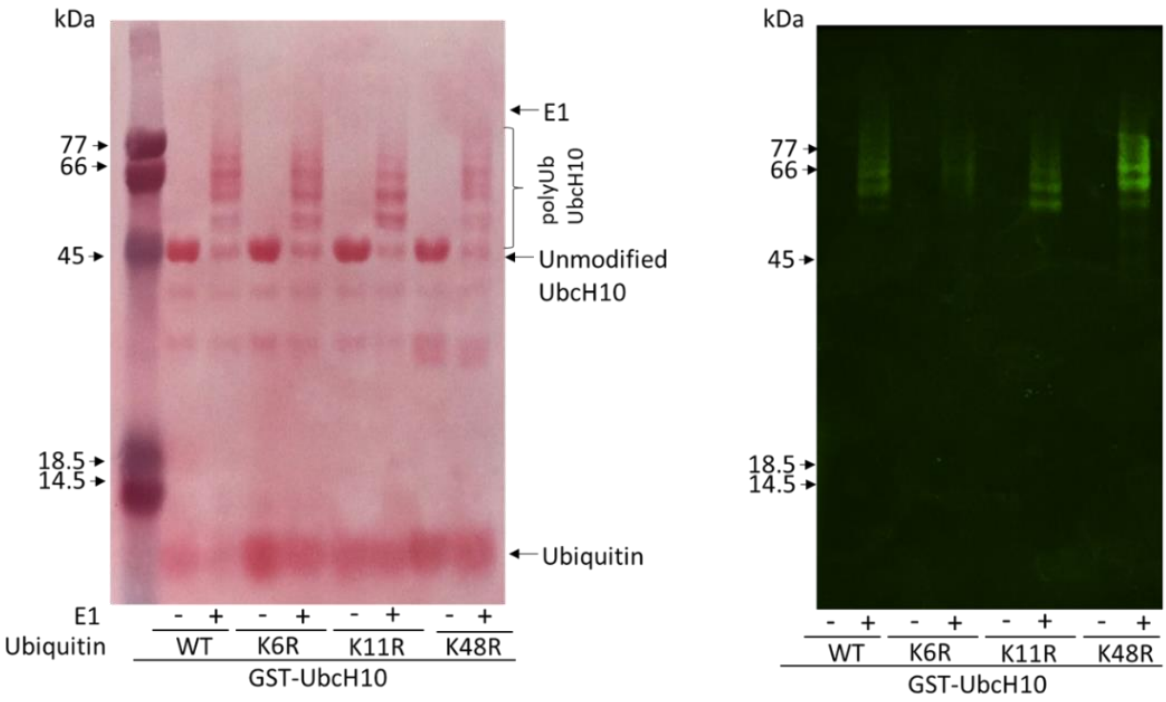

Figure 4.6: Ablation of K6, K11 or K48 ubiquitin linkages does not affect UbcH10 auto-polyubiquitylation. GST-UbcH10 was incubated with E1, Mg-ATP and either WT, K6R, K11R or K48R ubiquitin for one hour at 37 °C. Samples were resolved by SDS-PAGE and transferred to nitrocellulose. Proteins were stained with Ponceau S, whilst K6-specific diubiquitin linkages were detected with a K6-specific affimer (labelled with GFP). These data are representative of three identical experiments.

4.2.7 **Assignment of ubiquitin linkage specific sites on UbcH10**

In the ubiquitin-protein conjugation process, the C-terminal carboxyl group of ubiquitin conjugates to appropriate lysine acceptor residues in the target protein. To investigate the specific ubiquitylation sites on UbcH10, mass spectrometry analyses were performed in collaboration with Prof. Robert Layfield's laboratory at The University of Nottingham. Following the autoubiquitylation of GST-UbcH10 in the presence of His_6-E1, Mg-ATP and WT ubiquitin for one hour at 37°C, polyubiquitylated UbcH10 species were processed for analysis on an LTQ-Orbitrab-Velos spectrometer, as before (section 4.2.2), to identify ubiquitin K acceptor sites on UbcH10 (unpublished observations, Prof. Robert Layfield, The University of Nottingham).

The mass spectrometric analysis of UbcH10 K ubiquitin acceptor sites revealed that ubiquitin can conjugate with UbcH10 on six different lysine residues (**Fig. 4.7 A**). Of

the 11 Lysine residues contained in the UBC domain of UbcH10, six lysine residues located between amino acids 48-164 show apparent differential ability to be modified by ubiquitin (**Fig 4.7 A**; highlighted in **Fig. 4.7 B**). K121 appeared to be the most commonly modified residue as indicated in **Fig. 4.7 A**, a site previously known to undergo auto-monoubiquitylation in the absence of APC/C activity (Williamson, Banerjee et al. 2011). Residues K119 and K164 were also shown to undergo autoubiquitylation to appreciable levels whilst K48, K61 and K80 were all modified at apparently low levels (**Fig 4.7 A**). K119 has also been shown previously to undergo auto-monoubiquitylation in the absence of APC/C activity and is an important residue in the formation of UbcH10-ubiquitin adducts and in maintaining the conformation of the protein surrounding the catalytic cysteine (C114) residue (Lin, Hwang et al. 2002). Moreover, an alignment of UbcH10 species from *Homo sapiens*, *Mus musculus, Rattus norvegicus, Xenopus tropicalis* and *Danio rerio* show an extremely high conservation of the UbcH10 ubiquitylation sites identified by mass spectrometry (**Fig. 4.8**). Taken together, these data suggest an important role for multiple lysine residues on UbcH10 as ubiquitin acceptor sites.

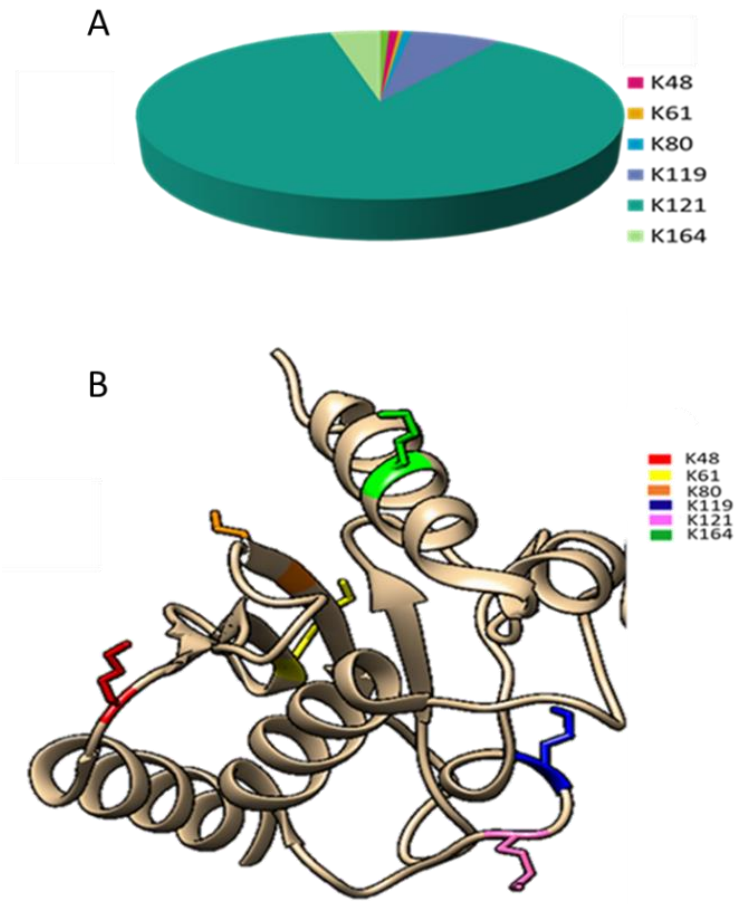

Figure 4.7: UbcH10 is ubiquitylated on multiple acceptor lysine residues. Trypsinized UbcH10-ubiquitin-conjugated peptides were subjected to mass spectrometry as described previously in section 4.2.2. (a) Pie chart indicating apparent proportion of UbcH10 ubiquitylation at different lysine residues. (b) Structural depiction of UbcH10 showing K acceptor sites on UbcH10 that conjugate with ubiquitin.

Figure 4.8: Sequence alignment of UbcH10 from different species showing UbcH10 ubiquitylation sites. using Clustal Omega software. Identified UbcH10 polyubiquitylation sites are underlined and highlighted in red and demonstrate that all lysine residues apart from K164 are fully conserved between the species investigated

4.2.8 **Generation of GST-UbcH10 K acceptor mutants**

In order to study the contribution of specific K acceptor sites on UbcH10 in more detail it was decided to generate K119R, K121R and K164R single, double and triple mutants in the context of full-length GST-UbcH10. Using the QuickChange site-directed mutagenesis kit from Agilent and using pGEX-2T-UbcH10 cDNA as a template, K119, K121 and K164 lysine residues were mutated to arginine using PCR as per the manufacturer's instructions (see section 2.5.7.1) Following PCR and digestion of parental, Dam-methylated pGEX-2T-UbcH10 cDNA with DpnI, PCR products were used to transform to XL1-Blue competent cells to isolate colonies for mutation screening by Sanger DNA sequencing. As such, the entire UbcH10 open-reading frame was sequenced and clones with the required mutation(s) isolated and plasmid DNA amplified. Mutants were made in sequence, such that single mutants were generated first, which were then used as templates for the double mutants, which were, in turn used as templates for the triple mutant (**Fig. 4.9 A-C**). GST-UbcH10 K acceptor single, double, and triple mutants were successfully generated as indicated

in the images generated by NCBI- BLAST software and Chromas (**Fig. 4.9 A-C**). Once appropriate pGEX-2T-UbcH10 mutants had been isolated the cDNAs were used to transform BL21 bacteria, which were then induced with IPTG to expression of the GST-UbcH10 fusion proteins (see section 2.3.7). GST fusion proteins were then purified by incubation with glutathione agarose, after which proteins were eluted with reduced glutathione and dialysed using a Tris-Glycerol dialysis buffer to remove the glutathione (see section 2.3.7). 5µg of the GST mutants were then separated on SDS-PAGE and stained with Coomassie blue staining to determine the purity of individual mutants and ensure that they were of the appropriate molecular weight (**Fig. 4.9 D**). For all GST-UbcH10 mutants a major 45 kDa species, corresponding to full-length GST-UbcH10 was observed, with minor, lower molecular weight protein bands (**Fig. 4.9 D**) that were immunoreactive with anti GST-antibodies (data not shown), and as such, likely represent GST-UbcH10 fragments that were not expressed fully.

Ai) K119R

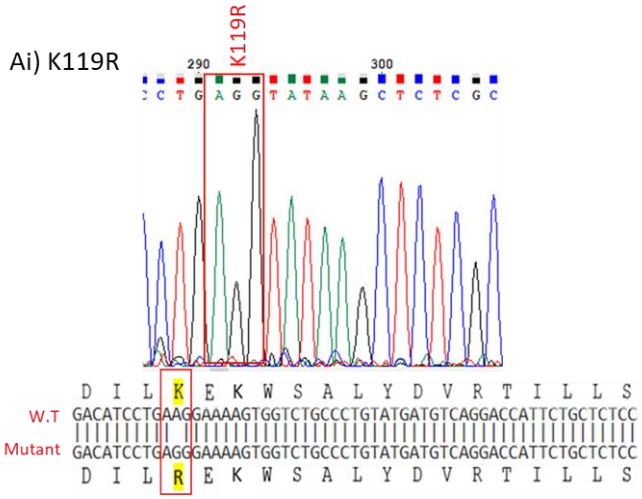

Aii) K121R

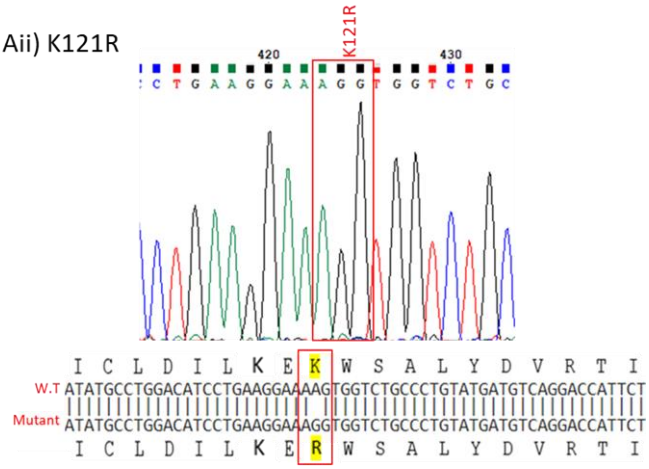

Aiii) K164R

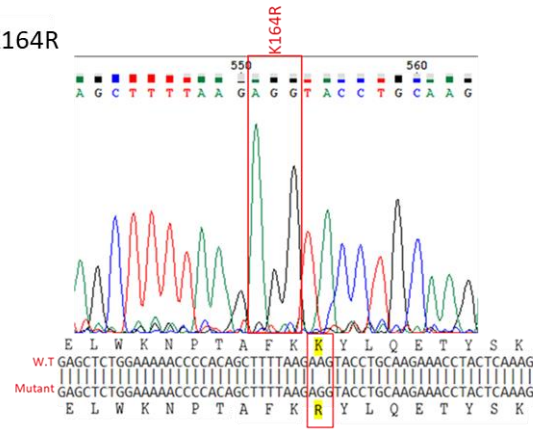

Bi) K119-121R

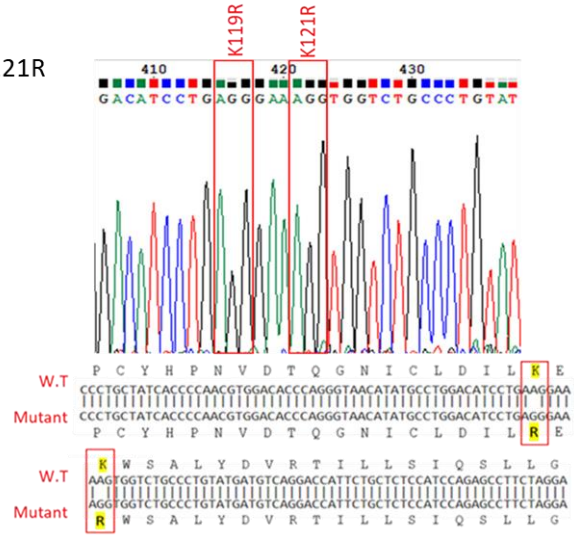

Bii) K119-164R

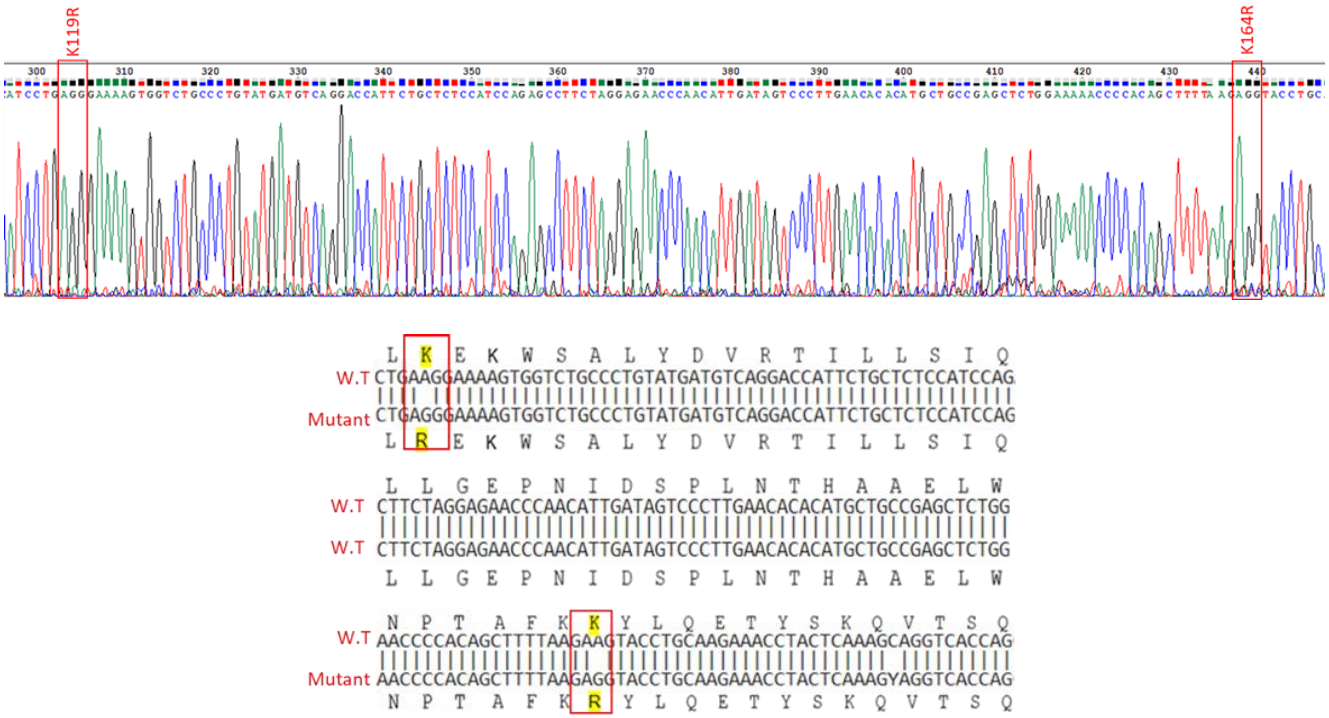

Biii) K121-164R

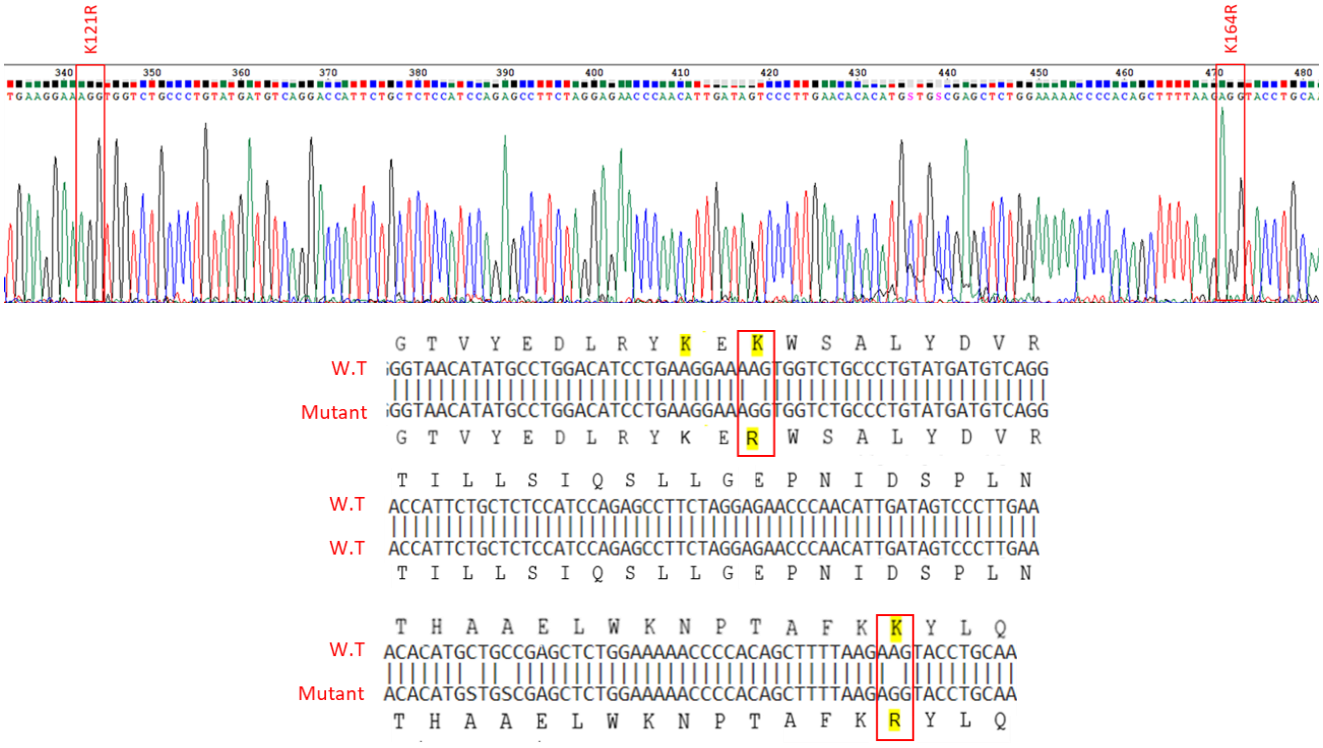

C) K119-121-164R

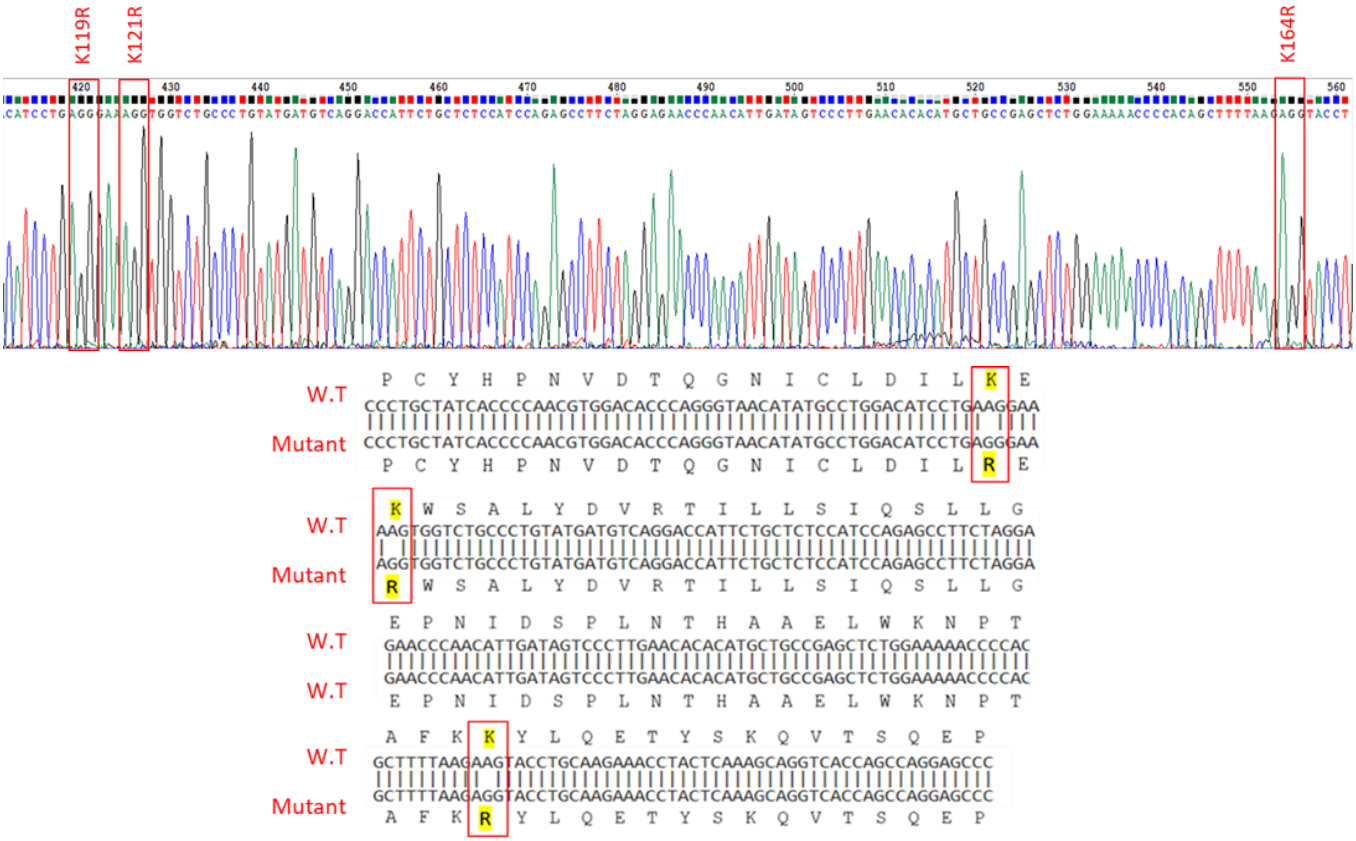

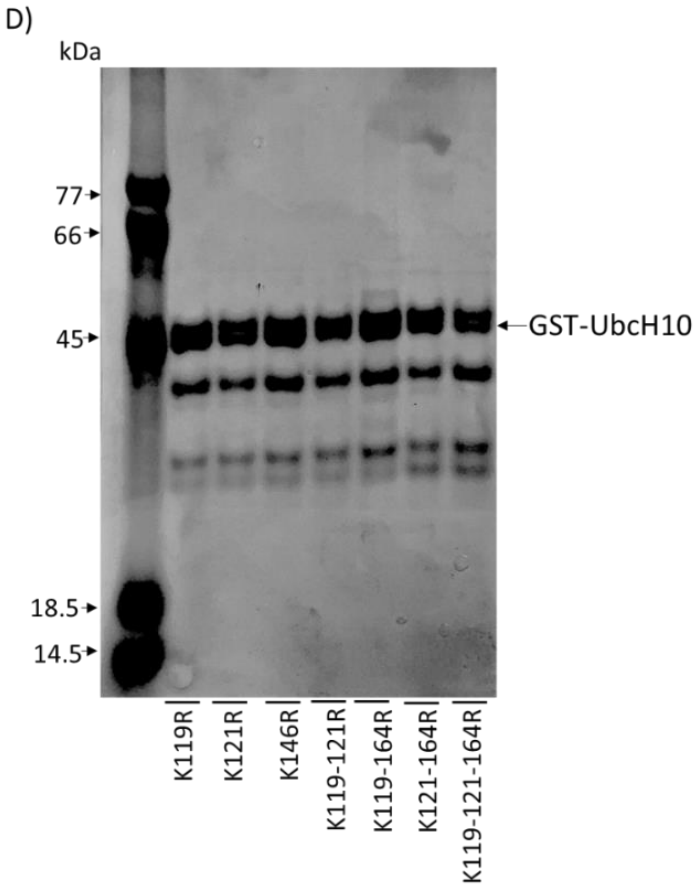

Figure 4.9: Generation of single, double, and triple pGEX-2T-UbcH10 K acceptor mutants. Using the QuikChange site-directed mutagenesis kit we successfully generated K acceptor site mutants in UbcH10, where specific lysine residues were mutated to arginine: (A) single mutants (K119R, K121R, and K164R), (B) double mutants (K119R-K121R, K119R-K164R, K121R-K164R) and (C) triple mutant (K119R-K121R-K164R). The images shown were produced by Chromas (Sanger sequencing) and NCBI-BLAST software. (D) 5µg of the generated GST-UbcH10 mutants were separated by SDS-PAGE and stained with Coomassie blue.

4.2.9 **K119 is the major UbcH10 autoubiquitylation K acceptor site *in vitro***

Mass spectrometric analysis of *in vitro* autoubiquitylated UbcH10 suggests that K121 is the major K acceptor site for ubiquitin conjugation, whilst K119 and K164 also contribute significantly as K acceptor sites for ubiquitin conjugation (**Fig. 4.6**). Given these findings it was investigated whether ablation of these lysine acceptor sites through mutation to arginine affected UbcH10 autoubiquitylation, hence the construction of the GST UbcH10 mutants (**Fig. 4.9**). In the first instance, a set of *in vitro* autoubiquitylation assays were performed using WT GST-UbcH10 and the single GST-UbcH10 KR mutants, GST-K119R, GST K121R and GST-K164. As such WT

GST-Ubch10 and UbcH10 mutants were incubated with His_6-E1, Mg-ATP and WT ubiquitin, for one hour 37°C, then separated on SDS-PAGE and transferred to nitrocellulose. As previously, the membrane was first stained with Ponceau S red stain and then WB for K6 diubiquitin linkages with the GFP-linked K6 diubiquitin affimer (**Fig. 4.10**).

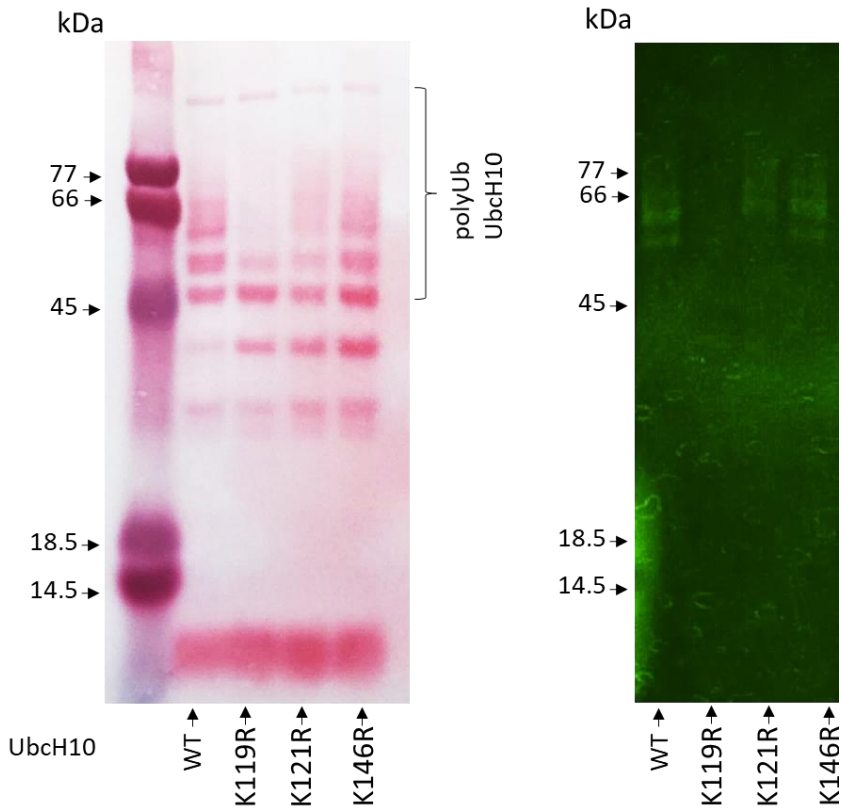

Figure 4.10: Ablation of the UbcH10 K119 acceptor site reduces polyubiquitin chain formation on UbcH10. GST-UbcH10, GST-UbcH10 K119R, GST-UbcH10 K121R and GST-UbcH10 K164 were incubated with E1, Mg-ATP and WT ubiquitin for one hour 37°C and resolved by SDS-PAGE and transferred to nitrocellulose. Proteins were stained with Ponceau S, whilst K6-specific diubiquitin linkages were detected with a K6-specific affimer (labelled with GFP). These data are representative of three identical experiments.

In contrast to the mass spectrometry data presented in **Fig. 4.6** the *in vitro* autoubiquitylation data with GST-UbcH10 K acceptor mutants suggests that K119 is the main UbcH10 acceptor K residue undergoing ubiquitin conjugation and polyubiquitin formation (**Fig. 4.10**). Both the Ponceau S staining and the detection of K6-linked diubiquitin with the GFP-linked K6 affimer show an appreciable reduction in

the level of UbcH10 polyubiquitylation when K119 is mutated to arginine, relative to WT GST-UbcH10, GST-UbcH10 K121R and GST-UbcH10 K164 (panels i and ii**, Fig. 4.10**). There was no appreciable reduction in polyubiquitin chain formation on UbcH10 when K121 and K164 acceptor sites were mutated to arginine (panels i and ii, **Fig. 4.10**). Taken together, these results suggest that UbcH10 K119 is the major acceptor for polyubiquitin chain formation on UbcH10.

To investigate further the contribution of K119 and K121 and K164 as ubiquitin acceptor sites in UbcH10 autoubiquitylation activity, a series of *in vitro* ubiquitylation assays were conducted using the double, and triple, GST-UbcH10 KR mutants generated previously (**Fig. 4.11**). Ponceau S red staining of nitrocellulose membranes revealed that ablation of K119 in any context (i.e. K119-K121R, K119-K164R and K119-K121-K164R) disrupted polyubiquitin formation on UbcH10, whilst polyubiquitin conjugation on WT GST-UbcH10 and GST-UbcH10 K121-K164R were very similar (panel i, **Fig. 4.11**). Likewise, WB analysis with the K6 diubiquitin affimer indicated that polyubiquitin conjugation to WT GST-UbcH10 and GST-UbcH10 K121-K164R were very similar (panel ii, **Fig. 4.11**). Taken together, these data confirm the importance of K119 as a major ubiquitylation site in agreement with single GST-UbcH10 KR mutant assay (**Fig. 4.10**). Interestingly, the mutation of K119 to arginine in the context of K121 and/or K164 had an effect on the formation of high molecular weight polyubiquitin chains containing K6 diubiquitin linkages as observed with the GFP-K6 diubiquitin affimer (panel ii, **Fig. 4.11**). As such, a smear of polyubiquitin was observed that was not apparent when K119 was intact (panel ii, **Fig. 4.11**). It is possible that in these situations other UbcH10 K residues act as major acceptors for ubiquitin conjugation. This will be discussed in more detail in section 4.3.

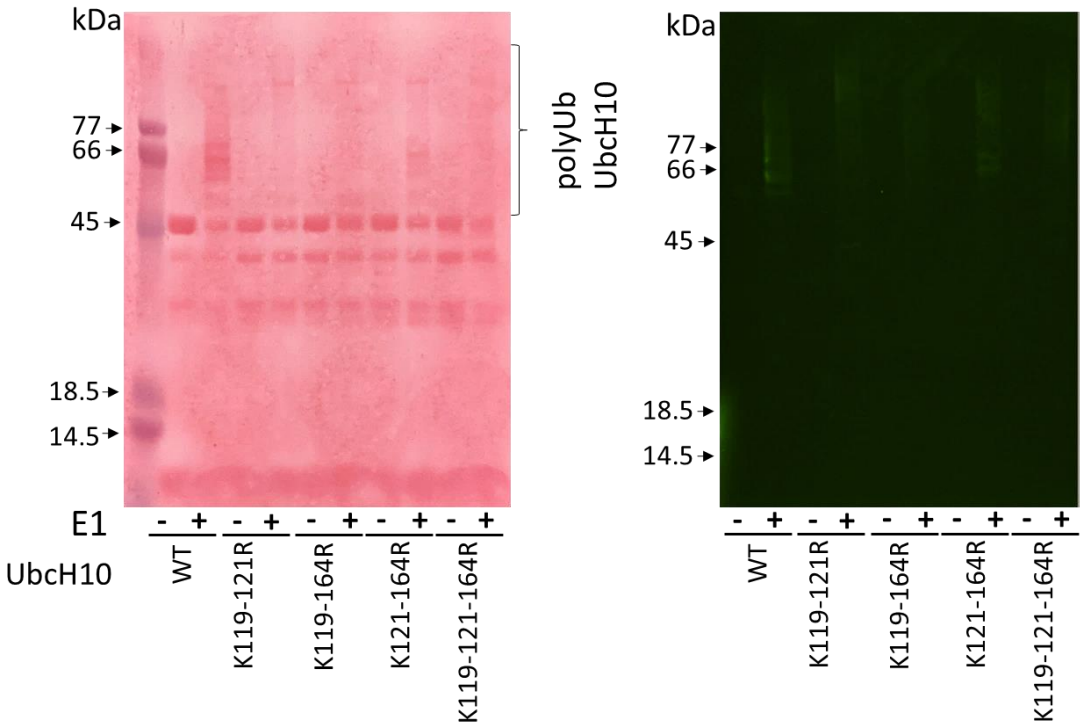

Figure 4.11: K119 is the major UbcH10 ubiquitylation site though K121 and K164 are also modified by ubiquitin. GST-UbcH10, GST-UbcH10 K119-121R, GST-UbcH10 K119-164R, GST-UbcH10 K121-164R and GST-UbcH10 K119-121-164R were incubated with E1, Mg-ATP and WT ubiquitin for one hour 37°C and resolved by SDS-PAGE and transferred to nitrocellulose. Proteins were stained with Ponceau S, whilst K6-specific diubiquitin linkages were detected with a K6-specific affimer (labelled with GFP). These data are representative of three identical experiments.

4.2.10 Investigating the role of K119 acceptor site inactivation on K121 UbcH10 polyubiquitylation

Results presented above suggest that UbcH10 K119 is the major K acceptor for ubiquitin conjugation following UbcH10 autopolyubiquitylation (**Fig. 4.10**) and that ablation of K119 in addition to K121 and/or K164 changes the pattern of UbcH10 polyubiquitylation (**Fig 4.11**). To study this phenomenon in more detail, specifically in relation to K121 ubiquitylation, a series of UbcH10 *in vitro* autoubiquitylation assays were conducted using the GST UbcH10 K119-K164R mutant as the UbcH10 species for autoubiquitylation. In this regard, it was decided to investigate whether ablation of K acceptor sites in ubiquitin modulated the pattern of UbcH10 autoubiquitylation (**Fig. 4.12**).

Consistent with our previous findings, the GST UbcH10 K119-K164R mutant was shown to be subject to low levels of autoubiquitylation with WT ubiquitin compared to WT GST UbcH10 (cf **Fig 4.12** and **Fig. 4.1**). Ponceau S staining clearly showed that a smaller proportion of the unmodified UbcH10 species had undergone polyubiquitylation with WT ubiquitin (cf lanes 1 and 2, panel i, **Fig 4.12 A** and **B**). Ponceau S staining also revealed that ablation of K6, K11 or K48 ubiquitin conjugation residues through mutation to arginine had little, or no effect, on polyubiquitylation conjugation to K121, and potentially other K residues in UbcH10 (panel i, **Fig 4.12 A**). Likewise, WB analyses with the K6 diubiquitin affimer indicated that polyubiquitin conjugation to K121 was only modestly affected by the use of K6R, K11R or K48R ubiquitin, instead of WT ubiquitin (panel ii, **Fig 4.12 A**). Taken together though, these data do heavily suggest that K121 of UbcH10 is polyubiquitylated and that higher molecular weight species of polyubiquitin form on K121 when compared to the K121-K164R GST-UbcH10 mutant, we cannot definitively exclude the possibility that other UbcH10 K residues are modified in this scenario, as we know that the triple UbcH10 mutant still undergoes modification with polyubiquitin.

Next, the ability of different ubiquitin donors to moderate autopolyubiquitylation of the K121 residue of UbcH10 were investigated. Thus, a series of UbcH10 *in vitro* autoubiquitylation assays were conducted using the GST UbcH10 K119-K164R mutant as the UbcH10 species for autoubiquitylation with WT ubiquitin or K6O, K11O or K48O ubiquitin as the ubiquitin source. The most striking observation of this experiment was that K6O and K48O formed distinctive polyubiquitin chains on K121, in comparison to WT ubiquitin and K11O ubiquitin (cf lane 4 and 8 with lane 2 and 6,

panels i and ii, **Fig. 4.12 B**). Indeed, although the K6O and K48O ubiquitin species were able to form high molecular weight polyubiquitin conjugates on GST-K119-164R UbcH10, they were not as high in molecular weight as those formed when WT ubiquitin or K11O ubiquitin was used as the ubiquitin source (cf lane 4 and 8 with lanes 2 and 6, panels i and ii, **Fig. 4.12 B**). These data suggest that K121 is likely to be a K acceptor site that undergoes autopolyubiquitylation and is able to utilise K6, K11 and K48 ubiquitin linkages in this regard.

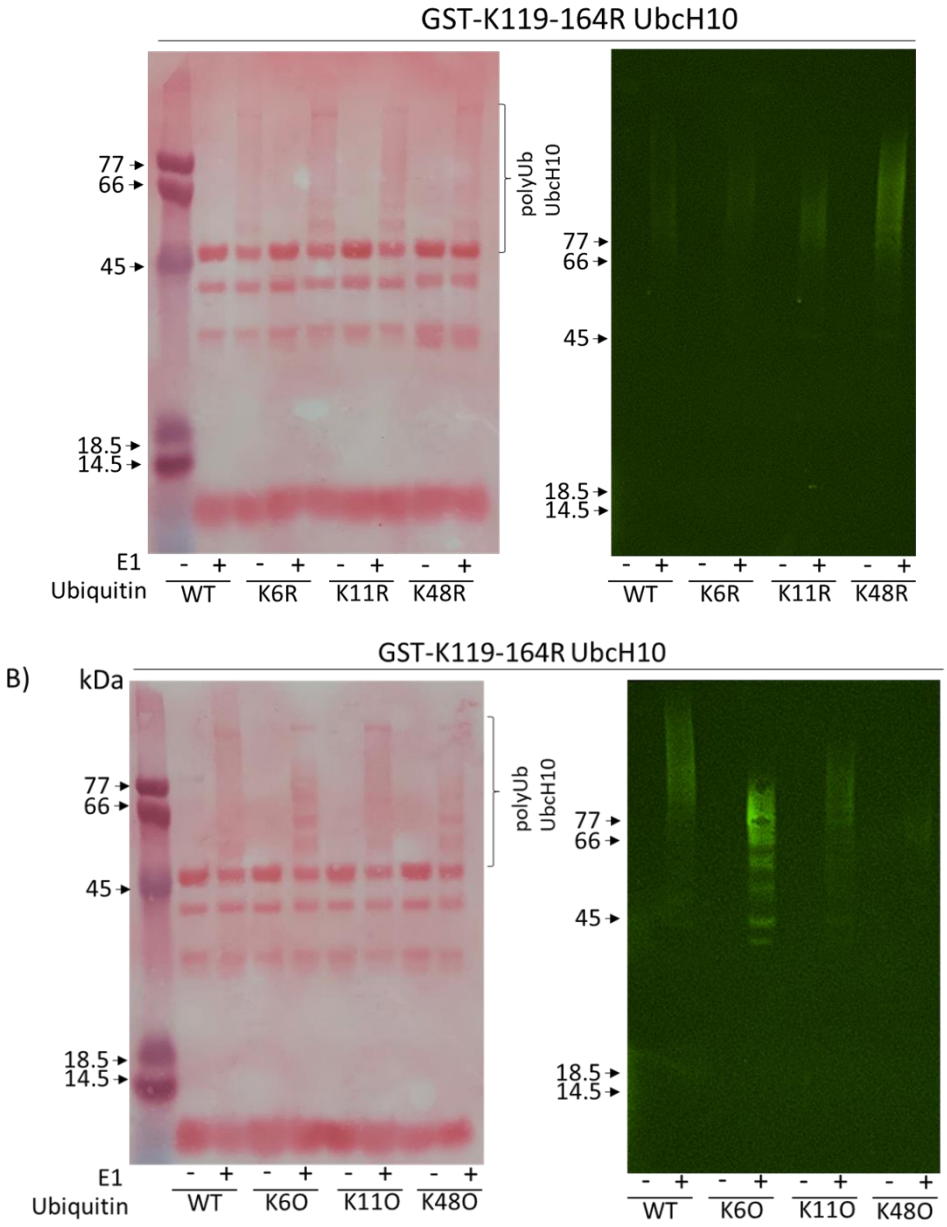

Figure 4.12: Investigating a role for K121 in UbcH10 ubiquitylation. GST-UbcH10 K119-164R was incubated with E1, Mg-ATP and either WT, K6R, K11R or K48R ubiquitin (A) or WT, K6O, K11O or K48O ubiquitin (B) for one hour at 37 °C. Samples were resolved by SDS-PAGE and transferred to nitrocellulose. Proteins were stained with Ponceau S, whilst K6-specific diubiquitin linkages were detected with a K6-specific affimer (labelled with GFP). These data are representative of three identical experiments.

4.2.11 Investigating the requirement for ubiquitin linkages in UbcH10 K119 autoubiquitylation

As the UbcH10 autoubiquitylation assays suggested that K119 is the major K acceptor for ubiquitin conjugation (**Fig. 4.10**) To confirm and extend, these observations, the GST UbcH10 K121-K164R mutant were used as the UbcH10 species for autoubiquitylation, which would facilitate a more focused consideration of UbcH10 ubiquitylation on K119. Therefore, a series of UbcH10 *in vitro* autoubiquitylation assays were performed with the GST UbcH10 K121-K164R mutant as the UbcH10 species for autoubiquitylation with WT ubiquitin K6R, K11R, K48R, K6O, K11O or K48O ubiquitin as the ubiquitin source.

In agreement with previous observations that indicate that K119 is the major acceptor site for UbcH10 autubiquitylation (**Fig 4.10**), Ponceau S staining revealed that GST-UbcH10 K121-164R was efficiently polyubiquitylated when WT ubiquitin was used as the ubiquitin source (panel i, **Fig. 4.13 A**). It was also determined that GST-UbcH10 K121-164R could still assemble polyubiquitin chains when K6, K11 or K48 acceptor sites were ablated through mutation to arginine, suggesting that there was no dependency for any linkage type in polyubiquitin assembly on UbcH10 (panel i, **Fig. 4.13 A**). Similarly, WB analyses with the K6 diubiquitin affimer indicated that polyubiquitin conjugation to K119 was not affected by the use of K6R, K11R or K48R ubiquitin, instead of WT ubiquitin (panel ii, **Fig 4.13 A**) but did highlight again that there was some cross-reactivity between the K6 diubiquitin affimer and other ubiquitin linkages (see K6R lanes, panel ii**, Fig 4.13 A**).

To validate these findings, a series of UbcH10 *in vitro* autoubiquitylation assays were conducted using the GST UbcH10 K121-K164R mutant as the UbcH10 species for

autoubiquitylation with WT ubiquitin or K6O, K11O or K48O ubiquitin as the ubiquitin source. Ponceau S staining of nitrocellulose membranes revealed that the GST UbcH10 K121-K164R mutant could self-assemble polyubiquitin chains as efficiently as WT ubiquitin, when WT ubiquitin was substituted with K6O, K11O or K48O ubiquitin (panel i, **Fig. 4.13 B**). These findings were corroborated when WB analyses were performed with the GFP-linked K6 diubiquitin affimer (panel ii, **Fig. 4.13 B**). Taken together, these data reaffirm that K119 is the major site for autopolyubiquitylation on UbcH10 and that polyubiquitin chains can be assembled through K6, K11 and K48 ubiquitin linkage.

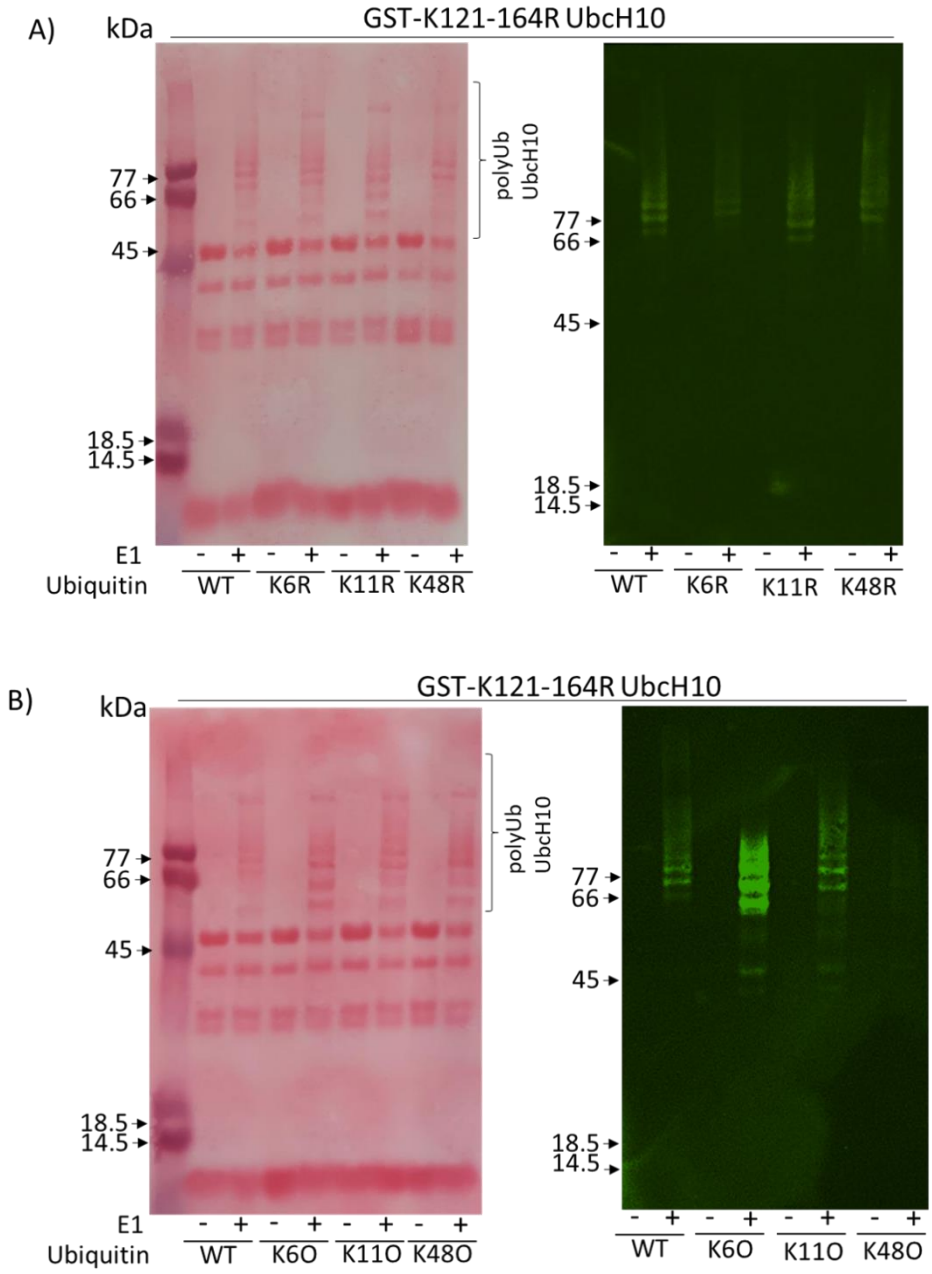

Figure 4.13: Investigating a role for K119 in UbcH10 ubiquitylation. GST-UbcH10 K121-164R was incubated with E1, Mg-ATP and either WT, K6R, K11R or K48R ubiquitin (A) or WT, K6O, K11O or K48O ubiquitin (B) for one hour at 37 °C. Samples were resolved by SDS-PAGE and transferred to nitrocellulose. Proteins were stained with Ponceau S, whilst K6-specific diubiquitin linkages were detected with a K6-specific affimer (labelled with GFP). These data are representative of three identical experiments.

4.2.12 Polyubiquitylated UbcH10 species containing mixed ubiquitin linkages are targeted for proteasomal degradation

It is well accepted that K11 and K48 ubiquitin linkages target proteins for 26S proteasome-mediated degradation (Xu, Duong et al. 2009). In this regard, it is known that polyubiquitin chains that possess both K11 and K48, or K48 alone, are targeted efficiently for proteasomal degradation, whilst K11O linkages are not targeted efficiently for degradation; K6 linkages are not thought to play a role in proteasomal degradation (Xu, Duong et al. 2009). As UbcH10 is known to be targeted for proteasomal degradation in an APC/C-Cdh1 dependent manner in G1 (Walker, Acquaviva et al. 2008). To investigate whether UbcH10 that had undergone autopolyubiquitylation was similiarly able to undergo 26S proteasome-mediated degradation, a 26S proteasome preparation from human HEK 293 cells (purchased form Ubiquigent) that had been treated with ubiquitin–vinylsulphone (Ub–VS) to inhibit the 26S proteasome deubiquitylase, USP14 (Lee et al. 2010). Initially, polyubiquitylated GST-UbcH10 species that had been subject to autoubiquitylation in the presence of either WT ubiquitin, K6O, K11O or K48O ubiquitin were generated. As non-ubiquitylated proteins are also known to be degraded by the proteasome in a ubiquitin-independent mechanism (Erales and Coffino 2014) the ability of unmodified UbcH10 to be degraded by the 26S proteasome was also investigated. GST-UbcH10 and polyubiquitylated GST-UbcH10 species were first isolated on glutathione agarose beads then incubated with 26S proteasome preparations in the presence of Mg-ATP, and incubated at 37°C for various times. Reactions were resolved by SDS-PAGE then subjected to WB with anti-GST antibodies to establish whether these UbcH10 species were targeted for degradation by the 26S proteasome (**Fig. 4.14**).

Results presented in **Figure 4.14** indicate that unmodified UbcH10 is targeted for proteasomal degradation during the course of the experiment but only after prolonged incubation periods (40 min +; **Fig. 4.14 A**). Interestingly, polyubiquitylated UbcH10 that had been generated with WT ubiquitin, was rapidly and efficiently targeted for 26-proteasome mediated degradation, as was K48 polyubiquitylated UbcH10 species with most of the substrate being degraded within 10 min of incubation (**Fig. 4.14 B** and **C**, respectively). Consistent with previous observations K11O polyubiquitin chains (in this instance on UbcH10) were not an efficient signal for 26S proteasomal degradation, with the majority of the K11 polyubiquitylated UbcH10 remaining after 60 min incubation (**Fig. 4.14 D**). Similarly, K6 polyubiquitylated UbcH10 was not an efficient signal for 26S proteasomal degradation, with the majority of the K6 polyubiquitylated UbcH10 remaining after 60 min incubation (**Fig. 4.14 E**). These data clearly suggest that UbcH10 possessing branched polyubiquitin chains through autoubiquitylation are substrates for 26S proteasomal degradation.

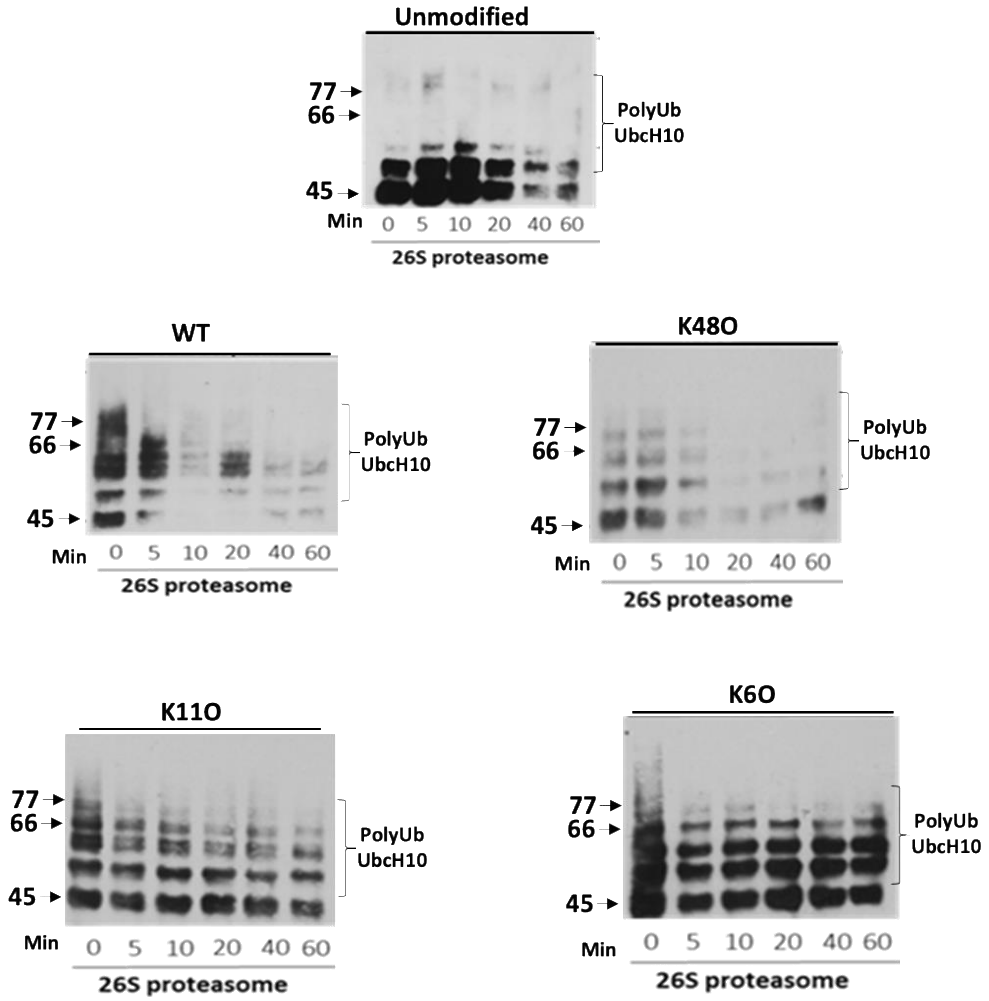

Figure 4.14: Self-decorated polyubiquitylated UbcH10 is a substrate for 26S proteasomal degradation. Unmodified GST-UbcH10 (A) or GST-UbcH10 ubiquitylated with WT (B), K48O (C), K11O (D) or K6O (E) ubiquitin, isolated on glutathione-agarose beads were incubated with purified 26S proteasome in the presence of Mg-ATP for various times at 37 °C. Samples were resolved by SDS-PAGE and transferred to nitrocellulose, whereupon the remaining levels of GST-were determined by WB with anti-GST antibodies. This experiment is representative of one other.

4.2.13 **UbcH10 autoubiquitylation activity *in vivo***

After demonstrating that UbcH10 underwent efficient autopolyubiquitylation *in vitro*, the next aim was to investigate whether UbcH10 underwent polyubiquitylation *in vivo*. To do this, the clonal TET-inducible UbcH10-HA U2OS Flp-in cell line was used previously generated in the laboratory that expresses UbcH10-HA to high levels in the presence of the tetracycline analogue, doxycycline (Foster, PhD thesis, University of Birmingham 2018) and then subjected them to an IP-WB to identify polyubiquitylated

UbcH10 species. Therefore, cells were initially treated with doxycycline to induce the exogenous expression of UbcH10-HA and then treated with +/- 5 µM proteasome inhibitor, MG132 for 4 hours to inhibit the proteasomal degradation of any polyubiquitylated UbcH10. Cells were then harvested in NETN and subjected to IP with IgG, anti-HA and anti-UbcH10 polyclonal antibodies. As such, a series of IPs were performed that were analysed for ubiquitylation by WB for UbcH10.

In agreement with the *in vitro* results (**Fig. 4.1**), WB analysis for UbcH10 revealed high molecular weight UbcH10 species, particularly in cells treated with both doxycycline and MG132 (cf lanes 11 and 12, **Fig. 4. 15**). Indeed, WB analysis revealed discrete UbcH10-monoubiquitin, UbcH10-diubiquitin and UbcH10-triubiquitin species as well as polyubiquitylated UbcH10 species that presented as a high molecular weight smear (see lane 12**, Fig. 4.15**). In the absence of MG132 only UbcH10-monoubiquitin was visible (see lane 11, **Fig. 4.15**). Control IPs with rabbit IgG antibody +/- MG132 failed to co-precipitate UbcH10 or any high molecular weight species, indicating that the high molecular weight species identified with anti-UbcH10 antibodies were most likely to be polyubiquitylated UbcH10. Overall, these data indicate that UbcH10 is subjected to polyubiquitylation *in vivo,* which is most apparent when cells are treated with the proteasome inhibitor, MG132, suggesting that at least some polyubiquitylated UbcH10 species are targeted to the proteasome for degradation.

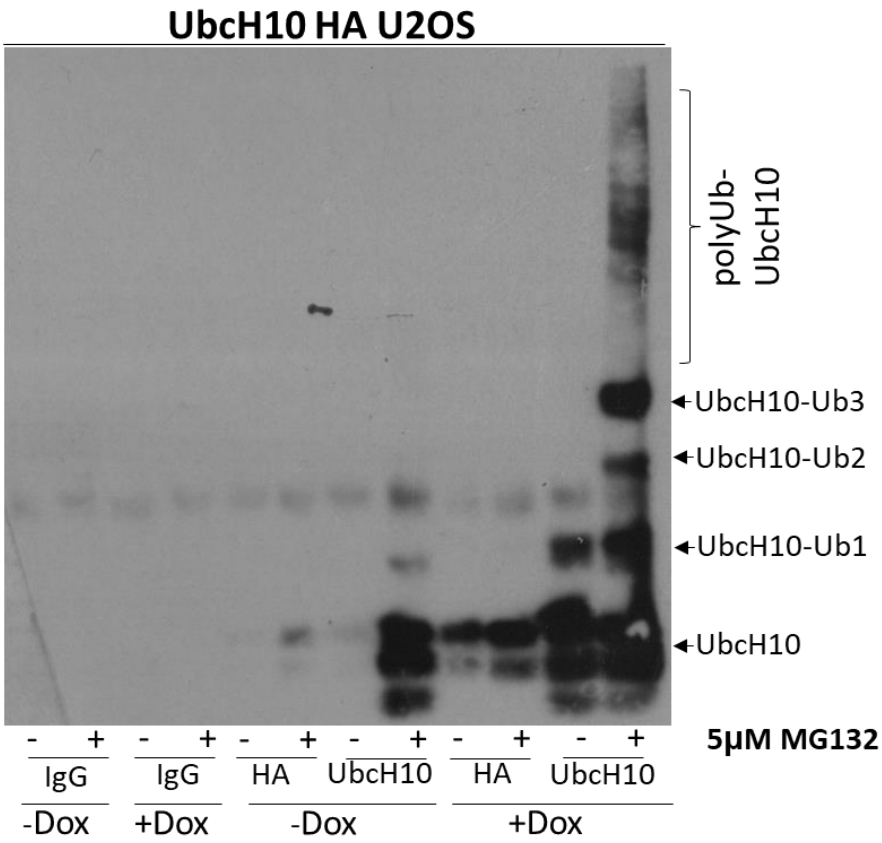

Figure 4.15: UbcH10 undergoes polyubiquitylation *in vivo*. TET-inducible UbcH10-HA U2OS cells were induced with doxycycline and incubated +/- 5 μM MG132 for 4h. Cells were subject to IP with an anti-UbcH10 polyclonal antibody, and subject to WB for UbcH10 with the UbcH10 polyclonal antibody, using a Protein G-HRP secondary. These data are representative of three identical experiments.

4.2.14 K119 is the major UbcH10 autoubiquitylation K acceptor site *in vivo*

Based on the results that show K119 is a major UbcH10 autoubiquitylation site *in vitro* (**Fig 4.10**) the next aim was to establish whether K119 was similarly polyubiquitylated *in vivo.* Thus, U2OS cells were transiently transfected with 5μg WT pcDNA5-FRT-UbcH10-HA or pcDNA5-FRT-K119R UbcH10-HA (see 4.2.15 for description of these constructs) then treated with +/- 5 μM proteasome inhibitor, MG132 for 4 hours to inhibit the proteasomal degradation of polyubiquitylated UbcH10. The cells were then harvested in NETN lysis buffer and subjected to IP with IgG and anti-UbcH10 polyclonal antibodies, then, following SDS-PAGE, to WB for UbcH10. The results presented in **Figure 4.16** re-affirmed earlier observations that UbcH10 was able to

form high molecular weight species following proteasomal inhibition, indicating that at least some polyubiquitylated UbcH10 is targeted for proteasomal degradation. In agreement with the *in vitro* ubiquitylation results presented in **Figure 4.10** ablation of the K119 ubiquitin acceptor site by mutation to R inhibited UbcH10 polyubiquitylation *in vivo* relative to WT UbcH10 (cf lane 8 with lane 4). Taken together, these results suggest that K119 is a major ubiquitylation acceptor site *in vivo*, although these experiments do not distinguish as to whether UbcH10 polyubiquitylation *in vivo* is due to intrinsic UbcH10 autoubiquitylation activity or due to the APC/C or another E3 ligase.

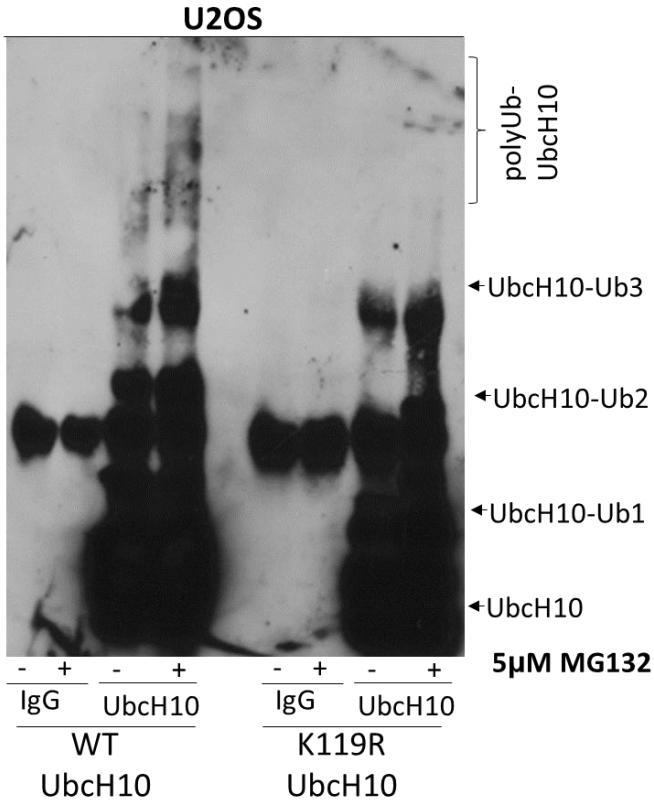

Figure 4.16: K119 is the major ubiquitylation site of UbcH10 *in vivo*. U2OS cells were transfected with WT UbcH10-HA and K119R UbcH10-HA. Four hours prior to harvesting the cells were treated with +/- 5 μM MG132; cells were then harvested in NETN lysis buffer. Cells were subjected to IP with an anti-UbcH10 polyclonal antibody and WB for UbcH10. These data are representative of three identical experiments.

4.2.15 Generation of an UbcH10-HA K121R U2OS FRT cell line

To investigate the role of UbcH10 autoubiquitylation activity *in vivo* in more detail it was decided to make TET-inducible FlpIn TREX U2OS cell lines that expressed K119R or K121R in a TET-responsive manner. To do this Quikchange site-directed mutagenesis was used to generate K119R and K121R using the TET-inducible, recombination-compatible vector, pcDNA5 FRT WT UbcH10-HA as a template. Following the validation of HA-UbcH10 mutants in the context of the whole UbcH10 gene, by Sanger sequencing, as described above for the pGEX-2T-UbcH10 mutants (section 4.2.10; data not shown), the products were used to produce hygromycin-resistant, TET-inducible USOS FRT monoclonal cell lines (as described in section 2.1.1.1). As such, individual colonies were isolated with a sterile pipette under low power microscopy in the tissue culture hood and expanded onto 24 well plates and then 6 well plates, respectively. WB analyses were then performed to determine the expression of each mutant. The results demonstrated that a number of cell lines expressing UbcH10-HA K121R to high levels upon Dox induction were isolated, although some isolated clones did not express UbcH10-HA K121R in response to Dox treatment (**Fig. 4.17 A**). Unfortunately, however, despite the isolation of a number of hygromycin-resistant clones we were not able to isolate any clones that expressed K119R in response to Dox treatment (**Fig. 4.17 B**). With time limitations, it was not possible to repeat this cloning procedure to generate TET-inducible K119R UbcH10-HA FlpIn TREX U2OS cells and investigate in more detail the requirement for APC/C and UbcH10 in the ubiquitylation of UbcH10 *in vivo*.

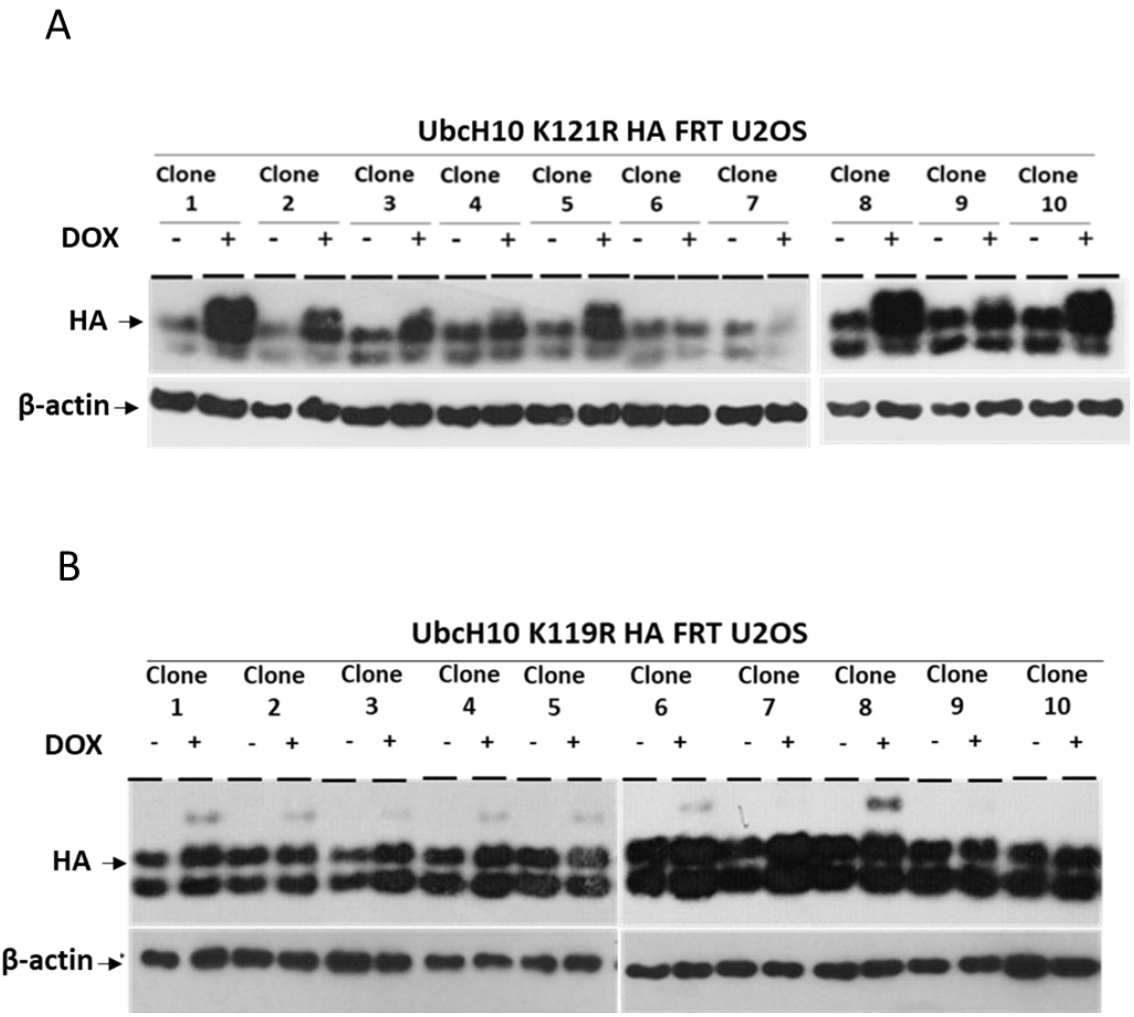

Figure 4.17: Generation of UbcH10-HA K121R U2OS FRT cell lines. The pcDNA5 FRT UbcH10-HA K121R (A) or K119R (B) plasmid was transfected into U2OS-FRT cells along with the recombination plasmid, pOG44. After the isolation of hygromycin-resistant colonies, the resultant monoclonal cell lines were treated +/- Dox, harvested and subjected to WB analyses to test the expression of each individual clone.

4.2.16 **UbcH10 is subjected to phosphorylation in mitosis**

Much of this chapter has been concerned with the investigation of UbcH10 autoubiquitylation. However, WB analyses of UbcH10 in mitosis are suggestive of lower molecular weight modifications of UbcH10 that might be monoubiquitylation, or potentially phosphorylation (data not shown). Indeed, some UBCs need to be phosphorylated for activation, though the requirement for UbcH10 phosphorylation in this regard is not known (Valimberti, Tiberti et al. 2015). Interestingly, the Phosphosite

plus web-site suggests that three distinct phosphorylation sites potentially exist in UbcH10, all identified through mass spectrometric screening, though these have yet to be confirmed by other means.

To investigate the possibility that UbcH10 might be subjected to phosphorylation in mitosis a phosphatase assay was performed upon α-UbcH10 immunoprecipitates isolated from asynchronously-grown and mitotic RPE1 and HeLa cells. Then, α-UbcH10 immunoprecipitates were incubated with the broad-range protein phosphatase, λ phosphatse (ppase) which can dephosphorylate all phosphorylation sites (pSer, pThr and pTyr) in a target protein (Mackiewicz, Seitzer et al. 2020). As such, asynchronous and nocodazole-arrested cells were harvested and subjected to IP with an α-UbcH10 antibody. Immunoprecipitates isolated on PrG beads were then treated with +/- λ ppase to remove any phosphate moieties attached to UbcH10. The reactions were then separated on SDS-PAGE and analysed for UbcH10 PTM by WB analysis. It is clear from the data presented in **Figure 4.18** that treatment of mitotically-derived UbcH10 with λ ppase reduced the levels of a higher molecular weight UbcH10 species indicating that UbcH10 is a substrate for phosphorylation during mitosis (cf lanes 7 and 8, panels i and ii, **Fig 4.18**).

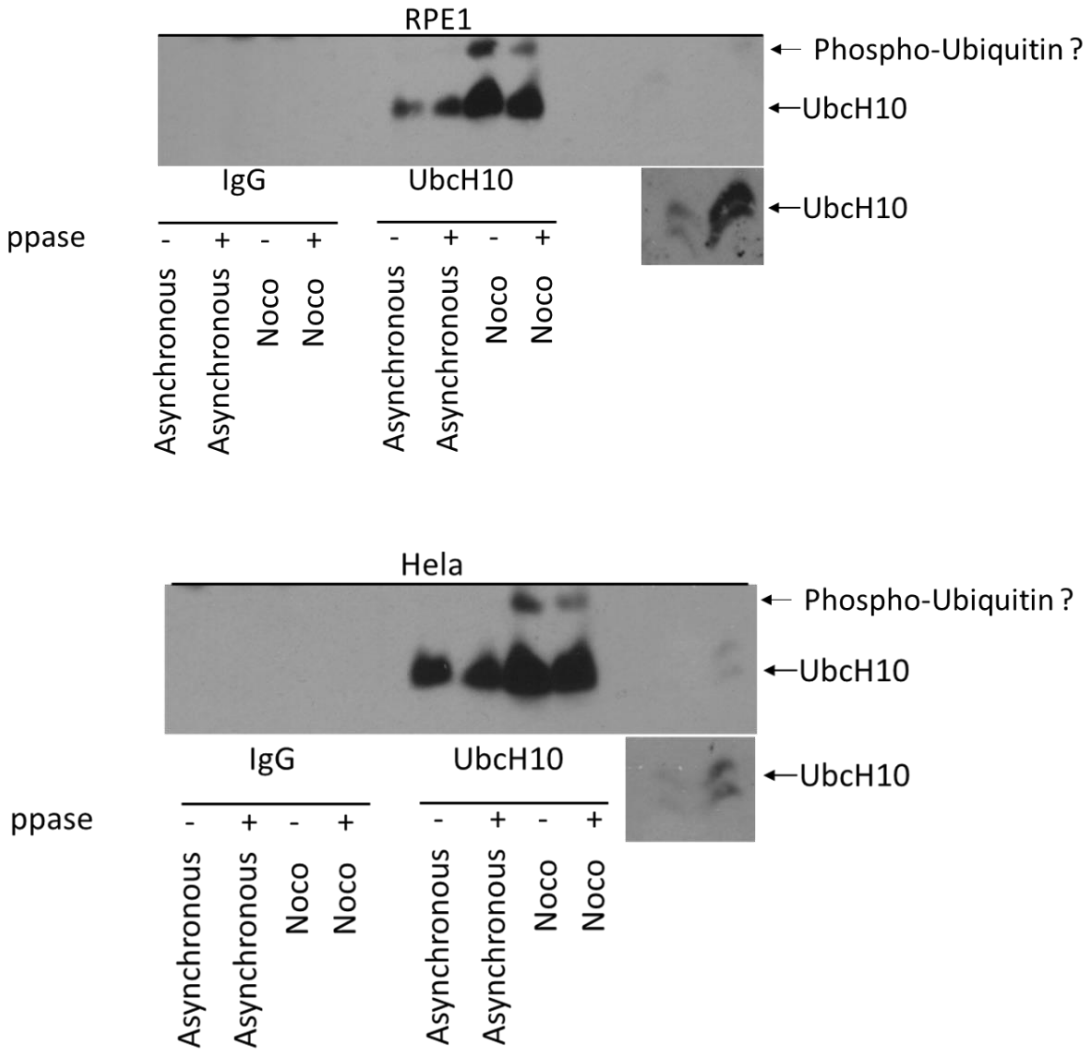

Figure 4.18: UbcH10 is phosphorylated in mitosis. Asynchronous and mitotically isolated RPE1 and Hela cells were harvested in NETN lysis buffer and incubated overnight at 4 °C with rabbit IgG or an anti-UbcH10 antibody. The lysates were then incubated for 3 hours at 4 °C with protein G Sepharose beads to isolate UbcH10. Immunoprecipitated proteins were then subjected to treatment with λ ppase for one hour at 37 °C. Immunoprecipitates and 50 µg of the total protein lysate were then separated on SDS-PAGE and analysed by WB with an anti-UbcH10 antibody.

4.2.17 Investigating the ubiquitin linkage preference of the FK2 anti-ubiquitin antibody for polyubiquitylated UbcH10

Up until now a combination of Ponceau S staining of nitrocellulose membranes and WB analyses with the GFP-K6 diubiquitin affimer has been used to investigate UbcH10 autoubiquitylation. As UbcH10 possesses intrinsic E3 ubiquitin ligase activity and undergoes auto-polyubiquitylation it might be possible to identify and/or generate UbcH10 active-site inhibitors that could be used therapeutically to inhibit the oncogenic

activity of UbcH10. As such, one of the major aims of this study was to develop a high throughput system that could be used to interrogate drug libraries for UbcH10 inhibitors. Although, potentially use the GFP-linked K6 diubiquitin affimer could be used in such a screening exercise the cost of the affimer makes this approach non-viable. As the FK2 antibody has been developed that identifies both conjugated monoubiquitin and polyubiquitin chains on substrates (Fujimuro, Sawada et al. 1994) whilst not detecting free monoubiquitin, this antibody is a more cost-effective alternative to the K6 affimer.

To investigate whether the FK2 antibody could recognise monoubiquitin and polyubiquitin chains conjugated to UbcH10 a UbcH10 autoubiquitylation assay was performed in the presence of WT ubiquitin, K6R, K11R or K48R ubiquitin. WB analyses with the FK2 anti-ubiquitin antibody clearly recognised monoubiquitin and polyubiquitin chains conjugated to UbcH10 when WT ubiquitin was used as the ubiquitin donor (see lane 2, **Fig. 4.19**). FK2 was also able to detect monoubiquitin and polyubiquitin chains conjugated to UbcH10 when K6R or K48R ubiquitin were used as the ubiquitin donor, though less efficiently than when WT ubiquitin was used as the donor (cf lanes 4 and 8 with lane 2, **Fig. 4.19**). Interestingly, however, the FK2 antibody was considerably less efficient at recognising, particularly, polyubiquitin chains conjugated to UbcH10 when K11R ubiquitin was the ubiquitin donor, relative to WT ubiquitin, or K6R or K48R ubiquitin (cf lane 6 with lanes 2, 4 and 8, **Fig. 4.19**). These data indicate that the FK2 antibody can be used effectively to detect polyubiquitin chjains conjugated to UbcH10, and moreover, suggest that FK2 might have a selective preference for K11 polyubiquitin chains.

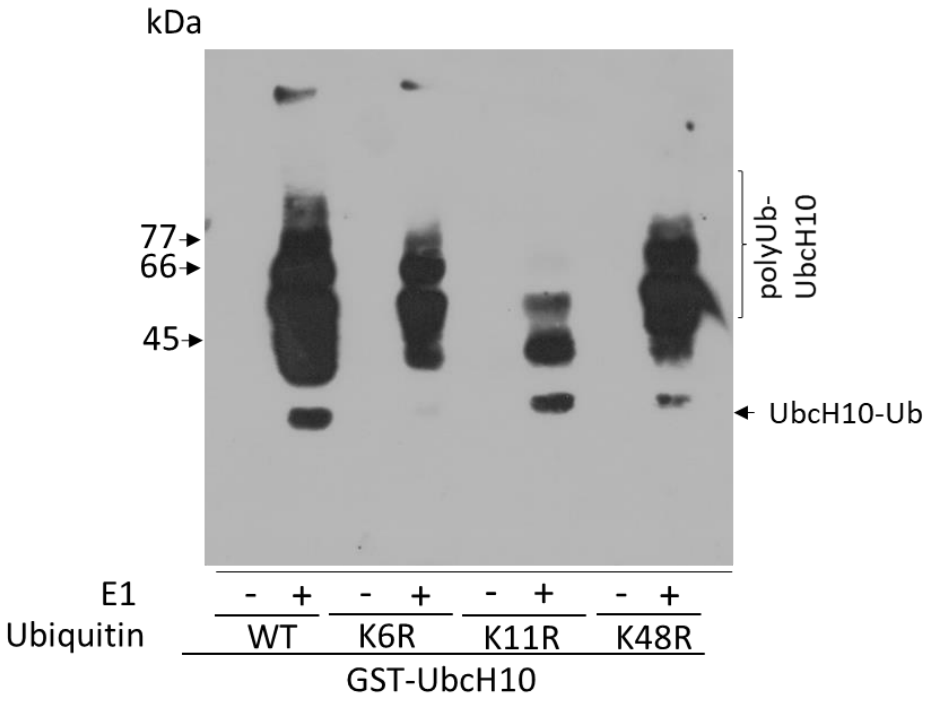

Figure 4.19: Detection of polyubiquitin chains on UbcH10 with the anti-ubiquitin, FK2 antibody. GST-UbcH10 was incubated with E1, Mg-ATP and either WT, K6R, K11R or K48R ubiquitin for one hour at 37°C. Samples were resolved by SDS-PAGE and transferred to nitrocellulose. Ubiquitin chains were detect using the FK2 anti-ubiquitin antibody which is purported to recognise both monoubiquitin and polyubiquitin chains conjugated to substrates, respectively. These data are representative of three identical experiments.

4.2.18 ELISA optimisation for a GST-UbcH10 *in vitro* ubiquitylation assay

As have been shown previously that the anti-ubiquitin antibody, FK2 recognizes polyubiquitylated UbcH10 by WB analysis (**Fig. 4.19**), it was thought appropriate to develop this assay for ELISA so that it is more amenable for high throughput screening and quantification of the effects of small molecule drugs on UbcH10 autoubiquitylation. To do this advantage was taken of a previous study that had developed a method to couple glutathione to Casein so that GST-coupled proteins could be coated in a 96 well plate format in a conformationally- ordered manner (Sehr et al. 2001). To establish that 96 well plates could be loaded efficiently with GST and GST-UbcH10, 96 well plates were coated with Glutathione-Casein overnight and GST and GST UbcH10 were then added at different concentrations, *i.e.* 0ng/well, 50ng/well, 100ng/well and

200ng/well in order to determine the right concentration of GST and GST UbcH10 to be used in the assay (see section 2.3.9). The plate was then incubated with an anti-GST antibody, followed by an HRP-coupled rabbit secondary antibody. After extensive washing plates were developed by incubating with the chromogenic HRP substrate, o-phenylenediamine dihydrochloride (OPD). The plate was then read after appropriate colour development using a SpectraMax ABS plus plate reader, Softmax pro 7 / ELISA endpoint with absorbance readings at 492nm (**Fig. 4.20**). ELISA readings indicated that 200ng/well of GST and GST-UbcH10 was the optimal concentration to use for the *in vitro* ubiquitylation assay (**Fig. 4.20 A-C**). These data indicated that there was no significant difference in the ability to load glutathione-Casein coated plates with GST or GST-UbcH10 (**Fig. 4.20 A-C**).

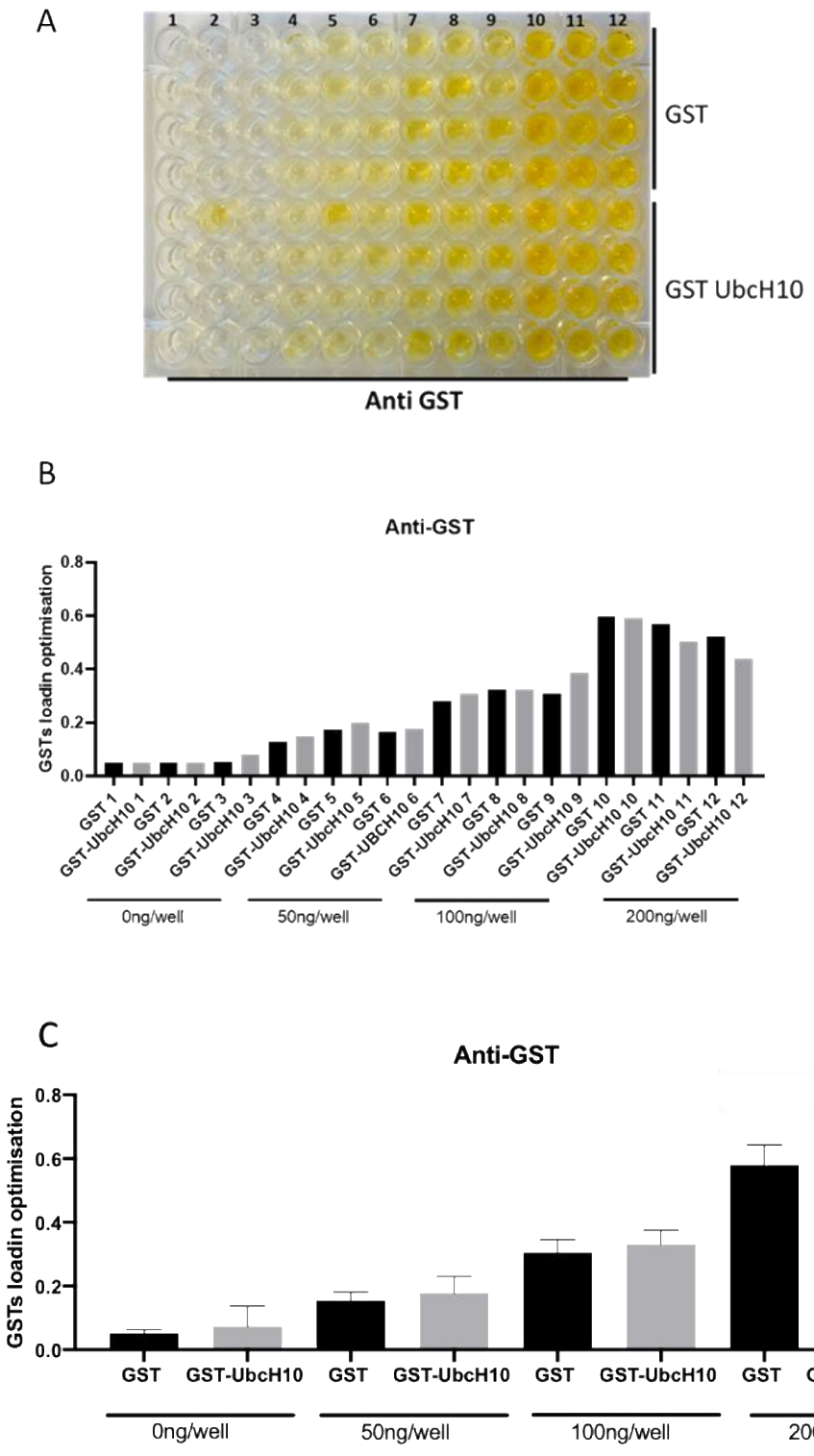

Figure 4.20: ELISA optimisation demonstrating equal loading of GST and GST-UbcH10 to glutathione-Casein coated 96 well plates. 96 wells plate were coated overnight with glutathione-Casein.GST and GST-UbcH10 at different concentrations (0ng/well, 50ng/well, 100ng/well and 200ng/well) were then loaded onto the plate which was subsequently incubated with an anti-GST antibody followed by incubation with a HRP-coupled rabbit secondary antibody and OPD for visualisation. Quantification was performed using a SpectraMax ABS plus ELISA reader. (A) Picture of the of the 96 wells plate following incubation with OPD. (B) Bar graph showing the mean column ELISA reading for GST and GST-UbcH10. (C) Bar graph showing the mean reading +/- Standard Deviation for both GST and GST UbcH10 loading. Data taken from one experiment, representative of one other

To demonstrate reproducibility GST and GST-UbcH10 were added at 200ng/well concentration to 96 well plates that had been coated previously with glutathione-Casein. The plate was then incubated, as before, with an anti-GST antibody, followed by an HRP-coupled rabbit secondary antibody. After development with the chromogenic HRP substrate, OPD the plate was then read using a SpectraMax ABS plus plate reader (**Fig. 4.21**). The data obtained indicated that GST and GST-UbcH10 could be reproducibly loaded to equal levels on 96 well plates (**Fig. 4.21 A-C**).

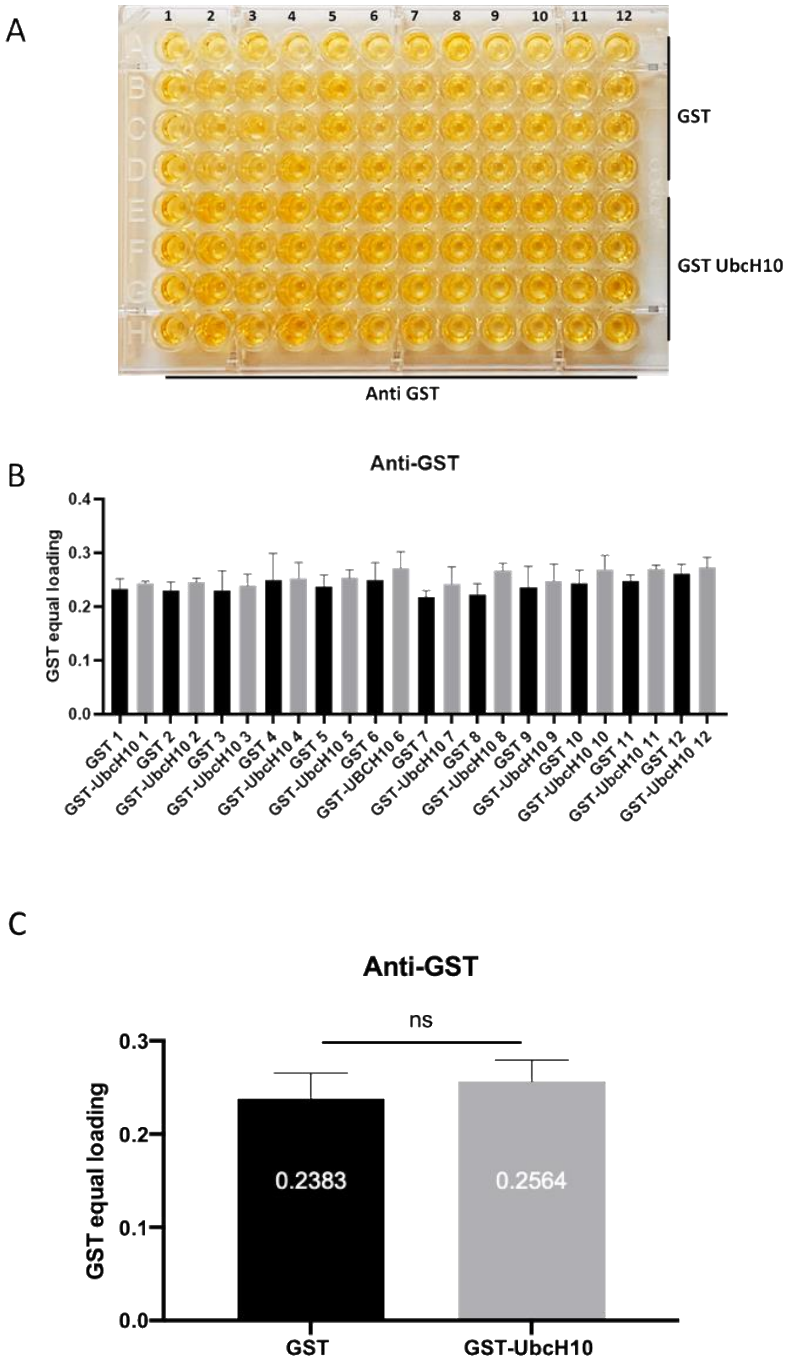

Figure 4.21: ELISA optimisation of GST and GST-UbcH10 loading on glutathione-Casein coated 96 well plates. 96 wells plate were coated overnight with glutathione-Casein. GST and GST-UbcH10 (200ng/well) were then loaded onto the plate which was subsequently incubated with an anti-GST antibody followed by incubation with a HRP-coupled rabbit secondary antibody and OPD for visualisation. Quantification was performed using a SpectraMax ABS plus ELISA reader. (A) Picture of the 96 wells plate following incubation with OPD. (B) Bar graph showing the mean column ELISA reading for GST and GST-UbcH10. (C) Bar graph showing the mean reading +/- Standard Deviation for both GST and GST UbcH10 loading. Data taken from one experiment, representative of one other. (ns) = P value >0.05, (*) P ≤ 0.05, (**) P ≤ 0.01, (***) P ≤ 0.001 and (****) P ≤ 0.0001

Finally, to confirm that GST could be discriminated from GST-UbcH10, plates were loaded with GST and GST-UbcH10 at 200ng/well concentration that had been coated previously with glutathione-Casein. The plate was then incubated with an anti-UbcH10 antibody, followed by an HRP-coupled rabbit secondary antibody. The plate was then read using a SpectraMax ABS plus plate reader after incubation with the HRP substrate, OPD (**Fig. 4:22**). The data obtained indicated that GST-UbcH10 could be discriminated from GST using this technique (**Fig. 4.22**).

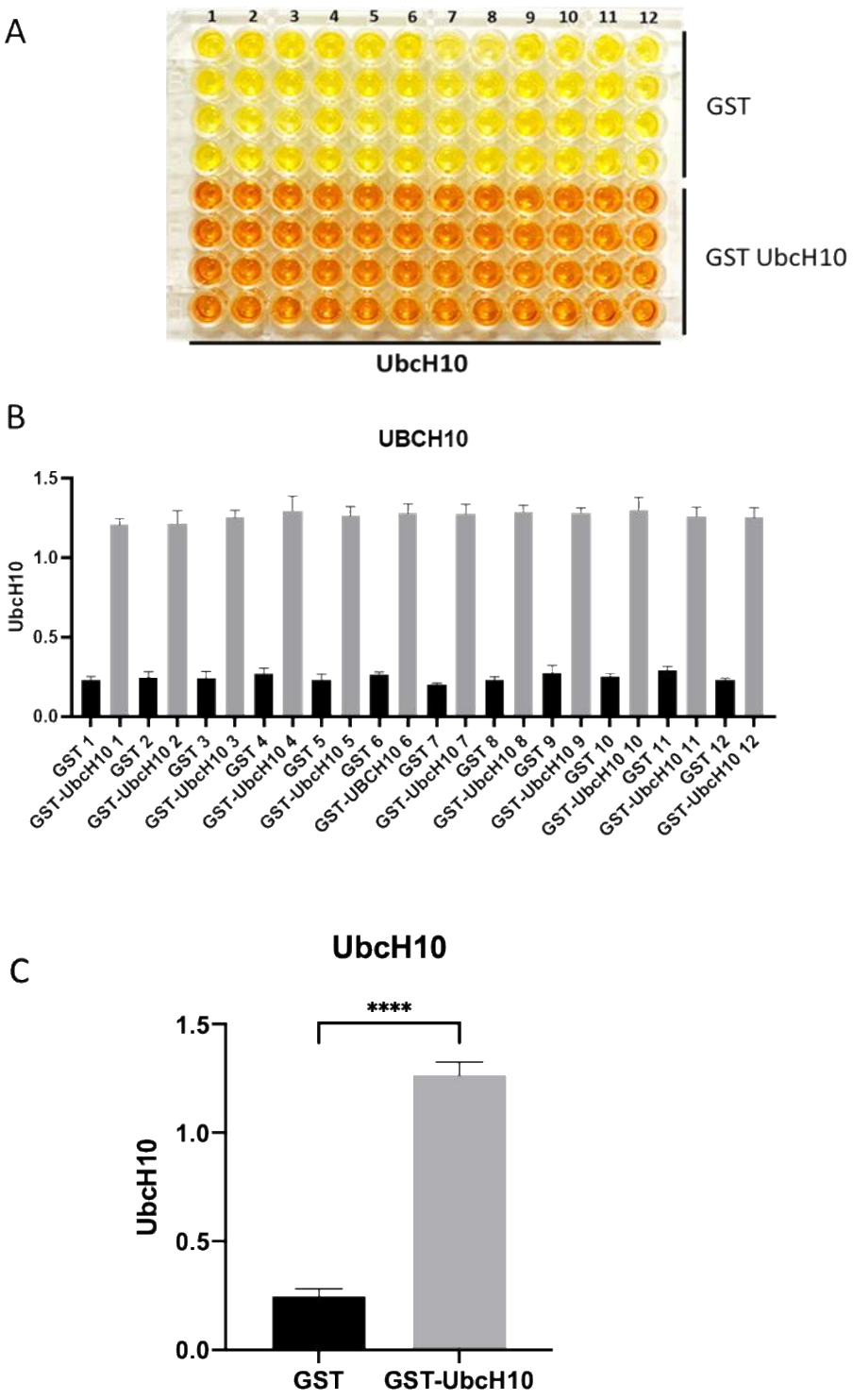

Figure 4.22: Identification of UbcH10 loaded onto glutathione-Casein coated 96 well plates as GST-UbcH10. 96 wells plate were coated overnight with glutathione-Casein. GST and GST-UbcH10 (200ng/well) were then loaded onto the plate which was subsequently incubated with an anti-UbcH10 antibody followed by incubation with a HRP-coupled rabbit secondary antibody and OPD for visualisation. Quantification was performed using a SpectraMax ABS plus ELISA reader. (A) Picture of the of the 96 wells plate following incubation with OPD. (B) Bar graph showing the mean column ELISA reading for GST and GST-UbcH10. (C) Bar graph showing the mean reading +/- Standard Deviation for both GST and GST UbcH10. Data taken from one experiment, representative of one other. (*) $P \leq 0.05$, (**) $P \leq 0.01$, (***) $P \leq 0.001$ and (****) $P \leq 0.0001$. (N=48 replicates)

Taken together, the results presented in **Figs. 4.20-4.22** confirmed successful optimization an ELISA technique for the loading of GST and GST-UbcH10 to glutathione-Casein coated 96 well plates that could be used to develop a quantitative method for UbcH10 autoubiquitylation activity and the screening of small drug inhibitors.

4.2.19 **Development of an ELISA-based UbcH10 autoubiquitylation assay**

Following optimisation of the ELISA for GST and GST-UbcH10 loading and quantitation, the next aim was to perform the UbcH10 autoubiquitylation assay quantitatively on 96 well plates. Thus, 96 wells plates were loaded with 200ng/well of GST and GST-UbcH10 that had previously been coated with glutathione-Casein. Next, the autoubiquitylation assay were performed for one hour at 37 °C, in the presence of a His_6-tagged E1 activating enzyme, Mg-ATP and WT ubiquitin. After this time the reactants were removed, plates washed and then blocked in Casein/Tween blocking buffer. After this time the plates were incubated with the FK2 anti-ubiquitin antibody followed by incubation with an anti-mouse HRP secondary antibody. Plates were then incubated with OPD and read with a SpectraMax ABS plus plate reader in an attempt to detect GST-UbcH10 species that had undergone autoubiquitylation. Significantly, this showed that GST-UbcH10, but not GST, underwent ubiquitin conjugation in the presence of E1 Mg-ATP and WT ubiquitin (**Fig. 4.23**). These data indicate successful development of a high-throughput assay to quantify UbcH10 autoubiquitylation activity that can be used to screen drug libraries for UbcH10 inhibitors.

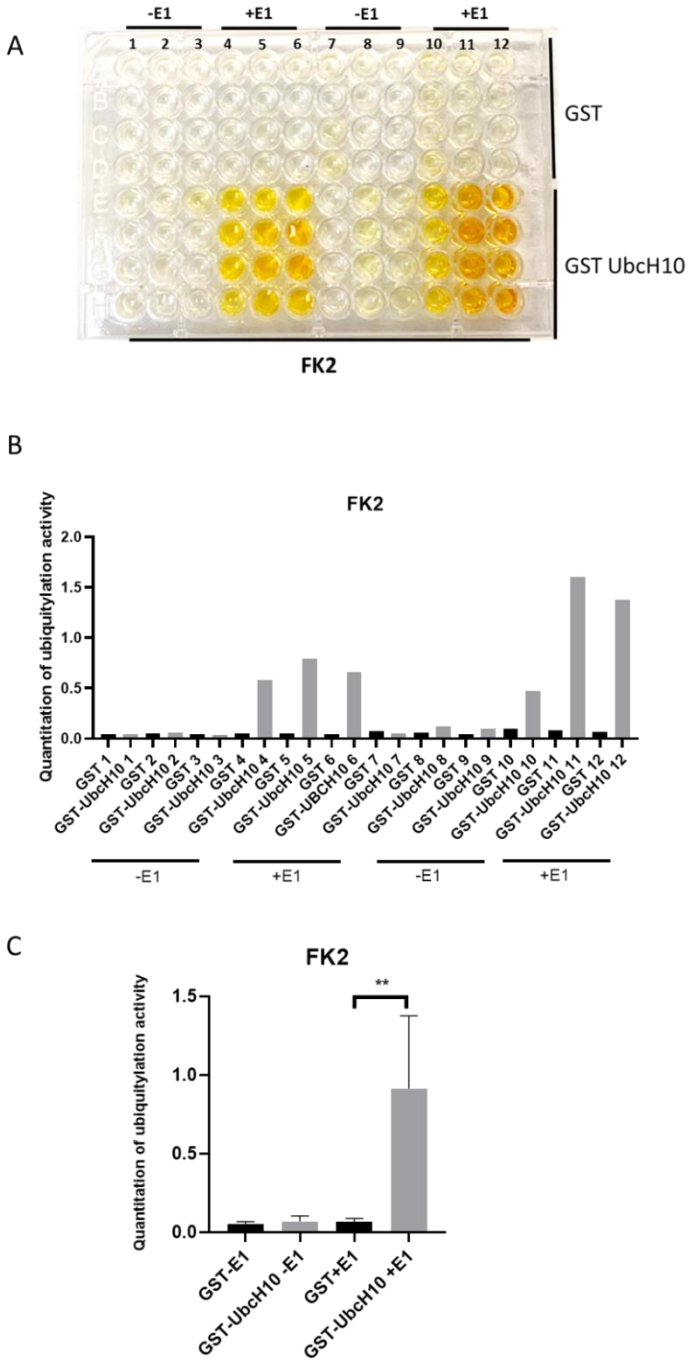

Figure 4.23: Validation of an in vitro ELISA-based method to assay UbcH10 ubiquitylation activity. 96 wells plates were coated overnight with glutathione-Casein. GST and GST-UbcH10 (200ng/well) were then loaded onto the plate which was subsequently incubated with His6-tagged E1 activating enzyme, Mg-ATP and WT ubiquitin at 37°C for 1 hour. Wells were then incubated with an FK2 anti-ubiquitin antibody with a HRP-coupled mouse secondary antibody and OPD for visualisation. Quantification was performed using a SpectraMax ABS plus ELISA reader. (A) Picture of the 96 wells plate following incubation with OPD. (B) Bar graph showing the mean column ELISA reading for FK2 detection (C) Bar graph showing the mean reading +/- Standard Deviation. Data taken from one experiment, representative of one other. (*) $P \leq 0.05$, (**) $P \leq 0.01$, (***) $P \leq 0.001$ and (****) $P \leq 0.0001$ indicating significant difference between GST + E1 and GST-UbcH10 + E1.

4.2.20 UbcH10 autoubiquitylation activity is reduced significantly upon ablation of K119, K121 and K164 acceptor sites

Based on earlier UbcH10 autoubiquitylation assays that established that K119, K121 and K164 were all sites for UbcH10 autoubiquitylation (**Figs. 4.2 and 4.11**), the next aim was to assay quantitatively the effect of K119, K121 and K164 mutation to R on UbcH10 autoubiquitylation. Therefore, GST-UbcH10 and GST K119-121-164R-UbcH10 were loaded onto the 96 well plate and the ubiquitylation assay carried out as before, in the presence of a His_6-tagged E1 activating enzyme, Mg-ATP and WT ubiquitin. After incubation with the FK2 anti-ubiquitin antibody followed by incubation with an anti-mouse HRP secondary antibody, the plate was incubated with OPD and read with a SpectraMax ABS plus plate reader to quantify the autoubiquitylation activity of WT GST-UbcH10, relative to mutant GST K119-121-164R-UbcH10 (**Fig. 4.24**). Interestingly, the results show that UbcH10 autoubiquitylation activity was reduced significantly upon mutation of the K119-121-164 residues to R, confirming the importance of these K ubiquitin acceptor sites in UbcH10 autoubiquitylation activity.

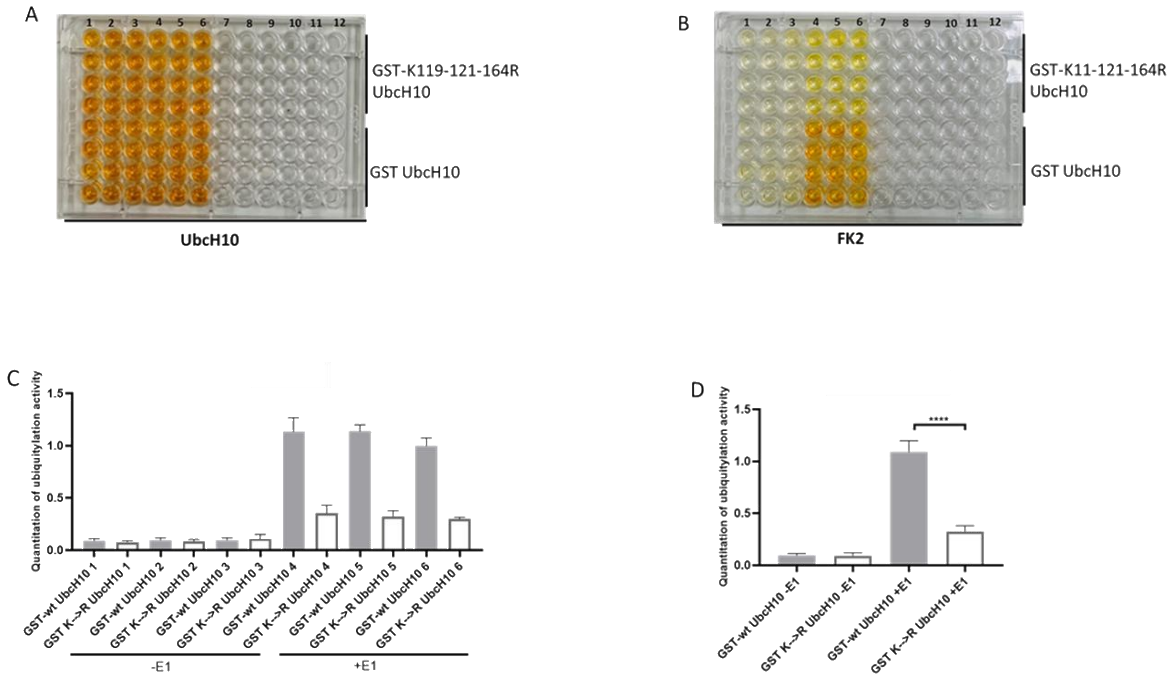

Figure 4.24: Ablation of the UbcH10 K119-K121 and K164 acceptor sites reduces polyubiquitin chain formation on UbcH10. 96 wells plate were coated overnight with glutathione-Casein. GST-UbcH10 and GST K119-121-164R-UbcH10 (200ng/well) were then loaded onto the plate which was subsequently incubated with His6-tagged E1 activating enzyme, Mg-ATP and WT ubiquitin at 37°C for 1 hour. Wells were then incubated with an FK2 anti-ubiquitin antibody and subsequently with a HRP-coupled mouse secondary antibody and OPD for visualisation. Quantification was performed using a SpectraMax ABS plus ELISA reader. (A) Picture of the 96 well plate showing the equal loading of both GST-UbcH10 and GST K119-121-164 R UbcH10 (B) Picture of the 96 well plate following incubation with the ant-ubiquitin antibody (C) Bar graph showing the mean column ELISA reading for FK2 detection (D) Bar graph showing the mean reading +/- Standard Deviation. Data taken from one experiment, representative of one other. (*) $P \leq 0.05$, (**) $P \leq 0.01$, (***) $P \leq 0.001$ and (****) $P \leq 0.0001$ indicating significant difference between GST Ubch10 + E1 and GST-UbcH10 K119, 121,164R + E1.

4.3 Discussion

UbcH10 is a class III E2-conjugating enzyme that operates specifically with the APC/C to facilitate substrate ubiquitylation and cell cycle progression throughout mitosis and G1. The processivity of APC/C related ubiquitin-mediated degradation is highly dependent on the level of UbcH10 (Jin et al. 2008). The main aim of the present study was to characterize UbcH10 autoubiquitylation and function in the absence of APC/C-Cdh1, the major APC/C species required for UbcH10 ubiquitylation and degradation. In this regard, key aims were to investigate whether UbcH10 could self-assemble polyubiquitin chains with different ubiquitin linkages and moreover, identify the major ubiquitylation K acceptor sites in UbcH10.

4.3.1 **UbcH10 exhibits an intrinsic E3 ligase activity**

The study presented herein sheds new light on a role of UbcH10 beyond its E2-conjugation activity as an accessory factor with Ube2S to promote the APC/C-dependent polyubiquitylation and proteasomal degradation of mitotic substrates by assembling polyubiquitin chains with K11 and K48 ubiquitin linkages (Jin . 2008). *In vitro* autoubiquitylation assays conducted with UbcH10 in the absence of the APC/C established that UbcH10 possesses intrinsic E3 ligase activity and is able to self-decorate with polyubiquitin chains in the absence of its cognate E3 ligase, the APC/C, in a mechanism dependent upon its catalytic cysteine residue (e.g. Fig. 4.1). Previous studies have suggested that some E2-conjugating enzymes do possess intrinsic E3 ligase activity and can self-decorate with ubiquitin chains independently of their E3 ubiquitin ligases (David et al. 2010). My observations however represent important new findings as it was not recognized previously the extent to which UbcH10 has the capacity to undergo autoubiquitylation in the absence of the APC/C.

My *in vitro* UbcH10 autopolyubiquitylation experiments also determined that UbcH10 forms polyubiquitin chains that possess, predominantly, K6, K11 and K48 ubiquitin linkages, highly suggestive that UbcH10 forms complex, branched polyubiquitin chains (e.g. **Figs. 4.2-4.5**). As indicated above, other E2-conjugating enzymes have been suggested to exhibit such autoubiquitylation activity. Ubc1 and CDC34, E2-conjugating enzymes from *Saccharomyces cerevisiae* have been shown to catalyze their own ubiquitylation and form polyubiquitin chains with K48 ubiquitin linkages (Banerjee et al. 1993). Additionally, a mammalian E2-25K, isolated from calf thymus, was also found to be capable of E3 ligase activity and the assembly of K48 'unanchored', free polyubiquitin chains in the absence of an E3 enzyme (Chen and Pickart 1990). Additionally, a more comprehensive study suggested that large number of E2-conjugating enzymes were capable of assembling polyubiquitin chains on either their catalytic cysteine or on acceptor lysine residues within their primary sequence (David et al. 2010).

The mechanism of action by which E2-conjugating enzymes form polyubiquitin chains has been suggested to occur in different ways. First, by catalysing the sequential addition of single ubiquitin moieties to other ubiquitin moieties already conjugated to the E2 enzyme, or by assembling a ubiquitin oligomer directly on the catalytic cysteine that is transferred en-bloc to an acceptor K residue; E2-25K was shown to catalyse the sequential addition of ubiquitin monomers to a growing chain (Chen and Pickart 1990). This study did not address the mechanism of UbcH10 autopolyubiquitylation, so it would be prudent in the future to address the kinetics of polyubiquitin chain formation on UbcH10 and whether UbcH10 can catalyse the transfer of ubiquitin oligomers assembled on its catalytic cysteine residue directly to a K acceptor, or

whether it favours the transfer of one ubiquitin moiety at a time. UbcH10 has previously been found to form short ubiquitin chains on its catalytic cysteine prior the elongation process by Ube2S (Rape et al. 2006).

Additional insights into E2 autopolyubiquitylation have been described elsewhere. Ubc1 for instance exhibits a mechanism that depends upon its ability to bind one molecule of ubiquitin covalently at its active-site and one molecule of ubiquitin non-covalently that has the potential to modulate polyubiquitin chain formation. The three-dimensional structure of Ubc1 shows that it is a two-domain protein possessing a catalytic cysteine residue that is surrounded by α/β folds and attached to a C-terminal UBA domain via a flexible linker; this structural arrangement allows Ubc1 to juxtapose a couple of ubiquitin molecules, such that the UBA domain interacts with mono-or poly ubiquitin and modulates catalytic cysteine activity (Hofmann 1996, Merkley et al. 2005). Interestingly, a number of E2-conjugating enzymes have been suggested to undergo spontaneous dimerization, and that both E2 molecules can be 'loaded' with ubiquitin (David et al. 2010). It has been suggested that one E2 monomer remains connected with the substrate while the other monomer allows for the transfer of ubiquitin moieties via intramolecular reactions. In the case of UbcH10, structural analyses have identified large interacting surfaces formed by residues 36, 39, 40, 43, 44, 51, 53–57, 63, 65, 78, and 80, suggesting that UbcH10 might behave as a dimer (Lin, Hwang et al. 2002). In agreement with this notion, the Clam E2-C, UbcH10 homologue, possesses similar interaction surfaces that might facilitate the functional dimerization of E2-C. Indeed, crystal structural analyses suggested that E2-C possesses an interaction area of 1318Å^2 which is in the range for functional dimerization. Indeed, part of these interaction surfaces were identified as one helix

locating against a symmetry partner on the other monomer, suggestive of dimerization. However, solution studies indicated that E2-C was a monomer (Jiang and Basavappa 1999). Thus, it is still to be determined whether UbcH10 functions as a dimer and how this might impact on autopolyuibiquitylation. It would be extremely interesting however, to see if mutation of residues comprising the proposed interaction motif interfere with UbcH10 autoubiquitylation.

4.3.2 **UbcH10 assembles branched polyubiquitin chains with K6 ubiquitin linkages**

As E2-conjugating enzymes are intermediates in ubiquitin chain assembly, they are suggested to play crucial role in the selection of ubiquitin linkages. The study by David, Ziv et al. (2010) determined an interesting relationship between an E2's polyubiquitylation activity and their preference for specific ubiquitin linkages. The study used a panel of single lysine-or arginine ubiquitin mutants linked to mass spectrometric analyses to show that many E2-conjugating enzymes have high specificity in directing the type of ubiquitin linkages and polyubiquitin topologies *in vivo*, with K11 and K48 being the most abundant. In this context, UbcH10 has been shown to facilitate the APC/C-dependent formation of K11 ubiquitin linkages on APC/C substrates (Jin et al. 2008). Indeed, UbcH10 is suggested to possess at least two APC/C-binding sites that help maintain UbcH10 binding to the APC/C in an appropriate orientation to facilitate the assembly of K11-linked polyubiquitin chains (Jin et al. 2008). It has been suggested that the preference of K11 over K48 linkages for APC/C substrates is in part a mechanism to allow the timely regulation of APC/C substrate degradation and prevent their deubiquitylation by DUBs, as DUBs distinguish substrates depending on their ubiquitin linkages (Nijman et al. 2005). Indeed, it has been postulated that the assembly of K11 linkages might distinguish substrates ubiquitylated by the APC/C in

mitosis from other substrates ubiquitylated by different E3 ligases, thus preventing their deubiquitylation (Jin et al. 2008). These findings support previous findings that UbcH10 can facilitate the formation of polyubiquitin chains with both K11 and K48 linkages. Indeed, mass spectrometric analyses suggest that K11 and K48 linkages are two of the most prevalent linkages used in the autoubiquitylation of UbcH10 (**Fig. 4.2**). However, these studies extend these observations to indicate that UbcH10 can also form non-degradative linkages including K6, K29 and K63 with K6 being the most common non-proteolytic linkages (**Fig. 4.2**).

These *in vitro* studies with specific ubiquitin mutants confirmed the mass spectrometry result and confirmed the ability of UbcH10 to form branched chain including K6, K11, and K48 (**Figs. 4.2 and 4.5**). It is known that different ubiquitin linkages direct targeted proteins to different cellular fates, with UbcH10 utilising degradative linkages such K11 and K48 for APC/C-targeted proteasomal degradation of substrates. K11 linkage assembly by APC/C on substrates requires the positioning of K11 ubiquitin in relation to the active site of UbcH10 as outlined above. This process is found to be highly dependent on the surface residues of ubiquitin particularly the TEK box formed by amino acid residues K6, E34 and T9 in addition to L8 and I36 (**Fig. 4.25**). The mutation of these residues in cell extracts stabilise the APC/C substrate, Securin to the same level of inactivation of the K11 acceptor site. Although APC/C substrates have not been documented to possess polyubiquitin chains with K6 linkages, the charge of the K6 residue in ubiquitin has been found to play an important role in enhancing APC/C dependent degradation by facilitating the efficient formation of K11 linkages on APC/C substrates (Jin et al. 2008). Given the apparent lack of ability of the APC/C to utilise K6 ubiquitin linkages, and these findings that indicate the ability of UbcH10 to form K6

linkages in absence of the APC/C, this data suggests that polyubiquitylated UbcH10, possessing K6 linkages might perform roles independently, that do not necessitate the APC/C, or require the activity of another E3 ligase.

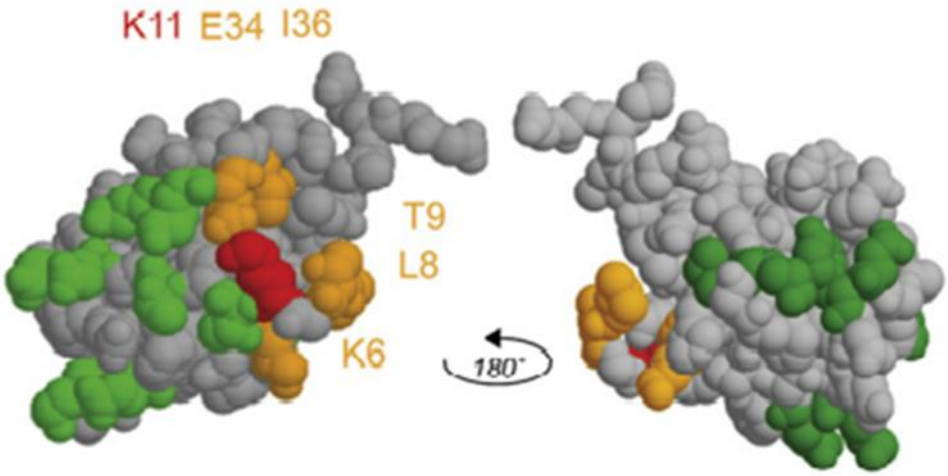

Figure 4.25 Localisation of the TEK box on ubiquitin in relation to the K11 residue. The surface ubiquitin residues form a cluster to allow the direct exposure of K11 to the active site of UbcH10. K11 in red and the ubiquitin surface residues in yellow. Taken from (Jin, Williamson et al. 2008).

Roles for K6 ubiquitin linkages have been found in autophagy and the DDR (Bingol et al. 2014, Ordureau et al. 2014, Cunningham et al. 2015, Liang et al. 2015, Ordureau et al. 2015), though a study has identified a role for K6 in mitosis. In *Xenopus* egg extracts, the E3 ligase TRAIP was found to assemble K6 and K63 ubiquitin chains on Mcm7 to facilitate replisome disassembly during prophase (Moreno, Jones et al. 2019). Given that UbcH10 can assemble both K6 and K63 ubiquitin linkages (**Fig. 4.2**) it would be interesting to investigate whether UbcH10 participates with TRAIP in this reaction, though studies to date suggest that TRAIP can utilise UbcH5a to ubiquitylate histones (Moreno et al. 2019). In the main, the role of K6 ubiquitin linkages in biology remains elusive due to the lack of appropriate tools. The generation of an affimer that has specificity for K6 diubiquitin linkages has helped to identify RNF144A, RNF144B, HUWE1 and Parkin as E3 ligases that can assemble branched chain including K6,

K11 and K48 for proteolysis (Michel et al. 2017). My data with this affimer suggested that although it had a high preference for K6 linkages it did cross-react slightly with K11 linkages (**Fig. 4.5**), such that any role determined with this affimer needs to be confirmed experimentally with ubiquitin mutants. It would be interesting to determine whether UbcH10 can function with these K6-utilising E3 ligases to promote K6-dependent ubiquitylation, although Parkin which is known to function to regulate mitosis, does not utilise UbcH10 in this capacity (Lee et al., 2015). It is not yet known whether UbcH10 could generate polyubiquitin chains with homotypic K6 linkages *in vivo* but the *in vitro* analyses indicate that homotypic K6 linkages do not target UbcH10 to the proteasome for degradation (**Fig. 4.14**).

Whereas the role of unconventional ubiquitin linkages in APC/C-dependent proteasomal degradation remains undetermined, it is worth mentioning that some quantitative studies in yeast show notable increases in the non-degradative ubiquitin linkages such as K6 following proteasomal inhibition with MG132 suggesting they might participate in proteasomal targeting as mixed, branched polyubiquitin chains (Xu, Duong et al. 2009). Moreover, studies with the proteasomal subunits Rpn1 and Rpn10 have demonstrated a significant binding preference towards K6 and K48, K11 and K48 and K48, consistent with a requirement for K6 chains in proteasomal degradation (Husnjak et al. 2008, Shi et al. 2016, Haakonsen and Rape 2019). In this regard it is possible that K6 might function as a seeding linkage that promotes the formation of K11 or K48 polyubiquitin chains and proteasomal degradation. As such, K63 linkages formed by the ITCH E3 ligase facilitate the recruitment of the K48 E3 ligase, UBR5 to target TXINP for proteasomal degradation (**Fig. 4.26**; Ohtake, et al.

2018). As such, heterotypic polyubiquitin chains on UbcH10 that possess K6 linkages might serve to target UbcH10 for degradation.

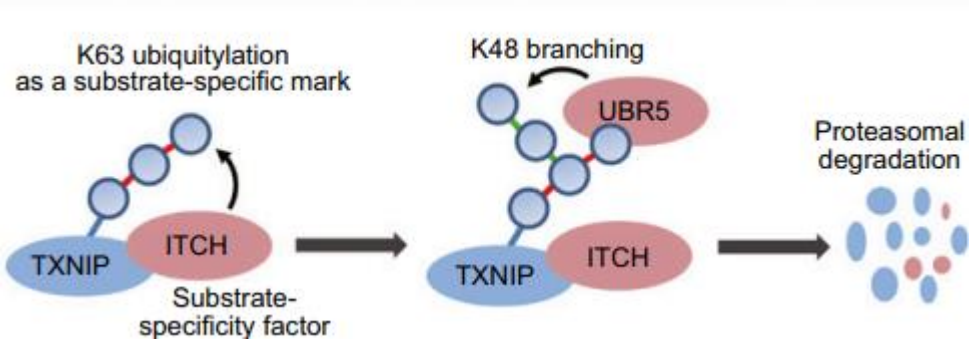

Figure 4.26 Figure 4.26 K63 serves as a seeding linkage for K48 linkages. The UBR5 E3 ligase targets TXNIP for degradation in a process highly dependent on the assembly of K63 linkages assembled by ITCH (Ohtake et al. 2018).

Given that UbcH10 functions predominantly in mitosis it would be interesting to identify UbcH10-APC/C substrates or UbcH10 substrates that utilise K6 linkages. This could be done by IP coupled to mass spectrometry utilising the K6 affimer to immunoprecipitate K6-linked substrates from mitotic cells (+/- proteasome inhibition) that could be identified by mass spectrometry and then validated by a combination of *in vitro* and *in vivo* ubiquitylation studies to determine the role of UbcH10 in these processes.

The BRCA1 E3 ligase has been shown to utilise K6 linkages in the DDR but these were not dependent on UbcH10 (Wu-Baer et al. 2003, Rajabi et al. 2017). However, a new role for UbcH10/Ube2S has been identified in the DDR, such that the RNF8 E3 ligase associates with Ube2S/UbcH10 on damaged chromatin to assemble K11 linkages on histone H2A and H2X in an ATM-dependent manner (**Fig. 4.27**). The study revealed a significant loss of K11 polyubiquitylation on damaged chromatin in Ube2s/UbcH10-depleted cells and that the association of UbcH10 at sites of damage was not dependent upon the APC/C (Paul and Wang 2017). Previous characterization

of the UbcH10 interactome from our laboratory (Jessica Foster, PhD thesis, University of Birmingham 2018) determined that UbcH10 interacts with the DTX3L E3 ligase and ADP-ribosyl transferase, PARP9 which both have been identified to play major roles in the DDR and immune response (Zhan et al. 2015). As such, DTX3L E3 ligase and PARP9 are responsible for the monoubiquitylation of histone 4 which facilitates the recruitment of 53BP1, RAP80 and BRCA1 to sites of DNA damage (Yan et al. 2009, Yan et al. 2013). In this context it would be interesting to determine if DTX3L/PARP9 assembles polyubiquitin chains on substrates with K6 linkages in a UbcH10-dependent manner.

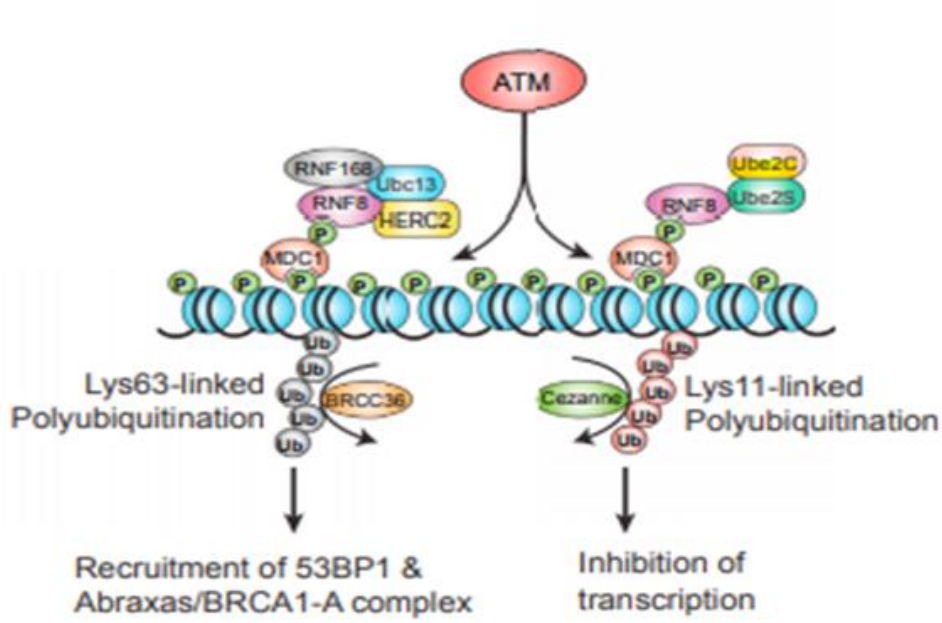

Figure 4.27 RNF8 associates with Ube2S/Ube2C to assemble K11 polyubiquitin chains on damaged chromatin. The schematic representation shows the assembly of K11 linkages on damaged site by RNF8/Ube2S/Ube2C in a manner that is distinctive to K63 assembly (Paul and Wang 2017).

4.3.3 **K119 as the major autopolyubiquitylation site on UbcH10**

This study indicates that UbcH10 autopolyubiquitylation is dependent on its catalytic cysteine as mutation of Cys114 to alanine or serine abrogates polyubiquitin chain assembly on UbcH10 (Figs. 4.1 and 4.3). Mass spectrometric analysis and

subsequent *in vitro* studies with UbcH10 revealed that UbcH10 can assemble polyubiquitin chains on different lysine residues including K48, K61, K80, K119 K121, with K121 being the most common linkages though *in vitro* analyses revealed that K119 was the major site of UbcH10 autoubiquitylation (cf Fig 4.7 and Fig. 4.10). The reason for this apparent discrepancy probably lies with the mass spectrometric spectral properties of peptides from different K modification sites, such that the K121 containing peptide might ionise better than other peptides, such as K119, so it appears more abundant. It is established that K119 and K121 are major ubiquitylation sites for APC/C-directed ubiquitylation of UbcH10 (Williamson et al. 2011) and that K119 is an important residue in the ubiquitin adduct function of UbcH10, as a component of the 3_{10} helix surrounding the UbcH10 catalytic Cys114, providing a more favourable and energetic environment (Lin et al. 2002). In this context, it is possible that K119 ubiquitylation modulates UbcH10-APC/C activity by regulating ubiquitin thiol-ester formation with Cys114. Consistent with this, these *in vitro* and *in vivo* studies support the notion that K119 is the major ubiquitin acceptor (Figs. 4.10 and 4.16) and that disruption of this specific site attenuates UbcH10 polyubiquitylation. It would however be interesting to see if the K119R mutant, that retains its positive charge affects the ability of the UbcH10 active site to associate with ubiquitin and affect APC/C- directed ubiquitylation of substrate proteins.

UbcH10 is a proto-oncogene and its overexpression in many cancers is associated with malignancy and poor prognosis (Welsh et al. 2001, Pallante et al. 2005, Lin et al. 2006, Berlingieri et al. 2007, Jiang et al. 2008, Fujita et al. 2009). Indeed, overexpression of UbcH10 promotes the premature segregation of sister chromatids during mitosis, aneuploidy, and cancer formation in mouse models (Van Ree,

Jeganathan et al. 2010). UbcH10 is therefore a *bona fide* cancer therapeutic target. Given that UbcH10 has a catalytic activity and directs its own polyubiquitylation this function can be used to screen drug libraries to identify potential inhibitors of UbcH10 autopolyubiquitylation activity that might have therapeutic benefit. In the first step to towards screening drug libraries a high throughput ELISA-based technique has been developed that recognises specifically polyubiquitylated UbcH10 with the FK2 anti-ubiquitin antibody (Figs. 4.23 and 4.24). Unfortunately, there was not the time to pursue this further, but in the future ,in the first instance, FDA-approved drug libraries will be screened to determine drugs, and classes of drugs, that inhibit UbcH10 activity *in vitro*, such that their ability to inhibit APC/C activity and cell cycle progression in cell-based systems will be studied to evaluate their potential usefulness for further studies.

5 Final Discussion

5.1 Role of RhoGEFs and Rho GTPases in mitosis

Work presented in chapter 3 established that PDZ-RhoGEF interacts with the APC/C E2-conjugating enzyme, UbcH10 and is targeted for proteasomal degradation early in mitosis (**Figs. 3.5, 3.6 and 3.8**). APC/C-Cdc20 was determined as likely to be the E3 ligase that targets PDZ-RhoGEF for degradation as PDZ-RhoGEF interacts with the APC/C activator Cdc20 in a KEN-box dependent manner, and KEN-box ablation stabilises PDZ-RhoGEF (**Figs. 3.24 and 3.25**). Consistent with these observations relating to the stability of PDZ-RhoGEF in mitosis, the APC/C has been found previously to modulate the activity of RhoA during mitosis. As such, APC/C-Cdh1 targets the Ect2 RhoGEF, which particpates in cell rounding and cytokinesis, for degradation at the end of mitosis (Niiya et al. 2006, Matthews et al. 2012, Nishimura and Yonemura 2006). The p190 RhoGAP is another RhoA regulator that partcipates in cell rounding and cytokinesis that has been identified as an APC/C-Cdh1 substrate at the end of mitosis (Naoe et al. 2010). Despite our studies, the biological role of PDZ-RhoGEF in mitotic entry/early mitosis, remains unclear. However, given the role of RhoA in cell rounding this seems an obvious area to investigate. Analysis of BioGRID and STRING databases suggests that PDZ-RhoGEF has many interacting proteins; most of those identified through experimentation alone (using the STRING database) are RhoGTPase family members (**Fig. 5.1**).

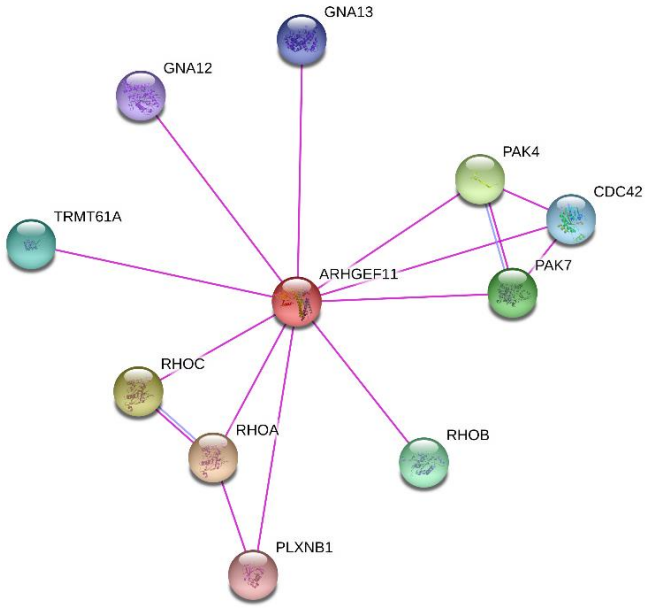

Figure 5.1 PDZ-RhoGEF (ARHGEF11) interacting proteins.STRING network of PDZ-RhoGEF known cellular-interacting proteins in Homo sapiens, using the String database using a medium confidence score of 0.40 (Szklarczyk et al., 2015).

It is well established that PDZ-RhoGEF cooperates with another RhoGEF, LARG to activate RhoA and promote growth cone collapse (Swiercz et al. 2002). Moreover, it is known that RhoA has many functions in mitosis, including cell rounding during mitotic entry and cytokinesis at the end of mitosis (Chircop, 2014). The enhanced activity of RhoA in early mitosis has been shown to be due to cellular inhibition of RhoGAPs and the high activity of RhoGEFs (Maddox and Burridge 2003). As PDZ-RhoGEF levels are depleted early during mitosis it would be of considerable interest to study by live cell imaging whether depletion of PDZ-RhoGEF by RNAi or CRISPR, or the overexpression of PDZ-RhoGEF modulates the ability of RhoA to promote cell rounding. Although it is known that the RhoGEF Ect2 participates in the activation of RhoA in this process, RhoGEFs are highly collaborative as illustrated by the dual role of PDZ-RhoGEF and LARG in the RhoA-dependent regulation of growth cones. Moreover, as the rigidity and rounding of the cell at early stage of mitosis is essential

for the spindle assembly (Carreno et al. 2008), it would be interesting to investigate whether the depletion of PDZ-RhoGEF affects spindle assembly, cetrosome separation or formation of the bipolar spindle.

Previous studies on cell rounding in early mitosis identified more than 60 genes that contributed to this process, many of which were Rho GTPases, namely RAC1, RAC2, RhoA, RhoB, RhoC and Cdc42 (Maddox and Burridge 2003). Given the roles of these other RhoGTPases in this process it would be of interest to investigate the interaction of PDZ-RhoGEF with RhoGTPases and other cellular proteins by mass spectrometry prior to its degradation in early mitosis, which might give further insight into its function. Additional roles for the Rho family member, Cdc42 in mitosis have also been determined. Cdc42 functions to ensure proper spindle orientation in polarised epithelial cells through the formation of cortical F-actin (Tuncay et al. 2015) and chromosomal alignment at metaphase, in non-polarised cells (Yasuda, Taniguchi et al. 2006). Although PDZ-RhoGEF has been shown to interact with Cdc42 effector PAK4 (p21-activated kinase 4) specifically (Barac et al. 2004), given the specific roles performed by Cdc42 in mitosis it iwould seem unlikely that PDZ-RhoGEF activates Cdc42 in its capacity to regulate metaphase spindle alignment and chromosome attachment as the cellular levels of PDZ-RhoGEF would be low at this time. Indeed, a very recent systems analysis of RhoGAPs and RhoGEFs established that PDZ-RhoGEF was very likely a RhoA-specific GEF that likely possessed pleiotropic functions as it localised to actin, the plasma membrane and the nucleus (Müller et al. 2020). Moreover, it was also established that PDZ-RhoGEF and LARG enhanced Cdc42 GTP-loading by enhancing the activity of the Cdc42-specific GEF, PLEKHG4B, whilst PLEKHG4B inhibited PDZ-RhoGEF and LARG activity towards RhoA,

suggesting molecular cross-talk between these pathways (Müller et al. 2020). Given these findings, it is possible that the phosphorylation and/or degradation of PDZ-RhoGEF early in mitosis negatively regulates Cdc42 activity. Although it is suggested that PDZ-RhoGEF also modulates RhoB and RhoC activity, there is no evidence to date to suggest that these proteins function in mitosis.

Given our current understanding of RhoGTPases, RhoGEFs and RhoGAPs it seems prudent to study the relationship between RhoA, Cdc42 and PDZ-RhoGEF during mitotic entry to gauge whether PDZ-RhoGEF particpates in cell rounding or other mitotic processes, yet to be uncovered, that would be identified by PDZ-RhoGEF knockdown/over-expression studies.

5.2 Role for post-translational modifications in UbcH10 function

Results presented in Chapter 4 indicated that UbcH10 possesses intrinsic E3 ligase activity and can self-decorate with polyubiquitin chains, particularly on K119, that possess multiple K linkages. As proteasomal inhibition increases the levels of UbcH10 polyubiquitylation *in vivo* on K119 (**Fig. 4.16**) it is likely that polyubiquitylation at this site promotes UbcH10 degradation. However, it is not clear at present as to whether K119 ubiquitylation *in vivo* is dependent upon the APC/C or not, and as such needs to be assessed by ablation of APC/C activity by APC/C inhibitors such as pro-TAME or apcin (Sackton et al. 2014) or knockdown/knockout of APC/C coactivators, Cdc20 and Cdh1. It is possible that polyubiquitylation on K119, or any of the other K acceptor sites identified in UbcH10 **(Fig 4.7**) serves a different role as an adaptor or protein-protein interaction motif and recruits proteins to UbcH10. In this regard, UbcH10 could serve to recruit APC/C substrates, or APC/C regulators to ensure the timely degradation of

APC/C substrates or could regulate other cellular pathways linked to distinct biological processes. Indeed, we have shown that UbcH10 can self-decorate with K6 ubiquitin linkages, which typically function in non-degradative pathways (Bingol et al. 2014, Ordureau et al. 2014, Cunningham et al. 2015, Liang et al. 2015, Ordureau et al. 2015). Moreover, a role for ubiquitin chains as protein-protein interaction domains is well established; Ubiquitin-Binding Domains (UBDs) such as Ubiquitin-Associated Domains (UBAs) and and Ubiquitin-Interaction Motifs (UIMs) associate with ubiquitin and polyubiquitin chains in a non-covalent manner to regulate not only protein stability but pathways involved in DDR, inflammation and receptor trafficking (Dikic et al. 2009).

Interestingly, a quantitative approach to identifying cellular proteins that interact with ubiquitin chains through UBDs has been devised; ubiquitin interactor affinity enrichment-massspectrometry (UbIA-MS) allows for the identification and quantification, using SILAC, of proteins that associate with diubiquitin species possessing different K linkages (Zhang et al. 2017). Pertinent to our studies with K6, diubiquitin species possessing K6 linkages were found to associate specifically with TGFβ-activated kinases 1 and 2 (TAB1 and TAB2) and associated with a number of DDR proteins following treatment of cells with the DNA-damaging agent, doxorubicin (Zhang, Smits et al. 2017). Pertinently, UbcH10 has also been linked to different E3 ligases that operate in the DDR. RNF8 E3 ligase is found to assemble K11 linkages on damaged chromatin in association with Ube2S/UbcH10 (Paul and Wang 2017) though it is possible that K6 linkages on UbcH10 are also involved in cell signalling pathways. Intriguingly, Cdc20, Bub1 and Ube2S all associate with diubiquitin species possessing K6 linkages following DNA damage (Zhang et al. 2017). As such, it would be extremely interesting to assess whether these proteins associated specifically with

polyubiquitylated UbcH10 in mitosis, or following DNA damage. To do this we could use WT or mutant GST-UbcH10, and WT or mutant GST-UbcH10 loaded differentially with ubiquitin species (e.g. WT, K6O and K6R ubiquitin) to perform pulldown assays with cell lysates from mitotic cells and those subjected to DNA damage. In a less-biased manner we could also identify GST-UbcH10 or GFP-K6 affimer interactors through a similar mass spectrometric approach adopted by Zhang and colleagues. If we identify UbcH10 interactors it will be important to determine fully the topology of UbcH10 linkages in this regard using a mass spectrometric approach that utilises specific DUBs and careful analysis of MS/MS fragmentation patterns to analyse linkage usage (Geis-Asteggiante et al. 2019).

More generally, the precise role of UbcH10 PTM is not known, despite the fact that UbcH10 is known to be modified by phosphorylation and methylation in addition to ubiquitylation (**Fig. 5.2**). Our collaborative analyses with the Layfield laboratory in Nottingham identified K48 and K61, in addition to K80, K119, K121 and K164 (**Fig 4.7**) that have been identified previously, though we did not identify K172 as a site that was ubiquitylated. It is not clear from the Phosphosite database, or the publications that identified these modifications as to whether they underwent mono- or poly-ubiquitylation, whilst our analyses suggested that polyubiquitylation was a common modification on K119, K121 and K164 at least (**Figs 4.12 and 4.13**). It will be interesting using the GST-pulldown approach coupled to mass spectrometry, as outlined above to determine whether these ubiquitylated species act to recruit proteins to UbcH10. It is well established that the N-terminal region of UbcH10 negatively regulates APC/C function (see Introduction, section 1.5.1.2). It will be of interest to see, via mutational analyses on UbcH10, if phosphorylation ot methylation in this

region modulates APC/C activity. Similarly, the role of phosphorylation at other sites need to be established. In this regard, we did identify a phosphorylated UbcH10 species (**Fig 4.18**) although we need to establish which site upon UbcH10 was phosphorylated in this instance.

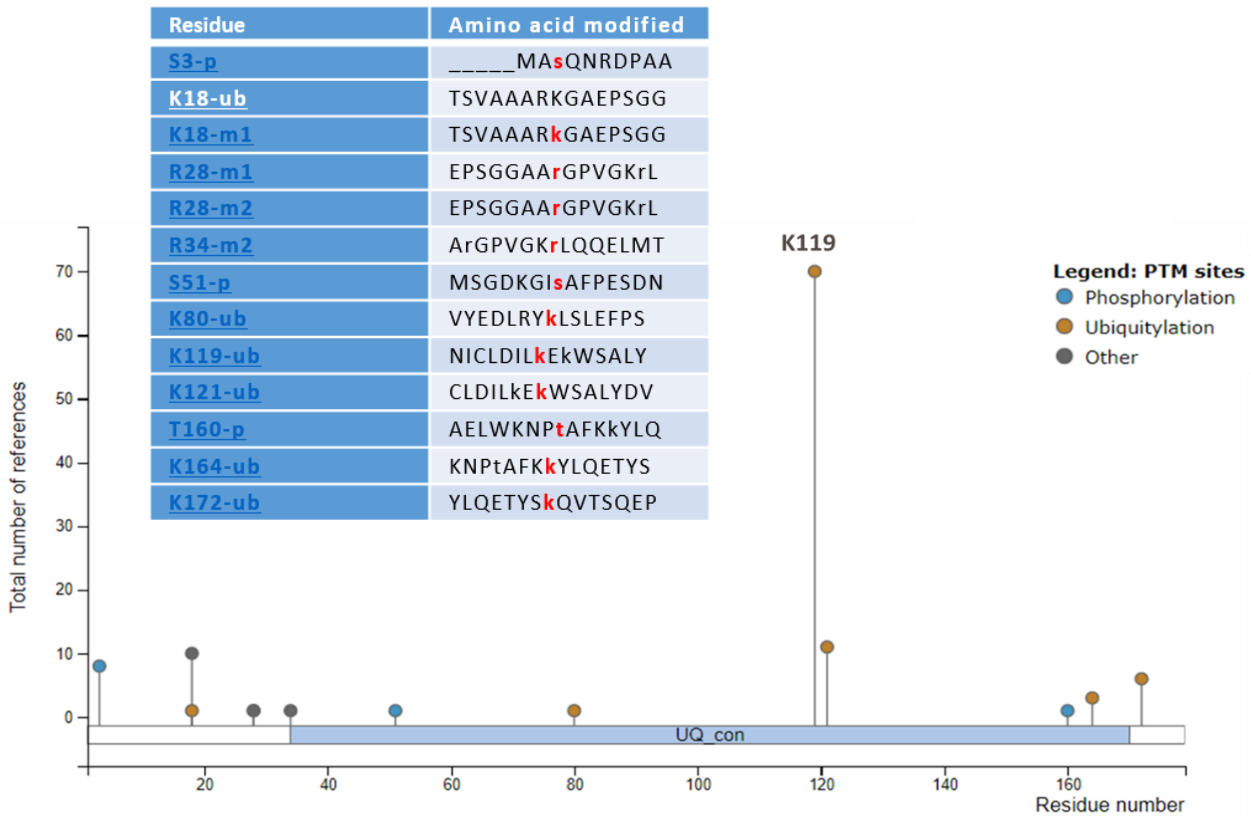

Figure 5.2 Post-translational modifications of UbcH10. Post-translational modifications occurring on human UbcH10 as identified by multiple mass spectrometry screening. Taken from PhosphoSitePlus (2020). p=phosphorylation; m1=mono-methylation; m2=di-methylation; ub=ubiquitylation.

UbcH10 is a proto-oncogene that is overexpressed in many cancers and whose overexpression is associated with poor prognosis (Welsh et al. 2001, Pallante et al. 2005). In this thesis we developed a high throughput assay ELISA assay to quantify UbcH10 ubiquitylation activity **(Fig. 4.23**). As such this will be a useful technique to

screen drug libraries for UbcH10 active site inhibitors that might have potential as cancer therapeutic agents. In addition to this approach we could develop an ELISA-based system to screen drugs and identify allosteric inhibitors of UbcH10 function- i.e. that prevent UbcH10 association with APC/C, Cdc20/Cdh1 and ubiquitin that might also have use as cancer therapeutic agents. Indeed, we could extend these analyses further to identify drugs that modulated UbcH10 phosphorylation or methylation status, which might also have use as therapeutic agents.

It is clear from the discussion above that there is still much to learn about the role of UbcH10 PTMs in UbcH10 function and how they cooperate/modulate to affect UbcH10 activity. It is apparent however that we could potentially target UbcH10 PTMs not only to further dissect UbcH10 function but also to inhibit the oncogenic activity of UbcH10 in cancer. An understanding of the role of UbcH10 PTMs is therefore, of considerable importance.

6 REFERENCES

Ajeawung, N. F., T. T. M. Nguyen, L. Lu, T. J. Kucharski, J. Rousseau, S. Molidperee, J. Atienza, I. Gamache, W. Jin and S. E. Plon (2019). "Mutations in ANAPC1, Encoding a Scaffold Subunit of the Anaphase-Promoting Complex, Cause Rothmund-Thomson Syndrome Type 1." The American Journal of Human Genetics 105(3): 625-630.

Alfieri, C., S. Zhang and D. Barford (2017). "Visualizing the complex functions and mechanisms of the anaphase promoting complex/cyclosome (APC/C)." Open biology **7**(11): 170204.

Alpi, A. F., P. E. Pace, M. M. Babu and K. J. Patel (2008). "Mechanistic insight into site-restricted monoubiquitination of FANCD2 by Ube2t, FANCL, and FANCI." Molecular cell **32**(6): 767-777.

Araki, M., H. Yu and M. Asano (2005). "A novel motif governs APC-dependent degradation of Drosophila ORC1 in vivo." Genes & development **19**(20): 2458-2465.

Aristarkhov, A., E. Eytan, A. Moghe, A. Admon, A. Hershko and J. V. Ruderman (1996). "E2-C, a cyclin-selective ubiquitin carrier protein required for the destruction of mitotic cyclins." Proceedings of the National Academy of Sciences **93**(9): 4294-4299.

Bailly, V., S. Lauder, S. Prakash and L. Prakash (1997). "Yeast DNA repair proteins Rad6 and Rad18 form a heterodimer that has ubiquitin conjugating, DNA binding, and ATP hydrolytic activities." Journal of Biological Chemistry **272**(37): 23360-23365.

Baldin, V., J. Lukas, M. J. Marcote, M. Pagano and G. Draetta (1993). "Cyclin D1 is a nuclear protein required for cell cycle progression in G1." Genes & development **7**(5): 812-821.

Banerjee, A., L. Gregori, Y. Xu and V. Chau (1993). "The bacterially expressed yeast CDC34 gene product can undergo autoubiquitination to form a multiubiquitin chain-linked protein." Journal of Biological Chemistry **268**(8): 5668-5675.

Banerjee, J. and P. B. Wedegaertner (2004). "Identification of a novel sequence in PDZ-RhoGEF that mediates interaction with the actin cytoskeleton." Molecular biology of the cell **15**(4): 1760-1775.

Barac, A., J. Basile, J. Vázquez-Prado, Y. Gao, Y. Zheng and J. S. Gutkind (2004). "Direct interaction of p21-activated kinase 4 with PDZ-RhoGEF, a G protein-linked Rho guanine exchange factor." Journal of Biological Chemistry 279(7): 6182-6189.

Barlow, P., B. Luisi, A. Milner, M. Elliott and R. Everett (1994). "Structure of the C3HC4 domain by 1H-nuclear magnetic resonance spectroscopy.: A new structural class of zinc-finger." Journal of molecular biology **237**(2): 201-211.

Bassermann, F., D. Frescas, D. Guardavaccaro, L. Busino, A. Peschiaroli and M. Pagano (2008). "The Cdc14B-Cdh1-Plk1 axis controls the G2 DNA-damage-response checkpoint." Cell 134(2): 256-267.

Berlingieri, M. T., P. Pallante, A. Sboner, M. Barbareschi, M. Bianco, A. Ferraro, G. Mansueto, E. Borbone, E. Guerriero and G. Troncone (2007). "UbcH10 is overexpressed in malignant breast carcinomas." European Journal of Cancer **43**(18): 2729-2735.

Berndsen, C. E., and Wolberger, C. (2014). New insights into ubiquitin E3 ligase mechanism. Nat. Struct. Mol. Biol. 21, 301–307. doi: 10.1038/nsmb.2780

Bingol, B., J. S. Tea, L. Phu, M. Reichelt, C. E. Bakalarski, Q. Song, O. Foreman, D. S. Kirkpatrick and M. Sheng (2014). "The mitochondrial deubiquitinase USP30 opposes parkin-mediated mitophagy." Nature **510**(7505): 370-375.

Borden, K., M. Boddy, J. Lally, N. O'reilly, S. Martin, K. Howe, E. Solomon and P. Freemont (1995). "The solution structure of the RING finger domain from the acute promyelocytic leukaemia proto-oncoprotein PML." The EMBO journal **14**(7): 1532-1541.

Bourne, H. R., D. A. Sanders and F. McCormick (1990). "The GTPase superfamily: a conserved switch for diverse cell functions." Nature **348**(6297): 125-132.

Bremm, A., S. M. Freund and D. Komander (2010). "Lys11-linked ubiquitin chains adopt compact conformations and are preferentially hydrolyzed by the deubiquitinase Cezanne." Nature structural & molecular biology **17**(8): 939.

Brito, D. A. and C. L. Rieder (2006). "Mitotic checkpoint slippage in humans occurs via cyclin B destruction in the presence of an active checkpoint." Current Biology **16**(12): 1194-1200.

Brown, N. G., R. VanderLinden, E. R. Watson, R. Qiao, C. R. Grace, M. Yamaguchi, F. Weissmann, J. J. Frye, P. Dube and S. E. Cho (2015). "RING E3 mechanism for ubiquitin ligation to a disordered substrate visualized for human anaphase-promoting complex." Proceedings of the National Academy of Sciences **112**(17): 5272-5279.

Brown, N. G., R. VanderLinden, E. R. Watson, F. Weissmann, A. Ordureau, K.-P. Wu, W. Zhang, S. Yu, P. Y. Mercredi and J. S. Harrison (2016). "Dual RING E3 architectures regulate multiubiquitination and ubiquitin chain elongation by APC/C." Cell **165**(6): 1440-1453.

Brown, N. G., E. R. Watson, F. Weissmann, M. A. Jarvis, R. VanderLinden, C. R. Grace, J. J. Frye, R. Qiao, P. Dube and G. Petzold (2014). "Mechanism of polyubiquitination by human anaphase-promoting complex: RING repurposing for ubiquitin chain assembly." Molecular cell **56**(2): 246-260.

Bu, J.-Y., A. S. Shaw and A. C. Chan (1995). "Analysis of the interaction of ZAP-70 and syk protein-tyrosine kinases with the T-cell antigen receptor by plasmon resonance." Proceedings of the National Academy of Sciences **92**(11): 5106-5110.

Burton, J. L. and M. J. Solomon (2001). "D box and KEN box motifs in budding yeast Hsl1p are required for APC-mediated degradation and direct binding to Cdc20p and Cdh1p." Genes & development **15**(18): 2381-2395.

Carreno, S., I. Kouranti, E. S. Glusman, M. T. Fuller, A. Echard and F. Payre (2008). "Moesin and its activating kinase Slik are required for cortical stability and microtubule organization in mitotic cells." The Journal of cell biology 180(4): 739-746.

Castro, A., S. Vigneron, C. Bernis, J.-C. Labbé and T. Lorca (2003). "Xkid is degraded in a D-box, KEN-box, and A-box-independent pathway." Molecular and cellular biology **23**(12): 4126-4138.

Ceccarelli, D. F., X. Tang, B. Pelletier, S. Orlicky, W. Xie, V. Plantevin, D. Neculai, Y.-C. Chou, A. Ogunjimi and A. Al-Hakim (2011). "An allosteric inhibitor of the human Cdc34 ubiquitin-conjugating enzyme." Cell **145**(7): 1075-1087.

Chang, L., Z. Zhang, J. Yang, S. H. McLaughlin and D. Barford (2014). "Molecular architecture and mechanism of the anaphase-promoting complex." Nature **513**(7518): 388-393.

Chang, L., Z. Zhang, J. Yang, S. H. McLaughlin and D. Barford (2015). "Atomic structure of the APC/C and its mechanism of protein ubiquitination." Nature **522**(7557): 450-454.

Chau, V., J. W. Tobias, A. Bachmair, D. Marriott, D. J. Ecker, D. K. Gonda and A. Varshavsky (1989). "A multiubiquitin chain is confined to specific lysine in a targeted short-lived protein." Science **243**(4898): 1576-1583.

Chen, Z. and C. M. Pickart (1990). "A 25-kilodalton ubiquitin carrier protein (E2) catalyzes multi-ubiquitin chain synthesis via lysine 48 of ubiquitin." Journal of Biological Chemistry **265**(35): 21835-21842.

Chen, Z., F. Medina, M.-y. Liu, C. Thomas, S. R. Sprang and P. C. Sternweis (2010). "Activated RhoA binds to the pleckstrin homology (PH) domain of PDZ-RhoGEF, a potential site for autoregulation." Journal of Biological Chemistry 285(27): 21070-21081.

Chen, Z. J. and L. J. Sun (2009). "Nonproteolytic functions of ubiquitin in cell signaling." Molecular cell 33(3): 275-286.

Chircop, M. (2014). "Rho GTPases as regulators of mitosis and cytokinesis in mammalian cells." Small GTPases 5(2): e29770.

Cho, K.-O., C. A. Hunt and M. B. Kennedy (1992). "The rat brain postsynaptic density fraction contains a homolog of the Drosophila discs-large tumor suppressor protein." Neuron **9**(5): 929-942.

Choi, E., H. Choe, J. Min, J. Y. Choi, J. Kim and H. Lee (2009). "BubR1 acetylation at prometaphase is required for modulating APC/C activity and timing of mitosis." The EMBO journal **28**(14): 2077-2089.

Chu, I., J. Sun, A. Arnaout, H. Kahn, W. Hanna, S. Narod, P. Sun, C.-K. Tan, L. Hengst and J. Slingerland (2007). "p27 phosphorylation by Src regulates inhibition of cyclin E-Cdk2." Cell **128**(2): 281-294.

Ciechanover, A., J. A. DiGiuseppe, B. Bercovich, A. Orian, J. D. Richter, A. L. Schwartz and G. M. Brodeur (1991). "Degradation of nuclear oncoproteins by the ubiquitin system in vitro." Proceedings of the National Academy of Sciences **88**(1): 139-143.

Ciehanover, A., Y. Hod and A. Hershko (1978). "A heat-stable polypeptide component of an ATP-dependent proteolytic system from reticulocytes." Biochemical and biophysical research communications **81**(4): 1100-1105.

Clague, M. J., I. Barsukov, J. M. Coulson, H. Liu, D. J. Rigden and S. Urbé (2013). "Deubiquitylases from genes to organism." Physiological reviews **93**(3): 1289-1315.
Clute, P. and J. Pines (1999). "Temporal and spatial control of cyclin B1 destruction in metaphase." Nature cell biology **1**(2): 82-87.

Clevers, H. and R. Nusse (2012). "Wnt/β-catenin signaling and disease." Cell 149(6): 1192-1205.

Coverley, D., H. Laman and R. A. Laskey (2002). "Distinct roles for cyclins E and A during DNA replication complex assembly and activation." Nature cell biology **4**(7): 523-528.

Coverley, D., C. Pelizon, S. Trewick and R. A. Laskey (2000). "Chromatin-bound Cdc6 persists in S and G2 phases in human cells, while soluble Cdc6 is destroyed in a cyclin A-cdk2 dependent process." Journal of cell science **113**(11): 1929-1938.

Cronin, N. B., J. Yang, Z. Zhang, K. Kulkarni, L. Chang, H. Yamano and D. Barford (2015). "Atomic-resolution structures of the APC/C subunits Apc4 and the Apc5 N-terminal domain." Journal of molecular biology **427**(20): 3300-3315.

Cunningham, C. N., J. M. Baughman, L. Phu, J. S. Tea, C. Yu, M. Coons, D. S. Kirkpatrick, B. Bingol and J. E. Corn (2015). "USP30 and parkin homeostatically regulate atypical ubiquitin chains on mitochondria." Nature cell biology **17**(2): 160-169.

Datta, A. B., G. L. Hura and C. Wolberger (2009). "The structure and conformation of Lys63-linked tetraubiquitin." Journal of molecular biology **392**(5): 1117-1124.

Davenport, J., L. D. Harris and R. Goorha (2006). "Spindle checkpoint function requires Mad2-dependent Cdc20 binding to the Mad3 homology domain of BubR1." Experimental cell research **312**(10): 1831-1842.

Davey, N. E. and D. O. Morgan (2016). "Building a regulatory network with short linear sequence motifs: lessons from the degrons of the anaphase-promoting complex." Molecular cell **64**(1): 12-23.

David, Y., T. Ziv, A. Admon and A. Navon (2010). "The E2 ubiquitin-conjugating enzymes direct polyubiquitination to preferred lysines." Journal of Biological Chemistry **285**(12): 8595-8604.

D'Avino, P. P. and L. Capalbo (2016). Regulation of midbody formation and function by mitotic kinases. Seminars in cell & developmental biology, Elsevier.

De Boer, L., V. Oakes, H. Beamish, N. Giles, F. Stevens, M. Somodevilla-Torres, C. DeSouza and B. Gabrielli (2008). "Cyclin A/cdk2 coordinates centrosomal and nuclear mitotic events." Oncogene **27**(31): 4261-4268.

den Elzen, N. and J. Pines (2001). "Cyclin A is destroyed in prometaphase and can delay chromosome alignment and anaphase." The Journal of cell biology **153**(1): 121-136.

Deshaies, R. J. and C. A. Joazeiro (2009). "RING domain E3 ubiquitin ligases." Annual review of biochemistry **78**.

Di Fiore, B., N. E. Davey, A. Hagting, D. Izawa, J. Mansfeld, T. J. Gibson and J. Pines (2015). "The ABBA motif binds APC/C activators and is shared by APC/C substrates and regulators." Developmental cell **32**(3): 358-372.

Díaz-Martínez, L. A. and H. Yu (2007). "Running on a treadmill: dynamic inhibition of APC/C by the spindle checkpoint." Cell division **2**(1): 23.

Didier, C., L. Broday, A. Bhoumik, S. Israeli, S. Takahashi, K. Nakayama, S. M. Thomas, C. E. Turner, S. Henderson and H. Sabe (2003). "RNF5, a RING finger protein that regulates cell motility by targeting paxillin ubiquitination and altered localization." Molecular and cellular biology **23**(15): 5331-5345.

Diffley, J. F. (2004). "Regulation of early events in chromosome replication." Current Biology **14**(18): R778-R786.

Dikic, I., S. Wakatsuki and K. J. Walters (2009). "Ubiquitin-binding domains—from structures to functions." Nature Reviews Molecular Cell Biology **10**(10): 659-671.

Donaldson, K. M., H. Yin, N. Gekakis, F. Supek and C. A. Joazeiro (2003). "Ubiquitin signals protein trafficking via interaction with a novel ubiquitin binding domain in the membrane fusion regulator, Vps9p." Current Biology **13**(3): 258-262.

Dong, X., K. H. Zavitz, B. J. Thomas, M. Lin, S. Campbell and S. L. Zipursky (1997). "Control of G1 in the developing Drosophila eye: rca1 regulates Cyclin A." Genes & development **11**(1): 94-105.

Dove, K. K., B. Stieglitz, E. D. Duncan, K. Rittinger and R. E. Klevit (2016). "Molecular insights into RBR E3 ligase ubiquitin transfer mechanisms." EMBO reports **17**(8): 1221-1235.

Dreijerink, K., E. Braga, I. Kuzmin, L. Geil, F.-M. Duh, D. Angeloni, B. Zbar, M. I. Lerman, E. J. Stanbridge and J. D. Minna (2001). "The candidate tumor suppressor gene, RASSF1A, from human chromosome 3p21. 3 is involved in kidney tumorigenesis." Proceedings of the National Academy of Sciences **98**(13): 7504-7509.
Driessens, M. H., C. Olivo, K.-i. Nagata, M. Inagaki and J. G. Collard (2002). "B plexins activate Rho through PDZ-RhoGEF." FEBS letters **529**(2-3): 168-172.

Eifler, K., S. A. Cuijpers, E. Willemstein, J. A. Raaijmakers, D. El Atmioui, H. Ovaa, R. H. Medema and A. C. Vertegaal (2018). "SUMO targets the APC/C to regulate transition from metaphase to anaphase." Nature communications 9(1): 1-15.

Eletr, Z. M., D. T. Huang, D. M. Duda, B. A. Schulman and B. Kuhlman (2005). "E2 conjugating enzymes must disengage from their E1 enzymes before E3-dependent ubiquitin and ubiquitin-like transfer." Nature structural & molecular biology **12**(10): 933-934.

Elia, A. E., A. P. Boardman, D. C. Wang, E. L. Huttlin, R. A. Everley, N. Dephoure, C. Zhou, I. Koren, S. P. Gygi and S. J. Elledge (2015). "Quantitative proteomic atlas of ubiquitination and acetylation in the DNA damage response." Molecular cell **59**(5): 867-881.

Elledge, S. J. (1996). "Cell cycle checkpoints: preventing an identity crisis." Science **274**(5293): 1664-1672.

Elsasser, S., D. Chandler-Militello, B. Müller, J. Hanna and D. Finley (2004). "Rad23 and Rpn10 serve as alternative ubiquitin receptors for the proteasome." Journal of Biological Chemistry **279**(26): 26817-26822.

Erales, J. and P. Coffino (2014). "Ubiquitin-independent proteasomal degradation." Biochimica et Biophysica Acta (BBA)-Molecular Cell Research 1843(1): 216-221.

Etienne-Manneville, S. and A. Hall (2002). "Rho GTPases in cell biology." Nature **420**(6916): 629-635.

Evans, T., E. T. Rosenthal, J. Youngblom, D. Distel and T. Hunt (1983). "Cyclin: a protein specified by maternal mRNA in sea urchin eggs that is destroyed at each cleavage division." Cell **33**(2): 389-396.

Ewen, M. E., H. K. Sluss, C. J. Sherr, H. Matsushime, J.-y. Kato and D. M. Livingston (1993). "Functional interactions of the retinoblastoma protein with mammalian D-type cyclins." Cell **73**(3): 487-497.

Fang, G., H. Yu and M. W. Kirschner (1998). "Direct binding of CDC20 protein family members activates the anaphase-promoting complex in mitosis and G1." Molecular cell **2**(2): 163-171.

Fei, C., Z. Li, C. Li, Y. Chen, Z. Chen, X. He, L. Mao, X. Wang, R. Zeng and L. Li (2013). "Smurf1-mediated Lys29-linked nonproteolytic polyubiquitination of axin negatively regulates Wnt/β-catenin signaling." Molecular and cellular biology **33**(20): 4095-4105.

Fiil, B. K. and M. Gyrd-Hansen (2014). "Met1-linked ubiquitination in immune signalling." The FEBS journal **281**(19): 4337-4350.

Finley, D., S. Sadis, B. P. Monia, P. Boucher, D. J. Ecker, S. T. Crooke and V. Chau (1994). "Inhibition of proteolysis and cell cycle progression in a multiubiquitination-deficient yeast mutant." Molecular and cellular biology **14**(8): 5501-5509.

Flick, K., S. Raasi, H. Zhang, J. L. Yen and P. Kaiser (2006). "A ubiquitin-interacting motif protects polyubiquitinated Met4 from degradation by the 26S proteasome." Nature cell biology **8**(5): 509-515.

Foe, I. T., S. A. Foster, S. K. Cheung, S. Z. DeLuca, D. O. Morgan and D. P. Toczyski (2011). "Ubiquitination of Cdc20 by the APC occurs through an intramolecular mechanism." Current Biology **21**(22): 1870-1877.

Foster, J. (2018). Investigating the relationship between ubch10 and the anaphase promoting complex/cyclosome (Unpublished PhD thesis). The University of Birmingham.

Freemont, P. S., I. M. Hanson and J. Trowsdale (1991). A novel gysteine-rich sequence motif, Cell Press.

Fritsch, J., M. Stephan, V. Tchikov, S. Winoto-Morbach, S. Gubkina, D. Kabelitz and S. Schütze (2014). "Cell fate decisions regulated by K63 ubiquitination of tumor necrosis factor receptor 1." Molecular and cellular biology **34**(17): 3214-3228.

Frye, J. J., N. G. Brown, G. Petzold, E. R. Watson, C. R. Grace, A. Nourse, M. A. Jarvis, R. W. Kriwacki, J.-M. Peters and H. Stark (2013). "Electron microscopy structure of human APC/C CDH1–EMI1 reveals multimodal mechanism of E3 ligase shutdown." Nature structural & molecular biology **20**(7): 827.

Fujimuro, M., H. Sawada and H. Yokosawa (1994). "Production and characterization of monoclonal antibodies specific to multi-ubiquitin chains of polyubiquitinated proteins." FEBS letters **349**(2): 173-180.

Fujita, T., H. Ikeda, N. Taira, S. Hatoh, M. Naito and H. Doihara (2009). "Overexpression of UbcH10 alternates the cell cycle profile and accelerate the tumor proliferation in colon cancer." BMC cancer **9**(1): 87.

Fukuhara, S., C. Murga, M. Zohar, T. Igishi and J. S. Gutkind (1999). "A novel PDZ domain containing guanine nucleotide exchange factor links heterotrimeric G proteins to Rho." Journal of Biological Chemistry **274**(9): 5868-5879.

Gatti, M., S. Pinato, A. Maiolica, F. Rocchio, M. G. Prato, R. Aebersold and L. Penengo (2015). "RNF168 promotes noncanonical K27 ubiquitination to signal DNA damage." Cell Reports **10**(2): 226-238.

Gautier, J., J. Minshull, M. Lohka, M. Glotzer, T. Hunt and J. L. Maller (1990). "Cyclin is a component of maturation-promoting factor from Xenopus." Cell 60(3): 487-494.

Gavet, O. and J. Pines (2010). "Progressive activation of CyclinB1-Cdk1 coordinates entry to mitosis." Developmental cell **18**(4): 533-543.

Gazdoiu, S., K. Yamoah, K. Wu and Z.-Q. Pan (2007). "Human Cdc34 employs distinct sites to coordinate attachment of ubiquitin to a substrate and assembly of polyubiquitin chains." Molecular and cellular biology **27**(20): 7041-7052.

Geis-Asteggiante, L., A. E. Lee and C. Fenselau (2019). Analysis of the topology of ubiquitin chains. Methods in enzymology, Elsevier. 626: 323-346.

Geley, S., E. Kramer, C. Gieffers, J. Gannon, J. Peters and T. Hunt (2001). "APC/C-dependent proteolysis of human cyclin A starts at the beginning of mitosis and is not subject to the spindle assembly checkpoint." J. Cell Biol **153**: 137-148.

Gerlach, B., S. M. Cordier, A. C. Schmukle, C. H. Emmerich, E. Rieser, T. L. Haas, A. I. Webb, J. A. Rickard, H. Anderton and W. W.-L. Wong (2011). "Linear ubiquitination prevents inflammation and regulates immune signalling." Nature **471**(7340): 591-596.

Gieffers, C., P. Dube, J. R. Harris, H. Stark and J.-M. Peters (2001). "Three-dimensional structure of the anaphase-promoting complex." Molecular cell **7**(4): 907-913.

Gilman, A. G. (1987). "G proteins: transducers of receptor-generated signals." Annual review of biochemistry **56**(1): 615-649.

Girard, F., U. Strausfeld, A. Fernandez and N. J. Lamb (1991). "Cyclin A is required for the onset of DNA replication in mammalian fibroblasts." Cell **67**(6): 1169-1179.

Glotzer, M., A. W. Murray and M. W. Kirschner (1991). "Cyclin is degraded by the ubiquitin pathway." Nature **349**(6305): 132-138.

Goitre, L., E. Trapani, L. Trabalzini and S. F. Retta (2014). The Ras superfamily of small GTPases: the unlocked secrets. Ras Signaling, Springer**:** 1-18.

Gong, D., J. R. Pomerening, J. W. Myers, C. Gustavsson, J. T. Jones, A. T. Hahn, T. Meyer and J. E. Ferrell Jr (2007). "Cyclin A2 regulates nuclear-envelope breakdown and the nuclear accumulation of cyclin B1." Current Biology **17**(1): 85-91.

Grimmler, M., Y. Wang, T. Mund, Z. Cilenšek, E.-M. Keidel, M. B. Waddell, H. Jäkel, M. Kullmann, R. W. Kriwacki and L. Hengst (2007). "Cdk-inhibitory activity and stability of p27Kip1 are directly regulated by oncogenic tyrosine kinases." Cell **128**(2): 269-280.

Grizot, S., J. Faure, F. Fieschi, P. Vignais, M.-C. Dagher and E. Pebay-Peyroula (2001). "Crystal structure of the Rac1− RhoGDI complex involved in NADPH oxidase activation." Biochemistry **40**(34): 10007-10013.

Haakonsen, D. L. and M. Rape (2019). "Branching out: improved signaling by heterotypic ubiquitin chains." Trends in cell biology **29**(9): 704-716.

Haas, A. L., J. Warms, A. Hershko and I. A. Rose (1982). "Ubiquitin-activating enzyme. Mechanism and role in protein-ubiquitin conjugation." Journal of Biological Chemistry **257**(5): 2543-2548.

Hagting, A., N. den Elzen, H. C. Vodermaier, I. C. Waizenegger, J.-M. Peters and J. Pines (2002). "Human securin proteolysis is controlled by the spindle checkpoint and reveals when the APC/C switches from activation by Cdc20 to Cdh1." The Journal of cell biology **157**(7): 1125-1137.

Hall, B. E., D. Bar-Sagi and N. Nassar (2002). "The structural basis for the transition from Ras-GTP to Ras-GDP." Proceedings of the National Academy of Sciences **99**(19): 12138-12142.

Hames, R. S., S. L. Wattam, H. Yamano, R. Bacchieri and A. M. Fry (2001). "APC/C-mediated destruction of the centrosomal kinase Nek2A occurs in early mitosis and depends upon a cyclin A-type D-box." The EMBO journal **20**(24): 7117-7127.

Handley, P. M., M. Mueckler, N. R. Siegel, A. Ciechanover and A. L. Schwartz (1991). "Molecular cloning, sequence, and tissue distribution of the human ubiquitin-activating enzyme E1." Proceedings of the National Academy of Sciences **88**(1): 258-262.

Hänzelmann, P., J. Stingele, K. Hofmann, H. Schindelin and S. Raasi (2010). "The yeast E4 ubiquitin ligase Ufd2 interacts with the ubiquitin-like domains of Rad23 and Dsk2 via a novel and distinct ubiquitin-like binding domain." Journal of Biological Chemistry **285**(26): 20390-20398.

Hara, T., M. Abe, H. Inoue, L. Yu, T. D. Veenstra, Y. Kang, K. Lee and T. Miki (2006). "Cytokinesis regulator ECT2 changes its conformation through phosphorylation at Thr-341 in G2/M phase." Oncogene 25(4): 566-578.

Hart, M. J., X. Jiang, T. Kozasa, W. Roscoe, W. D. Singer, A. G. Gilman, P. C. Sternweis and G. Bollag (1998). "Direct stimulation of the guanine nucleotide exchange activity of p115 RhoGEF by Gα13." Science **280**(5372): 2112-2114.

Hatakeyama, S., M. Yada, M. Matsumoto, N. Ishida and K.-I. Nakayama (2001). "U box proteins as a new family of ubiquitin-protein ligases." Journal of Biological Chemistry **276**(35): 33111-33120.

He, J., K. Kulkarni, P. C. da Fonseca, D. Krutauz, M. H. Glickman, D. Barford and E. P. Morris (2012). "The structure of the 26S proteasome subunit Rpn2 reveals its PC repeat domain as a closed toroid of two concentric α-helical rings." Structure **20**(3): 513-521.

Hershko, A., A. Ciechanover, H. Heller, A. L. Haas and I. A. Rose (1980). "Proposed role of ATP in protein breakdown: conjugation of protein with multiple chains of the polypeptide of ATP-dependent proteolysis." Proceedings of the National Academy of Sciences **77**(4): 1783-1786.

Hershko, A., E. Leshinsky, D. Ganoth and H. Heller (1984). "ATP-dependent degradation of ubiquitin-protein conjugates." Proceedings of the National Academy of Sciences **81**(6): 1619-1623.

Hicke, L., H. L. Schubert and C. P. Hill (2005). "Ubiquitin-binding domains." Nature Reviews Molecular Cell Biology **6**(8): 610-621.

Hinds, P. W., S. Mittnacht, V. Dulic, A. Arnold, S. I. Reed and R. A. Weinberg (1992). "Regulation of retinoblastoma protein functions by ectopic expression of human cyclins." Cell **70**(6): 993-1006.

Hirano, T., N. Kinoshita, K. Morikawa and M. Yanagida (1990). "Snap helix with knob and hole: essential repeats in S. pombe nuclear protein nuc2+." Cell **60**(2): 319-328.
Ho, S.-R., C. S. Mahanic, Y.-J. Lee and W.-C. Lin (2014). "RNF144A, an E3 ubiquitin ligase for DNA-PKcs, promotes apoptosis during DNA damage." Proceedings of the National Academy of Sciences **111**(26): E2646-E2655.

Hochstrasser, M. (1996). "Protein degradation or regulation: Ub the judge." Cell **84**(6): 813-815.

Hofmann, K. (1996). "The UBA domain: a sequence motif present in multiple enzyme classes of the ubiquitination pathway." Trends Biol Sci **21**: 172-173.

Holliday, G. L., D. E. Almonacid, G. J. Bartlett, N. M. O'Boyle, J. W. Torrance, P. Murray-Rust, J. B. Mitchell and J. M. Thornton (2007). "MACiE (Mechanism, Annotation and Classification in Enzymes): novel tools for searching catalytic mechanisms." Nucleic acids research **35**(suppl_1): D515-D520.

Holloway, S. L., M. Glotzer, R. W. King and A. W. Murray (1993). "Anaphase is initiated by proteolysis rather than by the inactivation of maturation-promoting factor." Cell **73**(7): 1393-1402.

Holt, L. J., A. N. Krutchinsky and D. O. Morgan (2008). "Positive feedback sharpens the anaphase switch." Nature 454(7202): 353-357.

Hook, S. S., A. Orian, S. M. Cowley and R. N. Eisenman (2002). "Histone deacetylase 6 binds polyubiquitin through its zinc finger (PAZ domain) and copurifies with deubiquitinating enzymes." Proceedings of the National Academy of Sciences **99**(21): 13425-13430.

Hornbeck, P. V., B. Zhang, B. Murray, J. M. Kornhauser, V. Latham and E. Skrzypek (2015). "PhosphoSitePlus, 2014: mutations, PTMs and recalibrations." Nucleic acids research 43(D1): D512-D520.

Hospenthal, M. K., S. M. Freund and D. Komander (2013). "Assembly, analysis and architecture of atypical ubiquitin chains." Nature structural & molecular biology **20**(5): 555.

Hoyt, M. A., L. Totis and B. T. Roberts (1991). "S. cerevisiae genes required for cell cycle arrest in response to loss of microtubule function." Cell **66**(3): 507-517.

Hsu, J. Y., J. D. Reimann, C. S. Sørensen, J. Lukas and P. K. Jackson (2002). "E2F-dependent accumulation of hEmi1 regulates S phase entry by inhibiting APC Cdh1." Nature cell biology **4**(5): 358-366.

Hu, H., G. C. Brittain, J.-H. Chang, N. Puebla-Osorio, J. Jin, A. Zal, Y. Xiao, X. Cheng, M. Chang and Y.-X. Fu (2013). "OTUD7B controls non-canonical NF-κB activation through deubiquitination of TRAF3." Nature **494**(7437): 371-374.

Hu, H., H. Wang, Y. Xiao, J. Jin, J.-H. Chang, Q. Zou, X. Xie, X. Cheng and S.-C. Sun (2016). "Otud7b facilitates T cell activation and inflammatory responses by regulating Zap70 ubiquitination." Journal of experimental medicine **213**(3): 399-414.

Hu, M., P. Li, M. Li, W. Li, T. Yao, J.-W. Wu, W. Gu, R. E. Cohen and Y. Shi (2002). "Crystal structure of a UBP-family deubiquitinating enzyme in isolation and in complex with ubiquitin aldehyde." Cell **111**(7): 1041-1054.

Huang, D. T., H. W. Hunt, M. Zhuang, M. D. Ohi, J. M. Holton and B. A. Schulman (2007). "Basis for a ubiquitin-like protein thioester switch toggling E1–E2 affinity." Nature 445(7126): 394-398.

Huang, H., M.-s. Jeon, L. Liao, C. Yang, C. Elly, J. R. Yates III and Y.-C. Liu (2010). "K33-linked polyubiquitination of T cell receptor-ζ regulates proteolysis-independent T cell signaling." Immunity **33**(1): 60-70.

Huibregtse, J. M., M. Scheffner, S. Beaudenon and P. M. Howley (1995). "A family of proteins structurally and functionally related to the E6-AP ubiquitin-protein ligase." Proceedings of the National Academy of Sciences **92**(7): 2563-2567.

Hurley, J. H. and H. Stenmark (2011). "Molecular mechanisms of ubiquitin-dependent membrane traffic." Annual review of biophysics **40**: 119-142.

Husnjak, K., S. Elsasser, N. Zhang, X. Chen, L. Randles, Y. Shi, K. Hofmann, K. J. Walters, D. Finley and I. Dikic (2008). "Proteasome subunit Rpn13 is a novel ubiquitin receptor." Nature **453**(7194): 481-488.

Iden, S. and J. G. Collard (2008). "Crosstalk between small GTPases and polarity proteins in cell polarization." Nature Reviews Molecular Cell Biology 9(11): 846-859.

Ishimi, Y., Y. Komamura-Kohno, Z. You, A. Omori and M. Kitagawa (2000). "Inhibition of Mcm4, 6, 7 helicase activity by phosphorylation with cyclin A/Cdk2." Journal of Biological Chemistry **275**(21): 16235-16241.

Itoh, M., A. Nagafuchi, S. Yonemura, T. Kitani-Yasuda and S. Tsukita (1993). "The 220-kD protein colocalizing with cadherins in non-epithelial cells is identical to ZO-1, a tight junction-associated protein in epithelial cells: cDNA cloning and immunoelectron microscopy." Journal of Cell Biology **121**(3): 491-502.

Izawa, D. and J. Pines (2011). "How APC/C–Cdc20 changes its substrate specificity in mitosis." Nature cell biology **13**(3): 223-233.

Jeganathan, K. B., L. Malureanu and J. M. Van Deursen (2005). "The Rae1–Nup98 complex prevents aneuploidy by inhibiting securin degradation." Nature **438**(7070): 1036-1039.

Jiang, F. and R. Basavappa (1999). "Crystal structure of the cyclin-specific ubiquitin-conjugating enzyme from clam, E2-C, at 2.0 Å resolution." Biochemistry **38**(20): 6471-6478.

Jiang, L., C.-G. Huang, Y.-C. Lu, C. Luo, G.-H. Hu, H.-M. Liu, J.-X. Chen and H.-X. Han (2008). "Expression of ubiquitin-conjugating enzyme E2C/UbcH10 in astrocytic tumors." Brain research **1201**: 161-166.

Jin, L., A. Williamson, S. Banerjee, I. Philipp and M. Rape (2008). "Mechanism of ubiquitin-chain formation by the human anaphase-promoting complex." Cell **133**(4): 653-665.

Jin, P., S. Hardy and D. O. Morgan (1998). "Nuclear localization of cyclin B1 controls mitotic entry after DNA damage." The Journal of cell biology **141**(4): 875-885.

Johnson, D. S. and Y. H. Chen (2012). "Ras family of small GTPases in immunity and inflammation." Current opinion in pharmacology 12(4): 458-463.

Kabeche, L., H. D. Nguyen, R. Buisson and L. Zou (2018). "A mitosis-specific and R loop–driven ATR pathway promotes faithful chromosome segregation." Science 359(6371): 108-114.

Kaiser, P., K. Flick, C. Wittenberg and S. I. Reed (2000). "Regulation of transcription by ubiquitination without proteolysis: Cdc34/SCFMet30-mediated inactivation of the transcription factor Met4." Cell **102**(3): 303-314.

Kamadurai, H. B., J. Souphron, D. C. Scott, D. M. Duda, D. J. Miller, D. Stringer, R. C. Piper and B. A. Schulman (2009). "Insights into ubiquitin transfer cascades from a structure of a UbcH5B~ ubiquitin-HECTNEDD4L complex." Molecular cell **36**(6): 1095-1102.

Kataria, M. and H. Yamano (2019). "Interplay between Phosphatases and the Anaphase-Promoting Complex/Cyclosome in Mitosis." Cells **8**(8): 814.

Kelsall, I. R., D. M. Duda, J. L. Olszewski, K. Hofmann, A. Knebel, F. Langevin, N. Wood, M. Wightman, B. A. Schulman and A. F. Alpi (2013). "TRIAD1 and HHARI bind to and are activated by distinct neddylated Cullin-RING ligase complexes." The EMBO journal **32**(21): 2848-2860.

Kikuchi, R., H. Ohata, N. Ohoka, A. Kawabata and M. Naito (2014). "APOLLON protein promotes early mitotic CYCLIN A degradation independent of the spindle assembly checkpoint." Journal of Biological Chemistry **289**(6): 3457-3467.

Kim, W., E. J. Bennett, E. L. Huttlin, A. Guo, J. Li, A. Possemato, M. E. Sowa, R. Rad, J. Rush and M. J. Comb (2011). "Systematic and quantitative assessment of the ubiquitin-modified proteome." Molecular cell **44**(2): 325-340.

King, E. M., S. J. van der Sar and K. G. Hardwick (2007). "Mad3 KEN boxes mediate both Cdc20 and Mad3 turnover, and are critical for the spindle checkpoint." PloS one **2**(4).

King, R. W., J.-M. Peters, S. Tugendreich, M. Rolfe, P. Hieter and M. W. Kirschner (1995). "A 20S complex containing CDC27 and CDC16 catalyzes the mitosis-specific conjugation of ubiquitin to cyclin B." Cell **81**(2): 279-288.

Klotzbücher, A., E. Stewart, D. Harrison and T. Hunt (1996). "The 'destruction box'of cyclin A allows B-type cyclins to be ubiquitinated, but not efficiently destroyed." The EMBO journal **15**(12): 3053-3064.

Koegl, M., T. Hoppe, S. Schlenker, H. D. Ulrich, T. U. Mayer and S. Jentsch (1999). "A novel ubiquitination factor, E4, is involved in multiubiquitin chain assembly." Cell **96**(5): 635-644.

Koff, A., F. Cross, A. Fisher, J. Schumacher, K. Leguellec, M. Philippe and J. M. Roberts (1991). "Human cyclin E, a new cyclin that interacts with two members of the CDC2 gene family." Cell **66**(6): 1217-1228.

Komander, D. and M. Rape (2012). "The ubiquitin code." Annual review of biochemistry 81: 203-229.

Kops, G. J., M. van der Voet, M. S. Manak, M. H. van Osch, S. Movahedi Naini, A. Brear, I. X. McLeod, D. M. Hentschel, J. R. Yates III and S. van den Heuvel (2015). "APC16 is a conserved subunit of the anaphase-promoting complex/cyclosome (vol 123, pg 1623, 2010)." Journal of cell science **128**(21): 4025-4025.

Kraft, C., H. C. Vodermaier, S. Maurer-Stroh, F. Eisenhaber and J.-M. Peters (2005). "The WD40 propeller domain of Cdh1 functions as a destruction box receptor for APC/C substrates." Molecular cell **18**(5): 543-553.

Kristariyanto, Y. A., S. A. A. Rehman, D. G. Campbell, N. A. Morrice, C. Johnson, R. Toth and Y. Kulathu (2015). "K29-selective ubiquitin binding domain reveals structural basis of specificity and heterotypic nature of k29 polyubiquitin." Molecular cell **58**(1): 83-94.

Kucharski, T. J., P. E. Minshall, M. Moustafa-Kamal, A. S. Turnell and J. G. Teodoro (2017). "Reciprocal Regulation between 53BP1 and the Anaphase-Promoting Complex/Cyclosome Is Required for Genomic Stability during Mitotic Stress." Cell Reports **18**(8): 1982-1995.

Kumar, K. S., J. J. Krolewski and S. Y. Fuchs (2004). "Phosphorylation and specific ubiquitin acceptor sites are required for ubiquitination and degradation of the IFNAR1 subunit of type I interferon receptor." Journal of Biological Chemistry **279**(45): 46614-46620.

Lake, M. W., M. M. Wuebbens, K. Rajagopalan and H. Schindelin (2001). "Mechanism of ubiquitin activation revealed by the structure of a bacterial MoeB–MoaD complex." Nature **414**(6861): 325-329.

Lara-Gonzalez, P., F. G. Westhorpe and S. S. Taylor (2012). "The spindle assembly checkpoint." Current Biology **22**(22): R966-R980.

Lauwers, E., C. Jacob and B. André (2009). "K63-linked ubiquitin chains as a specific signal for protein sorting into the multivesicular body pathway." Journal of Cell Biology **185**(3): 493-502.

Lee, B.-H., M. J. Lee, S. Park, D.-C. Oh, S. Elsasser, P.-C. Chen, C. Gartner, N. Dimova, J. Hanna and S. P. Gygi (2010). "Enhancement of proteasome activity by a small-molecule inhibitor of USP14." Nature **467**(7312): 179-184.

Lee, I. and H. Schindelin (2008). "Structural insights into E1-catalyzed ubiquitin activation and transfer to conjugating enzymes." Cell **134**(2): 268-278.

Li, R. and A. W. Murray (1991). "Feedback control of mitosis in budding yeast." Cell **66**(3): 519-531.

Li, W., M. H. Bengtson, A. Ulbrich, A. Matsuda, V. A. Reddy, A. Orth, S. K. Chanda, S. Batalov and C. A. Joazeiro (2008). "Genome-wide and functional annotation of human E3 ubiquitin ligases identifies MULAN, a mitochondrial E3 that regulates the organelle's dynamics and signaling." PloS one **3**(1).

Li, W., D. Tu, A. T. Brunger and Y. Ye (2007). "A ubiquitin ligase transfers preformed polyubiquitin chains from a conjugating enzyme to a substrate." Nature **446**(7133): 333-337.

Liang, J. R., A. Martinez, J. D. Lane, U. Mayor, M. J. Clague and S. Urbé (2015). "USP30 deubiquitylates mitochondrial Parkin substrates and restricts apoptotic cell death." EMBO reports **16**(5): 618-627.

Lin, J., D. A. Raoof, Z. Wang, M.-Y. Lin, D. G. Thomas, J. K. Greenson, T. J. Giordano, M. B. Orringer, A. C. Chang and D. G. Beer (2006). "Expression and effect of inhibition of the ubiquitin-conjugating enzyme E2C on esophageal adenocarcinoma." Neoplasia (New York, NY) **8**(12): 1062.

Lin, M.-Y., Y.-M. Lin, T.-c. Kao, H.-H. Chuang and R.-H. Chen (2011). "PDZ-RhoGEF ubiquitination by Cullin3–KLHL20 controls neurotrophin-induced neurite outgrowth." Journal of Cell Biology 193(6): 985-994.

Lin, Y., W. C. Hwang and R. Basavappa (2002). "Structural and functional analysis of the human mitotic-specific ubiquitin-conjugating enzyme, UbcH10." Journal of Biological Chemistry **277**(24): 21913-21921.

Littlepage, L. E. and J. V. Ruderman (2002). "Identification of a new APC/C recognition domain, the A box, which is required for the Cdh1-dependent destruction of the kinase Aurora-A during mitotic exit." Genes & development **16**(17): 2274-2285.

Liu, P., W. Gan, S. Su, A. V. Hauenstein, T.-m. Fu, B. Brasher, C. Schwerdtfeger, A. C. Liang, M. Xu and W. Wei (2018). "K63-linked polyubiquitin chains bind to DNA to facilitate DNA damage repair." Science signaling **11**(533): eaar8133.

Liu, Z., P. Chen, H. Gao, Y. Gu, J. Yang, H. Peng, X. Xu, H. Wang, M. Yang and X. Liu (2014). "Ubiquitylation of autophagy receptor Optineurin by HACE1 activates selective autophagy for tumor suppression." Cancer cell **26**(1): 106-120.

Lois, L. M. and C. D. Lima (2005). "Structures of the SUMO E1 provide mechanistic insights into SUMO activation and E2 recruitment to E1." The EMBO journal **24**(3): 439-451.

Lorenz, S. (2018). "Structural mechanisms of HECT-type ubiquitin ligases." Biological chemistry **399**(2): 127-145.

Lorick, K. L., J. P. Jensen, S. Fang, A. M. Ong, S. Hatakeyama and A. M. Weissman (1999). "RING fingers mediate ubiquitin-conjugating enzyme (E2)-dependent ubiquitination." Proceedings of the National Academy of Sciences **96**(20): 11364-11369.

Lu, D., J. Y. Hsiao, N. E. Davey, V. A. Van Voorhis, S. A. Foster, C. Tang and D. O. Morgan (2014). "Multiple mechanisms determine the order of APC/C substrate degradation in mitosis." Journal of Cell Biology **207**(1): 23-39.

Lu, Y., W. Wang and M. W. Kirschner (2015). "Specificity of the anaphase-promoting complex: a single-molecule study." Science **348**(6231): 1248737.

Lv, Z., K. M. Williams, L. Yuan, J. H. Atkison and S. K. Olsen (2018). "Crystal structure of a human ubiquitin E1–ubiquitin complex reveals conserved functional elements essential for activity." Journal of Biological Chemistry **293**(47): 18337-18352.

Mackiewicz, M., U. Seitzer, J. S. Ahmed and N. Reiling (2020). "Theileria annulata surface protein (TaSP) is a target of cyclin-dependent kinase 1 phosphorylation in Theileria annulata-infected cells." Transboundary and Emerging Diseases **67**: 40-55.

Maddox, A. S. and K. Burridge (2003). "RhoA is required for cortical retraction and rigidity during mitotic cell rounding." The Journal of cell biology 160(2): 255-265.

Mailand, N. and J. F. Diffley (2005). "CDKs promote DNA replication origin licensing in human cells by protecting Cdc6 from APC/C-dependent proteolysis." Cell 122(6): 915-926.

Mansfeld, J., P. Collin, M. O. Collins, J. S. Choudhary and J. Pines (2011). "APC15 drives the turnover of MCC-CDC20 to make the spindle assembly checkpoint responsive to kinetochore attachment." Nature cell biology **13**(10): 1234-1243.

Margarit, S. M., H. Sondermann, B. E. Hall, B. Nagar, A. Hoelz, M. Pirruccello, D. Bar-Sagi and J. Kuriyan (2003). "Structural evidence for feedback activation by Ras· GTP of the Ras-specific nucleotide exchange factor SOS." Cell **112**(5): 685-695.

Martz, M. K., E. Grabocka, N. Beeharry, T. J. Yen and P. B. Wedegaertner (2013). "Leukemia-associated RhoGEF (LARG) is a novel RhoGEF in cytokinesis and required for the proper completion of abscission." Molecular biology of the cell 24(18): 2785-2794.

Matsumoto, M. L., K. E. Wickliffe, K. C. Dong, C. Yu, I. Bosanac, D. Bustos, L. Phu, D. S. Kirkpatrick, S. G. Hymowitz and M. Rape (2010). "K11-linked polyubiquitination in cell cycle control revealed by a K11 linkage-specific antibody." Molecular cell **39**(3): 477-484.

Matthews, H. K., U. Delabre, J. L. Rohn, J. Guck, P. Kunda and B. Baum (2012). "Changes in Ect2 localization couple actomyosin-dependent cell shape changes to mitotic progression." Developmental cell 23(2): 371-383.

Matyskiela, M. E. and D. O. Morgan (2009). "Analysis of activator-binding sites on the APC/C supports a cooperative substrate-binding mechanism." Molecular cell **34**(1): 68-80.

Mayer, R. J., J. Arnold, L. László, M. Landon and J. Lowe (1991). "Ubiquitin in health and disease." Biochimica et Biophysica Acta (BBA)-Gene Structure and Expression **1089**(2): 141-157.

McGarry, T. J. and M. W. Kirschner (1998). "Geminin, an inhibitor of DNA replication, is degraded during mitosis." Cell **93**(6): 1043-1053.

McGrath, J. P., S. Jentsch and A. Varshavsky (1991). "UBA 1: an essential yeast gene encoding ubiquitin-activating enzyme." The EMBO journal **10**(1): 227-236.

Memon, A. R. (2004). "The role of ADP-ribosylation factor and SAR1 in vesicular trafficking in plants." Biochimica et Biophysica Acta (BBA)-Biomembranes **1664**(1): 9-30.

Merkley, N., K. R. Barber and G. S. Shaw (2005). "Ubiquitin manipulation by an E2 conjugating enzyme using a novel covalent intermediate." Journal of Biological Chemistry **280**(36): 31732-31738.

Metzger, M. B., J. N. Pruneda, R. E. Klevit and A. M. Weissman (2014). "RING-type E3 ligases: master manipulators of E2 ubiquitin-conjugating enzymes and ubiquitination." Biochimica et Biophysica Acta (BBA)-Molecular Cell Research **1843**(1): 47-60.

Meyer, H.-J. and M. Rape (2014). "Enhanced protein degradation by branched ubiquitin chains." Cell **157**(4): 910-921.

Meyer, H. H., Y. Wang and G. Warren (2002). "Direct binding of ubiquitin conjugates by the mammalian p97 adaptor complexes, p47 and Ufd1–Npl4." The EMBO journal **21**(21): 5645-5652.

Michel, M. A., P. R. Elliott, K. N. Swatek, M. Simicek, J. N. Pruneda, J. L. Wagstaff, S. M. Freund and D. Komander (2015). "Assembly and specific recognition of k29-and k33-linked polyubiquitin." Molecular cell **58**(1): 95-109.

Michel, M. A., K. N. Swatek, M. K. Hospenthal and D. Komander (2017). "Ubiquitin linkage-specific affimers reveal insights into K6-linked ubiquitin signaling." Molecular cell **68**(1): 233-246. e235.

Michelle, C., P. Vourc'h, L. Mignon and C. R. Andres (2009). "What was the set of ubiquitin and ubiquitin-like conjugating enzymes in the eukaryote common ancestor?" Journal of molecular evolution **68**(6): 616-628.

Miller, J. J., M. K. Summers, D. V. Hansen, M. V. Nachury, N. L. Lehman, A. Loktev and P. K. Jackson (2006). "Emi1 stably binds and inhibits the anaphase-promoting complex/cyclosome as a pseudosubstrate inhibitor." Genes & development **20**(17): 2410-2420.

Min, M., T. E. Mevissen, M. De Luca, D. Komander and C. Lindon (2015). "Efficient APC/C substrate degradation in cells undergoing mitotic exit depends on K11 ubiquitin linkages." Molecular biology of the cell **26**(24): 4325-4332.

Min, M., U. Mayor and C. Lindon (2013). "Ubiquitination site preferences in anaphase promoting complex/cyclosome (APC/C) substrates." Open biology 3(9): 130097.

Mocciaro, A. and M. Rape (2012). "Emerging regulatory mechanisms in ubiquitin-dependent cell cycle control." Journal of cell science **125**(2): 255-263.

Moniz, S., D. Bandarra, J. Biddlestone, K. J. Campbell, D. Komander, A. Bremm and S. Rocha (2015). "Cezanne regulates E2F1-dependent HIF2α expression." Journal of cell science **128**(16): 3082-3093.

Moon, S. Y. and Y. Zheng (2003). "Rho GTPase-activating proteins in cell regulation." Trends in cell biology **13**(1): 13-22.

Moore, M. S. (1998). "Ran and nuclear transport." Journal of Biological Chemistry 273(36): 22857-22860.

Moreno, S. P., R. M. Jones, D. Poovathumkadavil, S. Scaramuzza and A. Gambus (2019). "Mitotic replisome disassembly depends on TRAIP ubiquitin ligase activity." Life science alliance **2**(2).

Morisaki, H., A. Fujimoto, A. Ando, Y. Nagata, K. Ikeda and M. Nakanishi (1997). "Cell cycle-dependent phosphorylation of p27 cyclin-dependent kinase (Cdk) inhibitor by cyclin E/Cdk2." Biochemical and biophysical research communications **240**(2): 386-390.

Morris, J. R. and E. Solomon (2004). "BRCA1: BARD1 induces the formation of conjugated ubiquitin structures, dependent on K6 of ubiquitin, in cells during DNA replication and repair." Human molecular genetics **13**(8): 807-817.

Morris, L., K. E. Allen and N. B. La Thangue (2000). "Regulation of E2F transcription by cyclin E–Cdk2 kinase mediated through p300/CBP co-activators." Nature cell biology **2**(4): 232-239.

Moynihan, T. P., H. C. Ardley, U. Nuber, S. A. Rose, P. F. Jones, A. F. Markham, M. Scheffner and P. A. Robinson (1999). "The ubiquitin-conjugating enzymes UbcH7 and UbcH8 interact with RING finger/IBR motif-containing domains of HHARI and H7-AP1." Journal of Biological Chemistry **274**(43): 30963-30968.

Müller, P. M., J. Rademacher, R. D. Bagshaw, C. Wortmann, C. Barth, J. van Unen, K. M. Alp, G. Giudice, R. L. Eccles and L. E. Heinrich (2020). "Systems analysis of RhoGEF and RhoGAP regulatory proteins reveals spatially organized RAC1 signalling from integrin adhesions." Nature cell biology 22(4): 498-511.

Musacchio, A. (2015). "The molecular biology of spindle assembly checkpoint signaling dynamics." Current Biology **25**(20): R1002-R1018.

Nagy, O., M. Pál, A. Udvardy, C. A. Shirras, I. Boros, A. D. Shirras and P. Deák (2012). "lemmingA encodes the Apc11 subunit of the APC/C in Drosophila melanogaster that forms a ternary complex with the E2-C type ubiquitin conjugating enzyme, Vihar and Morula/Apc2." Cell division **7**(1): 9.

Nakayama, K., H. Nagahama, Y. A. Minamishima, M. Matsumoto, I. Nakamichi, K. Kitagawa, M. Shirane, R. Tsunematsu, T. Tsukiyama and N. Ishida (2000). "Targeted disruption of Skp2 results in accumulation of cyclin E and p27Kip1, polyploidy and centrosome overduplication." The EMBO journal **19**(9): 2069-2081.

Naoe, H., K. Araki, O. Nagano, Y. Kobayashi, J. Ishizawa, T. Chiyoda, T. Shimizu, K.-i. Yamamura, Y. Sasaki and H. Saya (2010). "The anaphase-promoting complex/cyclosome activator Cdh1 modulates Rho GTPase by targeting p190 RhoGAP for degradation." Molecular and cellular biology 30(16): 3994-4005.

Nath, S., T. Banerjee, D. Sen, T. Das and S. Roychoudhury (2011). "Spindle assembly checkpoint protein Cdc20 transcriptionally activates expression of ubiquitin carrier protein UbcH10." Journal of Biological Chemistry 286(18): 15666-15677.

Niiya, F., T. Tatsumoto, K. Lee and T. Miki (2006). "Phosphorylation of the cytokinesis regulator ECT2 at G2/M phase stimulates association of the mitotic kinase Plk1 and accumulation of GTP-bound RhoA." Oncogene 25(6): 827-837.

Nijman, S. M., M. P. Luna-Vargas, A. Velds, T. R. Brummelkamp, A. M. Dirac, T. K. Sixma and R. Bernards (2005). "A genomic and functional inventory of deubiquitinating enzymes." Cell **123**(5): 773-786.

Nilsson, J., M. Yekezare, J. Minshull and J. Pines (2008). "The APC/C maintains the spindle assembly checkpoint by targeting Cdc20 for destruction." Nature cell biology **10**(12): 1411-1420.

Nishimura, Y. and S. Yonemura (2006). "Centralspindlin regulates ECT2 and RhoA accumulation at the equatorial cortex during cytokinesis." Journal of cell science 119(1): 104-11

Ohtake, F., H. Tsuchiya, Y. Saeki and K. Tanaka (2018). "K63 ubiquitylation triggers proteasomal degradation by seeding branched ubiquitin chains." Proceedings of the National Academy of Sciences **115**(7): E1401-E1408.

oinuma, I., H. Katoh, A. Harada and M. Negishi (2003). "Direct interaction of Rnd1 with Plexin-B1 regulates PDZ-RhoGEF-mediated Rho activation by Plexin-B1 and induces cell contraction in COS-7 cells." Journal of Biological Chemistry 278(28): 25671-25677.

Olsen, S. K. and C. D. Lima (2013). "Structure of a ubiquitin E1-E2 complex: insights to E1-E2 thioester transfer." Molecular cell **49**(5): 884-896.

Ordureau, A., J.-M. Heo, D. M. Duda, J. A. Paulo, J. L. Olszewski, D. Yanishevski, J. Rinehart, B. A. Schulman and J. W. Harper (2015). "Defining roles of PARKIN and ubiquitin phosphorylation by PINK1 in mitochondrial quality control using a ubiquitin replacement strategy." Proceedings of the National Academy of Sciences **112**(21): 6637-6642.

Ordureau, A., S. A. Sarraf, D. M. Duda, J.-M. Heo, M. P. Jedrychowski, V. O. Sviderskiy, J. L. Olszewski, J. T. Koerber, T. Xie and S. A. Beausoleil (2014). "Quantitative proteomics reveal a feedforward mechanism for mitochondrial PARKIN translocation and ubiquitin chain synthesis." Molecular cell **56**(3): 360-375.

Ozkaynak, E., D. Finley, M. Solomon and A. Varshavsky (1987). "The yeast ubiquitin genes: a family of natural gene fusions." The EMBO journal **6**(5): 1429-1439.

Pachis, S. T., Y. Hiruma, E. C. Tromer, A. Perrakis and G. J. Kops (2019). "Interactions between N-terminal modules in MPS1 enable spindle checkpoint silencing." Cell Reports **26**(8): 2101-2112. e2106.

Palazzo, L., R. Della Monica, R. Visconti, V. Costanzo and D. Grieco (2014). "ATM controls proper mitotic spindle structure." Cell Cycle 13(7): 1091-1100.

Palicharla, V. R. and S. Maddika (2015). "HACE1 mediated K27 ubiquitin linkage leads to YB-1 protein secretion." Cellular signalling **27**(12): 2355-2362.

Pallante, P., M. Berlingieri, G. Troncone, M. Kruhoffer, T. Orntoft, G. Viglietto, A. Caleo, I. Migliaccio, M. Decaussin-Petrucci and M. Santoro (2005). "UbcH10

overexpression may represent a marker of anaplastic thyroid carcinomas." British journal of cancer **93**(4): 464-471.

Pan, Z.-Q., A. A. Amin, E. Gibbs, H. Niu and J. Hurwitz (1994). "Phosphorylation of the p34 subunit of human single-stranded-DNA-binding protein in cyclin A-activated G1 extracts is catalyzed by cdk-cyclin A complex and DNA-dependent protein kinase." Proceedings of the National Academy of Sciences **91**(18): 8343-8347.

Pareja, F., D. A. Ferraro, C. Rubin, H. Cohen-Dvashi, F. Zhang, S. Aulmann, N. Ben-Chetrit, G. Pines, R. Navon and N. Crosetto (2012). "Deubiquitination of EGFR by Cezanne-1 contributes to cancer progression." Oncogene **31**(43): 4599-4608.

Park, Y., H.-s. Jin, J. Lopez, J. Lee, L. Liao, C. Elly and Y.-C. Liu (2016). "SHARPIN controls regulatory T cells by negatively modulating the T cell antigen receptor complex." Nature immunology **17**(3): 286-296.

Passmore, L. A., C. R. Booth, C. Vénien-Bryan, S. J. Ludtke, C. Fioretto, L. N. Johnson, W. Chiu and D. Barford (2005). "Structural analysis of the anaphase-promoting complex reveals multiple active sites and insights into polyubiquitylation." Molecular cell **20**(6): 855-866.

Passmore, L. A., E. A. McCormack, S. W. Au, A. Paul, K. R. Willison, J. W. Harper and D. Barford (2003). "Doc1 mediates the activity of the anaphase-promoting complex by contributing to substrate recognition." The EMBO journal **22**(4): 786-796.
Paul, A. and B. Wang (2017). "RNF8-and Ube2S-dependent ubiquitin lysine 11-linkage modification in response to DNA damage." Molecular cell **66**(4): 458-472. e455.

Pelzer, C., I. Kassner, K. Matentzoglu, R. K. Singh, H.-P. Wollscheid, M. Scheffner, G. Schmidtke and M. Groettrup (2007). "UBE1L2, a novel E1 enzyme specific for ubiquitin." Journal of Biological Chemistry **282**(32): 23010-23014.

Peters, J.-M. (1998). "SCF and APC: the Yin and Yang of cell cycle regulated proteolysis." Current opinion in cell biology **10**(6): 759-768.

Petroski, M. D. and R. J. Deshaies (2005). "Mechanism of lysine 48-linked ubiquitin-chain synthesis by the cullin-RING ubiquitin-ligase complex SCF-Cdc34." Cell **123**(6): 1107-1120.

Pickart, C. M. (2004). "Back to the future with ubiquitin." Cell **116**(2): 181-190.
Pines, J. (1994). "Ubiquitin with everything." Nature **371**(6500): 742-743.

Pines, J. (2011). "Cubism and the cell cycle: the many faces of the APC/C." Nature Reviews Molecular Cell Biology **12**(7): 427-438.

Pornillos, O., S. L. Alam, R. L. Rich, D. G. Myszka, D. R. Davis and W. I. Sundquist (2002). "Structure and functional interactions of the Tsg101 UEV domain." The EMBO journal **21**(10): 2397-2406.

Rahighi, S., F. Ikeda, M. Kawasaki, M. Akutsu, N. Suzuki, R. Kato, T. Kensche, T. Uejima, S. Bloor and D. Komander (2009). "Specific recognition of linear ubiquitin chains by NEMO is important for NF-κB activation." Cell **136**(6): 1098-1109.

Rajabi, H., M. Hiraki, A. Tagde, M. Alam, A. Bouillez, C. L. Christensen, M. Samur, K.-K. Wong and D. Kufe (2017). "MUC1-C activates EZH2 expression and function in human cancer cells." Scientific reports **7**(1): 1-13.

Ramadan, K., R. Bruderer, F. M. Spiga, O. Popp, T. Baur, M. Gotta and H. H. Meyer (2007). "Cdc48/p97 promotes reformation of the nucleus by extracting the kinase Aurora B from chromatin." Nature **450**(7173): 1258-1262.

Rape, M., S. K. Reddy and M. W. Kirschner (2006). "The processivity of multiubiquitination by the APC determines the order of substrate degradation." Cell **124**(1): 89-103.

Rape, M., T. Hoppe, I. Gorr, M. Kalocay, H. Richly and S. Jentsch (2001). "Mobilization of processed, membrane-tethered SPT23 transcription factor by CDC48UFD1/NPL4, a ubiquitin-selective chaperone." Cell 107(5): 667-677.

Rape, M. and M. W. Kirschner (2004). "Autonomous regulation of the anaphase-promoting complex couples mitosis to S-phase entry." Nature 432(7017): 588-595.

Reimann, J. D., B. E. Gardner, F. Margottin-Goguet and P. K. Jackson (2001). "Emi1 regulates the anaphase-promoting complex by a different mechanism than Mad2 proteins." Genes & development 15(24): 3278-3285.

Reimann, J. D., E. Freed, J. Y. Hsu, E. R. Kramer, J.-M. Peters and P. K. Jackson (2001). "Emi1 is a mitotic regulator that interacts with Cdc20 and inhibits the anaphase promoting complex." Cell **105**(5): 645-655.

Reis, A., M. Levasseur, H. Y. Chang, D. J. Elliott and K. T. Jones (2006). "The CRY box: a second APCcdh1-dependent degron in mammalian cdc20." EMBO reports **7**(10): 1040-1045.

Repasky, G. A., E. J. Chenette and C. J. Der (2004). "Renewing the conspiracy theory debate: does Raf function alone to mediate Ras oncogenesis?" Trends in cell biology **14**(11): 639-647.

Reyes-Turcu, F. E., J. R. Horton, J. E. Mullally, A. Heroux, X. Cheng and K. D. Wilkinson (2006). "The ubiquitin binding domain ZnF UBP recognizes the C-terminal diglycine motif of unanchored ubiquitin." Cell **124**(6): 1197-1208.

Rieder, C. L., A. Schultz, R. Cole and G. Sluder (1994). "Anaphase onset in vertebrate somatic cells is controlled by a checkpoint that monitors sister kinetochore attachment to the spindle." The Journal of cell biology **127**(5): 1301-1310.

Rodrigo-Brenni, M. C., S. A. Foster and D. O. Morgan (2010). "Catalysis of lysine 48-specific ubiquitin chain assembly by residues in E2 and ubiquitin." Molecular cell **39**(4): 548-559.

Russell, P. and P. Nurse (1987). "Negative regulation of mitosis by wee1+, a gene encoding a protein kinase homolog." Cell **49**(4): 559-567.

Sackton, K. L., N. Dimova, X. Zeng, W. Tian, M. Zhang, T. B. Sackton, J. Meaders, K. L. Pfaff, F. Sigoillot and H. Yu (2014). "Synergistic blockade of mitotic exit by two chemical inhibitors of the APC/C." Nature 514(7524): 646-649.

Scheffner, M., B. A. Werness, J. M. Huibregtse, A. J. Levine and P. M. Howley (1990). "The E6 oncoprotein encoded by human papillomavirus types 16 and 18 promotes the degradation of p53." Cell **63**(6): 1129-1136.

Schmidt, A. and A. Hall (2002). "Guanine nucleotide exchange factors for Rho GTPases: turning on the switch." Genes & development **16**(13): 1587-1609.

Schwab, M., A. S. Lutum and W. Seufert (1997). "Yeast Hct1 is a regulator of Clb2 cyclin proteolysis." Cell **90**(4): 683-693.

Schwab, M., M. Neutzner, D. Möcker and W. Seufert (2001). "Yeast Hct1 recognizes the mitotic cyclin Clb2 and other substrates of the ubiquitin ligase APC." The EMBO journal **20**(18): 5165-5175.

Schwickart, M., J. Havlis, B. Habermann, A. Bogdanova, A. Camasses, T. Oelschlaegel, A. Shevchenko and W. Zachariae (2004). "Swm1/Apc13 is an evolutionarily conserved subunit of the anaphase-promoting complex stabilizing the association of Cdc16 and Cdc27." Molecular and cellular biology **24**(8): 3562-3576.

Sedgwick, G. G., D. G. Hayward, B. Di Fiore, M. Pardo, L. Yu, J. Pines and J. Nilsson (2013). "Mechanisms controlling the temporal degradation of Nek2A and Kif18A by the APC/C–Cdc20 complex." The EMBO journal **32**(2): 303-314.
Sehr, P., K. Zumbach and M. Pawlita (2001). "A generic capture ELISA for recombinant proteins fused to glutathione S-transferase: validation for HPV serology." Journal of immunological methods **253**(1-2): 153-162.

Sheehan, D., G. MEADE, V. M. FOLEY and C. A. DOWD (2001). "Structure, function and evolution of glutathione transferases: implications for classification of non-mammalian members of an ancient enzyme superfamily." Biochemical Journal **360**(1): 1-16.

Shi, Y., X. Chen, S. Elsasser, B. B. Stocks, G. Tian, B.-H. Lee, Y. Shi, N. Zhang, S. A. de Poot and F. Tuebing (2016). "Rpn1 provides adjacent receptor sites for substrate binding and deubiquitination by the proteasome." Science **351**(6275).

Shiba, Y., Y. Katoh, T. Shiba, K. Yoshino, H. Takatsu, H. Kobayashi, H.-W. Shin, S. Wakatsuki and K. Nakayama (2004). "GAT (GGA and Tom1) domain responsible for ubiquitin binding and ubiquitination." Journal of Biological Chemistry **279**(8): 7105-7111.

Shimura, H., N. Hattori, S.-i. Kubo, Y. Mizuno, S. Asakawa, S. Minoshima, N. Shimizu, K. Iwai, T. Chiba and K. Tanaka (2000). "Familial Parkinson disease gene product, parkin, is a ubiquitin-protein ligase." Nature genetics **25**(3): 302-305.

Sikorski, R. S., M. S. Boguski, M. Goebl and P. Hieter (1990). "A repeating amino acid motif in CDC23 defines a family of proteins and a new relationship among genes required for mitosis and RNA synthesis." Cell **60**(2): 307-317.

Singh, S. and J. Sivaraman (2020). "Crystal structure of HECT domain of UBE3C E3 ligase and its ubiquitination activity." Biochemical Journal **477**(5): 905-923.

Sivakumar, S. and G. J. Gorbsky (2015). "Spatiotemporal regulation of the anaphase-promoting complex in mitosis." Nature Reviews Molecular Cell Biology **16**(2): 82-94.

Sloper-Mould, K. E., J. C. Jemc, C. M. Pickart and L. Hicke (2001). "Distinct functional surface regions on ubiquitin." Journal of Biological Chemistry **276**(32): 30483-30489.

Smit, J. J., D. Monteferrario, S. M. Noordermeer, W. J. Van Dijk, B. A. Van Der Reijden and T. K. Sixma (2012). "The E3 ligase HOIP specifies linear ubiquitin chain assembly through its RING-IBR-RING domain and the unique LDD extension." The EMBO journal **31**(19): 3833-3844.

Spence, J., R. R. Gali, G. Dittmar, F. Sherman, M. Karin and D. Finley (2000). "Cell cycle–regulated modification of the ribosome by a variant multiubiquitin chain." Cell **102**(1): 67-76.

Stewart, M. D., T. Ritterhoff, R. E. Klevit and P. S. Brzovic (2016). "E2 enzymes: more than just middle men." Cell research **26**(4): 423-440.

Stieglitz, B., A. C. Morris-Davies, M. G. Koliopoulos, E. Christodoulou and K. Rittinger (2012). "LUBAC synthesizes linear ubiquitin chains via a thioester intermediate." EMBO reports **13**(9): 840-846.

Stracker, T. H., T. Usui and J. H. Petrini (2009). "Taking the time to make important decisions: the checkpoint effector kinases Chk1 and Chk2 and the DNA damage response." DNA repair 8(9): 1047-1054.

Su, K.-C., T. Takaki and M. Petronczki (2011). "Targeting of the RhoGEF Ect2 to the equatorial membrane controls cleavage furrow formation during cytokinesis." Developmental cell 21(6): 1104-1115.

Sudakin, V., D. Ganoth, A. Dahan, H. Heller, J. Hershko, F. C. Luca, J. V. Ruderman and A. Hershko (1995). "The cyclosome, a large complex containing cyclin-selective ubiquitin ligase activity, targets cyclins for destruction at the end of mitosis." Molecular biology of the cell 6(2): 185-197.

Sudakin, V., G. K. Chan and T. J. Yen (2001). "Checkpoint inhibition of the APC/C in HeLa cells is mediated by a complex of BUBR1, BUB3, CDC20, and MAD2." The Journal of cell biology **154**(5): 925-936.

Sugiura, A., S. Nagashima, T. Tokuyama, T. Amo, Y. Matsuki, S. Ishido, Y. Kudo, H. M. McBride, T. Fukuda and N. Matsushita (2013). "MITOL regulates endoplasmic reticulum-mitochondria contacts via Mitofusin2." Molecular cell **51**(1): 20-34.

Summers, M. K., B. Pan, K. Mukhyala and P. K. Jackson (2008). "The unique N terminus of the UbcH10 E2 enzyme controls the threshold for APC activation and enhances checkpoint regulation of the APC." Molecular cell **31**(4): 544-556.

Sun, L. and Z. J. Chen (2004). "The novel functions of ubiquitination in signaling." Current opinion in cell biology **16**(2): 119-126.

Swiercz, J. M., R. Kuner, J. Behrens and S. Offermanns (2002). "Plexin-B1 directly interacts with PDZ-RhoGEF/LARG to regulate RhoA and growth cone morphology." Neuron 35(1): 51-63.

Swiercz, J. M., T. Worzfeld and S. Offermanns (2009). "Semaphorin 4D signaling requires the recruitment of phospholipase Cγ into the plexin-B1 receptor complex." Molecular and cellular biology 29(23): 6321-6334.

Szczepanowski, R. H., R. Filipek and M. Bochtler (2005). "Crystal structure of a fragment of mouse ubiquitin-activating enzyme." Journal of Biological Chemistry **280**(23): 22006-22011.

Takai, Y., T. Sasaki and T. Matozaki (2001). "Small GTP-binding proteins." Physiological reviews **81**(1): 153-208.

Tang, Z., R. Bharadwaj, B. Li and H. Yu (2001). "Mad2-Independent inhibition of APCCdc20 by the mitotic checkpoint protein BubR1." Developmental cell **1**(2): 227-237.

Thornton, B. R. and D. P. Toczyski (2003). "Securin and B-cyclin/CDK are the only essential targets of the APC." Nature cell biology **5**(12): 1090-1094.

Tilotta, M. (2019). Investigating the role of the anaphase promoting complex/cyclosome subunit apc5 in mitosis (Unpublished PhD thesis). The University of Birmingham.

Torrecilla, I., J. Oehler and K. Ramadan (2017). "The role of ubiquitin-dependent segregase p97 (VCP or Cdc48) in chromatin dynamics after DNA double strand breaks." Philosophical Transactions of the Royal Society B: Biological Sciences **372**(1731): 20160282.

Torres, J. Z., K. H. Ban and P. K. Jackson (2010). "A specific form of phospho protein phosphatase 2 regulates anaphase-promoting complex/cyclosome association with spindle poles." Molecular biology of the cell **21**(6): 897-904.

Townsley, F. M., A. Aristarkhov, S. Beck, A. Hershko and J. V. Ruderman (1997). "Dominant-negative cyclin-selective ubiquitin carrier protein E2-C/UbcH10 blocks cells in metaphase." Proceedings of the National Academy of Sciences **94**(6): 2362-2367.

Tuncay, H., B. F. Brinkmann, T. Steinbacher, A. Schürmann, V. Gerke, S. Iden and K. Ebnet (2015). "JAM-A regulates cortical dynein localization through Cdc42 to control planar spindle orientation during mitosis." Nature communications 6(1): 1-12.

Turnell, A. S., G. S. Stewart, R. J. Grand, S. M. Rookes, A. Martin, H. Yamano, S. J. Elledge and P. H. Gallimore (2005). "The APC/C and CBP/p300 cooperate to regulate transcription and cell-cycle progression." Nature **438**(7068): 690-695.

Valimberti, I., M. Tiberti, M. Lambrughi, B. Sarcevic and E. Papaleo (2015). "E2 superfamily of ubiquitin-conjugating enzymes: constitutively active or activated through phosphorylation in the catalytic cleft." Scientific reports **5**(1): 1-13.

Van Ree, J. H., K. B. Jeganathan, L. Malureanu and J. M. Van Deursen (2010). "Overexpression of the E2 ubiquitin–conjugating enzyme UbcH10 causes chromosome missegregation and tumor formation." Journal of Cell Biology **188**(1): 83-100.

van Zon, W., J. Ogink, B. ter Riet, R. H. Medema, H. te Riele and R. M. Wolthuis (2010). "The APC/C recruits cyclin B1–Cdk1–Cks in prometaphase before D box recognition to control mitotic exit." Journal of Cell Biology **190**(4): 587-602.

Varghese, B., H. Barriere, C. J. Carbone, A. Banerjee, G. Swaminathan, A. Plotnikov, P. Xu, J. Peng, V. Goffin and G. L. Lukacs (2008). "Polyubiquitination of prolactin receptor stimulates its internalization, postinternalization sorting, and degradation via the lysosomal pathway." Molecular and cellular biology **28**(17): 5275-5287.

Vijay-Kumar, S., C. E. Bugg and W. J. Cook (1987). "Structure of ubiquitin refined at 1.8 Åresolution." Journal of molecular biology **194**(3): 531-544.

Visintin, R., S. Prinz and A. Amon (1997). "CDC20 and CDH1: a family of substrate-specific activators of APC-dependent proteolysis." Science **278**(5337): 460-463.

Vodermaier, H. C., C. Gieffers, S. Maurer-Stroh, F. Eisenhaber and J.-M. Peters (2003). "TPR subunits of the anaphase-promoting complex mediate binding to the activator protein CDH1." Current Biology **13**(17): 1459-1468.

Voitenleitner, C., E. Fanning and H. Nasheuer (1997). "Phosphorylation of DNA polymerase α-primase by cyclin A-dependent kinases regulates initiation of DNA replication in vitro." Oncogene **14**(13): 1611-1615.

Wagner, S. A., P. Beli, B. T. Weinert, M. L. Nielsen, J. Cox, M. Mann and C. Choudhary (2011). "A proteome-wide, quantitative survey of in vivo ubiquitylation sites reveals widespread regulatory roles." Molecular & Cellular Proteomics **10**(10).

Walker, A., C. Acquaviva, T. Matsusaka, L. Koop and J. Pines (2008). "UbcH10 has a rate-limiting role in G1 phase but might not act in the spindle checkpoint or as part of an autonomous oscillator." Journal of cell science **121**(14): 2319-2326.

Wang, J., B. T. Dye, K. R. Rajashankar, I. Kurinov and B. A. Schulman (2009). "Insights into anaphase promoting complex TPR subdomain assembly from a CDC26–APC6 structure." Nature structural & molecular biology **16**(9): 987.

Wang, Q., X. Liu, Y. Cui, Y. Tang, W. Chen, S. Li, H. Yu, Y. Pan and C. Wang (2014). "The E3 ubiquitin ligase AMFR and INSIG1 bridge the activation of TBK1 kinase by modifying the adaptor STING." Immunity **41**(6): 919-933.

Watanabe, N., H. Arai, Y. Nishihara, M. Taniguchi, N. Watanabe, T. Hunter and H. Osada (2004). "M-phase kinases induce phospho-dependent ubiquitination of somatic Wee1 by SCFβ-TrCP." Proceedings of the National Academy of Sciences **101**(13): 4419-4424.

Weis, K. (2003). "Regulating access to the genome: nucleocytoplasmic transport throughout the cell cycle." Cell **112**(4): 441-451.

Welsh, J. B., P. P. Zarrinkar, L. M. Sapinoso, S. G. Kern, C. A. Behling, B. J. Monk, D. J. Lockhart, R. A. Burger and G. M. Hampton (2001). "Analysis of gene expression profiles in normal and neoplastic ovarian tissue samples identifies candidate molecular markers of epithelial ovarian cancer." Proceedings of the National Academy of Sciences **98**(3): 1176-1181.

Wenzel, D. M., A. Lissounov, P. S. Brzovic and R. E. Klevit (2011). "UBCH7 reactivity profile reveals parkin and HHARI to be RING/HECT hybrids." Nature **474**(7349): 105-108.

Wiborg, O., M. Pedersen, A. Wind, L. Berglund, K. Marcker and J. Vuust (1985). "The human ubiquitin multigene family: some genes contain multiple directly repeated ubiquitin coding sequences." The EMBO journal **4**(3): 755-759.

Wild, T., M. S. Y. Larsen, T. Narita, J. Schou, J. Nilsson and C. Choudhary (2016). "The spindle assembly checkpoint is not essential for viability of human cells with genetically lowered APC/C activity." Cell Reports **14**(8): 1829-1840.

Williamson, A., S. Banerjee, X. Zhu, I. Philipp, A. T. Iavarone and M. Rape (2011). "Regulation of ubiquitin chain initiation to control the timing of substrate degradation." Molecular cell **42**(6): 744-757.

Williamson, A., K. E. Wickliffe, B. G. Mellone, L. Song, G. H. Karpen and M. Rape (2009). "Identification of a physiological E2 module for the human anaphase-promoting complex." Proceedings of the National Academy of Sciences **106**(43): 18213-18218.

Wirth, K. G., R. Ricci, J. F. Giménez-Abián, S. Taghybeeglu, N. R. Kudo, W. Jochum, M. Vasseur-Cognet and K. Nasmyth (2004). "Loss of the anaphase-promoting complex in quiescent cells causes unscheduled hepatocyte proliferation." Genes & development **18**(1): 88-98.

Wolf, S., F. Lottspeich and W. Baumeister (1993). "Ubiquitin found in the archaebacterium Thermoplasma acidophilum." FEBS letters **326**(1-3): 42-44.

Wolthuis, R., L. Clay-Farrace, W. van Zon, M. Yekezare, L. Koop, J. Ogink, R. Medema and J. Pines (2008). "Cdc20 and Cks direct the spindle checkpoint-independent destruction of cyclin A." Molecular cell **30**(3): 290-302.

Woods, D. F. and P. J. Bryant (1991). "The discs-large tumor suppressor gene of Drosophila encodes a guanylate kinase homolog localized at septate junctions." Cell **66**(3): 451-464.

Wu-Baer, F., K. Lagrazon, W. Yuan and R. Baer (2003). "The BRCA1/BARD1 heterodimer assembles polyubiquitin chains through an unconventional linkage involving lysine residue K6 of ubiquitin." Journal of Biological Chemistry **278**(37): 34743-34746.

Xie, C., C. Powell, M. Yao, J. Wu and Q. Dong (2014). "Ubiquitin-conjugating enzyme E2C: a potential cancer biomarker." The international journal of biochemistry & cell biology **47**: 113-117.

Xu, M., K.-A. Sheppard, C.-Y. Peng, A. S. Yee and H. Piwnica-Worms (1994). "Cyclin A/CDK2 binds directly to E2F-1 and inhibits the DNA-binding activity of E2F-1/DP-1 by phosphorylation." Molecular and cellular biology **14**(12): 8420-8431.

Xu, P., D. M. Duong, N. T. Seyfried, D. Cheng, Y. Xie, J. Robert, J. Rush, M. Hochstrasser, D. Finley and J. Peng (2009). "Quantitative proteomics reveals the function of unconventional ubiquitin chains in proteasomal degradation." Cell **137**(1): 133-145.

Yam, C., T. Fung and R. Poon (2002). "Cyclin A in cell cycle control and cancer." Cellular and Molecular Life Sciences CMLS **59**(8): 1317-1326.

Yamaguchi, M., R. VanderLinden, F. Weissmann, R. Qiao, P. Dube, N. G. Brown, D. Haselbach, W. Zhang, S. S. Sidhu and J.-M. Peters (2016). "Cryo-EM of mitotic checkpoint complex-bound APC/C reveals reciprocal and conformational regulation of ubiquitin ligation." Molecular cell **63**(4): 593-607.

Yamano, H. (2019). "APC/C: current understanding and future perspectives." F1000Research **8**.

Yan, Q., S. Dutt, R. Xu, K. Graves, P. Juszczynski, J. P. Manis and M. A. Shipp (2009). "BBAP monoubiquitylates histone H4 at lysine 91 and selectively modulates the DNA damage response." Molecular cell **36**(1): 110-120.

Yan, Q., R. Xu, L. Zhu, X. Cheng, Z. Wang, J. Manis and M. A. Shipp (2013). "BAL1 and its partner E3 ligase, BBAP, link Poly (ADP-ribose) activation, ubiquitylation, and double-strand DNA repair independent of ATM, MDC1, and RNF8." Molecular and cellular biology **33**(4): 845-857.

Ye, Y. and M. Rape (2009). "Building ubiquitin chains: E2 enzymes at work." Nature Reviews Molecular Cell Biology **10**(11): 755-764.

Young, P., Q. Deveraux, R. E. Beal, C. M. Pickart and M. Rechsteiner (1998). "Characterization of two polyubiquitin binding sites in the 26 S protease subunit 5a." Journal of Biological Chemistry **273**(10): 5461-5467.

Yu, H. (2002). "Regulation of APC–Cdc20 by the spindle checkpoint." Current opinion in cell biology **14**(6): 706-714.

Yuan, J., F. Eckerdt, J. Bereiter-Hahn, E. Kurunci-Csacsko, M. Kaufmann and K. Strebhardt (2002). "Cooperative phosphorylation including the activity of polo-like kinase 1 regulates the subcellular localization of cyclin B1." Oncogene 21(54): 8282-8292.

Yuan, W.-C., Y.-R. Lee, S.-Y. Lin, L.-Y. Chang, Y. P. Tan, C.-C. Hung, J.-C. Kuo, C.-H. Liu, M.-Y. Lin and M. Xu (2014). "K33-linked polyubiquitination of coronin 7 by Cul3-KLHL20 ubiquitin E3 ligase regulates protein trafficking." Molecular cell **54**(4): 586-600.

Zachariae, W., A. Shevchenko, P. D. Andrews, R. Ciosk, M. Galova, M. J. Stark, M. Mann and K. Nasmyth (1998). "Mass spectrometric analysis of the anaphase-promoting complex from yeast: identification of a subunit related to cullins." Science **279**(5354): 1216-1219.

Zerial, M. and H. McBride (2001). "Rab proteins as membrane organizers." Nature Reviews Molecular Cell Biology **2**(2): 107-117.

Zhang, S., L. Chang, C. Alfieri, Z. Zhang, J. Yang, S. Maslen, M. Skehel and D. Barford (2016). "Molecular mechanism of APC/C activation by mitotic phosphorylation." Nature **533**(7602): 260-264.

Zhang, Y., J. Gao, K. K. Chung, H. Huang, V. L. Dawson and T. M. Dawson (2000). "Parkin functions as an E2-dependent ubiquitin–protein ligase and promotes the degradation of the synaptic vesicle-associated protein, CDCrel-1." Proceedings of the National Academy of Sciences **97**(24): 13354-13359.

Zhang, Y., D. Mao, W. T. Roswit, X. Jin, A. C. Patel, D. A. Patel, E. Agapov, Z. Wang, R. M. Tidwell and J. J. Atkinson (2015). "PARP9-DTX3L ubiquitin ligase targets host histone H2BJ and viral 3C protease to enhance interferon signaling and control viral infection." Nature immunology **16**(12): 1215-1227.

Zhang, L., M. Xu, E. Scotti, Z. J. Chen and P. Tontonoz (2013). "Both K63 and K48 ubiquitin linkages signal lysosomal degradation of the LDL receptor." Journal of lipid research **54**(5): 1410-1420.

Zhang, Z., K. Kulkarni, S. J. Hanrahan, A. J. Thompson and D. Barford (2010). "The APC/C subunit Cdc16/Cut9 is a contiguous tetratricopeptide repeat superhelix with a homo-dimer interface similar to Cdc27." The EMBO journal **29**(21): 3733-3744.

Zhang, Z., S. M. Roe, M. Diogon, E. Kong, H. El Alaoui and D. Barford (2010). "Molecular structure of the N-terminal domain of the APC/C subunit Cdc27 reveals a

homo-dimeric tetratricopeptide repeat architecture." Journal of molecular biology **397**(5): 1316-1328.

Zou, H., T. J. McGarry, T. Bernal and M. W. Kirschner (1999). "Identification of a vertebrate sister-chromatid separation inhibitor involved in transformation and tumorigenesis." Science **285**(5426): 418-422.

Zur, A. and M. Brandeis (2001). "Securin degradation is mediated by fzy and fzr, and is required for complete chromatid separation but not for cytokinesis." The EMBO journal **20**(4): 792-801.